

Linköping Studies in Science and Technology. Dissertations  
No. 580

# Spark Advance Modeling and Control

Lars Eriksson

Division of Vehicular Systems  
Department of Electrical Engineering  
Linköping University, SE-581 83 Linköping, Sweden  
Linköping 1999

**Spark Advance  
Modeling and Control**

© 1999 Lars Eriksson

*larer@isy.liu.se*  
*<http://www.vehicular.isy.liu.se>*  
*Department of Electrical Engineering,*  
*Linköping University,*  
*SE-581 83 Linköping,*  
*Sweden.*

ISBN 91-7219-479-0

ISSN 0345-7524

Printed by Linus & Linnea AB, Linköping, Sweden 1999

*To Bodil and Emil*



## Abstract

The spark advance determines the efficiency of spark-ignited (SI) engines by positioning the combustion in relation to the piston motion. Today's spark-advance controllers are open-loop systems that measure parameters that effect the spark-advance setting and compensate for their effects. Several parameters influence the best spark-advance setting but it would be too expensive to measure and account for all of them. This results in a schedule that is a compromise since it has to guarantee good performance over the range of all the non-measured parameters. A closed-loop scheme instead measures the result of the actual spark advance and maintains an optimal spark-advance setting in the presence of disturbances. To cover this area two questions must be addressed: How to determine if the spark advance is optimal and how it can be measured? This is the scope of the present work.

One possible measurement is the in-cylinder pressure, which gives the torque, but also contains important information about the combustion. The cylinder pressure can accurately be modeled using well known single-zone thermodynamic models which include the loss mechanisms of heat transfer and crevice flows. A systematic procedure for identifying heat-release model parameters is presented.

Three well-known combustion descriptors have been presented in the literature that relate the phasing of the pressure signal to the optimal ignition timing. A parametric study was performed showing how changes in model parameters influence the combustion descriptors at optimum ignition timing.

Another possible measurement is the ionization current that uses the spark plug as a sensor, when it is not used for ignition. This is a direct in-cylinder measurement which is rich in information about the combustion. A novel approach to spark-advance control is presented, which uses the ionization current as a sensed variable. The feedback control scheme is closely related to schemes based on in-cylinder pressure measurements, that earlier have reported good results. A key idea in this approach is to fit a model to the measured ionization current signal, and extract information about the peak pressure position from the model parameters.

The control strategy is validated on an SI production engine, demonstrating that the spark-advance controller based on ionization current interpretation can control the peak pressure position to desired positions. A new method to increase engine efficiency is presented, by using the closed-loop spark-advance control strategy in combination with active water injection. However, the major result is that the controller maintains an optimal spark advance under various conditions and in the presence of environmental disturbances such as air humidity.

## Acknowledgments

First of all I would like to thank my supervisor, Lars Nielsen, and express my sincere gratitude for his guidance, encouragement, and for always taking time for discussions. Moreover, the positive atmosphere that he has created at the Division of Vehicular Systems for research and discussions is highly appreciated.

This work has been subsidized by the Swedish National Board for Industrial and Technical Development (NUTEK), under the competence centre ISIS, which is gratefully acknowledged. Also Mecel AB has supported the work and is further acknowledged for providing us at the division with an electronic engine control unit, SELMA, together with much knowledge and assistance.

I would like to thank the staff at the Division of Vehicular Systems. Andrej Perkovic for keeping the laboratory running and always giving assistance during the engine tests, without him the water experiments would have been very difficult. The questioning discussions with my former room-mate Mattias Nyberg have been very inspiring, in particular they increased my understanding and forced me to motivate the value of my research. Erik Frisk who has provided much time-consuming assistance on L<sup>A</sup>T<sub>E</sub>X and T<sub>E</sub>X. Simon Edlund, for support on the real-time system.

A well-functioning computer system is indispensable. Mattias Olofsson and Jens Larsson are acknowledged for keeping the computers going under crucial moments.

Andrej Perkovic, Per Andersson, and Maria Murphy are acknowledged for proof-reading parts of the material during the preparation of the thesis.

My family has always supported me and I wish to thank them all: My mother, Linnéa, for her encouragement. My sister, Anette, for her interest. My father, Hans, for always being curious this interest of his has greatly inspired me. My in-laws, Brita and Lennart, for all their support.

Finally, I would like to express my warmest gratitude to my wife, Bodil, and son, Emil, for bringing all their love and joyfulness into my life.

*One windy day in Linköping  
April 1999  
Lars Eriksson*

---

---

# Contents

<b>I</b>	<b>Introduction</b>	<b>1</b>
<b>1</b>	<b>Introduction</b>	<b>3</b>
1.1	Contributions . . . . .	5
<b>2</b>	<b>Introductory Background</b>	<b>7</b>
2.1	Ignition Control . . . . .	7
2.2	Spark Advance Control . . . . .	8
2.2.1	Approaches for Feedback . . . . .	9
2.3	Importance of In-Cylinder Pressure . . . . .	9
2.3.1	Cylinder Pressure Modeling . . . . .	10
2.3.2	Cylinder Pressure and MBT Timing . . . . .	12
2.4	Ion Sensing . . . . .	13
2.4.1	Ion Sensing for Ignition Control . . . . .	14
2.5	Performance Limits . . . . .	15
	<b>Bibliography</b>	<b>17</b>
<b>II</b>	<b>Publications</b>	<b>21</b>
<b>1</b>	<b>Ionization Current Interpretation for Ignition Control in Internal Combustion Engines</b>	<b>23</b>
1	Introduction . . . . .	24

2	Spark-Ignited Engines . . . . .	24
2.1	Cylinder pressure . . . . .	24
2.2	Ignition control . . . . .	25
2.3	Peak pressure algorithm . . . . .	26
3	The Ionization Current . . . . .	26
3.1	The ionization current signal . . . . .	27
4	Experimental Situation . . . . .	28
5	Ionization Current Interpretation . . . . .	29
5.1	Connection between ionization and pressure . . . . .	29
5.2	A model of the ionization signal . . . . .	31
6	Results from Ionization Current Interpretation . . . . .	31
7	Conclusions . . . . .	33
	References . . . . .	34
<b>2</b>	<b>A Real-Time Platform for Closed-Loop Spark-Advance Control</b>	<b>37</b>
1	Introduction . . . . .	38
1.1	Report Overview . . . . .	38
2	Experimental Platform . . . . .	38
2.1	Functionality Overview . . . . .	39
2.2	Electronic Control Unit (ECU) . . . . .	39
2.3	PC and Board Configuration . . . . .	40
2.4	Sample Timing . . . . .	42
3	Verification of the Experimental Platform . . . . .	43
4	Ionization Current Interpretation Algorithm . . . . .	44
4.1	Model description . . . . .	44
4.2	Criterion and Search Strategy . . . . .	45
4.3	Time Complexity . . . . .	45
5	Algorithm Suitable for the Platform . . . . .	46
5.1	Reparameterization of the Model . . . . .	46
5.2	Kullback Criterion . . . . .	47
5.3	Search Strategy . . . . .	47
6	Verification of the Estimation Algorithm . . . . .	50
7	Summary . . . . .	50
	References . . . . .	50
<b>3</b>	<b>Closed Loop Ignition Control by Ionization Current Interpretation</b>	<b>53</b>
1	Introduction . . . . .	54
2	Spark Timing . . . . .	54
2.1	Peak Pressure Concept . . . . .	54
3	Pressure and Torque Variability . . . . .	55
3.1	Measurements . . . . .	56
3.2	Principal Study of Variations . . . . .	57
4	Ionization Current . . . . .	58
4.1	Ionization Current Interpretation . . . . .	58

5	Spark Timing Controller . . . . .	60
5.1	Controller Tuning . . . . .	61
5.2	Influence of Cycle-To-Cycle Variations . . . . .	62
6	Experimental Setup . . . . .	63
7	Closed Loop Demonstration . . . . .	65
8	Conclusions . . . . .	66
	References . . . . .	67
A	Torque Variance . . . . .	67
<b>4</b>	<b>Increasing the Efficiency of SI-Engines by Spark-Advance Control and Water Injection</b>	<b>71</b>
1	Introduction . . . . .	72
2	Closed Loop Spark Advance Control . . . . .	72
2.1	Ionization current interpretation . . . . .	72
3	Experimental Setup . . . . .	73
4	Water Injection Experiments . . . . .	74
4.1	Test cycle 1 . . . . .	74
4.2	Test cycle 2 . . . . .	75
4.3	Test cycle 3 . . . . .	75
5	Torque Increase . . . . .	78
6	Conclusions . . . . .	78
	References . . . . .	78
<b>5</b>	<b>An Ion-Sense Engine-Fine-Tuner</b>	<b>81</b>
1	Introduction . . . . .	82
2	Outlook on Diagnosis and Feed-back Control . . . . .	82
2.1	Virtual Engine-Doctors . . . . .	82
2.2	Virtual Engine-Fine-Tuners . . . . .	83
3	Ionization current . . . . .	84
3.1	Detection . . . . .	85
3.2	Ionization Current Terminology . . . . .	86
3.3	Ionization current modeling . . . . .	88
4	Spark Advance Control . . . . .	89
4.1	Spark Advance and Cylinder Pressure . . . . .	90
4.2	Peak Pressure Concept . . . . .	91
4.3	Engine-tuning for efficiency . . . . .	91
4.4	Principle Study of Variations . . . . .	92
5	Structure and Design of Engine-Fine-Tuner . . . . .	94
5.1	PPP Estimate . . . . .	94
5.2	Controller structure . . . . .	96
5.3	Closed-Loop Control Parameters . . . . .	97
6	Performance of the Engine-Fine-Tuner . . . . .	97
6.1	Experimental set-up . . . . .	97
6.2	Response to set-point changes . . . . .	97
6.3	Water injection setup . . . . .	99

6.4	Humidity handled by the Engine-Fine-Tuner . . . . .	99
7	Conclusions . . . . .	100
	References . . . . .	102
<b>6</b>	<b>Requirements for and a Systematic Method for Identifying Heat-Release Model Parameters</b>	<b>105</b>
1	Introduction . . . . .	106
1.1	Parameter Identification . . . . .	106
2	Single-Zone Heat-Release Modeling . . . . .	107
2.1	Energy conservation equation . . . . .	108
2.2	Thermodynamic properties . . . . .	108
2.3	Temperature model . . . . .	109
2.4	Crevice Model . . . . .	109
2.5	Convective Heat Transfer . . . . .	110
2.6	Cylinder volume . . . . .	110
2.7	A commonly used family of simulation models . . . . .	111
3	Pressure Sensing and Sensor Modeling . . . . .	113
3.1	Pressure frequency contents . . . . .	113
3.2	Phasing of the pressure signal . . . . .	115
3.3	Filtering and data collection . . . . .	115
3.4	Sensor modeling . . . . .	117
3.5	Static sensor model . . . . .	118
4	Parameter Estimation Method . . . . .	121
4.1	Formulation of residuals . . . . .	121
4.2	Minimization procedure . . . . .	122
4.3	Parameter Evaluation . . . . .	123
4.4	Unknown parameters . . . . .	124
5	Parameter Estimation Results . . . . .	124
5.1	Pressure Residual . . . . .	126
5.2	Heat-Release Residual . . . . .	129
5.3	TDC determination, $\theta_0$ . . . . .	129
5.4	Cylinder pressure referencing . . . . .	130
5.5	Parameter variations . . . . .	131
5.6	Which criterion to minimize? . . . . .	131
6	Conclusions . . . . .	132
	References . . . . .	132
<b>7</b>	<b>A Parametric Study of Optimal Spark Advance and the Influence of Cycle-to-Cycle Variations</b>	<b>135</b>
1	Introduction . . . . .	136
1.1	Outline of Investigation . . . . .	137
2	Spark advance control . . . . .	138
2.1	Spark Advance and Cylinder Pressure . . . . .	139
3	Empirical Rules for Optimal Spark Advance . . . . .	139
3.1	Comparison of PR and MFB . . . . .	142

---

4	Heat-release model . . . . .	143
4.1	Heat-Release Calculation . . . . .	144
4.2	In-Cylinder Pressure Simulation . . . . .	144
5	Engine Data and Model Parameters . . . . .	145
5.1	Study of burn-angle variations . . . . .	146
5.2	Burn angles and spark advance . . . . .	146
5.3	Burn angles and engine speed . . . . .	148
5.4	Burn angles and engine load . . . . .	149
5.5	Summary of burn-angle variations . . . . .	149
5.6	Burn-angle parameters for 1500 rpm 50 Nm . . . . .	150
5.7	Nominal Model Parameters . . . . .	151
5.8	Mean values for the burn rates . . . . .	153
6	Simulation evaluation of engine efficiency . . . . .	153
6.1	Flame Development and Rapid Burn . . . . .	156
6.2	Heat Transfer and Burn Rate . . . . .	159
6.3	Crevice Volume and Heat Transfer . . . . .	163
6.4	$Q_{in}$ and $\gamma_{300}$ . . . . .	164
6.5	Evaluation of loss . . . . .	165
7	Summary of simulation evaluation . . . . .	168
7.1	Validation of relevance of study . . . . .	168
8	Cycle-to-cycle variations . . . . .	168
8.1	Derivation of the pdf . . . . .	170
8.2	Influence of cycle-to-cycle variations . . . . .	172
9	Issues Relevant for Feedback Control . . . . .	173
9.1	Ambiguity in PPP . . . . .	173
9.2	Determination of the Combustion Descriptors . . . . .	174
9.3	Gain evaluation . . . . .	175
10	Summary and Conclusions . . . . .	176
	References . . . . .	177
A	Heat-Release Model . . . . .	178
A.1	Energy conservation equation . . . . .	178
A.2	Thermodynamic properties . . . . .	179
A.3	Crevice model . . . . .	179
A.4	Temperature model . . . . .	180
A.5	Convective Heat Transfer . . . . .	180
B	Laminar burning velocity . . . . .	181
C	Early combustion development . . . . .	182



---

---

## List of Figures

2.1	Engine brake torque as function of ignition angle. The position for maximum brake torque (MBT) is marked, and MBT timing is approximately $24.5^\circ$ before top dead center (TDC). The spark is positioned to the right of the MBT timing, rather than the opposite, since it reduces $\text{NO}_x$ emissions and increases the margin to knock. . . . .	8
2.2	Four pressure traces resulting from four different ignition angles. The dashed line is the pressure from a motored cycle obtained by skipped firing. Ignition timing SA2 is close to optimum. . . . .	10
2.3	Model validation of a single-zone cylinder pressure model. Top: Plot of both measured and simulated cylinder pressure. Bottom: Difference between measured and simulated cylinder pressure. . . . .	11
2.4	Example of an ionization current with its three characteristic phases. The signal shape in the ignition phase is associated with the spark. In the flame front phase the signal is influenced by ions generated in and near the flame front. In the post flame phase the flame has propagated away from the spark plug and the signal is influenced by the cylinder temperature and pressure. . . . .	14
1	The cylinder pressure showing the motored cycle and three different positions for the ignition. (a) Motored cycle, MBT and early timing. (b) Motored cycle, MBT and late timing. . . . .	25
2	Measurement of the ionization current. (a) The spark plug-gap is used as a probe. (b) Measurement on the low voltage side. . . . .	27
3	An ionization signal showing the three phases: ignition, flame front, post flame. . . . .	28

4	The measurement situation. The pressure sensor is used only for validation. . . . .	29
5	Ionization current and cylinder pressure for one cycle. The post-flame phase corresponds to the pressure. . . . .	30
6	A case where the ionization current has two peaks in the flame-front phase and no peak in the post-flame phase, but there is still a correspondence with the pressure. . . . .	30
7	The pressure related part of the ionization signal compared with a Gaussian function. Solid; Measured cylinder pressure converted to ionization current through Eq. 1. Dashed; A Gaussian signal positioned at the cylinder pressure. . . . .	32
8	The measured ionization current and the fitted model. . . . .	32
9	The measured ionization current, and the two obtained Gaussian functions. The ICB pressure-function is positioned in the post-flame phase. . . . .	33
10	The peak positions of the cylinder pressure and the ICB pressure-function obtained. . . . .	34
11	A model with a extended flame front description. (a) The measured signal compared to the model. (b) The three Gaussian components. . . . .	35
12	The peak positions for the pressure related Gaussian signal (ICB) and the measured cylinder pressure corresponds well. . . . .	35
1	Block diagram over the system. . . . .	38
2	The ionization current showing the three characteristic phases: ignition phase, flame-front phase, and post-flame phase. . . . .	40
3	Sample timing system, the inputs and the output are shown. . . . .	42
4	The peak pressure position for several cycles. The controller is started at cycle 70, and successfully achieves the desired ignition timing. . . . .	44
5	Correlation plot between the true peak pressure position and the estimated peak position. Six different ignition timings, for one operating point with engine speed (2000 rpm) and load (100 Nm). Of course, some averaging improves the correlation. . . . .	51
1	The PPP (Peak Pressure Position) is the position in crank angles for the pressure peak. . . . .	55
2	Mean PPP (Peak Pressure Position) and output torque for 1500 rpm and four different throttle angles. Each circle is a mean value from 200 consecutive cycles with the same ignition timing. The optimal mean PPP is close to 15° for all loads. . . . .	56
3	Mean PPP (Peak Pressure Position) and output torque for 3000 rpm and four different throttle angles. Each circle is a mean value from 200 consecutive cycles with the same ignition timing. The optimal mean PPP is close to 15° for all loads. . . . .	57

---

4	Measured standard deviations for the peak pressure position, $\sigma_P$ , calculated for different engine speeds, loads and spark advances. The speeds are: solid – 1500 rpm, dashed – 2000 rpm, dash-dotted – 2500 rpm, dotted – 3000 rpm. . . . .	58
5	When the mean PPP (peak pressure position) is at optimum the variations in the output torque are minimal. At a) the mean peak pressure position lies at optimum which give small variations in output torque at a1). At b) the mean peak pressure position lies some degrees off from optimum and the resulting variations are larger at b1). . . . .	59
6	The spark plug functions as sensor for several parameters. Knock intensity, misfire, and cam-phase sensing has been implemented and lambda is also a potential output from an interpretation algorithm. The peak pressure position estimate is the information used here. . .	59
7	Ionization current with three clear phases, ignition, flame front, and post flame. . . . .	60
8	The peak pressure position estimated from the ionization current compared to the measured. Each point corresponds to the estimated and true PPP for one cycle. Close to 500 cycles are displayed in the plot. One to one correspondence is indicated by the solid line. . . .	61
9	The structure of the spark timing control system, where the spark plug operates as an integrated actuator and sensor. Information is extracted from the raw ionization current, and the estimate of the PPP is the input to the spark timing controller. . . . .	62
10	PPP and the estimate. Moving averages are computed with different lengths (measured in number of cycles) over the measured peak pressure positions and the estimated. The average lengths are; upper left - 3, upper right - 6, lower left - 9, lower right - 12. . . . .	63
11	Structure of a controller using feed back and feed forward in combination. . . . .	64
12	Experimental setup with the engine, the ECU, and the PC. . . . .	64
13	Closed loop control of spark advance with changing reference value, showing that the PPP can be controlled to the desired positions. Dash dotted – reference signal, solid – measured PPP, dashed – estimated PPP . . . . .	65
14	Closed loop control of spark advance with changing reference value, showing the step response time. Dash dotted – reference signal, solid – measured PPP, dashed – estimated PPP . . . . .	66
1	Left: A picture of the sprayer spraying water. Right: A schematic figure of the sprayer nozzle with the liquid spray, pressurized air, and the atomized liquid drops. . . . .	73

2	The sprayer is directed towards the intake port and throttle plate. At the lower side of the throttle plate, the spray of water can be seen as a pale shade of gray. When the picture was taken the engine ran at steady state with speed 1500 rpm and load 50 Nm. . . . .	74
3	A large part of the test cycle is displayed. The spark advance controller is shut off around cycle 100 and the spark advance is held constant. The water spraying starts around cycle 250 which leads to increased PPP and decreased output torque. The spark advance controller is switched on around cycle 400, controlling PPP back to MBT leading to increased output torque. The water spraying stops around cycle 550 and the parameters asymptotically goes back to their initial conditions, when the water still in the system, e.g. deposited on walls, decreases. . . . .	76
4	The interesting part of the test cycle. The spark advance controller is switched off at cycle 50 and the water injection starts at cycle 250. The controller is switched on again around cycle 500, controlling PPP to MBT which increases the output torque. . . . .	77
5	The interesting part of the test cycle. This test is run at a lower load condition than the tests shown in Figures 3 and 4, with output torque 38 Nm. The water injection starts around cycle 150 and the spark advance controller is switched on around cycle 225. The increase in output torque when the controller is switched on can also be observed here. . . . .	80
1	A medical doctor can from measurements like EEG or EKG, that are crude compared to human complexity, draw many conclusions. Ionization currents, like the one in the figure, are in-cylinder engine measurements that are directly coupled to the combustion. Virtual engine-doctors and virtual engine-fine-tuners are now being developed.	83
2	The introduction of computerized engine controllers (here above the engine) has revolutionized the engine control era. Already today they represent an impressive computing power and the development continues. . . . .	84
3	The spark plug can, using signal interpretation, function as sensor for several parameters. Knock intensity and misfire are already implemented in production cars as a basis for virtual engine-doctors. Lambda sensing and peak pressure position estimation can be used in virtual engine fine tuners. The peak pressure position (and a quality measure of it) is the information used in this paper. . . . .	85
4	Cycle to cycle variations are always present in the combustion. The plots show ten consecutive cycles at stationary engine operation that clearly exhibit the cyclic variations. . . . .	86
5	Measurement of the ionization current. (a) The spark plug-gap is used as a probe. (b) Measurement on the low voltage side of the ignition coil. . . . .	87

6	Ionization current showing three clear phases, ignition, flame front, and post flame. . . . .	87
7	Components of the model (Equation (2)) that captures the appearance and the phases of the ionization current. . . . .	89
8	Three different pressure traces resulting from three different spark advances. The different spark advances are; SA1: spark advance $32.5^\circ$ before top dead center (TDC), SA2: $22.5^\circ$ before TDC, SA3: $12.5^\circ$ before TDC. The optimal spark advance is close to SA2. . . . .	91
9	The PPP (Peak Pressure Position) is the position in crank angles for the pressure peak. It is one way of describing the position of the pressure trace relative to crank angle. . . . .	92
10	Mean PPP (Peak Pressure Position) and output torque for 1500 rpm and 3000 rpm and two different engine load conditions. Each circle is a mean value from 200 consecutive cycles with the same ignition timing. The optimal mean PPP is close to $15^\circ$ for all loads, even though the spark advance differs a lot. . . . .	93
11	The figure illustrates that when the mean PPP (peak pressure position) is at optimum the variations in the output torque are minimal. At a) the mean peak pressure position lies at optimum which give small variations in output torque at a1). At b) the mean peak pressure position lies some degrees off from optimum and the resulting variations are larger at b1). . . . .	94
12	The peak pressure position estimated from the ionization current compared to the measured. Each point corresponds to the estimated and true PPP for one cycle. Close to 500 cycles are displayed in the plot. One to one correspondence is indicated by the solid line. . . . .	95
13	The structure of the spark advance control structure, where the spark plug operates as an integrated actuator and sensor. Information is extracted from the raw ionization current, and the estimate of the PPP is the input to the spark timing controller. Reference values and feed forward signals are obtained using other sensors, e.g. engine speed and load. . . . .	96
14	Closed loop control of spark advance with changing reference value, showing that the PPP can be controlled to the desired positions. Dash dotted – reference signal, solid – PPP measured by an extra pressure sensor, dashed – PPP estimated from ionization current . . . . .	98
15	Left: A picture of the sprayer spraying water. Right: A schematic figure of the sprayer nozzle with the liquid spray, pressurized air, and the atomized liquid drops. . . . .	99
16	The interesting part of the test cycle. The spark advance controller is switched off at cycle 50 and the water injection starts at cycle 250, which leads to increased PPP. The controller is switched on again around cycle 500, controlling PPP to MBT which increases the output torque. . . . .	101

1	Using a systematic procedure for determining the model parameters enables an automated analysis of large data sets. For each operating condition the procedure provides parameters that are used in the heat release analysis. . . . .	107
2	Two traces with exactly the same parameters, but with changed starting points. The figure shows that the level of $Q_{ch}$ has changed significantly. . . . .	112
3	Example of a pressure measurement setup, that samples the cylinder pressure based on the crank angle. The sample rate, in this configuration, is equal to one sample per crank angle degree. . . . .	114
4	Spectra for two (motored) cylinder pressure traces measured at engine speeds of 800 rpm and 1600 rpm. Note that the frequency scales are different for the two spectra. The first harmonic in the signal occurs at the frequency of the engine cycle i.e. for 800 rpm at 6.7 Hz. For both engine speeds the frequency contents become difficult to distinguish from noise around the 40th harmonic. . . . .	114
5	Three pressure signals: Dash dotted – measured pressure, Solid – zero-phase filtered, Dashed – causally filtered. The two filters had the same order and the same cut-off frequency, but the causal filter causes a shift in peak pressure position of $10^\circ$ . . . . .	116
6	Impulse response for the charge amplifier. At $t=0s$ a charge of 2.91 nC is given as input to the charge amplifier. Solid line – model output with $\tau_c = 22$ s. Dotted line – measured output from the charge amplifier. . . . .	119
7	Pressure signals for two different charge amplifiers, one with an infinite time constant, $p_\infty$ , and one with a time constant of 2.2 s, $p_{2.2s}$ . . . . .	120
8	The upper plot shows the measured pressure (solid line), and the output from the model (dashed line) the pressure that the model predicts, the signals are extremely close. The lower plot shows the difference between the measured and the model, and the conclusion is that the difference is very small. . . . .	125
9	Log-log pV diagram for pressure that has been optimized and the crank angle offset, sensor gain, and pressure offset has been included. . . . .	126
10	Cylinder pressure, intake manifold pressure, and exhaust pressure for one motored cycle. A validation that with a known sensor gain, C, the initial pressure, $p_{ivc}$ , can be estimated and the cylinder pressure is close to the intake and exhaust pressures during the intake and exhaust strokes. . . . .	127
11	Estimated TDC offset for crank angle measurements. The values that are estimated for one operating condition is very close to each other (within $\sim 0.1^\circ$ ), but between the operating conditions the offset varies ( $\sim 0.5^\circ$ ). . . . .	131

1	Closed loop schemes for spark advance control have been presented that utilize the three combustion descriptors, shown in the figure, as a sensor for optimal spark advance. The three combustion descriptors are: peak pressure position (PPP), mass fraction burned (MFB), and the pressure ratio (PR). . . . .	136
2	Environmental and engine conditions affect how the cylinder pressure develops and thus the optimal spark advance. Changes in conditions can also be represented by changes in model parameters, and in the simulation evaluation the model parameters are varied and their influence on the combustion descriptors are mapped. . . . .	137
3	Three pressure traces resulting from three different spark advances. The different spark advances are; SA1: spark advance $32.5^\circ$ before top dead center (TDC), SA2: $22.5^\circ$ before TDC, SA3: $12.5^\circ$ before TDC. The optimal spark advance is close to SA2. . . . .	140
4	The PPP (Peak Pressure Position) is the position in crank angles for the pressure peak. It is one way of describing the position of the pressure trace relative to crank angle. . . . .	141
5	The mass fraction burned profile $x_b(\theta)$ with the three positions for 30%, 50%, and 90% mass fraction burned marked. . . . .	141
6	Comparison of pressure ratio (dotted) and mass fraction burned (solid) traces, for five ignition timings, $\theta_{ig} \in \{-60^\circ, -40^\circ, -20^\circ, 0^\circ, 20^\circ\}$ , and two rapid-burning angles, $\Delta\theta_b \in \{20^\circ, 40^\circ\}$ . The difference is small when the burning occurs around and after TDC. . . . .	142
7	The mass fraction burned profile with the flame development angle, $\Delta\theta_d$ , and rapid burning angle, $\Delta\theta_b$ marked. . . . .	145
8	Variations in $\Delta\theta_d$ and $\Delta\theta_b$ as a function of ignition angle. The different lines represent one operating condition with respect to engine speed and load. . . . .	146
9	Simulation of how the ignition angle influences the flame development angle, $\Delta\theta_d$ , through the laminar burning velocity, the result agrees well with the experimental data in Figure 8. The minimum for $\Delta\theta_d$ is $22^\circ$ which occurs around $\theta_{ig} \approx 11^\circ$ . . . . .	147
10	Standard deviations for $\Delta\theta_d$ and $\Delta\theta_b$ for different ignition angles. The standard deviations increase as the ignition angle is increased. . . . .	149
11	Correlation coefficient between $\Delta\theta_d$ and $\Delta\theta_b$ for different ignition angles. There is a clear correlation between $\Delta\theta_d$ and $\Delta\theta_b$ for several operating conditions and the trend is that the correlation increases as the ignition angle is increased. . . . .	150
12	Variations in $\Delta\theta_d$ and $\Delta\theta_b$ as a function of engine speed and engine load. . . . .	151
13	The standard deviations for $\Delta\theta_d$ and $\Delta\theta_b$ as a function of engine speed and engine load. . . . .	152
14	Coefficient of correlation between $\Delta\theta_d$ and $\Delta\theta_b$ as a function of engine speed and engine load. . . . .	152

15	Variations in the flame development angle, $\Delta\theta_d$ , and rapid burning angle, $\Delta\theta_b$ , for the data set. Each mark in the plot represents the mean value for the parameter, calculated from 150 cycles at each operating condition i.e. for one speed, load, and ignition timing. The different shapes represent different loads: $\circ$ -0 Nm, $\times$ -50 Nm, $+$ -90 Nm, and $*$ -130 Nm . . . . .	154
16	The method for studying the how different model parameters influence the combustion descriptors at optimal ignition timing and. . . . .	155
17	Validation that the ignition does not significantly change the intake and exhaust processes. In the engine data plotted the four ignition angles ranged from $-23^\circ$ to $-8^\circ$ BTDC. Even though, the ignition angle changed the pressure during the exhaust and intake strokes does not change, and thus the pumping work is not significantly influenced by the ignition timing. . . . .	155
18	Pressure traces for optimal spark advance for changes in rapid burning angle $\Delta\theta_b$ . The flame development angle is $\Delta\theta_d = 20^\circ$ for the plot in this figure. . . . .	157
19	Heat release traces for optimal spark advance for changes in rapid burning angle $\Delta\theta_b$ . The flame development angle is $\Delta\theta_d = 20^\circ$ for the plot in this figure. . . . .	158
20	Changes in the optimal ignition angle as a function of flame development angle, $\Delta\theta_d$ , and rapid burning angle, $\Delta\theta_b$ . The x-axis gives values for $\Delta\theta_b$ , the lines represent constant $\Delta\theta_d$ , and the y-axis gives the optimal ignition timing MBT timing. . . . .	159
21	The peak pressure position (PPP) for optimum spark advance (MBT timing) as a function of flame development angle, $\Delta\theta_d$ , and rapid burning angle, $\Delta\theta_b$ . . . . .	160
22	Enlargement of the mass fraction burned traces shown in Figure 19 and with all other traces traces added. The plot shows that mass fraction burned levels between 45% and 50% are contained in a narrow region for a variety of flame development and rapid burn angles. . . . .	160
23	Changes in the 45% mass fraction burned for optimum ignition as a function of flame development angle, $\Delta\theta_d$ , and rapid burning angle, $\Delta\theta_b$ . . . . .	161
24	Changes in the 50% mass fraction burned for optimum ignition as a function of flame development angle, $\Delta\theta_d$ , and rapid burning angle, $\Delta\theta_b$ . . . . .	162
25	Changes in the optimal ignition angle as a function of heat transfer coefficient $C_1$ and changes in burn rate through $\Delta\theta_b = 12 + (\Delta\theta_d - 15)/20 * 26$ . . . . .	163
26	Changes in the optimal peak pressure position (PPP) as a function of heat transfer coefficient $C_1$ and changes in burn rate through $\Delta\theta_b = 12 + (\Delta\theta_d - 15)/20 * 26$ . . . . .	164

27	Changes in the optimal position for 45% mass fraction burned position as a function of heat transfer coefficient $C_1$ and changes in burn rate through $\theta_b = 12 + (\theta_d - 15)/20 * 26$ . . . . .	165
28	Changes in the optimal peak pressure position as a function of heat transfer coefficient $C_2$ and changes in crevice volume. . . . .	166
29	Net indicated efficiency as a function of ignition angle, the optimal value for the ignition is $\theta_{ig} = 22.9^\circ$ . The plot is generated with the model parameters at their nominal values. . . . .	166
30	The loss of not maintaining the peak pressure position at its optimum. In the plots the peak pressure has been kept at a position of $14^\circ$ ATDC and the loss in efficiency compared to the optimal ignition. It can be seen that the loss is less than 0.4%. . . . .	167
31	Model of the combustion process where the parameters $\theta_{ig}$ , $\Theta_d$ , and $\Theta_b$ are inputs and the mass fraction burned, cylinder pressure, PPP, and work are outputs. $\theta_{ig}$ is a deterministic variable while $\Theta_d$ , and $\Theta_b$ are stochastic variables. . . . .	169
32	Four of the steps in deriving the pdf for the burn-rate parameters are shown. a) Find principal components. b) "Rotation" to principal components $(x, y)$ . c) pdf for principal components. d) Rotation back to burn rate parameters. . . . .	171
33	Test of normality for data averaged over the principal components. The x-component does not fit a Normal distribution while the y-components does. . . . .	171
34	The output torque, peak pressure position, 45% and 50% mass fraction burned as a function spark advance. Solid lines – no cycle-to-cycle variations. Dashed lines – parameters influenced by cycle-to-cycle variations. . . . .	172
35	A carpet plot showing the output torque $T$ as a function of the three values: peak pressure position $\theta_{pp}$ , rapid burning angle $\Delta\theta_b$ , and ignition angle $\theta_{ig}$ . The ignition timing was varied from $60^\circ$ BTDC to $10^\circ$ ATDC. For very late ignition timings TDC is detected as peak pressure position. The flame development angle was fixed to $\Delta\theta_d = 25^\circ$ for all conditions simulated. Note that the rapid burn angles were chosen very large compared to the engine data shown in Figure 15. . . . .	174
36	Evaluation of the how the gain changes for different ignition angles in one operating condition. The lines represent: xb50 – gain for $\theta_{50\%}$ , xb45 – gain for $\theta_{45\%}$ , and PPP – gain for PPP. . . . .	175



---



---

## List of Tables

1	Influence of charge amplifier time constant $\tau_c$ on the intra cycle measurement offset. $\Delta p$ is the difference between ideal sensor and actual sensor. $p$ is the maximum pressure during the cycle. . . . .	120
2	Tuning parameters in the heat release model. The values shown in the rightmost column give the approximate size. . . . .	124
3	Standard deviation for the estimated crevice volume, for an engine speed of 800 rpm. The standard deviation increases pronouncedly when the throttle angle decreases, which reduces the temperature difference between crevices and average charge temperature. . . . .	128
4	Data for the engine that is used in the experiments. . . . .	134
1	The difference in crank angle between 50% mass fraction burned and pressure ratio (PR)=0.5 for different rapid burn angles and ignition angles. The optimal ignition timing for these conditions are $\theta_{ig} \in [-30^\circ, -15^\circ]$ and for these ignition angles the difference is only in the order of one degree. . . . .	143
2	A qualitative representation of how the burn-angle parameters vary with increasing ignition angle $\theta_{ig}$ , engine speed $N$ , and engine load $T_L$ . The symbols have the following meaning: $\searrow$ – decreasing trend, $\nearrow$ – increasing trend, $\rightsquigarrow$ – no apparent trend, $\searrow \nearrow$ – first decreases then increases, $\nearrow \searrow$ – first increases then decreases, (?) – there are data that contradicts the trend. . . . .	153

- 3 Nominal model parameter values that has been used during the evaluation. The parameters are:  $\Delta\theta_d$  and  $\Delta\theta_b$  – burn rate parameters,  $C_1$  and  $C_2$  – heat transfer parameters,  $V_{cr}$  – crevice volume given in % of clearance volume,  $Q_{in}$  – input energy,  $\gamma_{300}$  – ratio of specific heats for the temperature  $T = 300K$ . . . . . 153
- 4 Summary of how much the different model parameters influence the different combustion descriptors in the simulations. . . . . 168

## Part I

# Introduction



## Introduction

Today's ignition timing systems are regulated by open-loop controllers which in turn rely on calibrated look-up tables. Much can be gained by a closed-loop scheme both in terms of increasing the efficiency and reducing the calibration effort. Aiming at feedback control we require some measurement of the result of the ignition and combustion, which poses the following two questions:

- What is good combustion?
- How can we measure good combustion?

The cover illustration highlights the key parts in the thesis, which focuses on efficiency: Center – Spark plug with a spark in the gap; Left figure – Cylinder pressures resulting from different spark timings; Left equation – Model for the cylinder pressure; Right figure – Ionization current obtained using the spark plug as sensor; Right equation – Model for the ionization current that is used to extract pressure information.

### Pressure modeling

The spark advance that maximizes engine efficiency also maximizes the produced work. The spark initiates the combustion, and positions the in-cylinder pressure development in relation to the crank rotation, which finally produces work. Cylinder pressure is thus very important. Measured cylinder pressure is a consequence of the combustion and a model is therefore required for analysis of the combustion process. Heat-release models are well-known tools that utilize the cylinder pressure to determine the position and rate of combustion. A simple one-zone model based on the first law of thermodynamics is shown to be accurate enough to describe the

pressure development. The studied model was developed by Gatowski et. al. [21] and includes the loss mechanisms of heat transfer and crevice flow. Such modeling requires determination of model parameters for example by identification from experimental data. A novel systematic method is presented for identifying parameters in heat-release models using only cylinder pressure data.

Simple combustion descriptors, derived from the cylinder pressure, have been suggested that relate the result from the ignition timing to optimal ignition timing. Two examples are the position for the pressure peak and the mass fraction burned trace. Control schemes based on the combustion descriptors from the in-cylinder pressure sensors have shown good results [28, 22, 44, 33, 6]. A desirable property of combustion descriptors is that they represent a good measure of optimal spark advance even for varying engine and environmental conditions. The impact that different model parameters have on three known combustion descriptors at optimum spark advance is investigated in the thesis. It is shown that all three descriptors have the good property of being relatively invariant to changes in the burn rate. Among other things it is also shown that a correlation between the burn angles is important when studying the invariance of descriptors and that the cycle-to-cycle variations can be neglected when analyzing the optimal ignition timing.

### **Ionization current interpretation**

The ionization current, measured using the spark plug as sensor, is a direct measure in the combustion chamber. It is already used in production cars to detect knock, misfire, and for cam-phase sensing [4]. Therefore, to incorporate an ionization current based spark advance system, only additional signal interpretation in the electronic engine control unit (ECU) is required. The current is rich on information about the combustion, but it is also complex with three characteristic phases that mix together in complicated ways. One of the phases contains information about the in-cylinder pressure, which is good since a pressure sensor that can withstand the high pressures and temperatures in the combustion is expensive and has not yet proven cost effective.

### **Feedback demonstration**

This thesis presents a novel approach to the spark-advance control problem, by using the ionization current as sensed variable. Information about the peak pressure position is extracted from the ionization current, and used in a feedback loop for spark advance control. Experimental and theoretical studies clearly demonstrate the value of ignition control regarding power and efficiency. Controller performance is demonstrated in real-time experiments showing that the position of the pressure peak is successfully controlled, the step response time is sufficient, and that non-measured environmental disturbances are successfully handled.

## 1.1 Contributions

The contributions in this thesis are summarized in the presentation of the enclosed publications. Some of the results are also summarized in Sections 2.3.2 and 2.4.1 of Chapter 2, which gives an introductory background to the thesis.

### Publication 1

“Ionization Current Interpretation for Ignition Control in Internal Combustion Engines” by Lars Eriksson and Lars Nielsen [17] was published in the 1997 August issue of *Control Engineering Practice*. It presents a method for extracting information, relevant for spark-advance control, from the ionization current. The proposed method is a key contribution. Essentially, the idea for extracting information is to use a parameterized model to fit the measured ionization current, and interpret the received parameters to get a peak pressure position (PPP) estimate. The evaluation is performed off-line and it shows that the information extracted from the ionization current can be used for spark-advance control.

### Publication 2

The report “A Real-Time Platform for Closed-Loop Spark-Advance Control” by Lars Eriksson [14] describes the hardware and software platform that has been developed, and contributes with a real-time algorithm for ionization current interpretation. The platform is used for on-line validation of a control system that utilize the ionization current as sensed variable for spark-advance control. The report consists of two parts, where the first part describes the hardware platform that is designed to meet the demands for measurement and control synchronized with the engine combustion events. In the second part, the development of an algorithm suitable for real-time implementation on the platform is described.

### Publication 3

“Closed Loop Ignition Control by Ionization Current Interpretation” by Lars Eriksson, Lars Nielsen and Mikael Glavenius [19] was presented at the SAE 1997 International Congress and Exposition in Detroit. It demonstrates that the ionization current interpretation method can be used to optimize the engine performance in real-time. The peak pressure position principle is verified for the SAAB 2.3 l engine in Vehicular Systems laboratory, and the optimal PPP lies close to  $14^\circ - 16^\circ$  after top dead center (ATDC). A principle study of variations is also performed, quantifying the relation between cycle-to-cycle variations in PPP and output torque. It is demonstrated that an optimal spark advance gives lower cycle-to-cycle variations in the output torque. This paper also shows that the peak pressure position can be controlled to the desired positions, in real-time on a running engine, using only information extracted from the ionization current. This demonstration is one of the main contributions of this thesis. This paper was selected for publication in the 1997 SAE Transactions.

**Publication 4**

“Increasing the Efficiency of SI-Engines by Spark-Advance Control and Water Injection” by Lars Eriksson and Lars Nielsen [18] was presented at the 1998 IFAC Workshop: Advances in Automotive Control in Mohican State Park, Ohio, USA. It presents a new method for increasing the efficiency of an SI-Engine using active water injection and a closed-loop spark-advance scheme. It shows that the output torque actually increases with water injection combined with closed-loop spark advance control. This leads to suggestions for a novel method to increase the efficiency of spark ignited engines, by combining active water injection with the developed spark advance control method.

**Publication 5**

“An Ion-Sense Engine Fine-Tuner” by Lars Nielsen and Lars Eriksson [36], that appeared in the 1998 October issue of IEEE Control Systems Magazine, provides an overview of the ion-sensing part of the thesis by summarizing some of the earlier results. The paper clearly demonstrates the value of on-line engine optimization where the closed-loop control system is successful in handling environmental, i.e. non-measured, disturbances that affect the optimal spark advance. Water is sprayed into the engine as an environmental disturbance. A conventional pre-calibrated spark-advance schedule results in a lower output torque, whereas the method presented in this thesis controls the engine to maximum efficiency.

**Publication 6**

“Requirements for and a Systematic Method for Identifying Heat-Release Model-Parameters” by Lars Eriksson [15] was presented at the 1998 SAE International Congress and Exposition in Detroit. A systematic method is presented for simultaneous identification of parameters of sensor characteristic and heat release model. The effect of dependence between variables when selecting parameters and determining their values is pointed out. The paper [15] has been selected to appear in the 1998 SAE Transactions.

**Publication 7**

This publication is an extended version of the paper “Spark Advance for Optimal Efficiency” by Lars Eriksson [16], that was presented at the 1999 SAE International Congress and Exposition in Detroit. Three known combustion characteristics, that are deduced from the cylinder pressure, are studied and compared for an ignition timing that is at MBT. The influence that different model parameters have on the combustion characteristics is examined, through modeling and simulation. The three combustion characteristics do not change much when the burn angles change. A correlation is shown to exist between the burn rates which influences the invariance of combustion descriptors. Additionally, cycle-to-cycle variations can be neglected when studying the spark advance for optimal efficiency.

## Introductory Background

A brief overview is given of spark-advance control, which places the material in this thesis in perspective. The presentation is intended for a reader with a background from areas other than combustion engines and engine control. Nevertheless, some of the results are summarized in Sections 2.3.2 and 2.4.1.

### 2.1 Ignition Control

In spark-ignition (SI) engines the fuel and air mixture is prepared in advance and the mixture is ignited by the spark discharge. The spark initiates a small flame kernel that develops into a turbulent flame which propagates through the cylinder. The combustion increases the temperature and pressure which produces work on the piston. The main goal for the spark is to ignite the fuel and initiate a stable combustion, at a position that meets demands of maximizing the efficiency, fulfilling emission requirements, and preventing the engine from being destroyed. The demands are sometimes conflicting; for example at high engine loads the ignition timing for maximum efficiency has to be abandoned in favor of prevention of engine destruction by way of engine knock.

Two essential parameters are controlled with the ignition: Ignition energy and ignition timing. The control of ignition energy is an important topic for assuring combustion initiation but the focus in this thesis is on the ignition timing that maximizes the engine efficiency.

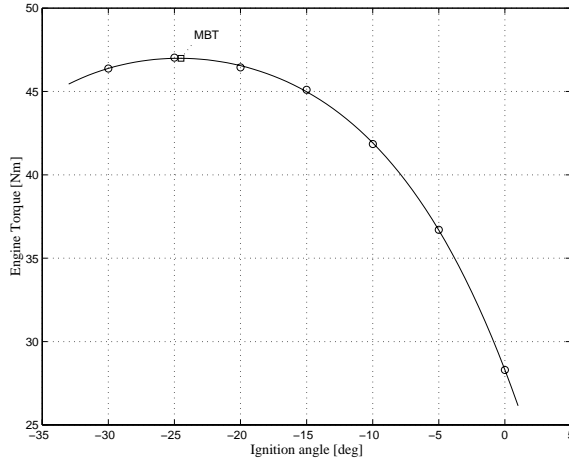


**Figure 2.1** Engine brake torque as function of ignition angle. The position for maximum brake torque (MBT) is marked, and MBT timing is approximately  $24.5^\circ$  before top dead center (TDC). The spark is positioned to the right of the MBT timing, rather than the opposite, since it reduces  $\text{NO}_x$  emissions and increases the margin to knock.

## 2.2 Spark Advance Control

The ignition timing itself influences nearly all engine outputs and is essential for efficiency, driveability, and emissions. Focusing on engine efficiency the *optimal ignition timing*, for a conventional SI engine, is defined as:

The ignition timing that for a given engine operating condition maximizes the work produced during a cycle.

This choice of definition narrows the problem down to the determination of only the ignition timing. The simple motivation for the definition is that when the produced work is maximized for a fixed engine geometry and operating condition with constant speed, constant amount of fuel, and constant air/fuel ratio then it gives best fuel economy. The ignition timing which gives the maximum brake torque is called the *maximum brake torque (MBT) timing*. A timing that deviates from MBT timing lowers the output torque, see Figure 2.1.

In today's production systems the ignition timing is controlled using open-loop schemes that rely on look-up tables. The look-up tables are determined through extensive calibration experiments in either an engine or chassis dynamometer. According to Heywood [26] a calibration procedure usually follows these guidelines: First the torque at MBT is determined. Then the ignition timing is retarded towards TDC until the torque is reduced by approximately 1% below the maximum

and that value is then used. There are three reasons for this: First, it is easier to determine this position, since the torque as a function of ignition timing is flat at the optimum. Second, with a slightly retarded schedule the margin to knocking conditions is increased. Third, the  $\text{NO}_x$  formation is reduced. The calibrated schedule is stored in a look-up table, covering the engine operating range, and compensation factors are added and used during e.g. cold start and idle conditions.

Optimal ignition timing depends on how the flame propagates through the combustion chamber and the losses such as heat transfer to the walls and piston, flows into and out of crevices, and piston blowby. The flame propagation in turn depends on many parameters such as engine speed, engine load, engine temperature, intake air temperature, fuel quality, air/fuel ratio, and humidity, to mention some of them. Optimal ignition timing thus depends on many engine parameters. Some of the parameters that are measured and accounted for, in today's systems, are: engine speed, engine load, coolant temperature, and intake air temperature [1]. To measure and account for all parameters that affect the ignition timing would be very expensive and time consuming. A calibrated scheme has to guarantee good performance over the range of the non measured parameters and is often chosen to be conservative, it is thus not optimal when the non measured parameters change. A feedback scheme on the other hand, that measures the result of the ignition instead of measuring and accounting for things that affect it, has the potential to guarantee good performance over the entire range of non-measured parameters, improve the efficiency, and additionally reduce the calibration effort and requirements.

### 2.2.1 Approaches for Feedback

Attempts have been made that utilize a dithering technique in combination with measurements of acceleration of the crank shaft speed. One of the first was made by Draper and Li [13] on a single cylinder engine. Schweitzer et. al. [46] extended the work to a multi cylinder engine. These schemes have the drawback of needing to constantly change the ignition to determine the optimality.

Another approach is to utilize some kind of sensor, for direct measurement of the combustion result, which relates to maximum efficiency. This is the main topic of the thesis and two related in-cylinder measurements are studied, the cylinder pressure and the ionization current.

## 2.3 Importance of In-Cylinder Pressure

Focusing on efficiency makes output torque and in-cylinder pressure the most important variables, since the work is integrated from the torque and the torque is generated by the pressure on the piston, i.e. the work per cycle and cylinder,  $W_c$ , can for a four stroke engine be expressed as

$$W_c = \int_{-2\pi}^{2\pi} T(\theta) d\theta = \int_{-2\pi}^{2\pi} p_{\text{cyl}}(\theta) A L(\theta) d\theta = \oint_{\text{cycle}} p(\theta) dV$$

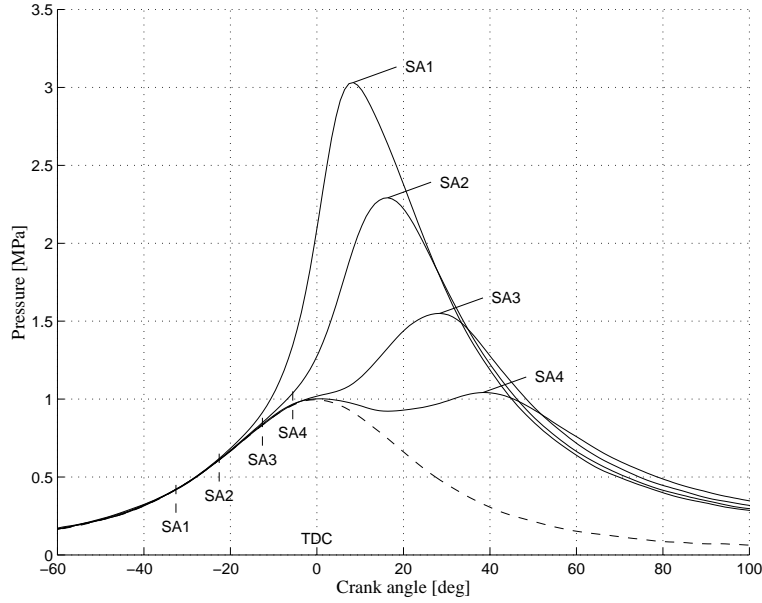


**Figure 2.2** Four pressure traces resulting from four different ignition angles. The dashed line is the pressure from a motored cycle obtained by skipped firing. Ignition timing SA2 is close to optimum.

where  $\theta$  is the crank angle,  $T$  torque,  $p_{\text{cyl}}$  pressure,  $A$  cylinder cross section area,  $L$  crankshaft lever, and  $V$  is the volume. Changing the spark advance influences how the fuel is burned in relation to the crank rotation and thus the pressure development, see Figure 2.2. An early ignition timing produces an early combustion and pressure development, which results in a high pressure peak that occurs early in the expansion stroke. Retarding the spark advance towards top dead center (TDC) results in a later pressure development with a lower pressure peak that occurs later in the expansion stroke.

### 2.3.1 Cylinder Pressure Modeling

The cylinder pressure development is prescribed by different sources of which the major ones are: volume change and addition of heat from the combustion. The loss mechanisms, e.g. heat transfer, flow into and out of crevices, and leakage, also influence the pressure development.

Heat-release analysis is a well established technique, based on the first law of thermodynamics, for estimating how the heat is released during the combustion. The *heat release* is calculated from a measured pressure trace using a model to subtract the influence of volume change and losses, which leaves the effect of heat

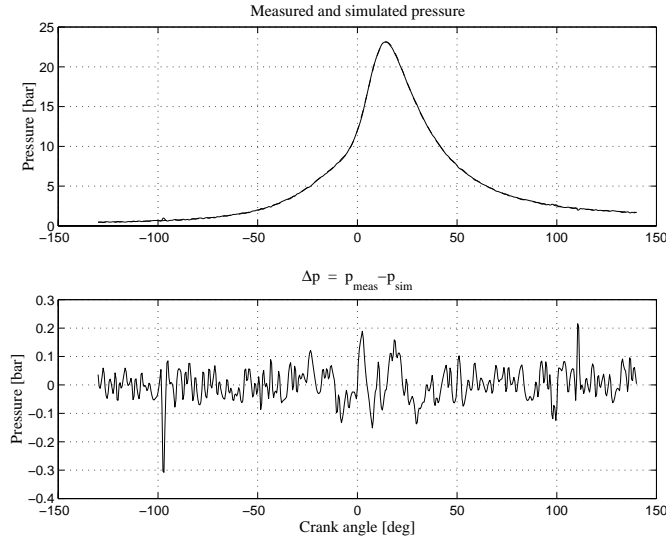


**Figure 2.3** Model validation of a single-zone cylinder pressure model. Top: Plot of both measured and simulated cylinder pressure. Bottom: Difference between measured and simulated cylinder pressure.

addition from the combustion. A wide variety of models can be derived by varying how the thermodynamic properties are modeled and what loss mechanisms are included. The most frequently cited references for heat release analysis are [39, 31, 21]. In a single-zone model the cylinder contents is treated as a single fluid, while a two-zone or multi-zone model treats the burned and unburned gases separately. Traditionally these models have been used to estimate the heat release but they can easily be reformulated and used to simulate the pressure provided a heat-release trace.

Here a single-zone combustion model is chosen based on the principle of “model only what you need”. A single zone-model is sufficient for producing a pressure trace that is accurate enough for engine torque and work calculations, see Figure 2.3. The selected model is the one developed and used in Gatowski et.al. [21]. The necessity to model the loss mechanisms is shown Publication 7, where the simulations show that heat transfer has a large influence on the optimal spark advance.

### Parameter Determination

Key issues in the modeling are accuracy of the pressure data and determination of model parameters. A number of excellent and discerning papers have been published on the determination of parameters associated with cylinder pressure

and heat-release models. However, most studies are limited in the sense that they only consider and analyze specific parameters under the assumption that all (or the majority) of the other parameters are known. Some examples are: offset in the measured pressure signal [9, 38], polytropic index [47], parameters in the heat transfer correlation [23], and TDC determination [34, 49]. Another important issue is how different parameters in the model and the pressure measurement influence the accuracy of the pressure and heat-release models [2, 8, 47].

The question addressed in Publication 6 is: What parameters can be identified from only cylinder pressure data? To answer the question a systematic method is developed and investigated for identifying the complete set of model parameters using data obtained from a motored cycle (cycle without combustion). The effect of dependences between variables is pointed out, especially how it influences the selection of parameters and the determination of their values.

### 2.3.2 Cylinder Pressure and MBT Timing

The torque and pressure development can accurately be simulated using the model and we can thus determine the optimum ignition timing through simulation. So now it is possible to focus on the question: How can we measure the efficiency of the combustion?

From the cylinder pressure a number of *combustion descriptors* have been deduced that relate the position of the combustion to when optimal spark advance is attained. The following three well known combustion descriptors are analyzed and compared in Publication 7. The first descriptor is the position for the pressure peak (PPP), it is sometimes also referred to as the location of the pressure peak (LPP). The second descriptor is based on the mass fraction burned profile, which is calculated from the heat release. The position when a certain percentage (45–50%) of the mass of mixture has burned is used as a descriptor. The third descriptor is based on calculating the ratio between the pressure for firing cycle and a motored cycle,  $PR = \frac{p_{fir}(\theta)}{p_{mot}(\theta)}$ . The position when the normalized ratio  $PR_N = \frac{PR(\theta)}{\max_{\theta} PR(\theta)}$  reaches 0.5 is used as a descriptor. A fourth descriptor, the position for the maximum cylinder pressure rise, has also been presented [11] but it is not analyzed. The statements made about the *combustion descriptors* at optimum ignition timing are identical to, or very similar to, the following:

- For MBT timing the pressure peak is positioned at  $16^\circ$  after TDC [28, 26].
- For MBT timing the position when 50% of the mass of mixture has burned is at  $10^\circ$  after TDC [26, 6].
- For MBT timing the position when  $PR = 0.5$  is at  $9^\circ$  after TDC [33].
- For MBT timing the position for the maximum pressure rise is at  $3^\circ$  after TDC [11].

These statements have been verified in both experiments and simulations and good results has been reported using them for spark advance control [28, 22, 44, 6, 35].

When using these combustion descriptors for feedback control a central question is: How sensitive are they with respect to changes in engine and environmental conditions? For robustness it is important that the descriptor is insensitive to changes in non-measured parameters. This is investigated in Publication 7 which study how changes in engine and environmental conditions change the optimal position that these criteria rely upon. The combustion descriptors are studied, using the single-zone model and parameters obtained from engine data, with respect to variations in the model parameters. The results are reported in Publication 7, on which the SAE paper [16] is based. The main results are summarized below.

All three combustion descriptors do not change much when burn angles change. Considering only the mass fraction burned profile it is shown that the positions between levels of 45 and 50% mass fraction burned are good candidates even under large variations in burn angles. Furthermore, analysis of experimental data show that there is a correlation between the flame development and rapid burning angles and when such a correlation exists it is shown that the position for 45% mass fraction burned is more robust than the position for 50%.

Cycle-to-cycle variations are always present in SI engines and must be taken under consideration since they pose limits on the engine performance [37, 26]. However, it is shown that cycle-to-cycle variations can be neglected when considering spark-advance control for maximum efficiency. The combustion descriptors are well suited as “sensors” for feedback control of the spark advance but the pressure sensor that can withstand the high pressures and temperatures in the cylinder chamber has not yet proven cost effective.

## 2.4 Ion Sensing

The ionization current, measured using the spark plug as sensor, is also a direct measure in the combustion chamber. The sensing technique is to apply a DC bias to the spark plug when it is not used for ignition and measure the current that flows through the circuit. The current is rich on information about the combustion, but it is also complex with three characteristic phases that mix together in complicated ways, see Figure 2.4. The mechanisms that contribute to the ions in the combustion have been investigated but their relative importance as contributors to the current is not yet fully understood. The following description of the three phases gives a picture of the underlying processes: The first phase, *ignition phase*, is influenced by the ignition itself and the ignition circuitry; The second phase, *flame front phase*, is influenced by the ions that are generated in or nearby the flame front; The third phase, *post flame phase*, is influenced by the pressure through its influence on the temperature. The third phase that contains information about the pressure trace is of interest for ignition control.

The ionization current is already used in production cars to detect knock, misfire, and for cam-phase sensing [4]. Therefore, to incorporate an ionization current based spark-advance system, only additional signal interpretation in the electronic engine control unit (ECU) is required.

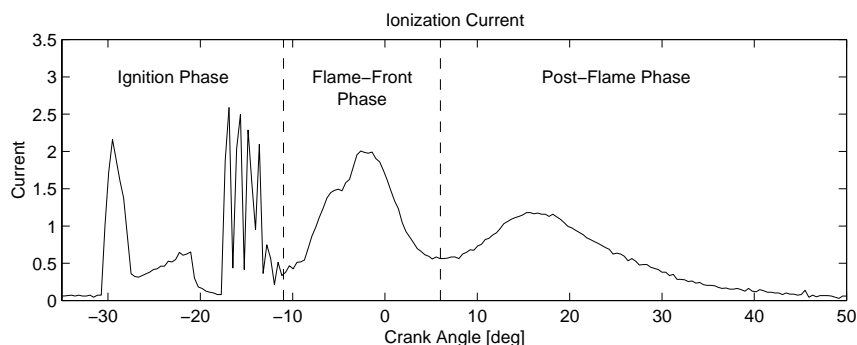


**Figure 2.4** Example of an ionization current with its three characteristic phases. The signal shape in the ignition phase is associated with the spark. In the flame front phase the signal is influenced by ions generated in and near the flame front. In the post flame phase the flame has propagated away from the spark plug and the signal is influenced by the cylinder temperature and pressure.

Ion sensing has been a hot topic in recent years concerning measurement techniques and its possible applications [3, 4, 5, 7, 10, 12, 20, 24, 25, 29, 30, 32, 48, 50]. More theoretical investigations, concerning physical and chemical modeling, have been performed and reported in [41, 42, 43, 40].

### 2.4.1 Ion Sensing for Ignition Control

The approach taken here is to estimate the peak pressure position from the ion current signal and use it for spark advance control. The paragraphs below outline what has been investigated and the results that are presented in this thesis. It is worth to mention that a method for estimating the mass fraction burned profile has been presented in Daniels [12].

The first publication shows that the peak pressure position can be estimated from the ion current trace using a simple model [17]. The model is to some extent physically justified. It is shown that a simple peak search is not feasible due to the complex appearance of the ion current signal.

The second publication shows that an algorithm has been developed and implemented for estimating the PPP in real time [14]. The prototype implementation of the algorithm is made on a PC. In Publication 3 controller performance is demonstrated, for an engine in a test bench. The experiments show that the ignition timing is successfully controlled and they quantify the step response time [19].

Publication 5 shows that the control scheme based on the ionization current can handle environmental disturbances and maintain an optimal spark advance schedule even under varying conditions [36]. It is also shown in Publication 4

that water injection in combination with a closed-loop spark-advance controller can increase the engine efficiency by a few percent [18]. The results also show that water injection alone does not improve the performance but the combination with the closed loop controller does.

## 2.5 Performance Limits

Since the focus is on efficiency, performance limiting factors such as knock and emissions are considered only implicitly. Knock and emissions restricts the spark advance in high load regions. The ignition controller usually has this information available and the optimal schedule is abandoned when knock occurs. The detection of knock has been investigated by many authors, see for example [45]. Systems that use a pressure transducer for closed-loop control of the spark advance in combination with detection and control of knock has been reported, see for example Hosey and Hubbard [27]. Production systems currently use accelerometers mounted on the engine block [1] or ionization current sensing [4] for knock control.

Emissions are also influenced by the ignition timing, it is foremost the influence that the pressure development has on the burned gas temperature that contributes to these formations. An earlier ignition timing results in higher maximum pressure and temperature. For  $\text{NO}_x$  formation these are the main contributors, see Heywood [26] Chapter 11 for a more thorough treatment of these issues.



---

---

## Bibliography

- [1] Ulrich Adler. *Automotive Electric/Electronic Systems*. Robert Bosch GmbH, 2 edition, 1995.
- [2] Charles A. Amann. Cylinder-pressure measurement and its use in engine research. *SAE Technical Paper 852067*, 1985.
- [3] Morito Asano, Tetsu Kuma, Mitsunobu Kajitani, and Manabu Tekeuchi. Development of new ion current combustion control system. *SAE paper 980162*, 1998.
- [4] J. Auzins, H. Johansson, and J. Nytomt. Ion-gap sense in missfire detection, knock and engine control. *SAE SP-1082*, (SAE paper No. 950004):21–28, 1995.
- [5] Eric N. Balles, Edward A. VanDyne, Alexandre M. Wahl, Kenneth Ratton, and Ming-Chi Lai. In-cylinder air/fuel ratio approximation using spark gap ionization sensing. *SAE paper 980166*, 1998.
- [6] Michael Bargende. Schwerpunkt-kriterium und automatische klingelerkennung. *Motor Technische Zeitschrift*, Vol. 56(10):632–638, 1995.
- [7] K. N. C. Bray and N. Collings. Ionization sensors for internal combustion engine diagnostics. *Endeavour, New Series*, 15(1), 1991.
- [8] Michael F. J. Brunt and Andrew L. Emtage. Evaluation of burn rate routines and analysis errors. *SAE Technical Paper 970037*, 1997.
- [9] Michael F. J. Brunt and Christopher R. Pond. Evaluation of techniques for absolute cylinder pressure correction. *SAE Technical Paper 970036*, 1997.

- 
- [10] Nick Collings, Steve Dinsdale, and Tim Hands. Plug fouling investigations on a running engine - an application of a novel multi-purpose diagnostic system based on the spark plug. *SAE paper No. 912318*, 1991.
- [11] H.A. Cook, O.H. Heinicke, and W.H. Haynie. Spark timing control based on correlation of maximum economy spark timing, flame front travel, and cylinder pressure rise. *NACA Report No.886*, November 22 1946.
- [12] Chao F. Daniels. The comparison of mass fraction burned obtained from the cylinder pressure signal and spark plug ion signal. *SAE Technical Paper 980140*, 1998.
- [13] C.S. Draper and Y.T. Li. Principles of optimizing control systems and an application to the internal combustion engine. *ASME Publication*, September 1951.
- [14] Lars Eriksson. A real-time platform for spark advance control. Technical Report LiTH-R-1938, ISSN 1400-3902, Department of Electrical Engineering, 1997.
- [15] Lars Eriksson. Requirements for and a systematic method for identifying heat-release model parameters. *Modeling of SI and Diesel Engines*, SP-1330(SAE Technical Paper no.980626):19–30, 1998.
- [16] Lars Eriksson. Spark advance for optimal efficiency. *SAE Technical Paper no.99-01-0548*, 1999.
- [17] Lars Eriksson and Lars Nielsen. Ionization current interpretation for ignition control in internal combustion engines. *IFAC Control Engineering Practice*, Issue 8, Volume 5:1107–1113, August 1997.
- [18] Lars Eriksson and Lars Nielsen. Increasing the efficiency of SI-engines by spark-advance control. In *IFAC Workshop - Advances in Automotive Control (Preprints)*, pages 211–216, 1998.
- [19] Lars Eriksson, Lars Nielsen, and Mikael Glavenius. Closed loop ignition control by ionization current interpretation. *SAE SP-1236*, (SAE paper No. 970854):159–166, 1997.
- [20] Jürgen Förster, Achim Gunther, Markus Ketterer, and Klaus-Jurgen Wald. Ion current sensing for spark ignition engines. *SAE 1999-01-0204*, 1999.
- [21] J. A. Gatowski, E. N. Balles, K. M. Chun, F. E. Nelson, J. A. Ekchian, and J. B. Heywood. Heat release analysis of engine pressure data. *SAE Technical Paper 841359*, 1984.
- [22] I. Glaser and J. D. Powell. Optimal closed-loop spark control of an automotive engine. *SAE paper No. 810058*, pages 11–21, 1981.

- [23] Yann G. Guezennec and Wajdi Hamama. Two-zone heat release analysis of combustion data and calibration of heat transfer correlation in an I.C. engine. *SAE Technical paper 1999-01-0218*, 1999.
- [24] M. Hellring, T. Munther, T. Rögnavaldsson, N. Wickström, C. Carlsson, M. Larsson, and J. Nytomt. Robust AFR estimation using the ion current and neural networks. *SAE 1999-01-991161*, 1999.
- [25] M. Hellring, T. Munther, T. Rögnavaldsson, N. Wickström, C. Carlsson, M. Larsson, and J. Nytomt. Spark advance control using the ion current and neural soft sensors. *SAE 1999-01-991162*, 1999.
- [26] J. B. Heywood. *Internal Combustion Engine Fundamentals*. McGraw-Hill series in mechanical engineering. McGraw-Hill, 1988.
- [27] R.J. Hosey and J.D. Powell. Closed loop, knock adaptive spark timing control based on cylinder pressure. *Journal of Dynamic Systems, Measurement, and Control*, 101(78-WA/DSC-15):64–70, March 1979.
- [28] M. Hubbard, P. D. Dobson, and J. D. Powell. Closed loop control of spark advance using a cylinder pressure sensor. *Journal of Dynamic Systems, Measurement and Control*, pages 414–420, December 1976.
- [29] Hans Johansson. Studie av parametrar för adaptiv tändningsstyrning. Master's thesis, Institutionen för förbränningsmotorteknik, Chalmers Tekniska Högskola, 1986. Swedish Only.
- [30] M. Krämer and K. Wolf. Approaces to gasoline engine control involving the use of ion current sensory analysis. *SAE paper No. 905007*, 1990.
- [31] R.B. Krieger and G.L. Borman. The computation of apparent heat release for internal combustion engines. *ASME*, 1967.
- [32] Anson Lee and Jan S. Pyko. Engine misfire detection by ionization current monitoring. *SAE SP-1082*, (SAE paper No. 950003):9–19, 1995.
- [33] Frederic A. Matekunas. Engine combustion control with ignition timing by pressure ratio management. US Pat., A, 4622939, Nov. 18 1986.
- [34] Mitsue Morishita and Tadashi Kushiyama. An improved method of determining the TDC position in a pv-diagram. *SAE Technical Paper 980625*, 1998.
- [35] Reiner Müller and Hans-Hubert Hemberger. Neural adaptive ignition control. *SAE paper 981057*, 1998.
- [36] Lars Nielsen and Lars Eriksson. An ion-sense engine-fine-tuner. *IEEE Control Systems (special issue on powertrain control)*, Vol. 18(5):43–52, October 1998.
- [37] D. J. Patterson. Cylinder pressure variations, a fundamental combustion problem. *SAE paper No. 660129*, 1966.

- [38] Andrew L. Randolph. Methods of processing cylinder-pressure transducer signals to maximize data accuracy. *SAE Technical Paper 900170*, 1990.
- [39] Gerald M. Rassweiler and Lloyd Withrow. Motion pictures of engine flames correlated with pressure cards. *SAE Technical Paper 800131*, 1980 (Originally presented 1938).
- [40] Reimond Reinman, André Saitzkoff, Bengt Lassesson, and Petter Strandh. Fuel and additive influend on the ion current. *SAE Technical Paper 980161*, 1998.
- [41] Raymond Reinmann, André Saitzkoff, and Fabian Mauss. Local air-fuel ratio measurements using the spark plug as an ionization sensor. *SAE paper No. 970856*, (SAE SP-1263):175–185, 1997.
- [42] A. Saitzkoff, R. Reinmann, T. Berglind, and M. Glavmo. An ionization equilibrium analysis of the spark plug as an ionization sensor. *SAE paper No. 960337*, 1996.
- [43] André Saitzkoff, Raymond Reinmann, and Fabian Mauss. In cylinder pressure measurements using the spark plug as an ionization sensor. *SAE paper No. 970857*, pages 187–197, 1997.
- [44] K. Sawamoto, Y. Kawamura, T. Kita, and K. Matsushita. Individual cylinder knock control by detecting cylinder pressure. *SAE paper No. 871911*, 1987.
- [45] K.P Schmillen and M. Rechs. Different methods of knock detection and knock control. *SAE 910858*, 1991.
- [46] P.H. Schweitzer, Carl Wolz, and Frank DeLuca. Control system to optimize engine power. *SAE Technical Paper 660022*, 1966.
- [47] P.J. Shayler, M.W. Wiseman, and T. Ma. Improving the determination of mass fraction burnt. *SAE Technical Paper 900351*, 1990.
- [48] Yuichi Shimasaki, Masaki Kanehiro, Shigeki Baba, Shigeru Maruyama, Takashi Hisaki, and Shigeru Miyata. Spark plug voltage analysis for monitoring combustion in an internal combustion engine. *SAE paper No. 930461*, 1993.
- [49] Marek J. Staś. Thermodynamic determination of T.D.C. in piston combustion engines. *SAE Technical Paper 960610*, 1996.
- [50] Devesh Upadhyay and Giorgio Rizzoni. AFR control on a single cylinder engine using the ionization current. *SAE paper 980203*, 1998.

**Part II**

**Publications**



# Ionization Current Interpretation for Ignition Control in Internal Combustion Engines<sup>1</sup>

Lars Eriksson<sup>†</sup> and Lars Nielsen<sup>‡</sup>

*Vehicular Systems, Department of Electrical Engineering,  
Linköping University, S-581 83 Linköping,  
Sweden. Fax: +46-13-282035*

*<sup>†</sup>e-mail: larser@isy.liu.se*

*<sup>‡</sup>e-mail: lars@isy.liu.se*

## Abstract

Spark advance setting in spark-ignited engines is used to place the in-cylinder pressure curve relative to the top dead center. A feedback scheme, not a calibration scheme, based on ionization current is proposed here. It is thus related to pressure sensor feedback schemes, that have reported good results, but have not yet been proved cost effective, due to the cost of the pressure sensor. The method proposed here is very cost-effective, since it uses exactly the same hardware and instrumentation (already used in production cars) that is used to utilize the spark plug as a sensor to detect misfire and as a sensor for knock control. A key idea in the method is to use parameterized functions to describe the ionization current. These parameterized functions are used to separate out the different phases of the ionization current. Special emphasis is laid on getting a correct description of the pressure development. The results are validated on a SAAB 2.3 l production engine by direct comparison with an in-cylinder pressure sensor (used only for validation, not for control), but also by using a physical model relating the ionization current to the pressure.

---

<sup>1</sup>This is an edited version of the article that was published in *Control Engineering Practice*, Vol. 5, No. 8, pp. 1107-1113, 1997.

## 1 Introduction

The spark plug can be used as a sensor during the part of the engine cycle where it is not used for ignition. This is done by setting a small voltage over the spark plug and measuring the current. This current is due to the ions in the gap of the spark plug, and the measurement is called the “ionization current”. The ions are formed during and after the combustion, and the type and amount of ions depend on combustion characteristics. The ionization current also depends on the pressure, the temperature, and so on. The signal is thus very rich in information, but it is also complex. It is a fast direct in-cylinder measurement, as opposed to sensors in the exhaust, and it is used on each cylinder individually. The potential for feedback control is thus obvious.

This paper deals with ignition control, or more specifically with spark advance control, i.e. how long before top dead center (TDC) to ignite. The idea is to control the spark advance so that the pressure peak is placed relative to TDC in an optimal way. Work is lost to compression and heat transfer if it is placed too early, and expansion work is lost if it is placed too late. A key problem is thus to find a description of the ionization current that is rich enough to capture the different variations, but still such that the relevant information can be extracted.

## 2 Spark-Ignited Engines

In spark-ignited (SI) internal combustion engines the cylinder is filled with fresh charge, which then is compressed. Before the piston has reached the uppermost position, top dead center (TDC), the mixture is ignited by the spark plug. A flame kernel develops in the mixture and turns to a turbulent flame. During combustion, the cylinder pressure rises due to the released energy and the new molecules produced by the chemical reactions. The flame reaches the wall, and the combustion completes. During the compression, work is transferred to the gases within the cylinder, and during the expansion, work is transferred from the gases. A thorough description of the combustion process is given in [6].

### 2.1 Cylinder pressure

The cylinder pressure is an important parameter in the combustion, since it gives the work produced by the combustion. In Figure 1 (a) three different pressure traces are displayed. The lowest dash-dotted trace, the motored cycle, is obtained by running the engine with an electric motor without firing the engine. The two other traces are from cycles when firing occurs. Two different ignition timings produce the signals shown; the dashed trace has an early timing and the solid line has an ignition timing that is optimal. The optimal ignition timing is called the “maximum brake torque timing” (MBT). A pressure trace with late ignition timing is shown by the dashed line in Figure 1 (b).

The influence of ignition timing on the work produced can be seen in Figure 1. With early ignition the pressure increases too early, before TDC, and work is lost

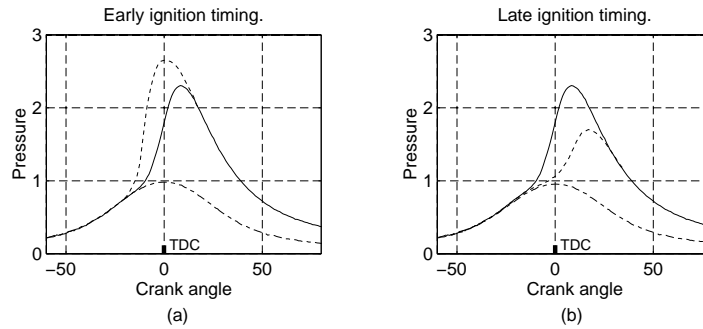


**Figure 1** The cylinder pressure showing the motored cycle and three different positions for the ignition. (a) Motored cycle, MBT and early timing. (b) Motored cycle, MBT and late timing.

during the compression of the gases. With too-late ignition work is lost due to the later pressure rise, after TDC.

## 2.2 Ignition control

In SI engines the ignition timing is an important parameter, among others, for the combustion efficiency. The ignition timing alone affects almost every engine output. In nearly all of today's production engines there is no feedback from the combustion to the ignition timing; the spark advance is based on a pre-calibrated system.

Several parameters affect the best spark advance setting, such as engine speed, load, air/fuel ratio, fuel characteristics, EGR, coolant temperature, air temperature, and humidity, among others. Present ignition-control systems measure several of these parameters, and adjust the spark advance. The spark advance setting is obtained by extensive testing and calibration during the design phase of the engine. Provided that all the parameters affecting the ignition timing were measured, and that all interactions were properly accounted for, it would be possible to determine the best spark advance. However, it is not possible to measure and account for all the parameters, since it would be extremely expensive to perform the measurement and testing required to incorporate such a system in a production engine.

The testing and calibration results in a nominal spark advance schedule. The schedule is conservative, since it has to guarantee that knock (or detonation) does not occur, as well as good performance over the entire range of the non-measured parameters. These systems are only calibrated during the design of the engine, and there is no feedback in the ignition control.

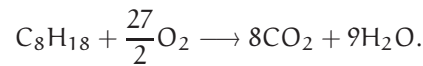
### 2.3 Peak pressure algorithm

A fundamentally different approach is to utilize the cylinder pressure as the sensed variable for the ignition control. As indicated earlier, the best ignition timing will position the pressure time history in some optimal way. Research in this area has shown that the position for the peak pressure is almost constant at optimal spark timing [7]. A spark control algorithm that maintains a constant pressure peak position (called the peak pressure algorithm), results in an ignition timing that is within  $2^\circ$  of optimum. The algorithm also results in optimal ignition timing for large changes in parameters that affect the flame speed, such as the fuel/air ratio and air humidity [7, 5]. Humidity is interesting, since it represents the largest environmental disturbance to optimal ignition timing.

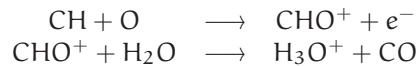
The optimum value for the peak pressure position, between  $12^\circ$  and  $20^\circ$  after TDC, varies with engine designs, mainly due to different heat flows to the cylinder walls [8]. The influence of cycle-by-cycle variations, in peak pressure position ( $\theta_{pp}$ ) with constant ignition timing, shall not inflect the ignition timing (IT) by more than  $1^\circ$ . Hence, cyclic variation of the order of  $10^\circ$  results in feedback to the ignition timing with a constant  $\Delta IT = \frac{1}{10} \Delta \theta_{pp}$ , where  $\Delta \theta_{pp} = (\text{desired } \theta_{pp}) - (\text{measured } \theta_{pp})$  and  $\Delta IT = (\text{Change in ignition timing})$  [8]. The peak pressure algorithm suffers from the fact that a pressure sensor that could stand the high temperatures and pressures would be very expensive. One manufacturer has implemented the concept and reported a 10% improvement in power and 5% improvement in efficiency [10].

## 3 The Ionization Current

In an ideal combustion, hydrocarbon molecules react with oxygen and generate carbon monoxide and water. An ideal reaction, with the hydrocarbon isooctane, gives



In the combustion there are also other reactions, which go through several steps before they are completed. Several reactions that include ions are present in the combustion; some examples are [11]



These ions, and several others, are generated by the chemical reactions in the flame. Additional ions are created when the temperature increases as the pressure rises. Thus, more ions are generated at higher internal energy of the gases.

To detect the ions, a DC bias is applied to the spark plug, generating an electrical field. The electrical field makes the ions move and generates an ion current,

a schematic illustration is shown in Figure 2 (a). The current is measured at the low-voltage side of the ignition coil, and does not require protection from the high-voltage pulses in the ignition, Figure 2 (b). Ionization current measurement systems are already in use in production engines for: individual cylinder knock control, cam phase sensing, pre-ignition detection, and misfire/combustion quality/lean limit [1]. Also, detection of spark plug fouling by using the ionization current is reported [2].

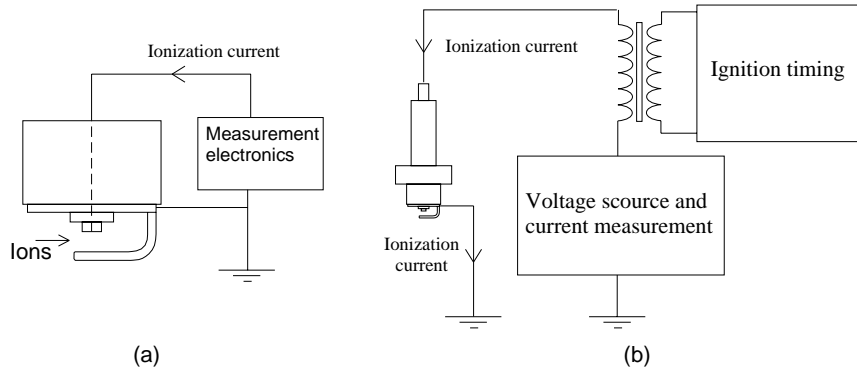


**Figure 2** Measurement of the ionization current. (a) The spark plug-gap is used as a probe. (b) Measurement on the low voltage side.

The ionization current is an interesting engine parameter to study, since it contains a lot of information about the combustion. Some of the parameters that affect the ionization current are: temperature, air/fuel ratio, time since combustion, exhaust gas recycling (EGR), fuel composition, engine load, and several others.

### 3.1 The ionization current signal

The ionization current, Fig. 3, has three characteristic phases; ignition, flame front, and post flame. In the ignition phase, the ionization current is large, with reversed polarity. Due to the high current in the ignition the measured signal shown in the figure is limited. What can be seen in Fig. 3 is the ringing phenomenon in the coil after the ignition. The high level of ions associated with the chemical reactions in the flame produces one or more characteristic peaks in the flame-front phase. The ions generated by the flame have different recombination rates. Some ions recombine very quickly to more-stable molecules, while others have longer residual times. The result is a high peak, that decays and flattens out when only the more stable ions remain.

In the post-flame phase the most stable ions remain, generating a signal that follows the cylinder pressure due to its effect on the molecule concentration. Ions are also created by the measurement voltage and the high temperature of the burned gases, since the temperature follows the pressure during the compression

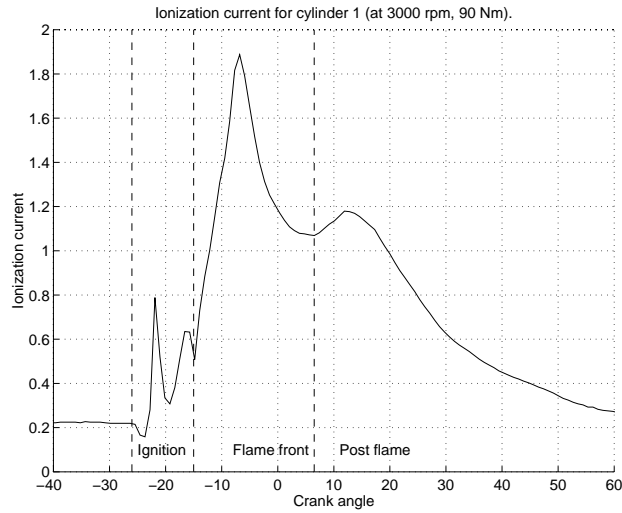


**Figure 3** An ionization signal showing the three phases: ignition, flame front, post flame.

of the burned gases, i.e when the flame propagates outwards and the combustion completes. The ionization current will hence depend on the pressure. The relatively low ionization energy of NO makes it a contributor to the ionization current in the post-flame phase [9].

## 4 Experimental Situation

The engine used for measurement and validation is a spark-ignited, SAAB 2.3 l, 16 valve, four-stroke, four-cylinder, fuel-injected, normally aspirated, production engine equipped with the Trionic engine control system. The ionization current measurement system is the production system developed by Mecel AB [4], which is used in the SAAB engine. A pressure transducer and amplifier from AVL, for in-cylinder pressure measurement, is used for validation of the algorithms. A cog wheel is attached to the crank, and an inductive sensor is used for computing the engine position. The experimental setup is shown in Figure 4.

The data was collected at several operating points in the mid-load and mid-speed range for the engine. The engine speed was in the range 2000 rpm to 4500 rpm, and the brake torque was in the range 50 Nm to 150 Nm. Approximately 100 cycles for each operating point were collected and evaluated.

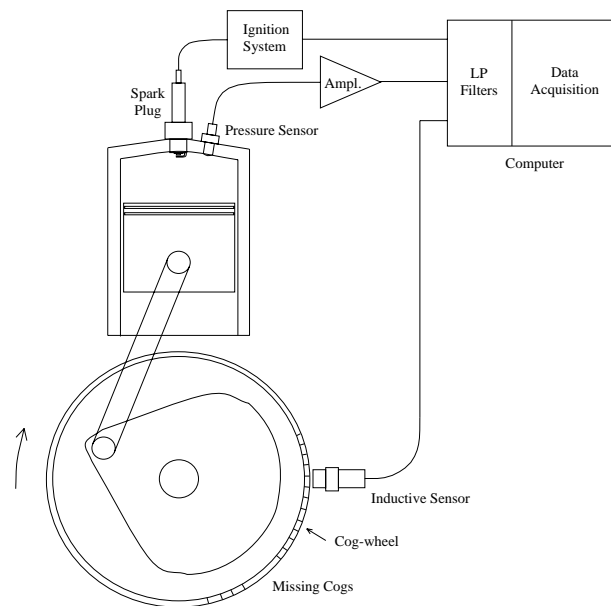


**Figure 4** The measurement situation. The pressure sensor is used only for validation.

## 5 Ionization Current Interpretation

The ionization current is affected by several parameters other than the cylinder pressure. Aiming at ignition control, using the ionization current and the peak pressure algorithm, special care must be taken when extracting the pressure information from the ionization current.

### 5.1 Connection between ionization and pressure

As mentioned earlier, and displayed in Figure 5, the pressure has most influence on the post-flame phase of the ionization current. Problems occur when searching for the peak pressure position: a peak search is not feasible since the flame-front phase often consists of more than one peak, and the post-flame phase often appears without a peak. In Figure 6 an ionization current signal with two peaks in the flame front and no peak in the post flame is displayed. It can be seen that the ionization signal contains information about the pressure in the post-flame phase, despite the fact that the post-flame phase does not contain a peak.

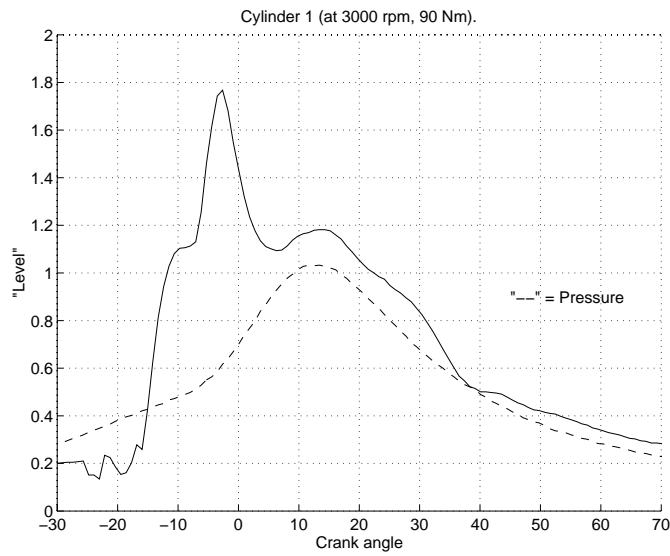


**Figure 5** Ionization current and cylinder pressure for one cycle. The post-flame phase corresponds to the pressure.

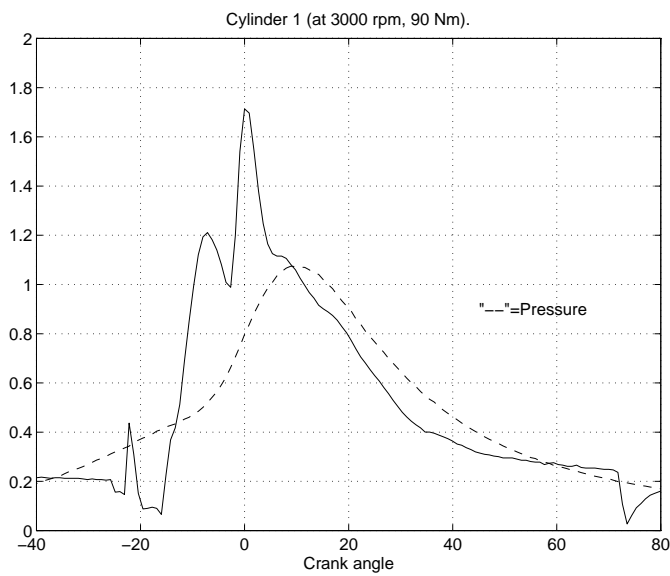


**Figure 6** A case where the ionization current has two peaks in the flame-front phase and no peak in the post-flame phase, but there is still a correspondence with the pressure.

## 5.2 A model of the ionization signal

An analytical expression for the ionization current has been presented [9], assuming that the gas in the spark plug is fully combusted, in thermodynamic equilibrium, and it undergoes adiabatic expansion, also assuming that the current is carried in a cylinder extending from the central electrode of the spark plug. Given the cylinder pressure, the analytical expression for the ionization current is

$$\frac{I}{I_m} = \frac{1}{\left(\frac{p}{p_m}\right)^{\frac{1}{2} - \frac{3}{4} \frac{\gamma-1}{\gamma}}} e^{-\frac{E_i}{2kT_m} \left[ \left(\frac{p}{p_m}\right)^{-\frac{\gamma-1}{\gamma}} - 1 \right]}. \quad (1)$$

The variables and constants are:  $I$ , Ionization current;  $I_m$ , Ionization current maximum;  $p$ , Cylinder pressure;  $p_m$ , Cylinder pressure maximum;  $T_m$ , Maximum temperature;  $\gamma$ , Specific heat ratio;  $k$ , Boltzmann's constant;  $E_i$ , Ionization energy.

Using the function and the measured cylinder pressure, the component of the ionization current related to the cylinder pressure has a shape close to a Gaussian function. In Figure 7 a Gaussian function is compared to the signal received by the pressure. Therefore, an idealized model of the ionization current, contains a Gaussian-shaped function for the component connected to the pressure. To the model, a description  $f(\theta)$  of the flame front must also be added,

$$I(\theta) = f(\theta) + \beta_1 e^{-\frac{1}{\beta_2}(\theta - \beta_3)^2} \quad (2)$$

( $\theta$  denotes the crank angle). A simple flame-front model is a Gaussian signal, which can capture a high peak in the flame front which decays. Thus the model is

$$I(\theta) = \alpha_1 e^{-\frac{1}{\alpha_2}(\theta - \alpha_3)^2} + \beta_1 e^{-\frac{1}{\beta_2}(\theta - \beta_3)^2}. \quad (3)$$

## 6 Results from Ionization Current Interpretation

The model, Equation 3, is fitted in the least-squares sense to the measured ionization current. The resulting fit, for six consecutive cycles, is displayed, together with the corresponding measured ionization current in, Figure 8. The components of the idealized ionization current are shown in Figure 9, together with the measured ionization current. The second Gaussian function is the ionization current-based (ICB) pressure-function. The figure shows that the first Gaussian function is positioned in the flame front, and the second Gaussian function in the post-flame phase. Accordingly the model captures the structure of the ionization current well.

The pressure and the ICB pressure-function are displayed in Figure 10. The correspondence is good. However, cycles three and four have a more complicated flame-front phase, with two peaks, which a simple Gaussian cannot describe. This also propagates to a lower correspondence between the pressure and the ICB

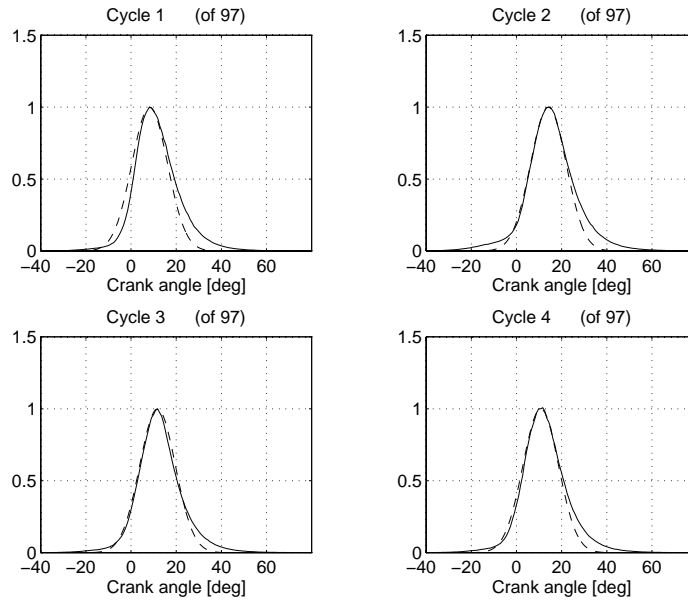


**Figure 7** The pressure related part of the ionization signal compared with a Gaussian function. Solid; Measured cylinder pressure converted to ionization current through Eq. 1. Dashed; A Gaussian signal positioned at the cylinder pressure.

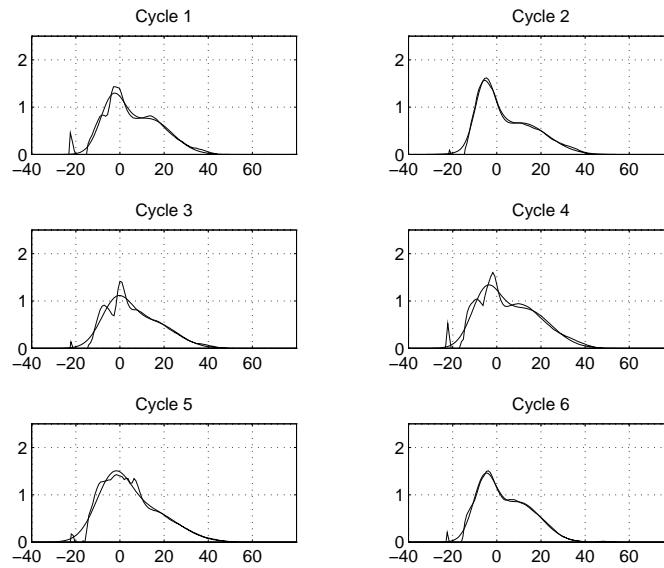


**Figure 8** The measured ionization current and the fitted model.

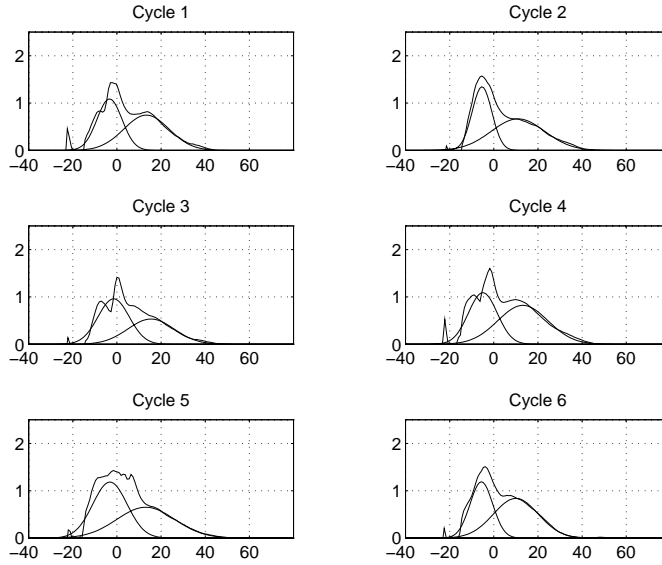


**Figure 9** The measured ionization current, and the two obtained Gaussian functions. The ICB pressure-function is positioned in the post-flame phase.

pressure-function. The solution is to use a description that is rich enough to capture the two peaks in the flame front. To validate this approach, the flame front  $f(\theta)$ , in Equation 2, is described by two Gaussian functions. Figure 11 shows the ionization current, the fitted model, and the components of the fit. The ICB pressure-function is still positioned in the post-flame phase of the ionization current.

The correspondence between the pressure and the ICB pressure, Figure 12, is much better with the enhanced model of the flame front than with the former, Cycle 3 in Figure 10.

Studies with varying ignition timing, and hence varying peak pressure position [3], show that the ICB pressure-function changes accordingly. This indicates that the ionization current can be used for ignition timing control.

## 7 Conclusions

It has been demonstrated that it is feasible to use ionization current interpretation for spark advance control to optimize engine performance. The proposed method is very cost-effective, since it uses exactly the same hardware and instrumentation (already used in production cars) that is used to employ the spark plug as a sensor for misfire detection and knock control. The only addition needed for the proposed feedback scheme is further signal interpretation in the electronic engine control unit.

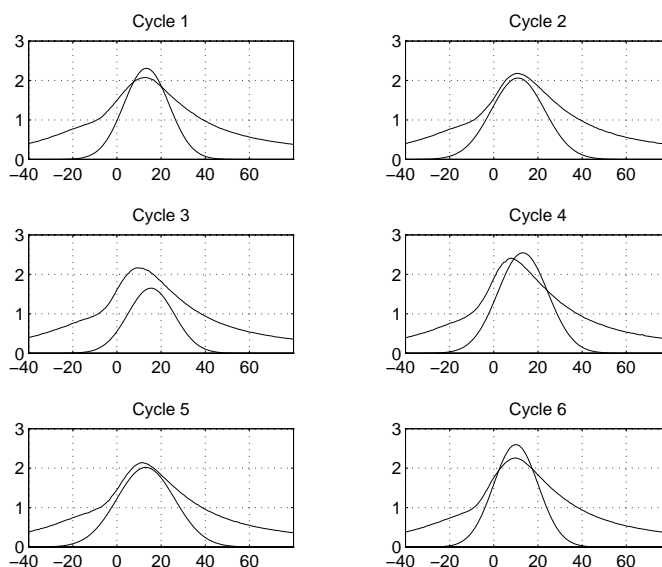


**Figure 10** The peak positions of the cylinder pressure and the ICB pressure-function obtained.

A key step in the method is to use parameterized functions to describe the ionization current. The different phases of the ionization current were separated out, and it was shown that this gives a good description of the pressure development. The results were validated by measurements on a SAAB 2.3 l, four-stroke, four-cylinder, 16-valve production engine.

It is also clear that, once the phase of the ionization current that is related to pressure development has been extracted, there is still a lot of information available in the signal. Ongoing and future work will, of course, try to utilize this information not only for ignition timing control, but also for other measures of combustion characteristics e.g. for use in EGR and air/fuel control.

## References

- [1] J. Auzins, H. Johansson, and J. Nytomt. Ion-gap sense in missfire detection, knock and engine control. *SAE SP-1082*, (SAE paper No. 950004):21–28, 1995.
- [2] Nick Collings, Steve Dinsdale, and Tim Hands. Plug fouling investigations on a running engine - an application of a novel multi-purpose diagnostic system based on the spark plug. *SAE paper No. 912318*, 1991.
- [3] Lars Eriksson, Lars Nielsen, and Jan Nytomt. Ignition control by ionization current interpretation. *SAE SP-1149*, (SAE paper No. 960045):73–79, 1996.

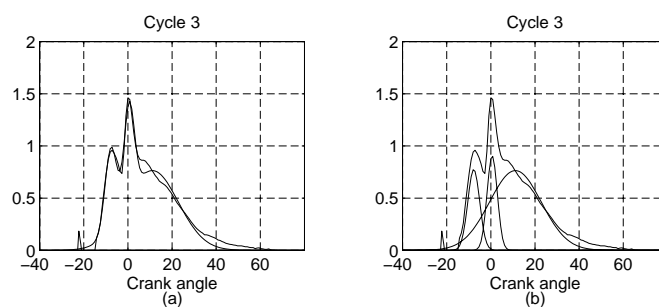


**Figure 11** A model with a extended flame front description. (a) The measured signal compared to the model. (b) The three Gaussian components.

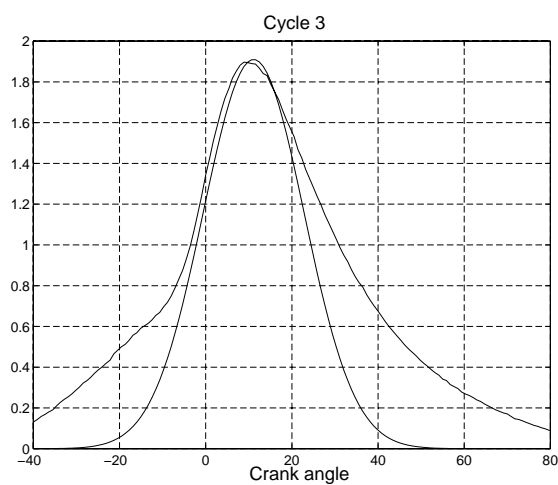


**Figure 12** The peak positions for the pressure related Gaussian signal (ICB) and the measured cylinder pressure corresponds well.

- [4] P. Gillbrand, H. Johansson, and J. Nytomt. Method and arrangement for detecting ionising current in an internal combustion engine ignition system. EP, C, 188180, December 19 1984.
- [5] I. Glaser and J. D. Powell. Optimal closed-loop spark control of an automotive engine. *SAE paper No. 810058*, pages 11–21, 1981.
- [6] J. B. Heywood. *Internal Combustion Engine Fundamentals*. McGraw-Hill series in mechanical engineering. McGraw-Hill, 1988.
- [7] M. Hubbard, P. D. Dobson, and J. D. Powell. Closed loop control of spark advance using a cylinder pressure sensor. *Journal of Dynamic Systems, Mea-*

*surement and Control*, pages 414–420, December 1976.

- [8] J. D. Powell. Engine control using cylinder pressure: Past, present, and future. *Journal of Dynamic System, Measurement, and Control*, 115:343–350, June 1993.
- [9] A. Saitzkoff, R. Reinmann, T. Berglind, and M. Glavmo. An ionization equilibrium analysis of the spark plug as an ionization sensor. *SAE paper No. 960337*, 1996.
- [10] K. Sawamoto, Y. Kawamura, T. Kita, and K. Matsushita. Individual cylinder knock control by detecting cylinder pressure. *SAE paper No. 871911*, 1987.
- [11] Yuichi Shimasaki, Masaki Kanehiro, Shigeki Baba, Shigeru Maruyama, Takashi Hisaki, and Shigeru Miyata. Spark plug voltage analysis for monitoring combustion in an internal combustion engine. *SAE paper No. 930461*, 1993.

# A Real-Time Platform for Closed-Loop Spark-Advance Control<sup>1</sup>

Lars Eriksson

*Vehicular Systems*  
*Department of Electrical Engineering*  
*Linköping University, S-581 83 Linköping, Sweden*  
*<http://www.vehicular.isy.liu.se>*  
*[larer@isy.liu.se](mailto:larer@isy.liu.se)*

## Abstract

With the aim at spark advance control, a method for estimating the peak pressure position (PPP) from the ionization current has previously been developed and validated off-line. To implement the concept on an engine a real-time platform is needed. A hardware platform, that consists of a PC, an electronic engine control unit (ECU), and a synchronization circuit, is described. The platform synchronizes the data acquisition with the engine and the functionality is validated. Also a refined interpretation algorithm for estimating the PPP is described and validated to give a good estimate. The algorithm is suitable for implementation on the described real-time platform.

---

<sup>1</sup>This report is also available from the Department of Electrical Engineering, Linköping University, 581 83 Linköping, SWEDEN. Reference number: LiTH-R-1938, ISSN 1400-3902.

## 1 Introduction

In [2] a method for extracting information from the ionization current about the peak pressure position (PPP) was presented. The validation of this estimation method was made off-line in that article. However, the PPP-estimate is to be used for closed-loop spark-advance control, and this report describes a hardware and software platform that has been developed for evaluating the method in real-time on an engine.

### 1.1 Report Overview

In Section 2 the functionality of the hardware platform and its subsystems, are described. A first step is to verify that the measurement system, computer system, and communication system work in collaboration with the electronic engine control unit. This is verified in Section 3, using feedback from the pressure sensor.

A second step is to develop an efficient algorithm, for estimating the peak pressure position from the ionization, that can be used in real time on the platform described above. This is treated in Sections 4 and 5. The results from the estimation algorithm is verified in Section 6, comparing measured data from the ionization current and cylinder pressure.

## 2 Experimental Platform

The complete experimental platform for ionization current based spark advance control is displayed in Figure 1. It consists of six subsystems. The subsystems are: the engine, the electronic engine control unit (ECU), the sample timing system, the data acquisition (DAQ) card, a personal computer (PC), and the CAN bus.

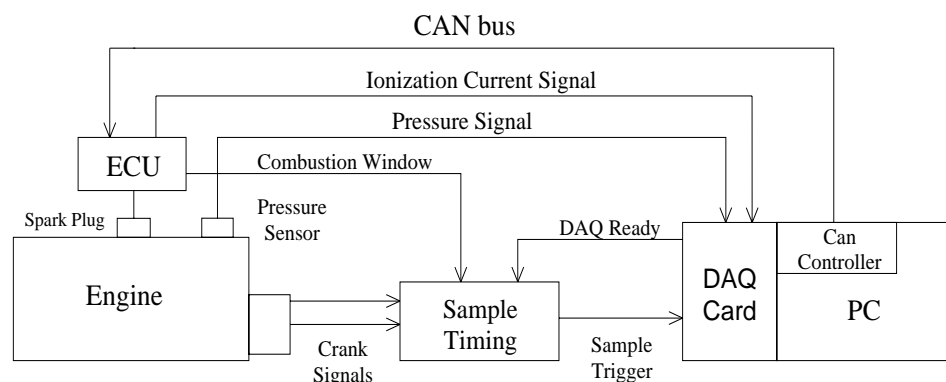


**Figure 1** Block diagram over the system.

## 2.1 Functionality Overview

A central part of this system is the Sample Timing block, since it synchronizes the PC with the engine, which is important for retrieving the correct engine position for the pressure and ionization current traces. It generates one pulse for every degree of the crank revolution during the interesting part of the cycle. The Sample timing block is further described in Section 2.4.

When the sample trigger signal goes high, the DAQ card samples the pressure signal and the ionization current. After 128 samples a buffer on the card is filled, and the data is transferred to the PC for signal interpretation.

The PC controls the DAQ and the CAN controller. The main tasks for the PC is to read the ionization current and pressure traces, and compute the estimated and true peak pressure positions. The estimated position is computed using the ionization current and the true position is computed from the pressure signal. The true peak position has been used for validation purposes only. The basic operating principle is that the PC reads ionization current data from the card and computes the estimated peak pressure position, the estimated position is then used to calculate an updated spark advance. The updated spark advance is sent via the CAN bus to the ECU. The PC block is further described in Section 2.3.

## 2.2 Electronic Control Unit (ECU)

The main task for the ECU, in the context here, is to operate as an actuator for the spark advance and as a sensor for the ionization current. It also has measurement electronics for using the spark plug as sensor and measuring the ionization current. The ionization current signal is available for measurement to other units such as the PC.

The actuator task for the ECU is to keep track of the correct engine position and produces a spark at the commanded engine position. The commanded position is computed from the correction to the spark timing that is sent from the PC via the CAN-bus. There is a switch in the ECU program so that the control functions, using the messages sent from the PC, can be easily turned on and off.

Another task for the ECU is to produce the combustion window pulse, i.e. tell when there is going to be a combustion in cylinder one. This information is used by the sample timing system to synchronize the sampling with the combustion.

### Ignition Phase Filtering

The ignition system in the ECU is of the inductive discharge type with one coil per spark plug. The ignition and measurement system gives an ionization current of the type displayed in Figure 2, showing the three characteristic phases of the ionization current (the ionization current is further described in [2]). The ignition phase is influenced by the ignition where the first sharp peak comes from the coil-on event, and the other peaks comes from a ringing in the ignition coil after spark has ended. The ignition system used in [2] was of the capacitive discharge type, which gives a different appearance of the ignition phase in the ionization current.

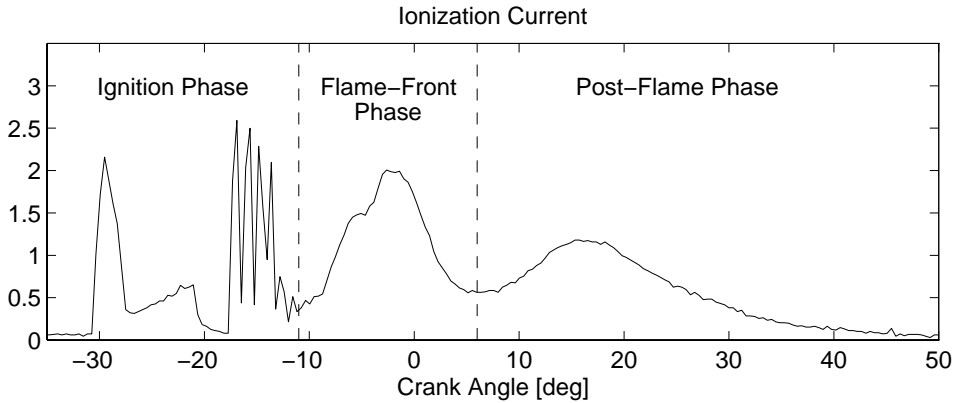


**Figure 2** The ionization current showing the three characteristic phases: ignition phase, flame-front phase, and post-flame phase.

The ringing of the coil has to be windowed away so that it will not affect the interpretation algorithm. Since the ringing has a well defined duration time, it can be filtered away using a time window. Knowing the crank angle for the spark timing  $\theta_{st}$ , and the engine speed  $n$ , the crank angle where the ringing ends  $\theta_{end}$ , can be calculated,

$$\theta_{end} = \theta_{st} + \frac{8^\circ}{1500 \text{ rpm}} \cdot n \quad (1)$$

With the setup in our ECU the ringing has been measured to end  $8^\circ$  after the spark initiation at 1500 rpm, which gives the quotient  $\frac{8^\circ}{1500 \text{ rpm}}$  in (1).

Thus, in order to window away the ignition phase of the ionization current, information about the engine speed and actual spark timing has to be transferred from the ECU to the PC. This is done using the CAN-bus.

### 2.3 PC and Board Configuration

The PC controls the data acquisition (DAQ) card and a CAN controller. The main purposes for the computer are to measure and interpret the ionization current signal, and send update information for the spark advance to the ECU. Pseudocode for the main program is given below to visualize the steps performed.

```

main()
{
    Configure_DAQ_Card();
    Configure_CAN_Controller(); /*Configure and setup CAN messages*/
    while (not key pressed) /*Repeat the loop until a key is pressed */
    {
        Clear_DAQ(); /*Clear DAQ from old values */
        Start_Acquisition(); /*Start the sampling process on the card */
        Set_DAQ_Ready(); /*Set the signal, DAQ ready, high (for
                           sample timing) */
        while (DAQ_Buffer_Not_Full)
        {
            Check_Can(); /*Just wait, and check CAN for messages */
        }
        Clear_DAQ_Ready(); /*Clear the signal DAQ ready */
        Read_Samples(); /*Read the last cycle data from the
                        DAQ card */
        Compute_PPP_Estimate(); /*Use the ionization current to estimate
                                the PPP */
        Compute_PPP(); /*Calculate the true PPP */
        Update_Spark_Advance();
        Send_Spark_Advance(); /*Send the peak position to ECU */
    }
}

```

The program first configures the DAQ card and the CAN controller, then it enters the main loop. The DAQ card is first cleaned from all old samples, whereafter the sampling is started and the “DAQ ready” bit is set. The “DAQ ready” is a signal that is sent to the sample timing circuit (Section 2.4) and indicates that the DAQ card is ready to sample data. The sample buffer size, on the DAQ card, can hold 256 samples of data and when it is full it sends a signal to the PC. Since two channels are sampled this gives 128 samples per channel.

While the sampling is running the PC checks for new messages on the CAN-bus from the ECU. The messages from the ECU contains engine speed and spark advance information which is used to window away the ignition phase (Section 2.2).

The card is externally triggered by the sample timing, and it samples 128 data points each of the ionization current and of the pressure trace. The “DAQ ready” pin is then cleared and the sampled data is transferred to the PC for interpretation. At the end of the main loop the estimated, and the true peak pressure positions (PPP) are computed. The estimated PPP is used to compute a correction to the spark advance, and the true (PPP) is used for validation. Finally the update to the spark advance is sent to the ECU via the CAN bus.

The software drivers supplied with the DAQ card were specialized for continuous sampling with no other tasks during the sampling process. Therefore, special software drivers for the card has been developed, that monitors the pressure and ionization current during the combustion events, and leaves the system available for other computational tasks.

## 2.4 Sample Timing

The ionization current, the cylinder pressure, and the engine position must be monitored to compute the estimated and true peak pressure position for the engine. The engine position can be retrieved in several ways; one is by measuring an extra signal that contains crank angle information and compute the crank angle (e.g. an inductive sensor and a cog-wheel connected to the crank), and another way is to use a signal that triggers sampling events synchronously with the crank revolutions. In the first case computational efficiency is lost due to the calculations that have to be performed when computing the engine position. In the second case no computations have to be performed but it requires additional hardware. The second alternative is used here in order to have computational power available for the signal interpretation algorithms.

In Figure 3 an overview of the system is displayed. It is designed to produce pulses at certain positions of the crank, where each pulse triggers a sampling event at the DAQ card. In this way each sample corresponds to a determined engine position. The spacing between the trigger pulses has currently been set to  $1^\circ$  of the crank angle, but it is possible to change this resolution in the system.

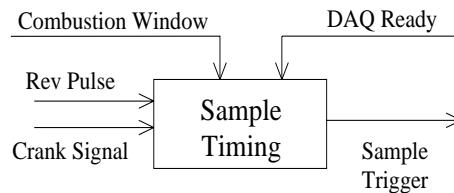


**Figure 3** Sample timing system, the inputs and the output are shown.

All four cylinders can be monitored regarding the ionization current signal, but only cylinder one has a pressure sensor mounted. Therefore, only cylinder one is sampled during the algorithm development and tests. Furthermore, it is only interesting to sample during the combustion in this cylinder, hence the system is designed to give pulses only from  $33^\circ$  BTDC until the DAQ buffer is filled (i.e. 128 samples later =  $128^\circ$  later).

### Signal and System Description

A short description of the signals that are available in the system follows.

**Sample Trigger** The output that triggers the sampling events at the DAQ card.

One pulse per degree from  $33^\circ$  BTDC and a total of 128 pulses. The pulses are generated when there is combustion in cylinder one and when the DAQ card is ready to read new samples.

**Crank Signal** Pulses that come from an optical encoder, connected to the crank shaft, which gives 1800 pulses per engine revolution. This is equal to 5 pulses per crank angle degree, and it is divided by a circuit to one pulse per crank angle degree.

**Rev Pulse** Also an output from the optical encoder with one pulse per engine revolution. This signal is used to get a fixed reference point for the crank angle. The pulse is high at 33° BTDC.

**Combustion Window** Output from the ECU that tells that there is going to be combustion in cylinder one.

**DAQ ready** Output from the DAQ card which tells that it is initialized and ready to sample data.

### 3 Verification of the Experimental Platform

This demonstration using feedback from the pressure sensor is only a verification that the data acquisition, the PC-hardware and -software, and the communication with the engine control unit all work together in real-time. This in order to make feedback control of the spark advance possible.

The optimum value for the mean peak pressure position (PPP), is between 12° and 20° after TDC, and it varies with engine designs due to different heat flows to the cylinder walls [5]. For our engine the optimal mean PPP is around 14°–16° ATDC [1]. The magnitude of the cycle-to-cycle variations is around 10°.

The spark timing controller measures the on-going combustion and updates the spark timing. The spark timing update is done through the following, PI like, control law

$$ST_{\text{new}} = ST_{\text{old}} - C(\text{PPP}_{\text{des}} - \text{PPP}_{\text{meas}})$$

where  $ST_{\text{new}}$  is the new spark timing correction,  $ST_{\text{old}}$  the old spark timing correction,  $\text{PPP}_{\text{des}}$  the desired PPP,  $\text{PPP}_{\text{meas}}$  the measured PPP, and  $C$  a gain that has to be tuned. The gain for the pressure based controller is tuned such that the influence of cycle-to-cycle variations in the peak pressure position ( $\theta_{\text{PPP}}$ ), shall not influence the ignition timing (IT) more than 1° [5]. Hence cyclic variation of magnitude 10° results in feed-back to the ignition timing with a constant  $C = \frac{1}{10}$ .

Figure 4 shows a plot of the peak pressure position for 193 consecutive cycles. To start with the spark advance timing is late with a PPP of around 30° ATDC. At cycle 70 the peak pressure controller is switched on. The reference value is 16° ATDC. It can be seen that the peak pressure position goes to the reference value when the controller is switched on.

In cycle 50 there is an outlier, which is either a misfire or a slow burn. Therefore, the TDC position is detected in that cycle. The fact that TDC is detected as peak pressure position is a further verification of that the platform is correctly synchronized with the engine. The probable cause of this slow burn or misfire, is the late ignition timing.

In this verification the measured peak pressure position has been used for spark advance control, but the platform is developed so that the pattern analysis algorithm for the ionization current can be analyzed.

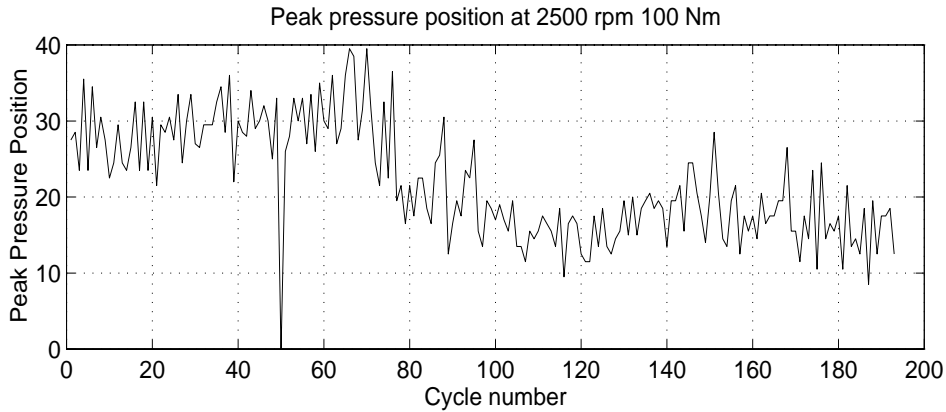


**Figure 4** The peak pressure position for several cycles. The controller is started at cycle 70, and successfully achieves the desired ignition timing.

## 4 Ionization Current Interpretation Algorithm

Having developed the experimental hardware and software platform, the second step is to tailor the ionization current interpretation method [2] to be used in real-time demonstrations.

The method for extracting information from the ionization current about the pressure is identified as a pattern recognition scheme. In this work the pattern recognition scheme has the following components.

**A signal** that shall be analyzed. In this work the signal that is studied is the ionization current.

**A model** with parameters such that it captures the appearance of the signal and include the patterns that shall be extracted.

**A criterion** used to select the parameters in the model that best describes the signal.

**A search strategy** that provides a way to search for the best parameters that minimizes the criterion. A fast search strategy is very valuable if there are demands for a fast algorithm.

Efficient search methods are often closely interlinked with the selection criterion.

### 4.1 Model description

The model of the ionization current,  $I(\theta)$ , used here was discussed in [2]. It contains a Gaussian shaped function for the post flame phase. The post flame phase is connected to the pressure, and it is important for the retrieval of the peak pressure position. To the post-flame model a description  $f(\theta)$  of the flame front is also

added,

$$I(\theta) = f(\theta) + \beta_1 e^{-\frac{1}{\beta_2}(\theta - \beta_3)^2}$$

where  $\theta$  denotes the crank angle. A simple flame-front model is a Gaussian signal, which can capture a high peak in the flame front which decays. Thus the model of the ionization current becomes

$$I(\theta, \bar{\alpha}) = \alpha_1 e^{-\frac{1}{\alpha_2}(\theta - \alpha_3)^2} + \beta_1 e^{-\frac{1}{\beta_2}(\theta - \beta_3)^2} \quad (2)$$

where  $\bar{\alpha}$  denotes the parameter vector

$$\bar{\alpha} = (\alpha_1, \alpha_2, \alpha_3, \beta_1, \beta_2, \beta_3)$$

The model is parameterized in six variables  $\alpha_1$ ,  $\alpha_2$ ,  $\alpha_3$ ,  $\beta_1$ ,  $\beta_2$ , and  $\beta_3$ , which are interpreted as:

$\alpha_1$	height of the flame front	$\beta_1$	height of the post flame
$\alpha_2$	width of the flame front	$\beta_2$	width of the post flame
$\alpha_3$	position of the flame front	$\beta_3$	position of the post flame

With this parameterization, the interpretation of the peak pressure position is simple, since the position of the second Gaussian signal,  $\beta_3$ , corresponds to the peak pressure position.

## 4.2 Criterion and Search Strategy

As a criterion to decide which set of parameters that best fit the model to the measured signal, a least squares criterion can be used. This means that the best parameters are chosen as the parameters that minimizes the following sum

$$V(\bar{\alpha}) = \sum_{i=1}^N (I(\theta_i, \bar{\alpha}) - I_{\text{samp}}(i))^2 \quad (3)$$

where

$i$	sample number
$N$	total number of samples
$\theta_i$	crank angle at sample $i$
$I(\theta_i, \bar{\alpha})$	model value at crank angle $\theta_i$
$I_{\text{samp}}(i)$	sampled ionization current at sample $i$

In the off-line study of the method [2], this criterion was used. The search method for the parameters that minimize this criterion was computed by performing a gradient search.

## 4.3 Time Complexity

With this approach, the time complexity is too large to be used in a real-time implementation on our platform. An approximation of the time complexity is

$O(i_{\text{steps}} \cdot (N_{\text{par}} + 1) \cdot N)$ , here  $N$  is the number of samples,  $N_{\text{par}}$  the number of parameters,  $i_{\text{steps}}$  the number of iteration steps. The complexity expression can be derived as follows: for each iteration step ( $i_{\text{steps}}$ ) one must update all parameters and the sum to be minimized ( $N_{\text{par}} + 1$ ) and finally to update the parameters and the sum one must go through the data set ( $N$ ). To get a good fit approximately 100 iteration steps,  $i_{\text{step}} = 100$ , has to be taken, which gives a too high time complexity.

A direct implementation of this algorithm would require a system with better computational performance than described above. This motivates the work in the next section developing the algorithm that is used in the real time experiments.

## 5 Algorithm Suitable for the Platform

The change from what was described in the previous section lies in the selection criterion and search strategy. By choosing a different criterion, for selecting the best parameters of the model, a search strategy can be found that is significantly faster than the one described earlier.

The algorithm determines a threshold between two unknown Gaussian functions from a measured signal and returns the parameters for the two Gaussian functions. The development of this algorithm, suitable for real time implementation, has been a major part of the work to achieve real-time control.

### 5.1 Reparameterization of the Model

For the algorithm development the model of the ionization current is reparameterized. First normalize the sampled data set  $I_{\text{samp}}(i)$  to  $I_{\text{norm}}(i)$ , i.e. divide every sample with the total sum,

$$I_{\text{norm}}(i) = \frac{I_{\text{samp}}(i)}{\sum_{j=1}^N I_{\text{samp}}(j)}$$

then write the model as,

$$I(\theta, \bar{\alpha}_r) = \frac{q_1}{\sqrt{2\pi}\sigma_1} e^{-\frac{1}{2}\left(\frac{\theta-\mu_1}{\sigma_1}\right)^2} + \frac{q_2}{\sqrt{2\pi}\sigma_2} e^{-\frac{1}{2}\left(\frac{\theta-\mu_2}{\sigma_2}\right)^2} \quad (4)$$

where  $q_1$  is the fraction of the first Gaussian component and  $q_2$  is the fraction of the second Gaussian component, i.e.  $q_1 + q_2 = 1$ , and  $\bar{\alpha}_r = (q_1, \sigma_1, \mu_1, q_2, \sigma_2, \mu_2)$ . The normalized data and the model has the following properties,

$$\begin{aligned} \sum I_{\text{norm}}(i) &= 1 \\ \int I(\theta, \bar{\alpha}_r) d\theta &= 1 \\ \sum I(\theta_i, \bar{\alpha}_r) \Delta\theta_i &\approx 1 \end{aligned}$$

where  $\theta_i$  is the crank angle at sample  $i$  and  $\Delta\theta_i$  is the difference in crank angle between the samples. Note that the data  $I(i)$  is sampled where the index  $i$  is the sample number, and that the model  $I(\theta_i, \bar{\alpha}_r)$  is described in crank angle.

The parameterization in (4) is equivalent to the one described in (2). Especially, the parameters, corresponding to the positions of the phases,  $\alpha_3$  and  $\beta_3$  are equal to  $\mu_1$  and  $\mu_2$ .

## 5.2 Kullback Criterion

The input to the estimation algorithm is a function that is assumed to consist of a sum of two Gaussian functions. The algorithm returns the parameters of the best fit and the threshold between the functions (the threshold is not interesting for our purposes).

The criterion for selecting the best parameters is called the Kullback directed divergence  $J$ , which is computed as

$$J(\bar{\alpha}_r) = \sum_{i=1}^N I_{\text{norm}}(i) \log \frac{I_{\text{norm}}(i)}{I(\theta_i, \bar{\alpha}_r)}$$

where  $I_{\text{norm}}(i)$  is the normalized dataset and  $I(\theta_i, \bar{\alpha}_r)$  the model.

The Kullback measure  $J$  has the following properties [4]: (1)  $J \geq 0$  (2)  $J = 0$  if and only if  $I(\theta_i, \bar{\alpha}_r) = I_{\text{norm}}(i)$  for all  $i$ . However  $J$  is not symmetric and it does not satisfy the triangle inequality, and therefore it is not a metric.

The criterion,  $J$ , can be rewritten as

$$J(\bar{\alpha}_r) = \sum_{i=1}^N I_{\text{norm}}(i) \log I_{\text{norm}}(i) - \sum_{i=1}^N I_{\text{norm}}(i) \log I(\theta_i, \bar{\alpha}_r)$$

Here the first sum is independent of the model parameters and will be constant during the search. Therefore, it is only necessary to compute the second sum during the search, which reduces the minimization criterion to

$$J_1(\bar{\alpha}_r) = - \sum_{i=1}^N I_{\text{norm}}(i) \log I(\theta_i, \bar{\alpha}_r)$$

## 5.3 Search Strategy

A fast search strategy can be developed [3] if one assumes that the two Gaussian functions are well separated. With separated Gaussians  $I(\theta_i, \bar{\alpha}_r)$  the model can be approximated by

$$I(\theta_i, \bar{\alpha}_r) \approx \begin{cases} \frac{q_1}{\sqrt{2\pi}\sigma_1} e^{-\frac{1}{2}\left(\frac{\theta_i - \mu_1}{\sigma_1}\right)^2} & \text{if } i \leq t \\ \frac{q_2}{\sqrt{2\pi}\sigma_2} e^{-\frac{1}{2}\left(\frac{\theta_i - \mu_2}{\sigma_2}\right)^2} & \text{if } i > t \end{cases}$$

The assumption that the modes are well separated means that if the threshold that separates the modes is  $t$ , then the mean and variance estimated from the  $t$  first values  $I_{\text{norm}}(1)$  to  $I_{\text{norm}}(t)$  will be close to the true values of these parameters i.e

$\mu_1$  and  $\sigma_1$ . The converse is true for the values  $I_{\text{norm}}(t+1)$  to  $I_{\text{norm}}(N)$  that gives the estimates for the parameters  $\mu_2$  and  $\sigma_2$ .

Given the data  $I_{\text{norm}}(i)$  and the threshold  $t$  the parameters of the model can be computed. The parameters for the first Gaussian function,  $q_1$ ,  $\sigma_1$ ,  $\mu_1$ , are estimated from the first part of the data set  $I_{\text{norm}}(1)$  to  $I_{\text{norm}}(t)$  and the parameters for the second Gaussian function  $q_2$ ,  $\sigma_2$ ,  $\mu_2$ , are estimated from the second part of the data set  $I_{\text{norm}}(t+1)$  to  $I_{\text{norm}}(N)$ .

### Efficient Criterion Evaluation

With the assumption described earlier the minimizing problem becomes

$$J_1(\bar{\alpha}_r) = - \sum_{i=1}^t I_{\text{norm}}(i) \log \left( \frac{q_1}{\sqrt{2\pi}\sigma_1} e^{-\frac{1}{2} \left( \frac{\theta_i - \mu_1}{\sigma_1} \right)^2} \right) - \sum_{i=t+1}^N I_{\text{norm}}(i) \log \left( \frac{q_2}{\sqrt{2\pi}\sigma_2} e^{-\frac{1}{2} \left( \frac{\theta_i - \mu_2}{\sigma_2} \right)^2} \right) \quad (5)$$

Using the assumption of well separated modes and the parameter estimates,  $J_1$  can be rewritten to

$$J_1(\bar{\alpha}_r) = \frac{1 + \log 2\pi}{2} - \hat{q}_1 \log \hat{q}_1 - \hat{q}_2 \log \hat{q}_2 + \frac{1}{2} (\hat{q}_1 \log \hat{\sigma}_1^2 + \hat{q}_2 \log \hat{\sigma}_2^2) \quad (6)$$

This criterion is efficient to evaluate, in comparison with (5), since it has no evaluation of exponential functions or sums. What is necessary for the evaluation of the criterion is the model parameters.

The search strategy for the optimal parameters is now

```

for t=1 to N
  compute the means and variances for this t
  compute J1
  if J1 < min
    save t, means, and variances as best so far
    min = J1
  end
end
end

```

### Recursive Parameter Updating

The computation of the means,  $\hat{\mu}_1$  and  $\hat{\mu}_2$ , and the variances,  $\hat{\sigma}_1$  and  $\hat{\sigma}_2$ , can be made incremental such that the values from one step,  $t$ , can be used for updating the parameters in the next step,  $t+1$ . Using also the variable  $\mu$ , to denote the mean value for the whole dataset, the parameter updating can be computed in the

following way

$$\begin{aligned}
\hat{q}_1(t+1) &= \hat{q}_1(t) + I_{\text{norm}}(t+1) \\
\hat{q}_2(t+1) &= 1 - \hat{q}_1(t+1) \\
\hat{\mu}_1(t+1) &= \frac{\hat{q}_1(t)\hat{\mu}_1(t) + \theta_{t+1}I_{\text{norm}}(t+1)}{\hat{q}_1(t+1)} \\
\hat{\mu}_2(t+1) &= \frac{\mu - \hat{q}_1(t+1)\hat{\mu}_1(t+1)}{1 - \hat{q}_1(t+1)} \\
\hat{\sigma}_1^2(t+1) &= \frac{\hat{q}_1(t)(\hat{\sigma}_1^2(t) + (\hat{\mu}_1(t) - \hat{\mu}_1(t+1))^2) + I_{\text{norm}}(t+1)(\theta_{t+1} - \hat{\mu}_1(t+1))^2}{\hat{q}_1(t+1)} \\
\hat{\sigma}_2^2(t+1) &= \frac{(1 - \hat{q}_1(t))(\hat{\sigma}_2^2(t) + (\hat{\mu}_2(t) - \hat{\mu}_2(t+1))^2) - I_{\text{norm}}(t+1)(\theta_{t+1} - \hat{\mu}_2(t+1))^2}{1 - \hat{q}_1(t+1)}
\end{aligned}$$

### Algorithm Tailoring Based on Prior Knowledge

The assumption of well separated modes makes the minimization problem simple and straight forward, but under certain conditions it is important that the interaction between the modes is taken into account. Therefore, a correction is computed to J1, which is based on a priori knowledge obtained from studies of measured ionization current under different operating conditions. The correction is computed such that it takes into account some interaction of the two modes, and still maintains a low time complexity of the algorithm.

Including the correction and exchanging  $\mu$  with  $m$  and  $\sigma$  with  $s$ , the pseudocode for the algorithm becomes

```

PeakEstimator()
{
  initialize q1, q2, m1, m2, s1, s2;
  min = large_value;
  for t=1 to N
  {
    compute J1
    H=Compute_correction(J1,t);
    if (H < min)
    {
      min=H;
      m2_best=m2;
    }
    update q1, q2, m1, m2, s1, s2;
  }
  return m2_best;
}

```

The algorithm returns the best value of  $\mu_2$  which is the estimate of the peak pressure position.

## 6 Verification of the Estimation Algorithm

The estimates produced by the least squares method were good [2]. Therefore, the first step is to compare the results that the Kullback measure gives, with the results from the least squares method. The estimated parameters differs between the algorithms since different criteria are used to select the best parameters. The difference between the important parameters  $\beta_3$  and  $\mu_2$  (corresponding to the peak position of the pressure) is very small, compared to the cyclic variations. The two algorithms produce nearly the same estimate of the mean peak pressure position.

In Figure 5 the results from the Kullback based algorithm is compared to the true peak pressure position. The operating point for the data in the figure is 2000 rpm and 100 Nm. Only the ignition timing is changed for the different points in the figure. It is changed between 30° BTDC and 5° BTDC. If the peak pressure position was exactly estimated, all points would lie on the straight line. Due to measurement noise and process noise the peak pressure position can not be exactly estimated. As can be seen, the algorithm gives sufficiently good results which in mean gives a good estimate of the peak position. With some averaging the correlation is even better.

## 7 Summary

A hardware and software system for spark advance control research has been developed and verified to work. The experimental platform includes the ECU, sample timing, DAQ-card, CAN-bus, and PC.

Furthermore, an efficient algorithm for extracting information from the ionization current has been described. The algorithm gives a good estimate of the peak pressure position, and can be used for feedback control of the spark-advance.

## Acknowledgment

The CAN controller and the ECU together with a base program for running the engine have been provided by Mecel AB. This equipment is foundational for the platform described, and their support is greatly acknowledged.

## References

- [1] Lars Eriksson, Lars Nielsen, and Mikael Glavenius. Closed loop ignition control by ionization current interpretation. *SAE SP-1236*, (SAE paper No. 970854):159–166, 1997.
- [2] Lars Eriksson, Lars Nielsen, and Jan Nytoft. Ignition control by ionization current interpretation. *SAE SP-1149*, (SAE paper No. 960045):73–79, 1996.
- [3] J. Kittler and J. Illingworth. On threshold selection using clustering criteria. *IEEE Transactions on Systems, Man, and Cybernetics*, SMC-15:652–655, 1985.

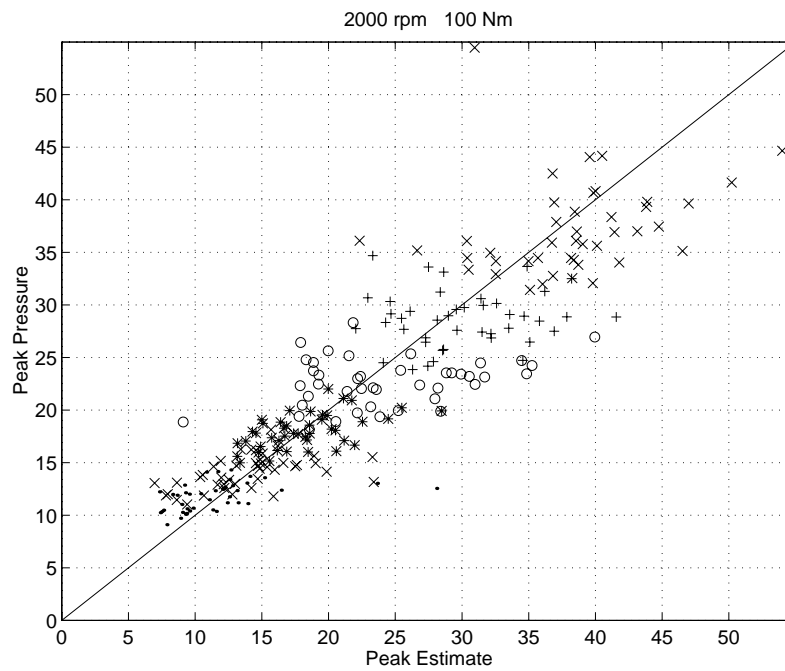


**Figure 5** Correlation plot between the true peak pressure position and the estimated peak position. Six different ignition timings, for one operating point with engine speed (2000 rpm) and load (100 Nm). Of course, some averaging improves the correlation.

- [4] S. Kullback. *Information Theory and Statistics*. Wiley, New York, 1959.
- [5] J. D. Powell. Engine control using cylinder pressure: Past, present, and future. *Journal of Dynamic System, Measurement, and Control*, 115:343–350, June 1993.



# Closed Loop Ignition Control by Ionization Current Interpretation<sup>1</sup>

Lars Eriksson<sup>†</sup>, Lars Nielsen<sup>†</sup>, and Mikael Glavenius<sup>‡</sup>

<sup>†</sup>*Vehicular Systems*  
*Linköping University, SE-581 83 Linköping, Sweden*

<sup>‡</sup>*Mecel AB*  
*Box 73, SE-662 22 Åmål, Sweden*

3

## Abstract

The main result of this paper is a real-time closed loop demonstration of spark advance control by interpretation of ionization current signals. The advantages of such a system is quantified. The ionization current, obtained by using the spark plug as a sensor, is rich on information, but the signal is also complex. A key step in our method is to use parameterized functions to describe the ionization current [1].

The results are validated on a SAAB 2.3 l, normally aspirated, production engine, showing that the placement of the pressure trace relative to TDC is controlled using only the ionization current for feedback.

---

<sup>1</sup>This is an edited version of the article that was published in the *SAE 1997 Transactions, Journal of Engines*, Vol. 106, Section 3, pp. 1216-1223, 1997.

## 1 Introduction

Spark advance timing is crucial for engine efficiency and power. The reason is that the spark advance determines how the pressure evolution is placed relative to TDC. Work is lost to heat transfer and to the compression if it is placed too early, and expansion work is lost if it is placed too late. In most of today's spark-ignited (SI) engines there is no feedback from the combustion to the spark advance, though there exist on-line methods of measuring the engine efficiency. Two methods, among others, are measurements of in-cylinder pressure and ionization current.

The idea in using in-cylinder pressure is to control the spark advance so that the pressure peak is placed relative to TDC in an optimal way. Systems using such feedback from a pressure sensor have reported good results, but have not yet proven cost effective due to the cost of the pressure sensor.

The other possibility is the ionization current, which is obtained from the spark plug. It is rich on information both about the pressure but also about many other combustion properties [2, 3, 4]. The sensor signal is thus relatively complex. The key step in our method, for deducing information, is to use parameterized functions to describe the ionization current. Special emphasis is made to get a correct description of the pressure development, using a physical model relating the ionization current to the pressure [5].

## 2 Spark Timing

Several parameters affect the best spark advance setting such as engine speed, load, air/fuel ratio, fuel characteristics, EGR, coolant temperature, air temperature, humidity, among others. Current ignition control systems measure several of these parameters and adjust the spark advance. The spark advance setting is chosen by extensive testing and calibration during the design phase of the engine. However, it is not possible to measure and account for all parameters that effect the spark advance, since it would be extremely expensive to perform the measurements and testing required to incorporate such a system in a production engine.

The testing and calibration results in a nominal spark advance schedule, which is conservative since it has to guarantee both that knock (or detonation) does not occur, as well as good performance over the entire range of the non measured parameters.

### 2.1 Peak Pressure Concept

A different approach is to continuously monitor the combustion and use information about the in-cylinder pressure to set the spark advance. The spark advance is used to position the in-cylinder pressure in some optimal way relative TDC (top dead center). To define the position of the in-cylinder pressure relative to TDC, the concept of peak pressure position (PPP) is used. The PPP is the position in crank angle where the in-cylinder pressure takes its maximal value. The PPP is shown in the Figure 1.

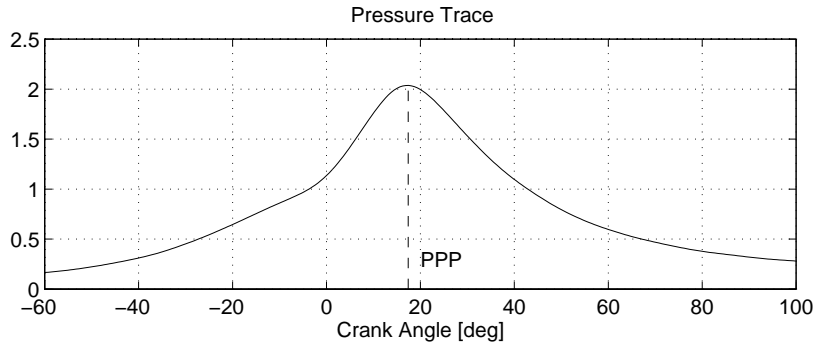


**Figure 1** The PPP (Peak Pressure Position) is the position in crank angles for the pressure peak.

In Figure 2 the mean value PPP is plotted together with the mean value of the produced torque at four different operating points, with an engine speed of 1500 rpm and with four different throttle angles. The PPP for maximum output torque in the figure is around  $15^\circ$  ATDC (after TDC) for all these operating points. Doubling the engine speed to 3000 rpm, the peak pressure position still remains close to  $15^\circ$  ATDC, as shown in Figure 3.

Note that the load, and speed are changed over large intervals, and that the PPP for maximum output torque at the different operating points, does not differ much. The PPP versus torque curve is also flat around the position for the maximum. Therefore a spark schedule that maintains a constant PPP at  $15^\circ$  is close to optimum. Considering only the work produced, it has been shown that an optimal spark schedule maintains almost the same position for the peak pressure [6]. However, the optimal PPP changes slightly with the operating points.

The efficiency can be improved a little bit further by mapping the optimal PPP for each operating point, and provide these values as reference signal to the spark timing controller. The peak pressure positioning principle can also be used for meeting emission standards. In [7] this question is addressed by rephrasing the emission regulations on the spark advance to desired peak pressure positions. Using feedback from the combustion guarantees that the peak pressure is held at the desired position even though the environmental conditions change. Other work using the peak pressure concept with a pressure sensor, together with a knock control algorithm, has shown a 10 % improvement in power and 5 % improvement in efficiency [8].

### 3 Pressure and Torque Variability

The PPP varies from cycle-to-cycle, and since the output torque depends on the peak pressure position, these variations in PPP will effect the cycle-to-cycle varia-

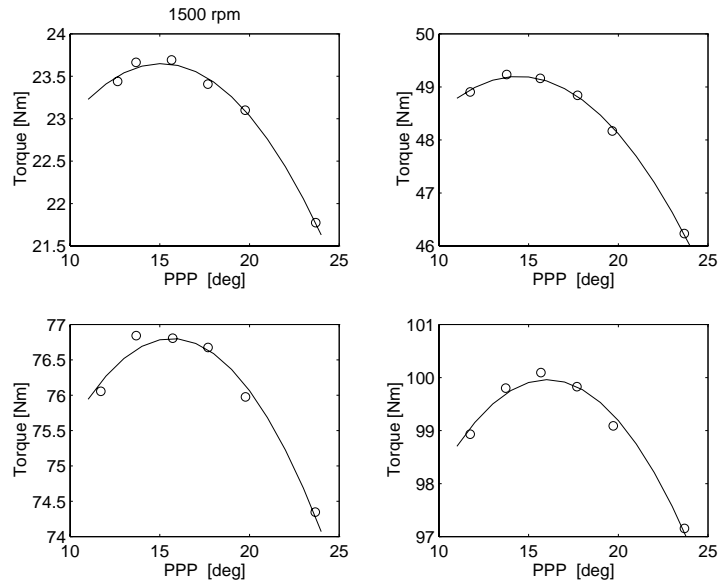


**Figure 2** Mean PPP (Peak Pressure Position) and output torque for 1500 rpm and four different throttle angles. Each circle is a mean value from 200 consecutive cycles with the same ignition timing. The optimal mean PPP is close to  $15^\circ$  for all loads.

tions in the output torque. The cycle-to-cycle variations in PPP and output torque depend on several parameters where spark advance is interesting in this context but also engine speed and load is considered here.

### 3.1 Measurements

In Figures 2, and 3, the engine has been run at 48 operating points. In each plot only the spark timing is changed while the injected fuel, engine speed, and throttle angle are held constant. Each circle in the plots is computed as a mean value from 200 consecutive cycles in the same operating points. A quadratic polynomial is fitted to the points and the resulting curve is plotted. Within the range in the figures the quadratic polynomial gives a good fit to the measured values.

The variation in PPP is shown in Figure 4, with respect to different engine speeds, engine loads, and PPP. The y-axis shows the standard deviation for the PPP,  $\sigma_p$ . For each plot in the figure the engine load is approximately the same, and for each line in the plots the engine speed is held constant and the spark advance is the only thing that has changed. For a given PPP lower loads tend to give higher cycle-to-cycle variations, and lower speeds tend to give lower cycle-to-cycle variations.

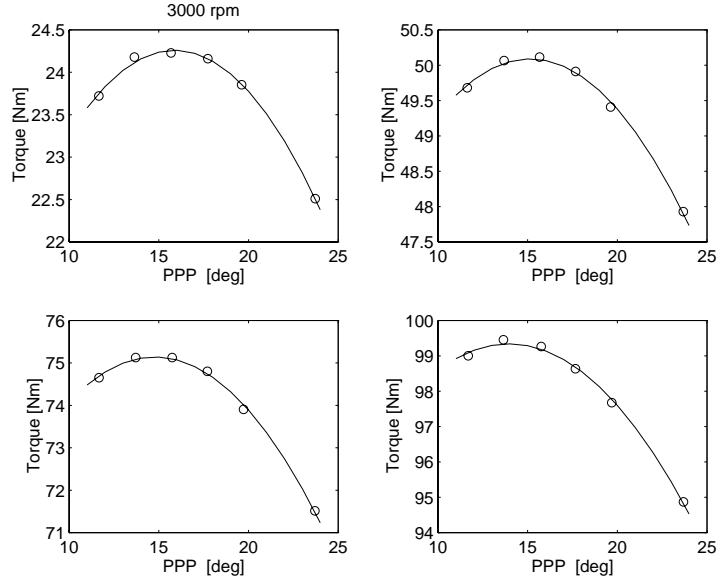


**Figure 3** Mean PPP (Peak Pressure Position) and output torque for 3000 rpm and four different throttle angles. Each circle is a mean value from 200 consecutive cycles with the same ignition timing. The optimal mean PPP is close to 15° for all loads.

### 3.2 Principal Study of Variations

The following principal study illustrates that variations in the output torque are smaller when the mean PPP is held at its optimum. In Figure 5, a quadratic polynomial, similar to those in Figures 2, and 3, is plotted. The polynomial represents an ideal relation between the PPP,  $x_p$ , and the output torque,  $y_T$ . The polynomial can be parameterized as

$$y_T = -c \cdot (x_p - x_{max})^2 + y_{max} \quad (1)$$

Using Equation 1, the standard deviation of the variations in the output torque,  $\sigma_T$ , can be derived as

$$\sigma_T^2 = 2c^2 \sigma_p^2 (\sigma_p^2 + 2d^2) \quad (2)$$

where,  $d$ , is the deviation from the optimal mean PPP and  $\sigma_p$  is the standard deviation for the PPP. This is derived and further described in the appendix. Equation 2 gives a useful rule of thumb, and another useful quantification of the value of spark advance feedback control. The influence of cycle-to-cycle variations in PPP on the output torque is minimal if the mean peak pressure position is controlled to its optimal value.

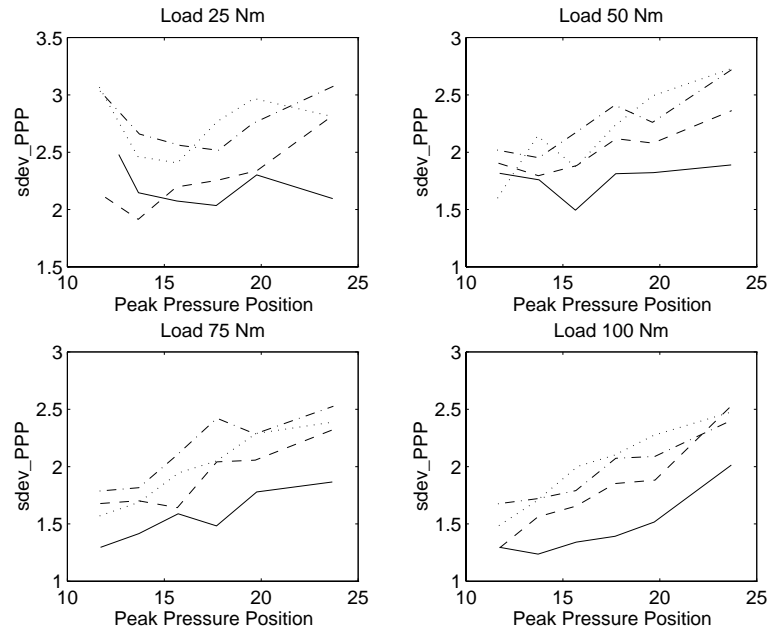


**Figure 4** Measured standard deviations for the peak pressure position,  $\sigma_P$ , calculated for different engine speeds, loads and spark advances. The speeds are: solid – 1500 rpm, dashed – 2000 rpm, dash-dotted – 2500 rpm, dotted – 3000 rpm.

## 4 Ionization Current

Sensing the ionization current in the cylinder, provides a possibility to estimate the efficiency of the combustion and control the spark advance. Ionization current interpretation has also proven cost effective and is already in use, for example for misfire detection and cam phase sensing, in production cars as well as in other applications [2]. Figure 6, displays the possibility to use the spark plug as sensor for several parameters related to the combustion. The spark plug acts both as an actuator and a multiple sensor. The peak pressure position is the signal that is used for spark advance control. The measure of fit tells how much the measured ionization current and the model differs.

### 4.1 Ionization Current Interpretation

The ionization current typically has three phases: a phase related to ignition, a phase related to ions from the flame development and propagation, and a phase related to pressure and temperature development. In Figure 7, the three phases of the ionization are displayed. Each of these phases have varying characteristics and

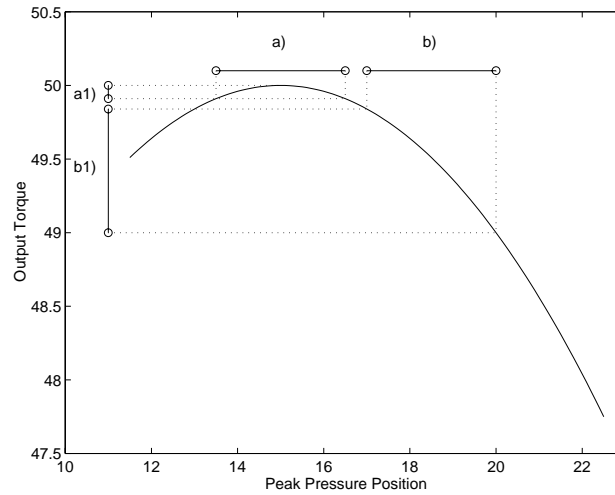


**Figure 5** When the mean PPP (peak pressure position) is at optimum the variations in the output torque are minimal. At a) the mean peak pressure position lies at optimum which give small variations in output torque at a1). At b) the mean peak pressure position lies some degrees off from optimum and the resulting variations are larger at b1).

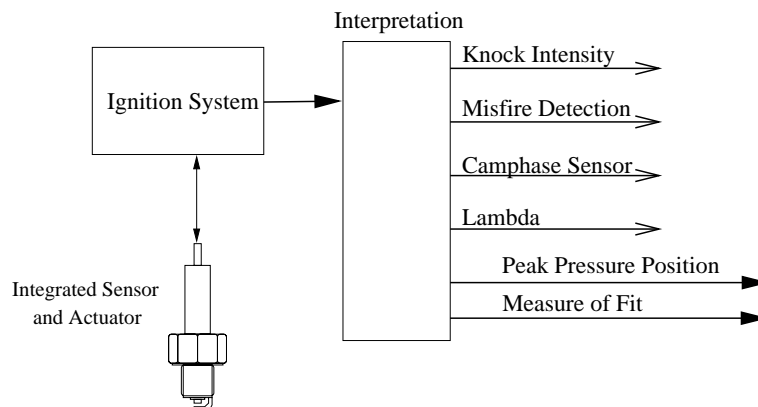


**Figure 6** The spark plug functions as sensor for several parameters. Knock intensity, misfire, and cam-phase sensing has been implemented and lambda is also a potential output from an interpretation algorithm. The peak pressure position estimate is the information used here.

they also mix together in complicated ways.

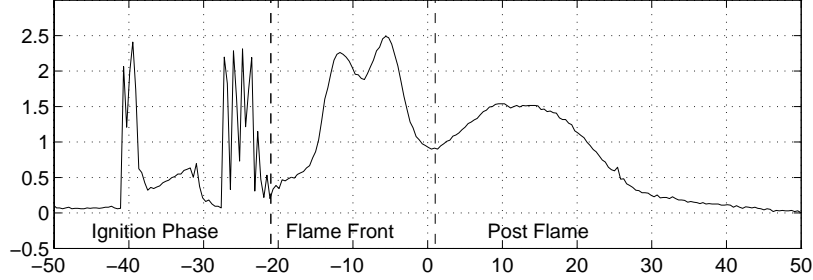


**Figure 7** Ionization current with three clear phases, ignition, flame front, and post flame.

The key step in our method for deducing information, is to use parameterized functions to describe the ionization current. These functions must be rich enough to capture the different variations, but they must also be such that the relevant information can be extracted. The parameterized functions are used to separate out the different phases of the ionization current, and get an estimate of the peak pressure position. As a simple model, with 6 parameters, a sum of two Gaussian function were used

$$I(\theta) = \alpha_1 e^{-\frac{1}{\alpha_2}(\theta - \alpha_3)^2} + \beta_1 e^{-\frac{1}{\beta_2}(\theta - \beta_3)^2}$$

The results were validated by direct comparison with an in-cylinder pressure sensor [1]. The ideas for extracting information, has been implemented using an algorithm suitable for real time. The algorithm estimates bimodal functions, using the Kullback measure to determine the best choice of parameters.

In Figure 8, the results from the ionization interpretation algorithm is compared to the measured peak pressure positions. In the figure the engine speed and the throttle angle are held constant, and the ignition timing is positioned at six different spark timings from 35° BTDC (before TDC) to 4° BTDC. The estimate correlates quite well with the measured peak pressure position. Since there is not a one to one correspondence, there is a need for a filtering of the estimate. The filtering is further described in Section 5.1.

## 5 Spark Timing Controller

A simple controller structure for the spark timing is shown in Figure 5, where the spark plug works as integrated actuator and sensor. The spark plug that is used is a conventional spark plug. The ionization current is produced by the integrated ignition and measurement system, described in [2], and the interpretation algorithm gives an estimate of the PPP. The reference value for the PPP gives a possibility to

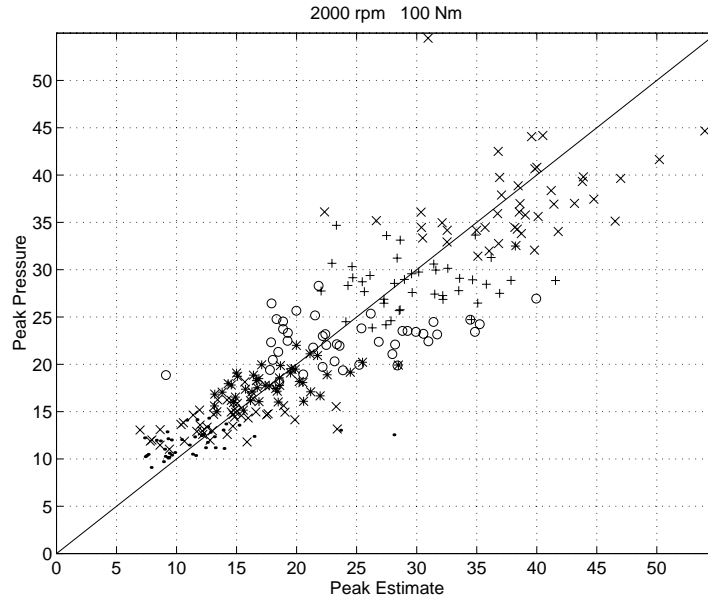


**Figure 8** The peak pressure position estimated from the ionization current compared to the measured. Each point corresponds to the estimated and true PPP for one cycle. Close to 500 cycles are displayed in the plot. One to one correspondence is indicated by the solid line.

have different spark schedules for different operating points, i.e meeting other goals than to maximize the work. For example in mid-load mid-speed ranges a schedule close to MBT, with peak around  $15^\circ$ , and in high load ranges a conservative schedule, with late peak, for holding down the  $\text{NO}_x$  emissions.

The spark timing controller measures the on-going combustion and updates the spark timing. The spark timing update is done through the following, PI like, control law

$$ST_{\text{new}} = ST_{\text{old}} - C(\text{PPP}_{\text{des}} - \text{PPP}_{\text{est}}) \quad (3)$$

where  $ST_{\text{new}}$  is the new spark timing,  $ST_{\text{old}}$  the old spark timing,  $\text{PPP}_{\text{des}}$  the desired peak pressure position,  $\text{PPP}_{\text{est}}$  the estimated of the PPP from the ionization current, and  $C$  a gain that has to be tuned.

## 5.1 Controller Tuning

The gain  $C$  is selected such that the cycle-to-cycle variations in the estimate does not affect the spark timing too much. One criterion is that the spark timing shall not move more than  $1^\circ$  due to the cyclic variations. For this engine the cycle to cycle variations for the estimate of the PPP is around  $10^\circ$ .

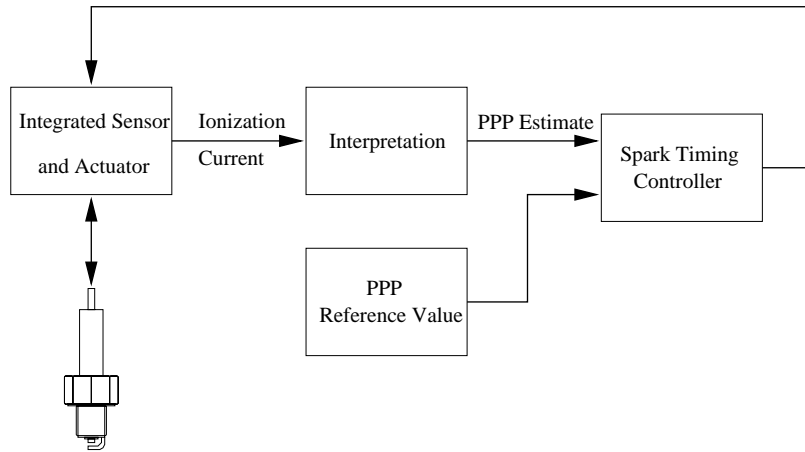


**Figure 9** The structure of the spark timing control system, where the spark plug operates as an integrated actuator and sensor. Information is extracted from the raw ionization current, and the estimate of the PPP is the input to the spark timing controller.

Another consideration to take into account is how well the estimate correlates with the PPP. In Figure 10, moving averages, with different lengths, are computed for the measured peak pressure positions and the estimated. In the upper left plot a moving average over three cycles is computed for the measure peak pressure position and the estimated. Improvements are visible in the figure when the average lengths increases from 3 to 6 and from 6 to 9, i.e the points in the plot moves closer to the solid line. But the improvement is not that large when the average length is increased from 9 to 12.

This indicates that a good choice for the gain  $C$  in the feedback control law is  $C = \frac{1}{10}$  measured in inverse number of cycles. This gain has been used in the on line tests. The small values of the gain can be viewed as low-pass filtering of the measurement signal. This filtering comes at a price, it slows down the feedback loop. Though it can be made faster using feed forward, that can be a nominal spark advance table.

A structure using feed forward is shown in Figure 11. Information about changes in reference value and engine transients are directly affecting spark timing controller. This structure is similar to the conventional lambda controllers.

## 5.2 Influence of Cycle-To-Cycle Variations

The magnitude of the cycle-to-cycle variations influences the spark timing controller in the feed back gain,  $C$ . With larger variations the feedback gain has to be selected smaller so that the variations does not effect the spark timing too much. Decreasing

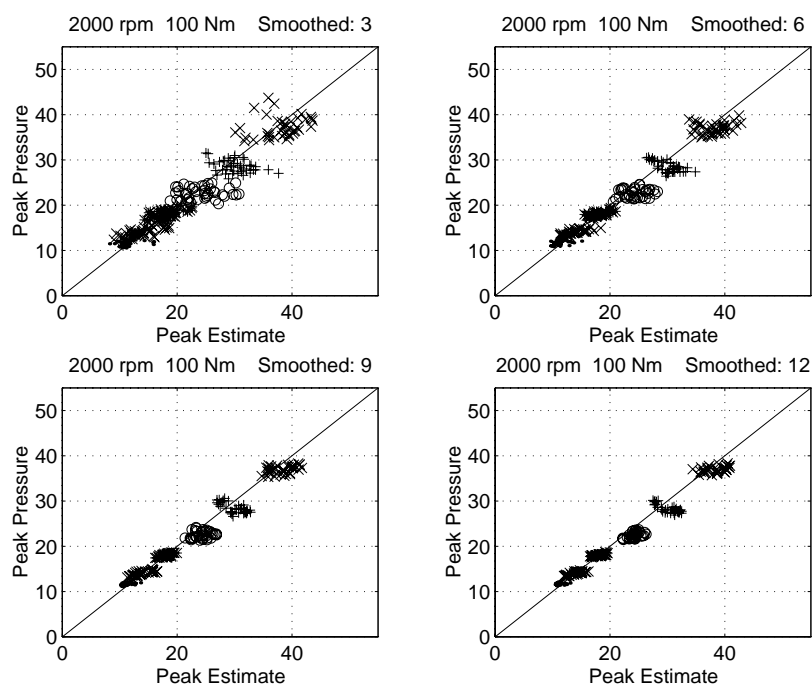


**Figure 10** PPP and the estimate. Moving averages are computed with different lengths (measured in number of cycles) over the measured peak pressure positions and the estimated. The average lengths are; upper left - 3, upper right - 6, lower left - 9, lower right - 12.

the sensitivity of the controller with a smaller gain results in a slower feed back loop.

## 6 Experimental Setup

Data collection and controller evaluation has been performed on a SAAB 2.3 l, four cylinder, four stroke, 16 valve, fuel injected, normally aspirated, production engine equipped with an ECU. The engine is connected to a Schenck “DYNAS NT 85” AC dynamometer, with an electronic control system.

In Figure 12, the setup for the closed loop experiments is shown. A PC is used for algorithm development and evaluation. The ionization current and the pressure signal (used only for validation) are sampled with a data acquisition card (DAQ). An optical incremental encoder is connected to the crank and used to trigger the DAQ at certain engine positions. The PC computes the updated spark advance and sends it via a CAN-network to the electronic control unit (ECU).

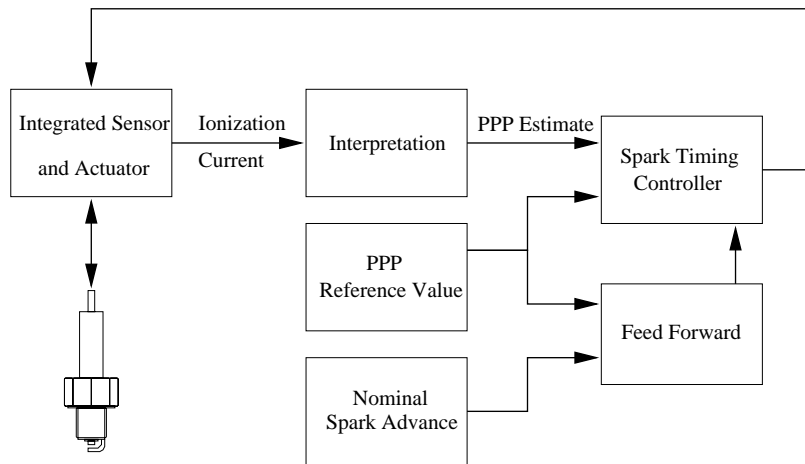


Figure 11 Structure of a controller using feed back and feed forward in combination.

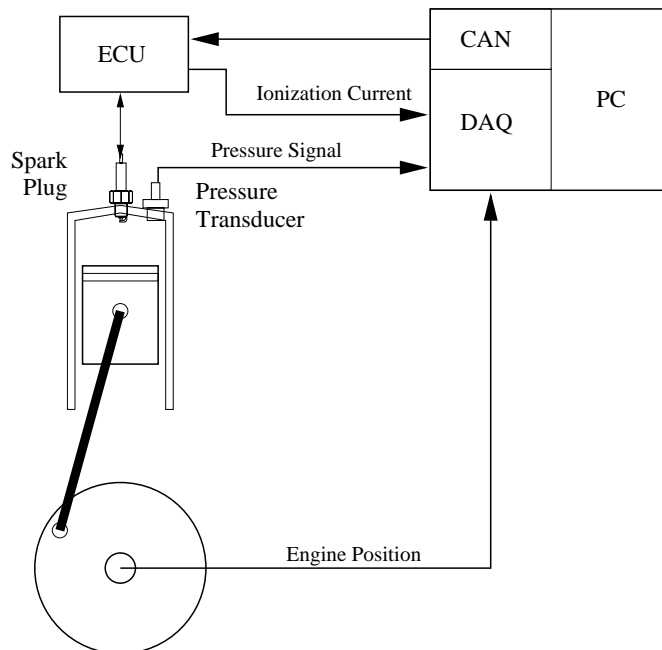
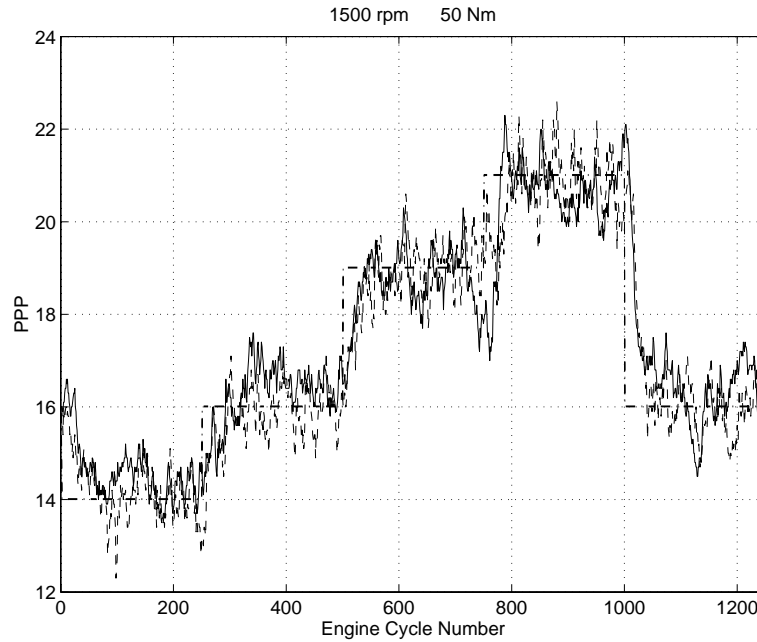


Figure 12 Experimental setup with the engine, the ECU, and the PC.

## 7 Closed Loop Demonstration

In Figure 13, it is shown that the ionization current based controller achieves the goal of controlling the peak pressure position to the desired values. The reference



**Figure 13** Closed loop control of spark advance with changing reference value, showing that the PPP can be controlled to the desired positions. Dash dotted – reference signal, solid – measured PPP, dashed – estimated PPP

value (dash dotted) shifts every 250'th engine cycle, from the initial value of 16° to 14° to 16° to 19° to 21° and back to 16°. The mean values for the PPP estimate from the ionization current (dashed) and the PPP (solid) and is computed using a first order LP filter with static gain 1,

$$PPP_{\text{new}} = 0.9 * PPP_{\text{old}} + 0.1 * PPP_{\text{measured}}$$

which is similar to the gain used in the controller for smoothing the PPP estimate. The results are very good, taken into account that the cycle-to-cycle variations of the PPP and its estimate is of the order 10°, and PPP is controlled to within  $\pm 1^\circ$  in mean.

The step response time for the controller can be seen in Figure 14. In this test the reference signal to the controller shifts every 60'th engine cycle, and it shifts between 14° and 20°. The step response time is approximately 30 cycles, which is

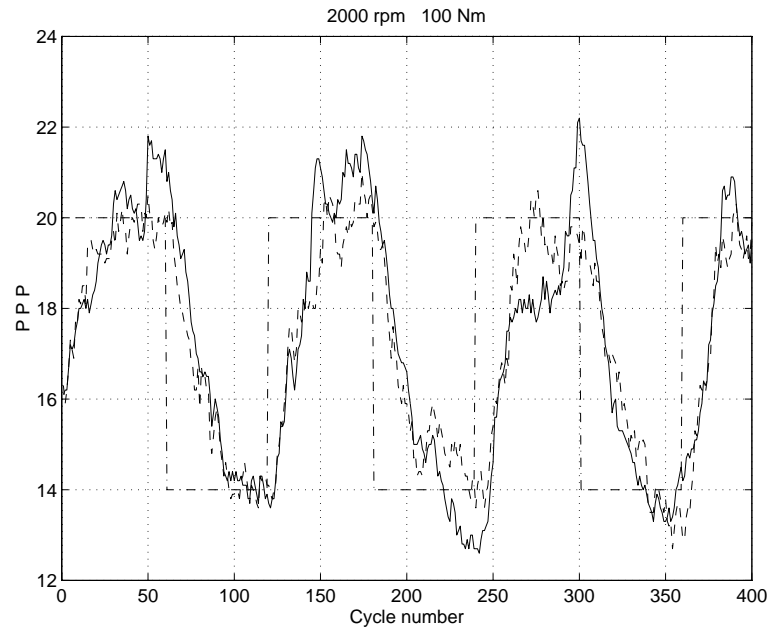


**Figure 14** Closed loop control of spark advance with changing reference value, showing the step response time. Dash dotted – reference signal, solid – measured PPP, dashed – estimated PPP

without feed forward compensation. Since no feed forward compensation is used this step response time for the reference signal will be the same as for environmental disturbances. With a feed forward loop the step response can be made faster to fit the needs during engine transients e.g. quick changes in the manifold pressure.

It is now demonstrated that the peak pressure position can be controlled using the ionization current signal. The step response time for the closed loop controller is also shown.

## 8 Conclusions

Closed loop control of the spark advance using the ionization current has been demonstrated. The scheme implemented is a feed back scheme, not a calibration scheme, which is related to the pressure based schemes that has earlier shown good results. The method is very cost effective since it uses exactly the same hardware and instrumentation (already used in production cars) that is used to utilize the spark plug as sensor, to detect misfire and for knock control. The only addition for ignition control is further signal interpretation in the electronic engine control unit.

Tuning of the feedback gain in the control law is discussed, and the main issue under consideration is that cyclic variations shall have a smooth effect on the spark timing. This introduces a time lag and a feed forward loop can be used for compensation during engine transients. The step response for the closed loop system is approximately 30 cycles, which is sufficient for environmental disturbances.

Non-measured environmental variables, like humidity, can significantly change the burn-rate and thus the peak pressure position. Experimental and theoretical studies (Figures 2 and 3, and Equation 2) clearly demonstrate the value of ignition timing control regarding power and efficiency. The controller based on ionization current interpretation reaches the goal, to control the peak pressure to desired mean position.

## References

- [1] Lars Eriksson, Lars Nielsen, and Jan Nytomt. Ignition control by ionization current interpretation. *SAE SP-1149*, (SAE paper No. 960045):73–79, 1996.
- [2] J. Auzins, H. Johansson, and J. Nytomt. Ion-gap sense in missfire detection, knock and engine control. *SAE SP-1082*, (SAE paper No. 950004):21–28, 1995.
- [3] Anson Lee and Jan S. Pyko. Engine misfire detection by ionization current monitoring. *SAE SP-1082*, (SAE paper No. 950003):9–19, 1995.
- [4] Nick Collings, Steve Dinsdale, and Tim Hands. Plug fouling investigations on a running engine - an application of a novel multi-purpose diagnostic system based on the spark plug. *SAE paper No. 912318*, 1991.
- [5] A. Saitzkoff, R. Reinmann, T. Berglind, and M. Glavmo. An ionization equilibrium analysis of the spark plug as an ionization sensor. *SAE paper No. 960337*, 1996.
- [6] M. Hubbard, P. D. Dobson, and J. D. Powell. Closed loop control of spark advance using a cylinder pressure sensor. *Journal of Dynamic Systems, Measurement and Control*, pages 414–420, December 1976.
- [7] I. Glaser and J. D. Powell. Optimal closed-loop spark control of an automotive engine. *SAE paper No. 810058*, pages 11–21, 1981.
- [8] K. Sawamoto, Y. Kawamura, T. Kita, and K. Matsushita. Individual cylinder knock control by detecting cylinder pressure. *SAE paper No. 871911*, 1987.

## A Torque Variance

Given the relation between the PPP (peak pressure position),  $x_P$ , and the output torque,  $y_T$ ,

$$y_T = -c \cdot (x_P - x_{\max})^2 + y_{\max} \quad (4)$$

an equation for the standard deviation of the output torque,  $\sigma_T$ , will be derived. The key part is to describe how  $\sigma_T$  depends on how much the mean PPP is offsetted from optimum.

One good assumption is that the variations in PPP can be described by a Gaussian distributed stochastic variable

$$X_P \in N(m_P, \sigma_P)$$

with mean value  $m_P$  and standard deviation  $\sigma_P$ .

Using Equation 4 to transform the stochastic variable for the peak pressure position,  $X_P$ , to a stochastic variable for the output torque,  $Y_T$ .

$$Y_T = -c \cdot (X_P - x_{max})^2 + y_{max}$$

We are interested in investigating the variance when the mean peak pressure position is placed  $d$  degrees from optimum. This means that we have a stochastic variable with a mean value of,  $m_P = x_{max} + d$ . Now  $X_P - x_{max}$  can be rewritten to  $X_P - x_{max} = X_0 + d$ ,  $X_0 \in N(0, \sigma_P)$ . Which gives the following transformation of the stochastic variable

$$Y_T = -c \cdot (X_0 + d)^2 + y_{max}$$

### Useful identities

In the following let  $X \in N(0, \sigma)$ , and also note that  $E[X] = 0$  and  $E[X^3] = 0$  which gives the following

$$\frac{X}{\sigma} \in N(0, 1) \Rightarrow \left(\frac{X}{\sigma}\right)^2 \in \chi^2(1)$$

$$\text{Var}[X^2] = \sigma^4 \cdot \text{Var}\left[\left(\frac{X}{\sigma}\right)^2\right] = \sigma^4 \cdot 2$$

$$\begin{aligned} \text{Var}[Y] &= E[(Y - m_Y)^2] = E[Y^2] - E[Y]^2 \\ &\Leftrightarrow E[Y^2] = \text{Var}[Y] + E[Y]^2 \end{aligned}$$

$$\text{Var}[Z^2] = E[Z^4] - E[Z^2]^2 \Leftrightarrow E[Z^4] = \text{Var}[Z^2] + E[Z^2]^2$$

$$\begin{aligned} E[(X + d)^2] &= E[X^2 + 2Xd + d^2] \\ &= E[X^2] + 2dE[X] + d^2 \\ &= E[X^2] + d^2 \end{aligned}$$

$$\begin{aligned} E[(X + d)^4] &= E[X^4 + 4X^3d + 6X^2d^2 + 4Xd^3 + d^4] \\ &= E[X^4] + 6d^2E[X^2] + d^4 \end{aligned}$$

$$\begin{aligned} \text{Var}[(X + d)^2] &= E[X^4 + 6d^2X^2 + d^4] - E[(X + d)^2]^2 \\ &= 2\sigma^4 + 4d^2(\text{Var}[X] + E[X^2]) \\ &= 2\sigma^4 + 4d^2\text{Var}[X] \\ &= 2\sigma^4\left(1 + 2\frac{d^2}{\sigma^2}\right) \end{aligned}$$

### Variance Formula

Using the identities above the variance of  $Y_T$  can be calculated

$$\begin{aligned}\sigma_T^2 &= \text{Var}[Y_T] = \text{Var}[-c \cdot (X_0 + d)^2 + y_{\max}] \\ &= c^2 \cdot \text{Var}[(X_0 + d)^2] = 2c^2 \sigma_p^2 (\sigma_p^2 + 2d^2) \\ &= 2c^2 \sigma_p^4 \left(1 + \frac{d^2}{\sigma_p^2}\right)\end{aligned}\tag{5}$$

where  $\sigma_p$  is the standard deviation for the peak pressure position.



# Increasing the Efficiency of SI-Engines by Spark-Advance Control and Water Injection<sup>1</sup>

Lars Eriksson<sup>†</sup> and Lars Nielsen<sup>‡</sup>

*Vehicular Systems*  
*Department of Electrical Engineering*  
*Linköping University, S-581 83 Linköping, Sweden*  
*<http://www.vehicular.isy.liu.se>*  
*<sup>†</sup>larer@isy.liu.se, <sup>‡</sup>lars@isy.liu.se*

4

## Abstract

Engine efficiency can be maximized by directly measuring in-cylinder parameters and adjusting the spark advance, using a feedback scheme based on the ionization current as sensed variable. Water injection is shown to increase the engine efficiency, if at the same time the spark advance is also changed when water is injected to obtain maximum efficiency. A spark-advance control scheme, that takes the water injection into account, is thus necessary to increase the efficiency.

---

<sup>1</sup>This is an edited version of the conference paper that was presented at *IFAC Workshop: Advances in Automotive Control (Preprints)*, pp. 211-216, Mohican State Park, Loudonville, OH, 1998.

## 1 Introduction

The efficiency of a spark ignited engine can be increased by using information from the combustion to control the spark advance. The peak pressure position (PPP) of the in-cylinder pressure trace is a parameter that indicates how efficient the spark advance is [5, 2]. This information about the combustion can be derived using the spark plug as sensor [3, 2].

The issue here is to demonstrate a new method to increase engine efficiency. The basis for the method is a combination of closed-loop spark advance control and injection of water, i.e. actively supplying water into the engine air intake. Water injection by itself will give a decrease in engine efficiency, but in combination with the spark advance controller it will be shown to increase efficiency.

Water injection is a well known method to increase engine power and efficiency at high loads and high compression ratios, the increase is achieved since water injection moves the knock limit and to gain the benefit of under these conditions it is necessary to change the spark advance. These performance limiting conditions occurs at high loads which is significantly different from the mid-load operating conditions that the scheme presented here is directed to.

## 2 Closed Loop Spark Advance Control

Under mid-load operating conditions the goal for the spark advance controller is to initiate and position the combustion in such a way that the engine output power is maximized. Different operating conditions results in different spark advance settings. Most of todays spark advance systems are based on calibrated fixed lookup tables, that accounts for some of the parameters effecting the spark advance.

The *Peak Pressure Position Principle* introduced by [5] states that a spark advance control scheme that maintains a constant Peak Pressure Position (PPP) is very close to optimum. This fact has been verified under different operating conditions for the SAAB 2.3 l engine in our laboratory [2], showing that the optimum PPP lies in the range  $14 - 16^\circ$  after top dead center (ATDC). The spark advance control problem is thus rephrased to controlling the spark advance such that the PPP appears at a given crank angle. Such schemes have not yet been proved cost effective, due to the cost of an additional in-cylinder pressure sensor.

### 2.1 Ionization current interpretation

The ionization current, obtained by applying a DC bias on the spark plug and measure the current that flows through the circuit, is a direct measure of in-cylinder combustion properties. The resulting signal has a complex shape and it also influenced by the in-cylinder pressure. A pattern recognition scheme that extracts information about the peak pressure position from the ionization current has been presented in [3]. The scheme has been validated showing that the peak pressure position can be controlled to the desired positions by a spark advance controller only using information obtained from the ionization current [1, 2]. A key idea in

the pattern recognition scheme is to fit a parameterized model of the ionization current signal to the actual measured signal and interpret the received parameter values.

Ionization current is already measured in production cars and the scheme therefore only requires further signal interpretation in the electronic engine control unit.

### 3 Experimental Setup

To inject water into the engine a sprayer is used. The sprayer is originally a color sprayer that has a valve which delivers a liquid spray. This liquid spray is further atomized by two opposing holes that blows pressurized air on the spray. Figure 1 shows a photo of the sprayer with the water spray, and a schematic enlargement of the sprayer nozzle with the liquid spray and the pressurized air. The liquid is not fully atomized by the pressurized air but the droplets are made much smaller. The container of the sprayer is mainly made of aluminum, while most other parts of the sprayer are made of stainless steel.

In Figure 2 the water injection setup is shown together with the engine. As can be seen in the figure, the injection procedure is carried out by hand. The water spray is directed into the induction system towards the throttle plate. The water spray is then drawn, by the lower pressure, into the intake manifold.

The amount of water sprayed into the engine was not measured but it had no audible effect on the engine during the tests. Though, there were enough water present to change the in-cylinder pressure trace so that the mean peak pressure position moved to a position around four to five degrees later.

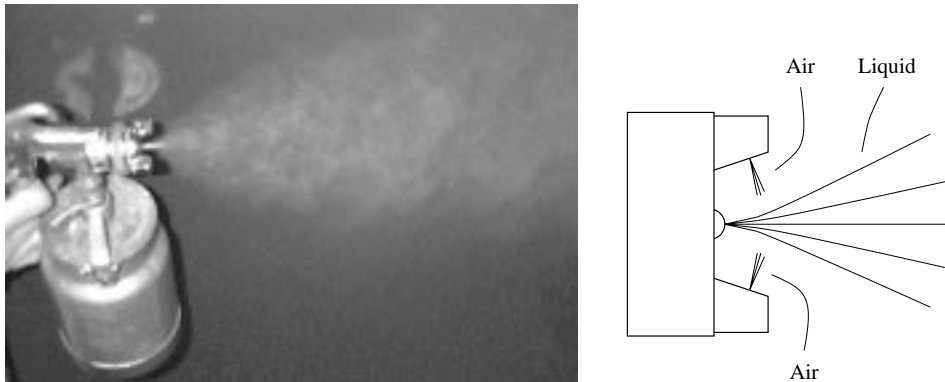


**Figure 1** Left: A picture of the sprayer spraying water. Right: A schematic figure of the sprayer nozzle with the liquid spray, pressurized air, and the atomized liquid drops.

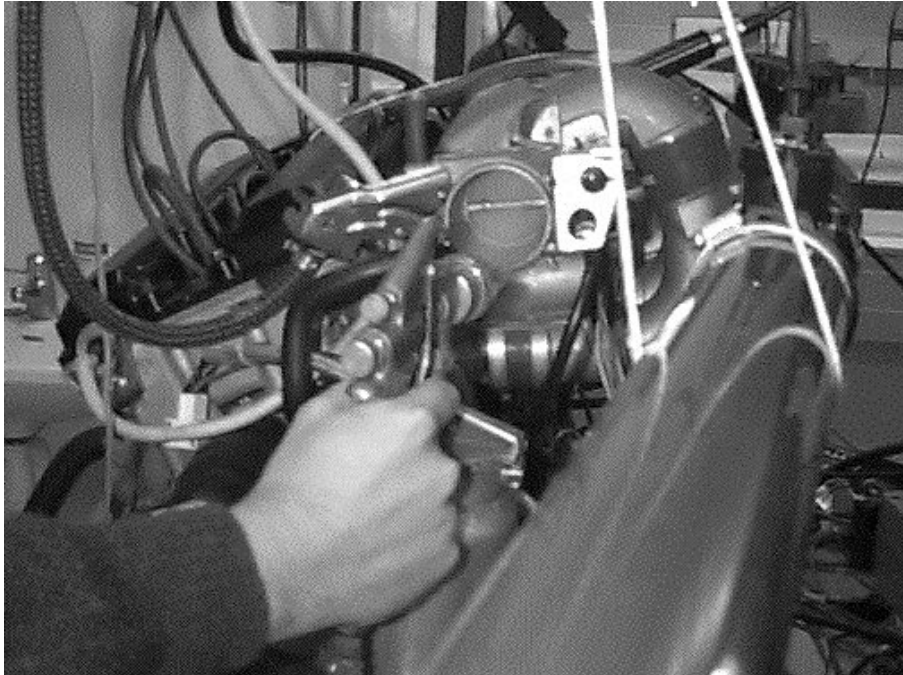


**Figure 2** The sprayer is directed towards the intake port and throttle plate. At the lower side of the throttle plate, the spray of water can be seen as a pale shade of gray. When the picture was taken the engine ran at steady state with speed 1500 rpm and load 50 Nm.

## 4 Water Injection Experiments

During all test cycles shown in Figures 3, 4, and 5, the throttle angle and the injection time are held constant. The engine speed is also held constant by a controller for the dynamometer. The engine is running at steady state and the A/F ratio is tuned to  $\lambda = 1$  before the test cycle starts, and then the injection time is locked and held constant during the test cycle.

### 4.1 Test cycle 1

Figure 3 shows a large part of the test cycle. The speed and load condition is 1500 rpm and 55 Nm. Initially in the test cycle, the spark advance controller is running and the controller changes the spark advance controlling the peak pressure position close to MBT, i.e.  $16^\circ - 17^\circ$  after TDC. The ionization current is used as input to the controller, and the in-cylinder pressure is only used for validation. Around cycle number 100 the spark advance controller is turned off and the con-

troller holds the present value. Around cycle 250 the spraying of water is started. Note that the peak pressure position is moved to a position  $4^\circ$  later and that the output torque decreases. Around cycle 400 the spark advance controller is turned on again and it controls the peak pressure position back to its optimal value. The controller needs to change the spark advance with around  $5^\circ$  to get back to the optimal position.

Around cycle 550 the water spraying stops. This can be seen in the figure when the change in spark advance starts to decrease. When the water spraying stops it takes a while before all water has passed through the system, in the figure it can be seen that the states asymptotically goes back to their initial conditions.

The signals: PPP, output torque, manifold pressure, and lambda has been filtered off-line with a non-causal filtering procedure with zero phase shift. This filtering procedure is included in the signal processing toolbox in Matlab. The filter that is used is a Butterworth filter with order 3, and with normalized cut-off frequency at 0.3.

## 4.2 Test cycle 2

Another test cycle is shown in Figure 4, where the speed and load conditions also are 1500 rpm and 55 Nm. Only the part of the test cycle showing the water spraying and the controller switching on and off is displayed in the figure. The test cycle that has been run is the same as described above, but in this test the reference value of the controller is changed one degree to  $17^\circ$  after TDC.

At cycle 50 the controller is turned off and the spark advance is held at its present value. At cycle 250 the water spraying is started, and two things can be noted at this point. Firstly, which is the most important point is that the PPP moves 4 degrees. Secondly, that the actual spark advance changes in the wrong direction due to the change in intake pressure. When the controller is turned off, the spark advance can be viewed as a pre-calibrated schedule with a spark advance close to MBT. The parameters that affect the spark advance is then the engine speed and the manifold pressure. Note that the calibrated scheme changes the spark advance in the wrong direction, since increased manifold pressure indicates higher load and therefore less spark advance.

The spark advance controller is switched on again at cycle 500. The PPP is controlled to  $17^\circ$  ATDC by using information from the ionization current. Note that the output torque increases when the controller is switched on, since the spark advance goes back to a point close to optimum.

## 4.3 Test cycle 3

In Figure 5, a test cycle with a different load condition is displayed. The operating condition is 1500 rpm and 38 Nm, and the desired peak pressure position is  $16^\circ$  after TDC. The same effect as in Figure 4 can be seen: the presence of water moves the peak pressure position, and the controller compensates for the changed environmental condition and increases the output torque.

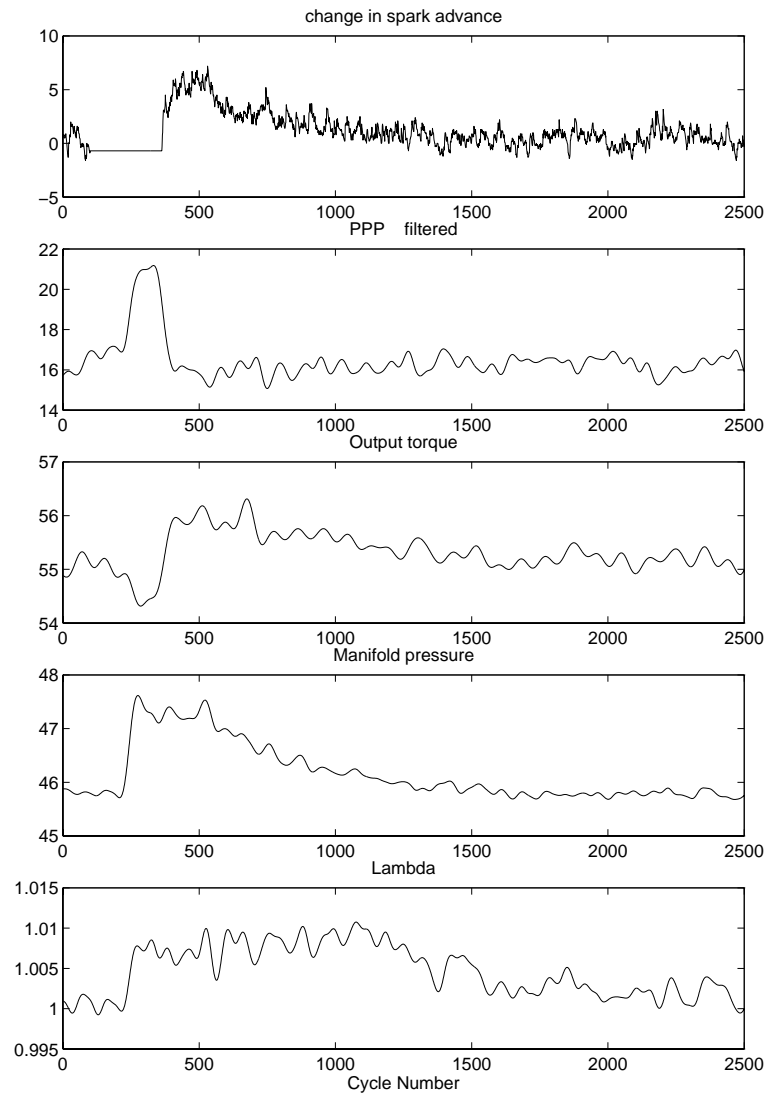


**Figure 3** A large part of the test cycle is displayed. The spark advance controller is shut off around cycle 100 and the spark advance is held constant. The water spraying starts around cycle 250 which leads to increased PPP and decreased output torque. The spark advance controller is switched on around cycle 400, controlling PPP back to MBT leading to increased output torque. The water spraying stops around cycle 550 and the parameters asymptotically goes back to their initial conditions, when the water still in the system, e.g. deposited on walls, decreases.

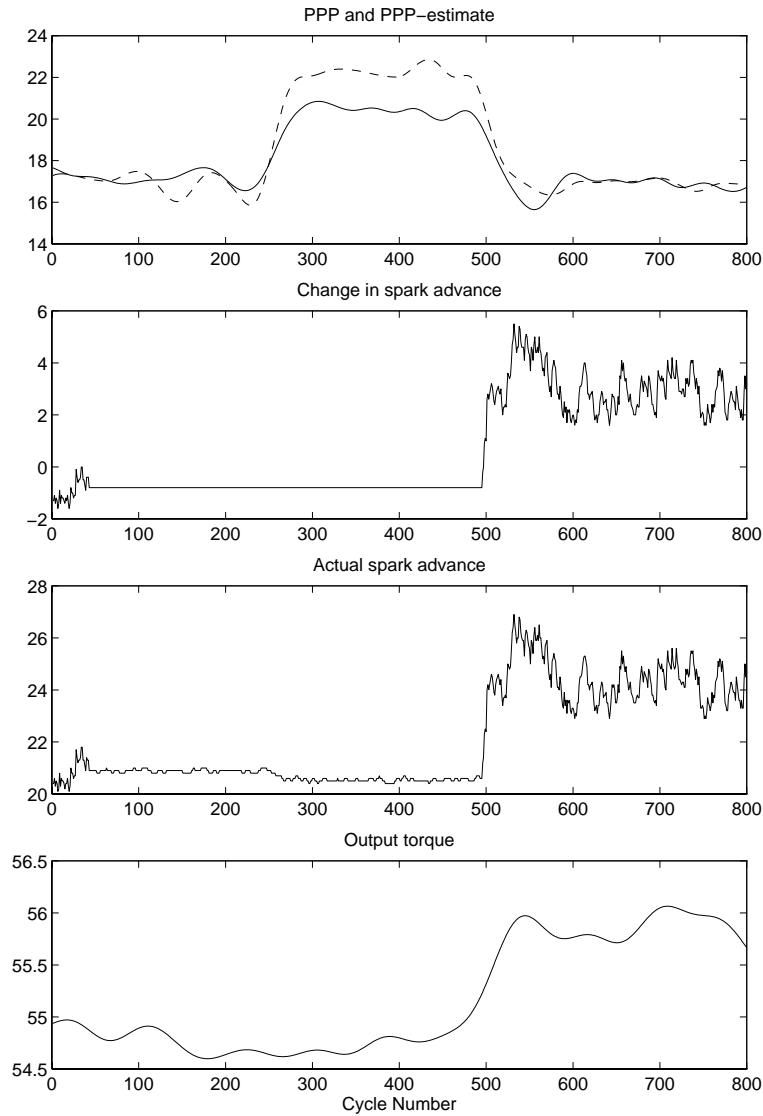


**Figure 4** The interesting part of the test cycle. The spark advance controller is switched off at cycle 50 and the water injection starts at cycle 250. The controller is switched on again around cycle 500, controlling PPP to MBT which increases the output torque.

## 5 Torque Increase

In all three figures the start of the controller increases the output torque with 1.5–3 % above the initial level. The increase in power just by adding water and controlling the spark advance may seem surprising at first but it comes from different sources. In Figure 3 it is shown that the A/F ratio increases which increases the fuel conversion efficiency, and since the amount of fuel is constant this implies an increase in output torque. A 1 % increase in A/F can change the fuel conversion efficiency with 0.4 % (this increase is derived from [4] page 182).

Figure 3 also shows that the manifold pressure increases with 2 %. Increasing the manifold pressure lowers the losses to the pumping work, indicating that the output torque should increase. In the figure it can be seen that the manifold pressure does not drop directly when the spraying stops, instead it slowly decreases as the water evaporates. Hence, it is the presence of water in the intake manifold that raises the pressure and not that the sprayer blows air and water on the throttle plate.

The presence of water also cools the air which, for the same pressure, makes the air density higher. The lower temperature and the presence of water also have a favorable influence on the thermodynamic cycle which increases the output torque.

Important to note is that to get the increase in output torque with water injection, it is necessary to change the spark advance to gain the benefits. In Figure 3 the output torque actually decreases when the water is injected, the increase in efficiency comes when the spark advance controller is switched on.

## 6 Conclusions

Spark advance control utilizing the spark plug as sensor in combination with water injection has been shown to increase the efficiency of the engine. The spark control algorithm compensates for the changes in burn rate of the combustion, and the spark advance for the engine is controlled close to optimum using feedback.

The results give a new method to actively increase engine efficiency by combining water injection with ionization current based spark advance control.

## References

- [1] Lars Eriksson. A real-time platform for spark advance control. Technical Report LiTH-R-1938, ISSN 1400-3902, Department of Electrical Engineering, 1997.
- [2] Lars Eriksson, Lars Nielsen, and Mikael Glavenius. Closed loop ignition control by ionization current interpretation. *SAE SP-1236*, (SAE paper No. 970854):159–166, 1997.
- [3] Lars Eriksson, Lars Nielsen, and Jan Nytomt. Ignition control by ionization current interpretation. *SAE SP-1149*, (SAE paper No. 960045):73–79, 1996.

- 
- [4] J. B. Heywood. *Internal Combustion Engine Fundamentals*. McGraw-Hill series in mechanical engineering. McGraw-Hill, 1988.
  - [5] M. Hubbard, P. D. Dobson, and J. D. Powell. Closed loop control of spark advance using a cylinder pressure sensor. *Journal of Dynamic Systems, Measurement and Control*, pages 414–420, December 1976.

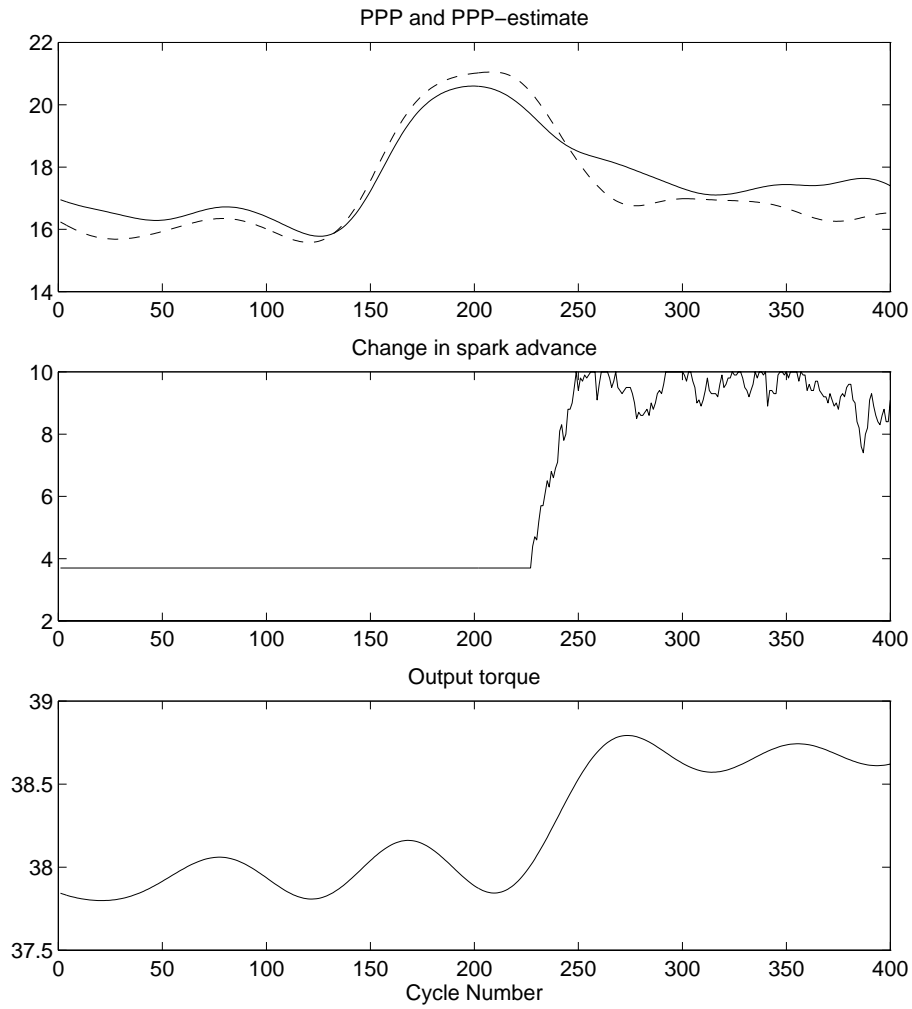


**Figure 5** The interesting part of the test cycle. This test is run at a lower load condition than the tests shown in Figures 3 and 4, with output torque 38 Nm. The water injection starts around cycle 150 and the spark advance controller is switched on around cycle 225. The increase in output torque when the controller is switched on can also be observed here.

# An Ion-Sense Engine-Fine-Tuner<sup>1</sup>

Lars Nielsen and Lars Eriksson

*Vehicular Systems*

*Department of Electrical Engineering*

*Linköping University, SE-581 83 Linköping, Sweden.*

## Abstract

Combustion engines are highly engineered complex system. Many variables like engine speed and load are measured, but there are many other variables influencing engine performance that are not measured. One such variable that strongly influences efficiency and power is air humidity. Even with such varying unmeasured variables, it is well known that a skilled human mechanic can diagnose and fine tune a car according to the environment and circumstances at a certain place and day. Inspired by these skills in combination with the development of computing power, it is possible to think of virtual engine-doctors and virtual engine-fine-tuners. Here an ion-sense engine-fine-tuner has been developed based on spark advance feed-back control using ionization current interpretation. It is shown, as a main result, that it can control the engine back to its optimal operation even when subjected to humidity in the intake air.

5

---

<sup>1</sup>This is an edited version of the article that was published in *IEEE Control Systems Magazine*, Vol. 18, no. 8, Oct 1998.

## 1 Introduction

Environmental issues and lower fuel consumption require improved combustion engines. Several trends desire use of feed back control directly from the combustion instead of using indirect measurements as is mostly done today. The development is based on new sensors or improved interpretation of available sensor signals. One example is ionization current sensing which is obtained by applying a sense voltage on the spark plug when it is not used for firing. The sensed current depends on the ions created, on their relative concentration and recombination, on pressure, and on temperature to mention some of the more important factors. The signal is very rich in information but also complex to analyze.

The main result of this paper is real-time closed loop demonstration of spark advance control by interpretation of ionization current signals. It is shown to be able to handle variations in air humidity, which is a major factor influencing burn rates, and consequently pressure build-up and useful work transferred via piston to drive shaft. This leads to a clear improvement in engine efficiency compared to traditional systems using only engine speed and load. The experiments are performed on a SAAB 2.3 l, normally aspirated, production engine.

Inspired by the type of challenges and potential usefulness in interpretation of ionization current signals, the paper starts in Section 2 with an outlook. Thereafter, the presentation focuses in on closed loop ignition control by ionization current interpretation. Section 3 deals with the basics of ionization currents. Spark advance control is treated in Section 4, especially principles relating pressure information to efficiency. Section 5 presents the structure of the ion-sense spark advance controller. Experimental demonstrations are found in Section 6, and conclusions are drawn in Section 7.

## 2 Outlook on Diagnosis and Feed-back Control

The main message in this outlook section is: Research in modern engine control is challenging and fun! It is not the case that engine development is so mature that everything has been tested already. Instead, the availability of computing power has revolutionized the possibilities of sensor interpretation and combination. Another, perhaps more common, saying within the field is that engines are so difficult and complex that analysis of combustion quality, for example, is almost hopeless. Nevertheless, progress is being made that leads to the ideas of virtual engine-doctors and virtual engine-fine-tuners.

### 2.1 Virtual Engine-Doctors

Engines are difficult and complex, but before ruling out interpretation of complex signals one could consider the progress in human medicine. A medical doctor can draw conclusions from measurements like EEG or EKG, that are indirect crude clues to what is going on inside the body. Engine measurements, like e.g. ionization currents being in-cylinder engine measurements, are signals that are more

directly coupled to the physics and chemistry of the process of interest i.e. the combustion (see Figure 1). Virtual engine-doctors that detect and diagnose serious

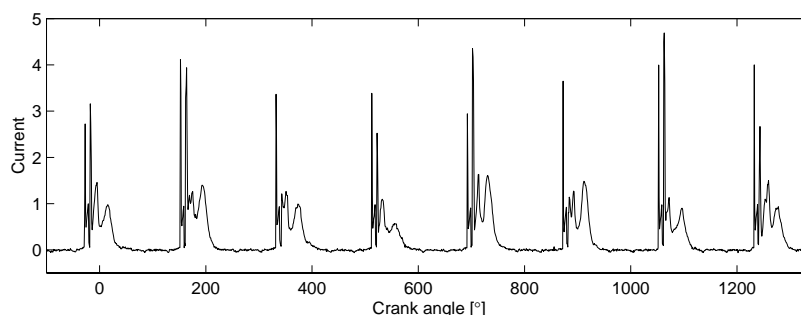


**Figure 1** A medical doctor can from measurements like EEG or EKG, that are crude compared to human complexity, draw many conclusions. Ionization currents, like the one in the figure, are in-cylinder engine measurements that are directly coupled to the combustion. Virtual engine-doctors and virtual engine-fine-tuners are now being developed.

malfunctions like knock that will destroy the engine and misfire that will destroy the catalyst, are not a farfetched idea in that perspective. They also already exist. Ionization current interpretation can be used for both purposes. Knock is a pressure oscillation in the cylinder with a frequency determined by the geometry of the combustion chamber. The oscillation is present in the current measurement and can be extracted mainly by using a band pass filter in a well chosen time window of the current signal. When there is a misfire, then there are no resulting ions and hence no current which is easily detected. These systems are already used in production cars [1, 10]. Therefore, the basic hardware is already available and to develop a virtual engine-doctor for combustion requires only additional signal interpretation in the electronic engine control unit (ECU), Figure 2.

## 2.2 Virtual Engine-Fine-Tuners

The term virtual engine-fine-tuner is more inspired by a skilled auto mechanic than a medical doctor. A human performing the task of tuning an engine, e.g. for best performance, would use several clues like test measurements and the sound of the engine, but also experience, e.g. about the actual weather situation. The result can typically be an increase of several percent in engine efficiency. One way to achieve engine tuning that has been shown previously is to use feedback schemes that use a pressure sensor [8, 7, 16], but these systems have not yet been proven cost effective due to expensive pressure sensors.

With the increasing computational power it is now becoming possible to do engine tuning by feed back control from more advanced interpretation of signals

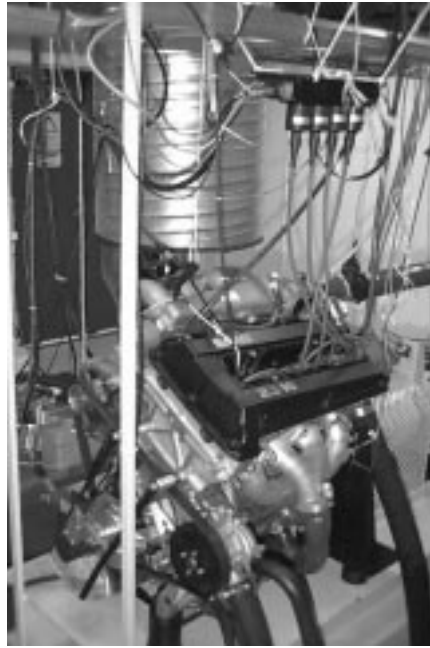


**Figure 2** *The introduction of computerized engine controllers (here above the engine) has revolutionized the engine control era. Already today they represent an impressive computing power and the development continues.*

to take care of circumstances previously not possible to easily measure. A multi-sensor idea is developed where a basic signal, like engine speed or ionization current, is measured and several other sensor signals can be deduced from it (Figure 3). Variations in engine speed together with crank shaft models can be used to conclude misfire by for example lacking torque pulse or to estimate cylinder pressure from derived torque fluctuations [18, 2]. Usage of the spark plug as an integrated actuator and sensor leading to ionization current interpretation is the path taken here.

The rest of the paper is thus about one example of continuous engine tuning. Ionization current interpretation is used to derive in-cylinder pressure characteristics, and this information is used for feed back control to optimize engine efficiency, compensating for example for air humidity.

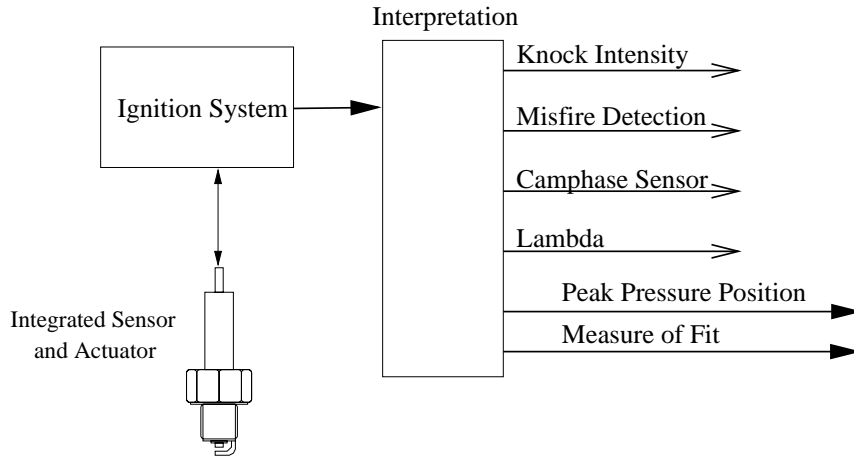
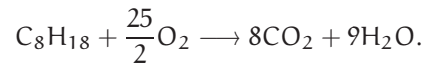


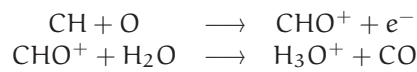
**Figure 3** The spark plug can, using signal interpretation, function as sensor for several parameters. Knock intensity and misfire are already implemented in production cars as a basis for virtual engine-doctors. Lambda sensing and peak pressure position estimation can be used in virtual engine fine tuners. The peak pressure position (and a quality measure of it) is the information used in this paper.

### 3 Ionization current

In an ideal combustion reaction, hydrocarbon molecules react with oxygen and generate only carbon dioxide and water, e.g. isoctane gives



In the combustion there are also other reactions present, that include ions, which go through several steps before they are completed; some examples are [17]



These ions, and several others, are generated by the chemical reactions in the flame front. Additional ions are created when the temperature increases as the pressure rises.

The processes creating the ionization current are complex and are also varying from engine cycle to engine cycle. Figure 4 shows ten consecutive cycles of the cylinder pressure and the ionization current operating at constant speed and load. As can be seen, the cycle-by-cycle variations are significant. An important part of this paper is to derive pressure characteristics from ionization current.

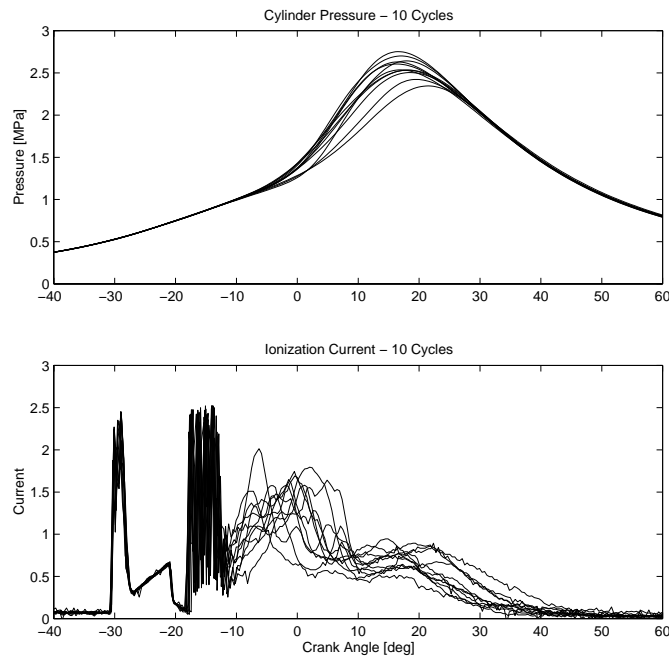


**Figure 4** Cycle to cycle variations are always present in the combustion. The plots show ten consecutive cycles at stationary engine operation that clearly exhibit the cyclic variations.

### 3.1 Detection

To detect the ions, a DC bias is applied to the spark plug, generating an electrical field. The electrical field makes the ions move and generates an ion current. A schematic illustration is shown in Figure 5 (a). The current is measured at the low-voltage side of the ignition coil, and does not require protection from the high-voltage pulses in the ignition, Figure 5 (b). Ionization current measurement systems are already in use in production engines for: individual cylinder knock control, cam phase sensing, pre-ignition detection, and misfire/combustion quality/lean limit [1]. Also, work on detection of spark plug fouling by using the ionization current has been reported [3].

The ionization current is an interesting engine parameter to study. It is a direct measure of the combustion result that contains a lot of information about the combustion, and several challenges remain in the interpretation of it. Some of the parameters that affect the ionization current are: temperature, air/fuel ratio, time since combustion, exhaust gas recycling (EGR), fuel composition, engine load, and several others.

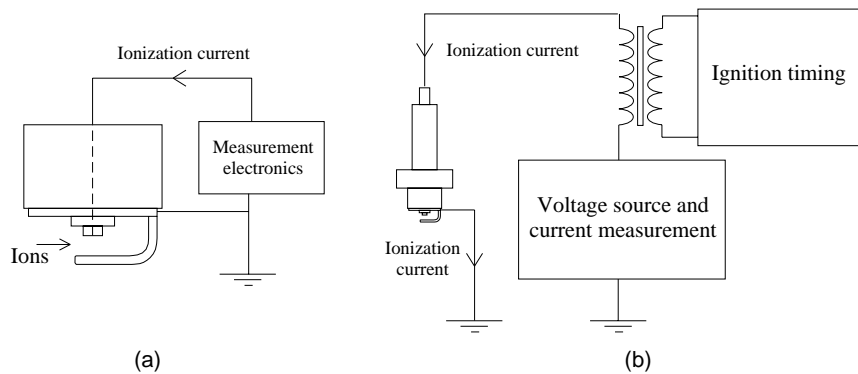


**Figure 5** Measurement of the ionization current. (a) The spark plug-gap is used as a probe. (b) Measurement on the low voltage side of the ignition coil.

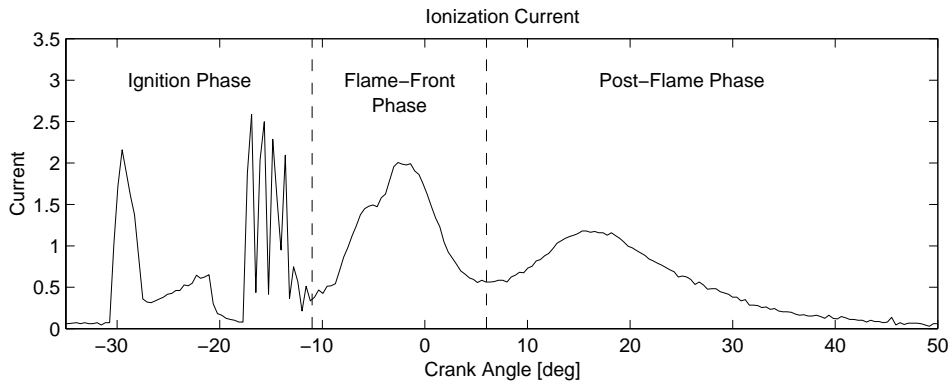


**Figure 6** Ionization current showing three clear phases, ignition, flame front, and post flame.

### 3.2 Ionization Current Terminology

The ionization current typically has three phases: a phase related to ignition, a phase related to ions from the flame development and propagation, and a phase related to pressure and temperature development. In Figure 6, the three phases of the ionization current are displayed. Each of these phases has varying characteristics and they also mix together in complicated ways. In the ignition phase, the ionization current is large, with reversed polarity. Due to the high current in the ignition the measured signal shown in the figure is limited. What can be seen in Figure 6 is the ringing phenomenon in the coil after the ignition.

In the flame-front phase, the high level of ions associated with the chemical re-

actions in the flame produces one or more characteristic peaks. The ions generated by the flame have different recombination rates. Some ions recombine very quickly to more-stable molecules, while others have longer residual times. The result is a high peak which after some time decays as the ions recombine.

In the post-flame phase the most stable ions remain, generating a signal that follows the cylinder pressure due to its effect on the temperature and molecule concentration. Ions are created by the combination of the measurement voltage and the high temperature of the burned gases, since the temperature follows the pressure during the compression and expansion of the burned gases, i.e when the flame propagates outwards and the combustion completes. The ionization current thus depends on the pressure.

### 3.3 Ionization current modeling

The ionization current can be studied by thermodynamical and chemical kinetic modeling [14, 15, 13]. Concentrating on the pressure-related post-flame phase, an analytical expression for the ionization current has been presented. Some of the fundamental assumptions in the model are that the gas in the spark plug is: fully combusted, in thermodynamic equilibrium, undergoes adiabatic expansion, and that the current is carried in a cylinder extending from the central electrode of the spark plug [14]. Given the cylinder pressure, the analytical expression for the ionization current is

$$\frac{I}{I_m} = \frac{1}{\left(\frac{p}{p_m}\right)^{\frac{1}{2} - \frac{3}{4} \frac{\gamma-1}{\gamma}}} e^{-\frac{E_i}{2kT_m} \left[ \left(\frac{p}{p_m}\right)^{-\frac{\gamma-1}{\gamma}} - 1 \right]}. \quad (1)$$

Where:

$I$ ,	Ionization current	$I_m$ ,	Ionization current maximum
$p$ ,	Cylinder pressure	$p_m$ ,	Cylinder pressure maximum
$T_m$ ,	Maximum temperature	$\gamma$ ,	Specific heat ratio
$k$ ,	Boltzmann's constant;	$E_i$ ,	Ionization energy.

#### Interpretation model

A key step in our method for deducing information is to use parameterized functions based on a phenomenological description of the ionization current, i.e. the signal consists of two combustion related phases. These functions must be rich enough to capture the different variations, but they must also be such that the relevant information can be extracted. The parameterized functions are used to separate out the different phases of the ionization current, and to get an estimate of the pressure. As a model, with 6 parameters, a sum of two Gaussian functions is used

$$I(\theta) = \alpha_1 e^{-\frac{1}{\alpha_2}(\theta - \alpha_3)^2} + \beta_1 e^{-\frac{1}{\beta_2}(\theta - \beta_3)^2} \quad (2)$$

Note that this model is not based on combustion physics with respect to the flame-front phase. Even though this may seem ad hoc, the model is physically motivated

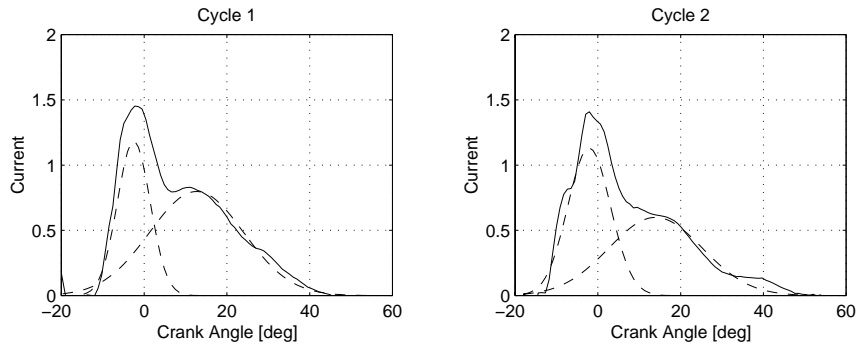


**Figure 7** Components of the model (Equation (2)) that captures the appearance and the phases of the ionization current.

in [5] with regard to pressure information. Measured pressure traces are recalculated to ionization currents using Equation (1), and the result is shown to be close to a Gaussian function.

For ionization current interpretation, the model, Equation (2), is fitted to the measured ionization current. Figure 7 shows two ionization currents together with the Gaussian components of the model. The first component corresponds to the flame-front phase and the second to the post-flame phase. This second part, corresponding to the post-flame phase, is the experimentally and physically motivated basis for obtaining pressure information.

## 4 Spark Advance Control

Spark-advance control deals with determination of the engine position where the spark plug shall ignite the air-fuel mixture and start the combustion. It is thus used to position the combustion and pressure trace relative to the crank shaft motion. Engine efficiency and emissions are directly affected by the spark advance, due to its influence on the in-cylinder pressure. Work is lost to heat transfer and to the compression if it is placed too early, and expansion work is lost if it is placed too late. The optimal spark advance setting depends on several parameters, e.g. engine speed, engine load, air/fuel ratio, fuel characteristics, air humidity, EGR, air temperature, and coolant temperature. Emission regulations and engine knock also affect the best spark advance setting, but this is not a topic here.

Today, most spark-advance controllers are open-loop systems, which measure a number of parameters that affect the spark advance and compensate for their effects. Extensive testing and calibration, during the design phase of the engine, results in a nominal spark-advance schedule. Such a calibrated schedule is conservative since it has to guarantee good performance over the entire range of the non-measured parameters, and also be robust to aging. If all parameters that affect

the spark advance were measured, and their effects and interactions were properly accounted for, it would be possible to determine the best spark advance. However, such a system would be too expensive due to the measurements and testing required to incorporate it in a production car.

### Feed back schemes

A different approach is to use closed-loop spark-advance control. Such a system measures the result of the spark setting rather than measuring all the parameters known to affect the spark advance. This requires measurement of parameters directly resulting from the actual combustion, such as the in-cylinder pressure or the ionization current. It is an accepted fact that the position for the pressure peak is nearly constant with the optimal spark advance, regardless of operating condition [8]. A spark-advance control algorithm that maintains a constant peak pressure position (PPP) is therefore close to optimum. Even for large changes in parameters that affect the flame speed, such a feedback scheme still maintains the optimal spark advance. This has been shown previously by using feedback schemes that utilize a pressure sensor [8, 7, 16], but these systems have not yet been proven cost effective due to expensive pressure sensors.

## 4.1 Spark Advance and Cylinder Pressure

The spark advance is used to position pressure development in the cylinder such that the combustion produces maximum work. Under normal driving conditions the mixture is ignited around  $15 - 30^\circ$  in crank angle before the piston has reached top dead center (TDC), and the pressure peak comes around 20 degrees after TDC. In Figure 8 three different pressure traces, resulting from three different spark timings, are shown. Earlier spark advance normally gives higher maximum pressures and maximum temperatures that appear at earlier crank angles.

The optimal spark advance for maximum output torque is close to SA2 for the operating point in the figure, and the resulting peak pressure position lies around  $17^\circ$  after TDC. With too early ignition timing the pressure rise starts too early and counteracts the piston movement. This can be seen for the pressure trace with spark advance SA1 where the pressure rise starts already at  $-20^\circ$  due to the combustion. There are also losses due to heat and crevice flow from the gas to the combustion chamber walls, and with an earlier spark advance the loss mechanisms start earlier reducing the work produced by the gas. Higher pressures give higher temperatures which also decrease the difference in internal energy between the reactants and products in the combustion, thus resulting in lower energy-conversion ratios. The heat loss mechanisms and the lower conversion ratio can be seen in Figure 8, at crank angles over  $30^\circ$ , where the pressure trace from the SA1 spark advance is lower than the others.

Too late ignition gives a pressure increase that comes too late so that work is lost during the expansion phase. In Figure 8, the pressure increase for spark advance SA3 starts as late as at TDC. But work is also gained due to the later

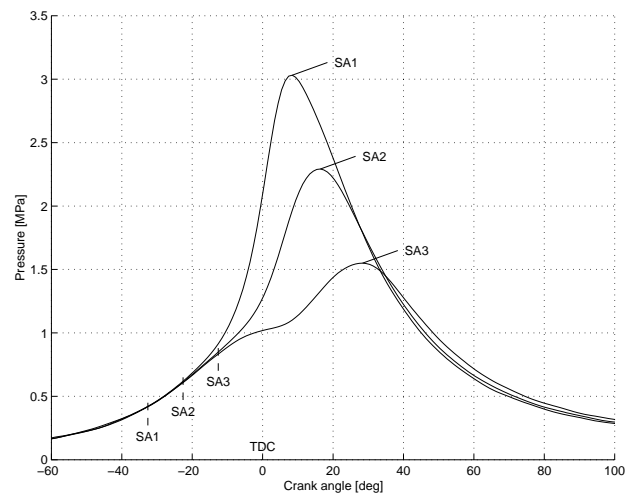


**Figure 8** Three different pressure traces resulting from three different spark advances. The different spark advances are; SA1: spark advance  $32.5^\circ$  before top dead center (TDC), SA2:  $22.5^\circ$  before TDC, SA3:  $12.5^\circ$  before TDC. The optimal spark advance is close to SA2.

start of the effects mentioned above, which also can be seen in the figure. The pressure trace from the spark advance, SA3, is higher than the others at crank angles over  $30^\circ$ . However, this gain in produced work can not compensate for the losses early in the expansion phase.

## 4.2 Peak Pressure Concept

Thus, optimal spark advance positions the pressure trace in a way that compromise between the effects mentioned above. To define the position of the in-cylinder pressure relative to TDC, the peak pressure position (PPP) is used, Figure 9. The PPP is the position in crank angle where the in-cylinder pressure takes its maximal value. There also exist other ways of describing the positioning of the combustion relative to crank angle, e.g. based on the mass fraction burned curve.

## 4.3 Engine-tuning for efficiency

Development of an engine-fine-tuner for efficiency requires experiments to describe optimal engine output. Such a description is the basis for determining the set-point values to be used in the feed back scheme. In Figure 10, mean values, over 200 cycles, of the PPP are plotted together with the mean value of the produced torque at four different operating points covering a large part of the road load operating

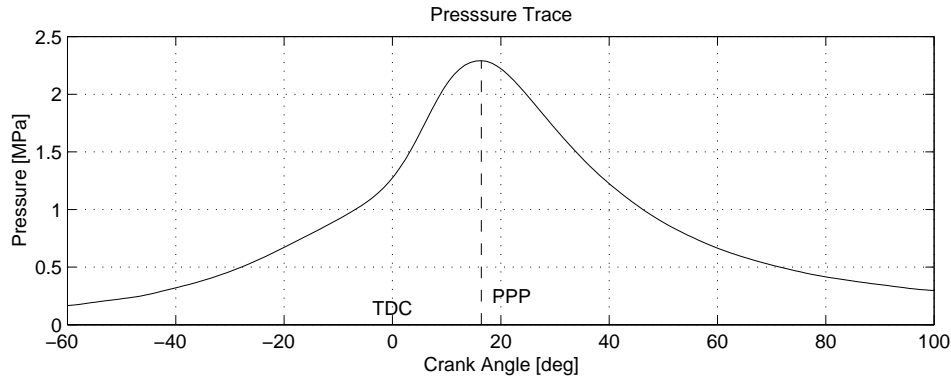


**Figure 9** The PPP (Peak Pressure Position) is the position in crank angles for the pressure peak. It is one way of describing the position of the pressure trace relative to crank angle.

range for the engine. Two of the operating points have an engine speed of 1500 rpm with different throttle angles, and for the two other operating points the engine speed is doubled to 3000 rpm. The PPP for maximum output torque in the figure lies around  $15^\circ$  ATDC (after TDC) for all these operating points.

Note that the load and speed are changed over large intervals, and that the PPP for maximum output torque at the different operating points does not differ much. The PPP versus torque curve is flat around the position for the maximum. Therefore a spark schedule that maintains a constant PPP at  $15^\circ$  is close to optimum. Considering only the work produced, this motivates that an optimal spark schedule maintains almost the same position for the peak pressure [8]. However, the optimal PPP changes slightly with the operating points. The efficiency can thus be improved a little bit further by mapping the optimal PPP for each operating point, and provide these values as reference signal to the spark timing controller. The peak pressure positioning principle can also be used for meeting emission standards. In [7] this question is addressed by rephrasing the emission regulations on the spark advance to desired peak pressure positions.

#### 4.4 Principle Study of Variations

The experiments in Figure 10 are interesting not only for determining the optimal point. They can also be used to illustrate the effect of cycle-by-cycle variations, which limits the performance of SI Engines [11, 9]. Recall that these variations are significant as previously illustrated in Figure 4.

The following principle study illustrates that variations in the output torque are smaller when the mean PPP is held at its optimum. In Figure 11, a quadratic polynomial is plotted, which is the same as those in Figure 10. The polynomial

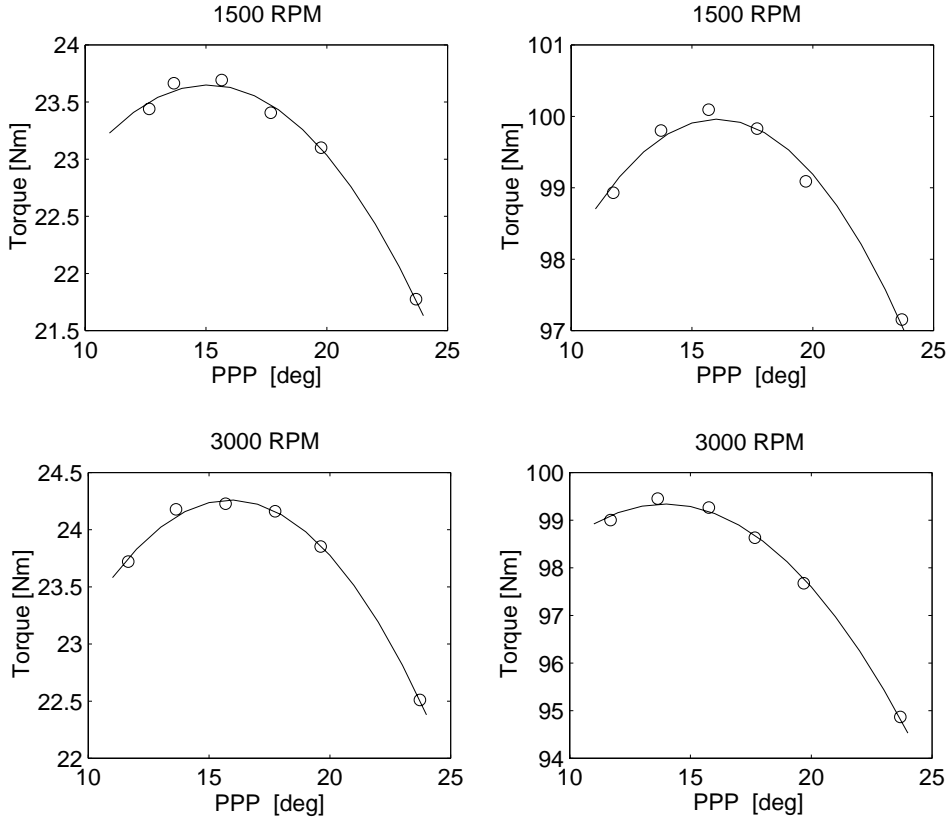


**Figure 10** Mean PPP (Peak Pressure Position) and output torque for 1500 rpm and 3000 rpm and two different engine load conditions. Each circle is a mean value from 200 consecutive cycles with the same ignition timing. The optimal mean PPP is close to  $15^\circ$  for all loads, even though the spark advance differs a lot.

represents an idealized relation between the PPP,  $x_p$ , and the output torque,  $y_T$ . The polynomial can be parameterized as

$$y_T = -c \cdot (x_p - x_{max})^2 + y_{max}$$

Using this equation the standard deviation of the variations in the output torque,  $\sigma_T$ , can be derived as a function of the standard deviation of PPP,  $\sigma_p$ , and the deviation of PPP from the optimal,  $d$ , [6]

$$\sigma_T^2 = 2c^2 \sigma_p^2 (\sigma_p^2 + 2d^2) \quad (3)$$

Equation (3) gives a useful rule of thumb, and another useful quantification of the value of spark advance feedback control. The interpretation is that the influence of

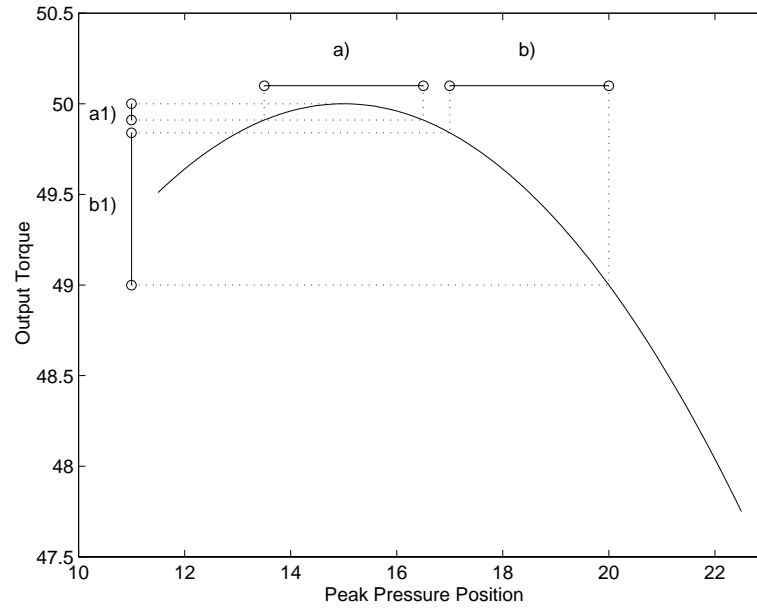


**Figure 11** The figure illustrates that when the mean PPP (peak pressure position) is at optimum the variations in the output torque are minimal. At a) the mean peak pressure position lies at optimum which give small variations in output torque at a1). At b) the mean peak pressure position lies some degrees off from optimum and the resulting variations are larger at b1).

cycle-to-cycle variations in PPP on the output torque is minimal if the mean peak pressure position is controlled to its optimal value  $d = 0$ .

The conclusion is that if an engine is not kept at its optimum point then not only is efficiency lost. It also increases variability that leads to harsher operation, which of course is not desired for driveability reasons.

## 5 Structure and Design of Engine-Fine-Tuner

The developed engine-fine-tuner relies on ionization current interpretation to obtain an estimate of the peak pressure position (PPP), and it relies on the analysis in mainly Section 4.3 to obtain set-points and feed forward values.

### 5.1 PPP Estimate

The ionization current interpretation method is presented in somewhat more detail in [5]. The phenomenological model in Equation (2) is fitted to the measured

ionization current, and the model parameters  $\alpha_1, \alpha_2, \alpha_3, \beta_1, \beta_2, \beta_3$  corresponding to the flame front and post-flame phases are extracted. The second phase, the post-flame phase, is used as the estimate of the in-cylinder pressure development.

In Figure 12, the peak pressure position (PPP) estimate from the ionization interpretation algorithm is compared to the measured PPP. For the experiments

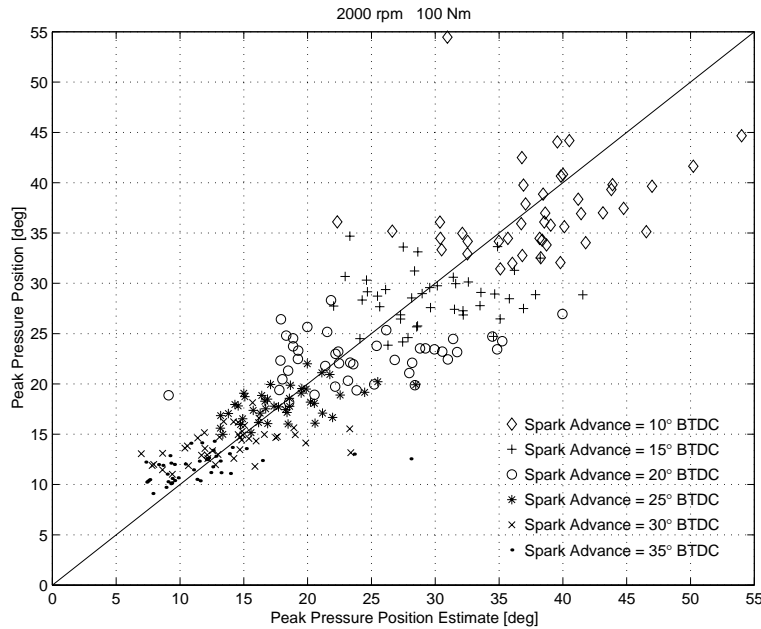


**Figure 12** The peak pressure position estimated from the ionization current compared to the measured. Each point corresponds to the estimated and true PPP for one cycle. Close to 500 cycles are displayed in the plot. One to one correspondence is indicated by the solid line.

shown in the figure the engine speed and the throttle angle are held constant, and the ignition timing is positioned at six different spark timings from 35° BTDC (before TDC) to 4° BTDC. The resulting PPPs range from 7° ATDC (after TDC) to 55° ATDC as can be seen in the figure. The estimate correlates quite well with the measured peak pressure position. The correlation is best around the point of optimal efficiency at 15 degrees after TDC, which is yet another way of pointing out the increase in engine variations when moving away from optimal position. The correlation is improved by further filtering which is discussed in Section 5.3.

The implementation to obtain the model parameters,  $\alpha_1, \alpha_2, \alpha_3, \beta_1, \beta_2, \beta_3$ , can be done in different ways, but there is a real-time requirement since it is pattern recognition in a fast inner loop. The algorithm used in the real-time implementation [4] estimates bimodal functions based on the Kullback directed divergence.

## 5.2 Controller structure

The controller structure for the spark timing is shown in Figure 13. The spark plug that is used is a conventional spark plug. The ionization current is produced by the integrated ignition and measurement system, described in [1], and the interpretation algorithm gives an estimate of the PPP. The reference value for the PPP gives a possibility to have different spark schedules for different operating points, i.e. meeting other goals than to maximize the work. For example in mid-load mid-speed ranges it is desirable to have a spark advance close to MBT, with PPP around  $15^\circ$ , and in high load ranges a more conservative schedule, with late PPP, for reducing engine noise and  $\text{NO}_x$  emissions. The feed forward structure shown in Figure 13 incorporates information about how changes in reference value and engine transients affect the spark advance. This structure is similar to the ones used in conventional lambda controllers.

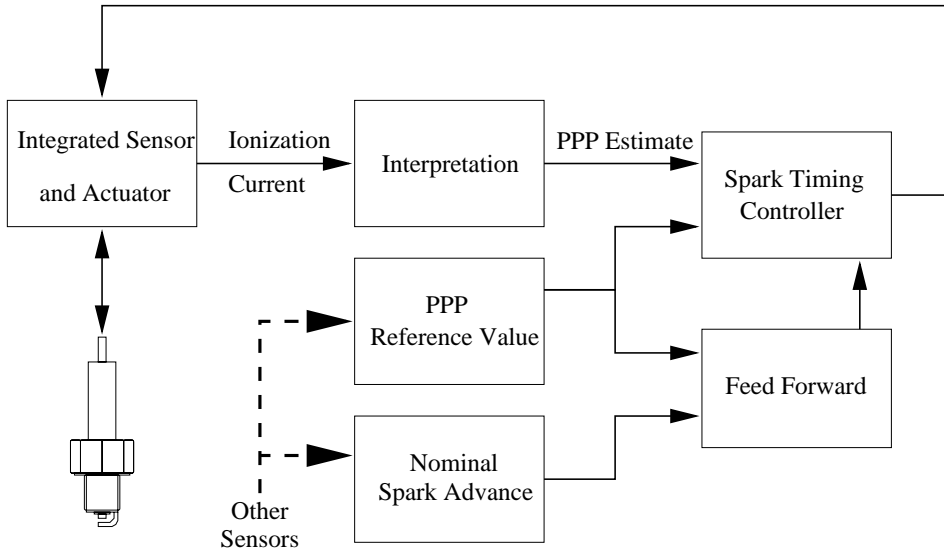


**Figure 13** The structure of the spark advance control structure, where the spark plug operates as an integrated actuator and sensor. Information is extracted from the raw ionization current, and the estimate of the PPP is the input to the spark timing controller. Reference values and feed forward signals are obtained using other sensors, e.g. engine speed and load.

The spark advance controller measures the on-going combustion and updates the spark timing to the next combustion. Without the feed forward the spark timing update is done through the following, PI like, control law

$$ST[n + 1] = ST[n] - C \cdot (PPP_{ref}[n] - PPP_{est}[n]) \quad (4)$$

where  $ST$  is the spark timing,  $PPP_{ref}$  the desired peak pressure position,  $PPP_{est}$  the PPP estimation from the ionization current, and  $C$  a gain that has to be tuned.

### 5.3 Closed-Loop Control Parameters

The gain  $C$  in Equation (4) is selected as a balance between attenuation of cycle-to-cycle variations and response speed. The filtering comes at the price of slowing down the feedback loop, but this can be compensated by using feed forward schemes, shown in Figure 13, based on a nominal spark advance table. Since environmental parameters like humidity do not change rapidly, very quick responses is not an issue. One criterion is that the spark timing shall not move more than  $1^\circ$  due to the cyclic variations [12]. For this engine the cycle to cycle variations for the estimate of the PPP is around  $10^\circ$ .

Another consideration to take into account is how well the PPP estimate correlates with the actual PPP. Moving averages of different lengths have been computed for the measured and the estimated peak pressure positions [6]. This indicates that a good choice for the gain in the feedback control law is  $C = \frac{1}{10}$ , which is the gain used in the on-line tests.

## 6 Performance of the Engine-Fine-Tuner

Experiments with the engine-fine-tuner will be presented. Responses to set-point changes are presented together with measurements from an extra pressure sensor to prove that the pressure trace is correctly positioned. The high light of the experiments is the demonstration in Section 6.4 where the engine is being exposed to increased humidity. There is an increase in power and efficiency when the engine-fine-tuner is turned on.

### 6.1 Experimental set-up

The engine used for measurement and validation is a spark-ignited, SAAB 2.3 *l*, 16 valve, four-stroke, four-cylinder, fuel-injected, normally aspirated, production engine equipped with the Trionic engine control system. The ionization current measurement system is the production system developed by Mecel AB [1], which is used in the SAAB engine. A pressure transducer and amplifier from AVL, for in-cylinder pressure measurement, is used for algorithm validation.

The ionization current interpretation scheme is implemented in a PC that is connected to the ECU by a CAN bus. Ionization current and pressure data are sampled into the PC synchronously with the crank shaft rotation, and a new updated spark advance is calculated and sent to the ECU using the CAN bus.

### 6.2 Response to set-point changes

In Figure 14, it is shown that the ionization current based controller achieves the goal of controlling the peak pressure position to the desired values. The reference

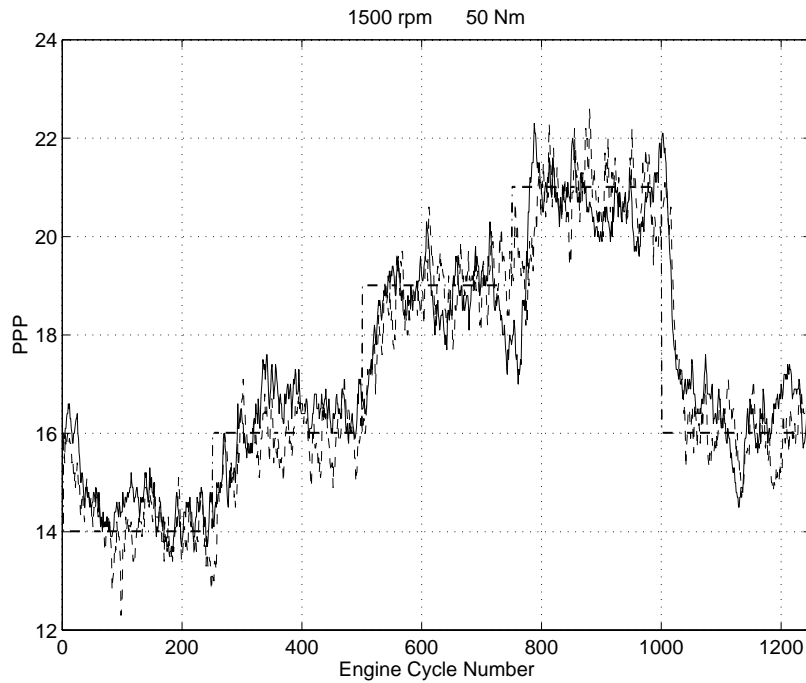


**Figure 14** Closed loop control of spark advance with changing reference value, showing that the PPP can be controlled to the desired positions. Dash dotted – reference signal, solid – PPP measured by an extra pressure sensor, dashed – PPP estimated from ionization current

value (dash dotted) shifts every 250<sup>th</sup> engine cycle, from the initial value of 16° to 14° to 16° to 19° to 21° and back to 16°. The mean values for the PPP estimate from the ionization current (dashed) and the PPP (solid) are computed using a first order LP filter with unity static gain,  $y[n+1] = 0.9 \cdot y[n] + 0.1 \cdot u_{\text{measured}}[n]$ .

The results are very good, taking into account that the cycle-to-cycle variations of the PPP and its estimate are of the order 10°, and the actual mean PPP is controlled to within  $\pm 1^\circ$  of the desired position, as can be seen in Figure 14. It is thus demonstrated that the peak pressure position can be controlled to desired positions using only information from the ionization current signal.

The response time for the controller has been evaluated using a reference square wave with a fast duty cycle, showing that the step response time is approximately 30 cycles without feed forward compensation [6]. Since no feed forward compensation is used this step response time for the reference signal will be the same as for environmental disturbances. With a feed forward loop the step response can be made faster to fit the needs during engine transients e.g. quick changes in the manifold pressure.

### 6.3 Water injection setup

To create a change in air humidity in the laboratory a water sprayer is used. The sprayer is originally a color sprayer that has a valve which delivers a liquid spray. This liquid spray is further atomized by two opposing holes that blows pressurized air on the spray. In Figure 15 a photo of the sprayer with the water spray is displayed. The figure also shows a schematic figure that displays an enlargement of the nozzle with the liquid spray and the pressurized air. The liquid is not fully atomized by the pressurized air but the droplets are made significantly smaller. By directing the water spray towards the throttle plate the water is drawn into the induction system by the lower pressure in the intake manifold.

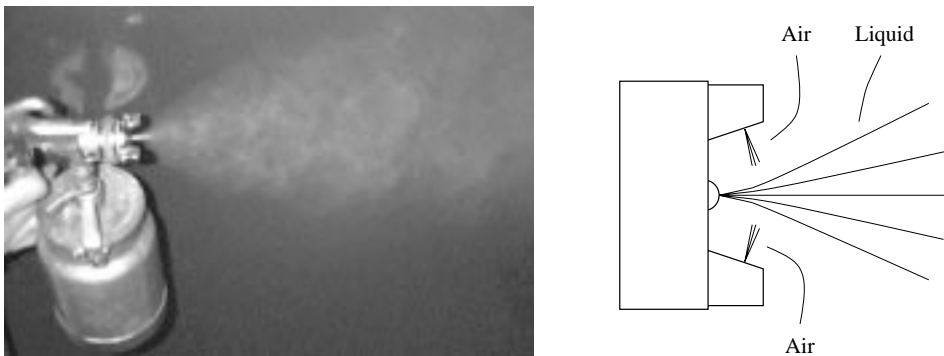


**Figure 15** Left: A picture of the sprayer spraying water. Right: A schematic figure of the sprayer nozzle with the liquid spray, pressurized air, and the atomized liquid drops.

The amount of water sprayed into the engine was not measured during the tests but it had no audible effect on the engine during the tests. Nevertheless, there was enough water present to change the in-cylinder pressure trace so that the mean peak pressure position moved to a position four to five degrees later than optimal.

### 6.4 Humidity handled by the Engine-Fine-Tuner

Humidity slows down combustion speed, leading to delayed pressure development and thus decreased power and efficiency. This is normally not possible to compensate for, and the ultimate test of the engine-fine-tuner is of course if it really has an effect on the overall engine output in terms of power and efficiency when subjected to an air humidity change.

During the water injection tests, the throttle angle, fuel injection time, and engine speed are held constant. The engine is running at steady state and the A/F ratio is tuned to  $\lambda = 1$  before the test cycle starts. Then the injection time is frozen and held constant during the test cycle. A controller structure that includes

a feed-forward coupling, Figure 13, using a conventional look-up table with engine speed and manifold pressure as inputs was used during the tests.

Figure 16 shows a part of a test cycle where water is sprayed into the engine air intake, and the closed loop spark advance controller is switched on and off. The speed and load condition is 1500 rpm and 55 Nm. Initially in the test cycle, the closed-loop spark-advance controller is running and it changes the spark advance controlling the peak pressure position to a position close to MBT, i.e.  $17^\circ$  after TDC. The ionization current is used as input to the controller, and the in-cylinder pressure is only used for validation. The signals PPP and output torque have been filtered off-line with the filtering procedure with zero phase shift, which is included in the signal processing toolbox in Matlab. The filter that is used is a Butterworth filter with order 3, and normalized cut-off frequency at 0.3.

At cycle 50 the closed-loop controller is turned off and the spark advance is held constant, changing only slightly due to the measurement noise in the manifold pressure signal used for feed forward. At cycle 250 the water spraying is started, and two things can be noted at this point: Firstly, the most important point is that the PPP moves 4 degrees. Secondly, the actual spark advance changes slightly,  $0.5^\circ$ , in the wrong direction due to a change in intake manifold pressure. When the controller is turned off, the spark advance can be viewed as a conventional pre-calibrated schedule with a spark advance close to MBT. The parameters that affect the spark advance is then the engine speed and the manifold pressure. Note that a conventional scheme changes the spark advance in the wrong direction, since increased manifold pressure indicates higher load and therefore would require a smaller spark advance.

The spark advance controller is switched on again at cycle 500. The PPP is controlled to  $17^\circ$  ATDC by using information from the ionization current. Note that the output torque increases by  $\sim 2\%$  when the controller is switched on. It is thus shown that the engine-fine-tuner can handle external disturbances such as air humidity, and control the engine to an optimal operating condition.

## 7 Conclusions

Developments of virtual engine-doctors and virtual engine-fine-tuners are trends that add to the challenges and joys of modern research in engine control. Here an ion-sense engine-fine-tuner has been presented. It is a feed back scheme, not a calibration scheme, based on ionization current interpretation. The method is very cost effective since it uses exactly the same hardware and instrumentation (already used in production cars) that is used to utilize the spark plug as sensor, to detect misfire and for knock control. The only addition for ignition control is further signal interpretation in the electronic engine control unit.

Humidity significantly changes the burn-rate in the combustion, and thus the peak pressure position which in turn affects power and efficiency. Humidity is not easily measured, and is therefore usually not compensated for. Both experimental and theoretical studies (Figures 10 and 16, and Equation 3) clearly demonstrate

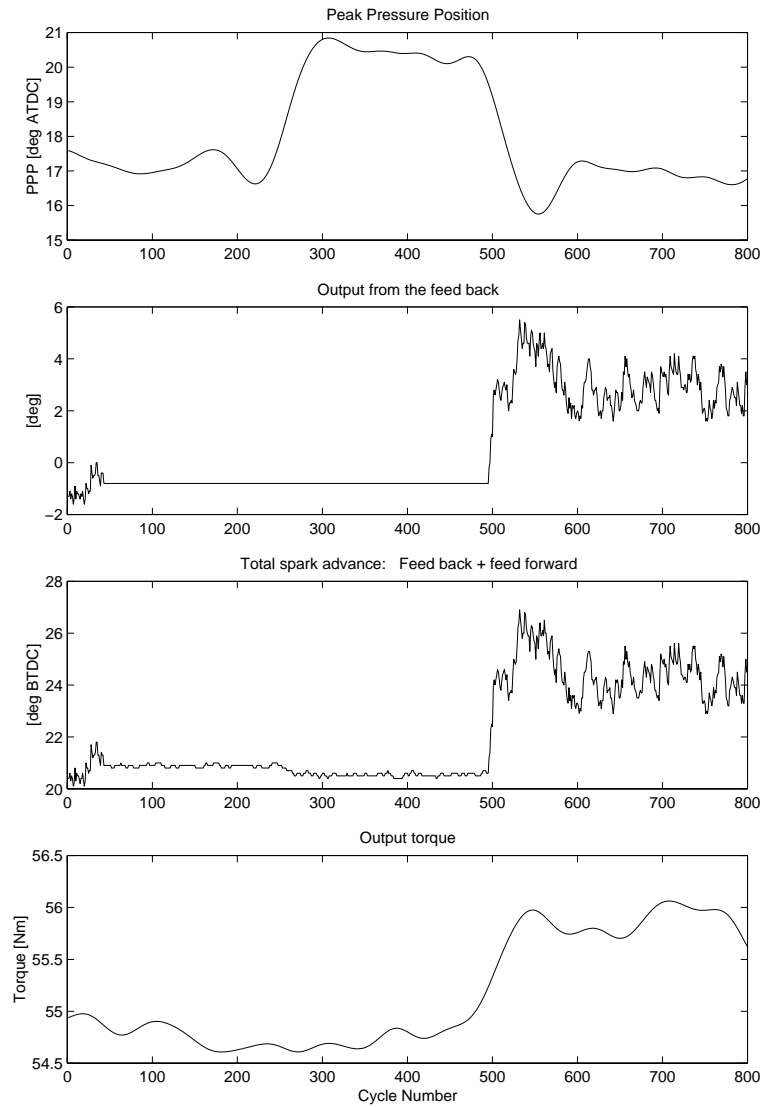


**Figure 16** The interesting part of the test cycle. The spark advance controller is switched off at cycle 50 and the water injection starts at cycle 250, which leads to increased PPP. The controller is switched on again around cycle 500, controlling PPP to MBT which increases the output torque.

the value of spark advance control regarding power and efficiency. The ion-sense engine-fine-tuner has a response time more than sufficient to follow environmental changes. And it was shown, as a main result, that it can control the engine back to its optimal operation when subjected to humidity in the intake air.

## References

- [1] J. Auzins, H. Johansson, and J. Nytomt. Ion-gap sense in missfire detection, knock and engine control. *SAE SP-1082*, (SAE paper No. 950004):21–28, 1995.
- [2] S. X. Chen and J. J. Moskwa. Application of nonlinear sliding mode observers for cylinder pressure reconstruction. *IFAC Control Engineering Practice*, 5(8):1115–1121, August 1997.
- [3] Nick Collings, Steve Dinsdale, and Tim Hands. Plug fouling investigations on a running engine - an application of a novel multi-purpose diagnostic system based on the spark plug. *SAE paper No. 912318*, 1991.
- [4] Lars Eriksson. Closed-loop spark-advance control using the spark plug as ion probe. Technical report, 1997. LiU-TEK-LIC-1997:14, Thesis No. 613.
- [5] Lars Eriksson and Lars Nielsen. Ionization current interpretation for ignition control in internal combustion engines. *IFAC Control Engineering Practice*, Issue 8, Volume 5:1107–1113, August 1997.
- [6] Lars Eriksson, Lars Nielsen, and Mikael Glavenius. Closed loop ignition control by ionization current interpretation. *SAE SP-1236*, (SAE paper No. 970854):159–166, 1997.
- [7] I. Glaser and J. D. Powell. Optimal closed-loop spark control of an automotive engine. *SAE paper No. 810058*, pages 11–21, 1981.
- [8] M. Hubbard, P. D. Dobson, and J. D. Powell. Closed loop control of spark advance using a cylinder pressure sensor. *Journal of Dynamic Systems, Measurement and Control*, pages 414–420, December 1976.
- [9] Bengt Johansson. *On Cycle to Cycle Variations in Spark Ignition Engines*. PhD thesis, Lund Institute of Technology, 1995.
- [10] Anson Lee and Jan S. Pyko. Engine misfire detection by ionization current monitoring. *SAE SP-1082*, (SAE paper No. 950003):9–19, 1995.
- [11] D. J. Patterson. Cylinder pressure variations, a fundamental combustion problem. *SAE paper No. 660129*, 1966.
- [12] J. D. Powell. Engine control using cylinder pressure: Past, present, and future. *Journal of Dynamic System, Measurement, and Control*, 115:343–350, June 1993.

- 
- [13] Raymond Reinmann, André Saitzkoff, and Fabian Mauss. Local air-fuel ratio measurements using the spark plug as an ionization sensor. *SAE paper No. 970856*, (SAE SP-1263):175–185, 1997.
  - [14] A. Saitzkoff, R. Reinmann, T. Berglind, and M. Glavmo. An ionization equilibrium analysis of the spark plug as an ionization sensor. *SAE paper No. 960337*, 1996.
  - [15] André Saitzkoff, Raymond Reinmann, and Fabian Mauss. In cylinder pressure measurements using the spark plug as an ionization sensor. *SAE paper No. 970857*, pages 187–197, 1997.
  - [16] K. Sawamoto, Y. Kawamura, T. Kita, and K. Matsushita. Individual cylinder knock control by detecting cylinder pressure. *SAE paper No. 871911*, 1987.
  - [17] Yuichi Shimasaki, Masaki Kanehiro, Shigeki Baba, Shigeru Maruyama, Takashi Hisaki, and Shigeru Miyata. Spark plug voltage analysis for monitoring combustion in an internal combustion engine. *SAE paper No. 930461*, 1993.
  - [18] Y-Y. Wang, V. Krishnaswami, and G. Rizzoni. Event-based estimation of indicated torque for IC engines using sliding-mode observers. *IFAC Control Engineering Practice*, 5(8):1123–1129, August 1997.



# Requirements for and a Systematic Method for Identifying Heat-Release Model Parameters<sup>1</sup>

Lars Eriksson

*Vehicular Systems  
Department of Electrical Engineering  
Linköping University, SE-581 83 Linköping  
Sweden*

## Abstract

Heat release analysis by using a pressure sensor signal is a well recognized technique for evaluation of the combustion event, and also for combustion diagnostics. The analysis includes tuning of several parameters in order to accurately explain measured data. This work presents and investigates a systematic method for estimating parameters in heat release models and minimizing the arbitrary choices. In order for the procedure to be systematic there are also the requirements on the model, that it includes no inherent ambiguities, like over-parameterization with respect to the parameters and to the information contained in the measurements.

The question asked is: Which parameters, in the heat release model, that can be identified using only cylinder pressure data. The parameter estimation is based on established techniques, that constructs a predictor for the model and then minimizes a least-squares objective function of the prediction error. The effect of dependencies between parameters, when selecting parameters and parameter values, is pointed out. The study is performed on data measured on a SAAB 2.3 liter, four stroke four cylinder, normally aspirated, gasoline engine.

---

<sup>1</sup>This is an extended version of the conference paper "Requirements for and a Systematic Method for Identifying Heat-Release Model Parameters", by Lars Eriksson, *SI Engine Modeling*, SAE Technical Paper 980626, Detroit, MI, February, 1998. The conference paper has been selected for publication in *SAE 1998 Transactions*.

## 1 Introduction

The compensation of the effects of volume change, heat transfer, and blowby from the cylinder pressure is called heat release analysis and is done within the framework of the first law of thermodynamics. The heat release analysis can also provide a consistency check of the pressure data itself. The more simple one-zone analysis relates the pressure changes to the amount of the fuel's chemical energy which is released as thermal energy, while the more complex two-zone analysis relates the pressure rise to changes in thermodynamic properties which occur as the mixture burns [1]. A one-zone model, which is used here, has the advantage of including heat transfer and gas flow to the crevices more simply.

Many studies have been performed on analysis and determination of parameters essential for the heat release analysis, but most studies focus only on specific subproblems such as thermodynamic TDC determination [2, 3], cylinder pressure measuring [4, 5], absolute cylinder pressure referencing [6, 7], heat transfer correlations [8, 9, 10], and the influence of polytropic index [11]. When the different effects are considered they are often treated separately, and each effect yielding parameters to be tuned for each engine and operating condition.

Here, one commonly used model structure is studied which is a one-zone heat-release model that includes the effects of net heat-release, convective heat-transfer, and crevice-flow. The model structure has previously been summarized by Gatowski et. al. 1984 [12]. Furthermore, a sensor model is important to include because it also contributes with parameters that has to be determined. Two different models are considered for the piezo-electric pressure-sensor, where the first one describes the unknown offset and the sometimes unknown gain, and the second additionally includes the leakage effect in the charge amplifier.

### 1.1 Parameter Identification

The heat release model includes several parameters that have to be determined and the issue here is to investigate which parameters are identifiable only by measuring the in-cylinder pressure. A systematic framework makes identification of the model parameters possible and also allows a consistency check of both the model and the data. Furthermore, the time consuming analysis of large data sets can be automatized with a systematic method which reduces or eliminates the arbitrary choices. Figure 1 shows how the systematic procedure is applied to a number of datasets collected at different operating conditions from an engine.

An optimization procedure for estimating the parameters in the heat-release models will be described and analyzed. The parameter estimation is based on established techniques by constructing a predictor and minimizing a least-squares objective function of the prediction error [13]. At each step the parameters at hand are used to predict the output and based on the prediction error the parameters are updated. Two different predictors based on the model are considered. The first uses the in-cylinder pressure signal as input to predict the heat released (which should be zero for the motored cycle). The second predictor uses the model parameters

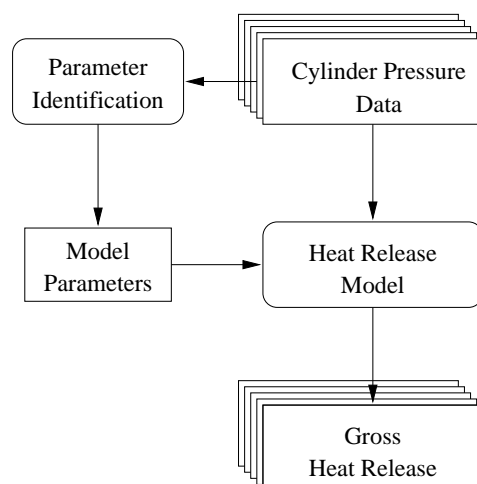


**Figure 1** Using a systematic procedure for determining the model parameters enables an automated analysis of large data sets. For each operating condition the procedure provides parameters that are used in the heat release analysis.

and the knowledge of zero heat release during the motored cycle to predict the in-cylinder pressure. With these two predictors two different objective functions can be formulated that are used in an optimization procedure for finding the best parameters. To tune the model parameters, a pressure signal from a motored cycle obtained by skipped firing is used.

## 2 Single-Zone Heat-Release Modeling

The following section describes the one-zone heat-release model that has been used in this work. The model has been widely used and the phenomena that it takes into account has been described earlier in the literature [12, 14]. Therefore, only a short summary of the model is given and the attention is turned to the parameters that are not fully known and requires determination.

Basically the model is a one-zone model based on the first thermodynamic law. Some of the processes that influence the cylinder pressure are combustion, volume change, heat transfer to the chamber walls, and mass leakage to the crevices. The article by Gatowski et.al. [12] develops, tests, and applies the heat release analysis procedure that is used here. The heat release procedure maintains simplicity while still including the effects of heat transfer and crevice flows.

## 2.1 Energy conservation equation

The combustion process is considered as a separate heat addition process and the contents of the chamber are regarded as a single fluid. The thermodynamic properties of the fluid are represented by a linear approximation for  $\gamma(T)$ . Straightforward heat transfer and crevice models are used to complete the energy balance in the first thermodynamic law

$$\delta Q_{ch} = dU_s + dW + \delta Q_{ht} + \sum_i h_i dm_i$$

Here the conventions, following [12, 14], are used:  $\delta Q_{ch}$  is the chemical energy that is added to the fluid through combustion;  $dU$  is the increase in internal energy which is considered as only a function of mean charge temperature,  $U_s = m_c u(T)$ , where both products and reactants are referred to the same datum.  $m_c$  is the cylinder charge mass;  $dW$  is the work that the fluid produces on the piston, i.e.  $p dV$ ;  $\delta Q_{ht}$  is the heat transfer from the fluid to the cylinder walls;  $h_i dm_i$  is the enthalpy for the mass flow out of the cylinder.

The single mass flux that is considered is the gas flow into and out of crevices,  $dm_i = dm_{cr} = -dm_c$ . In this model no blow-by is considered. The energy balance equation is rewritten, following the treatment in [12], by carrying out these steps: 1) The internal energy differential is  $dU_s = m_c du + u dm_c$  where  $du = c_v dT$ . 2) Use the ideal gas law  $T = (mR)^{-1}pV$  to determine  $dT$ . 3) Assume that the change in gas constant  $R$  can be neglected. The resulting energy balance is,

$$\delta Q_{ch} = \frac{c_v V}{R} dp + \frac{(c_v + R)}{R} p dV + \frac{h'}{h' - u + c_v T} dm_{cr} + \delta Q_{ht} \quad (1)$$

where  $dm_{cr} > 0$  for flows out of the cylinder into the crevice, and  $h'$  is evaluated at cylinder conditions when  $dm_{cr} > 0$  and at crevice conditions otherwise.

## 2.2 Thermodynamic properties

The most important thermodynamic property that is used when calculating the heat release for engines is the ratio of specific heats,  $\gamma$ . It is important since it affects how accurate changes in the internal energy of the working fluid can be represented. The ratio of specific heats,  $\gamma$ , decreases with temperature and is also influenced by the fuel/air ratio.

### Model of $\gamma$

A simple model of  $\gamma$  describes it as a linear function of temperature which can be parameterized as,

$$\gamma(T) = \gamma_{300} + b(T - 300)$$

where  $\gamma_{300}$  and  $b$  are constants. The approximation in this model is consistent with the other components of the one-zone heat release model, and it is sufficient for calculating burning rates and the overall energy balance [12].

The parameter  $\gamma_{300}$  provides the flexibility for changing the offset of  $\gamma(T)$  with changes in for example air/fuel ratio, while  $b$  captures the temperature dependence.

Changing the air/fuel ratio and amount of residual gases mainly changes the parameter  $\gamma_{300}$ , while the change in  $b$  is relatively small, see e.g. Chapter 4 in Heywood [14]. For tuning the heat-release model to a motored cycle the parameter  $b$  is fixed to  $b = -2.487 \cdot 10^{-4}$  which represents the slope of  $\gamma(T)$  in the range  $T \in [300\text{K}, 1000\text{K}]$ , and for analysis of firing data  $b$  is fixed to  $b = -7 \cdot 10^{-5}$  which gives a good fit over temperature range  $T \in [300\text{K}, 3000\text{K}]$ . The parameter  $\gamma_{300}$  is left for identification since for example the A/F ratio and the residual gases are not precisely determined. For air  $\gamma_{300}$  is close to 1.40.

The commonly made assumption that  $\bar{\gamma}$  is constant or a linear function of mean temperature is not sufficiently accurate during the period for the combustion event. However, appropriate assumptions can be made within the simple one-zone analysis framework which can provide accurate predictions [1].

### 2.3 Temperature model

The mean charge temperature for calculating the internal energy is computed by using the ideal gas law  $pV = m_c R T$ , which is close to the mass averaged cylinder temperature since the molecular weights of the reactants and the products are nearly identical [12, 14]. If the temperature and pressure is known at some known datum, e.g. IVC, then we get

$$pV = \frac{p_{\text{ivc}} V_{\text{ivc}}}{T_{\text{ivc}}} T = c T$$

which eliminates  $m$  and  $R$ . The volume at IVC is fairly well known while the datum values for  $p_{\text{ivc}}$  and  $T_{\text{ivc}}$  might need to be determined. Reasonable values are for  $T_{\text{ivc}}$  around 300 K and  $p_{\text{ivc}}$  around intake manifold pressure. The in-cylinder pressure at IVC is not necessarily equal to the intake manifold pressure due to pressure drop over the valves, ram effects, and pressure waves in the intake system.

### 2.4 Crevice Model

The crevice walls cool the gas in the crevices to a temperature close to the wall temperature, therefore crevices may contain substantial amounts of gas when the cylinder pressure is very high. The percentage of the original charge present in the crevices at the end of the combustion can approach 10% [12]. A simple crevice model, which does not account for blow-by, is to consider a single aggregate crevice volume that has same gas temperature as the walls and the same pressure as the cylinder, i.e.  $m_{\text{cr}} = \frac{(pV_{\text{cr}})}{RT_w}$ .

The factor that multiplies  $dm_{\text{cr}}$  in Equation (1) can be rewritten, using the model for  $\gamma$ , and with the crevice model the energy balance then becomes,

$$\begin{aligned} \delta Q_{\text{ch}} = & \frac{\gamma}{\gamma-1} p dV + \frac{1}{\gamma-1} V dp + \delta Q_{\text{ht}} \\ & + \frac{dp V_{\text{cr}}}{T_w} \left( \frac{T}{\gamma-1} - \frac{1}{b} \ln \left( \frac{\gamma-1}{\gamma'-1} \right) + T' \right) \end{aligned} \quad (2)$$

## 2.5 Convective Heat Transfer

The magnitude of the rate of energy transfer by convection, which occurs in a direction perpendicular to the surface fluid interface,  $\dot{Q}_{ht}$ , is obtained from Newton's law of cooling

$$\dot{Q}_{ht} = h A \Delta T = h A (T - T_w) \quad (3)$$

where  $A$  is the surface area of the body which is in contact with the fluid,  $\Delta T$  is the appropriate temperature difference, and  $h$  is the convection heat transfer coefficient. The most important task is to accurately predict the magnitude of the convection heat transfer coefficient. Since this quantity is a composite of both microscopic and macroscopic phenomena, many factors must be taken into consideration. For many flow geometries,  $h$ , is given by the relation [15, 8, 9]

$$Nu = C (Re)^m (Pr)^n$$

The correlation used to calculate the instantaneous spatially averaged heat transfer is based on the form proposed by Woschni [9], which essentially is a Nusselt-Reynolds number of the form  $Nu = 0.035Re^m$  with  $m = 0.8$ .

$$h = \frac{131B^{0.2}C_1p^{0.8}w^{0.8}}{T^{0.53}} \quad (4)$$

The characteristic speed  $w$  was chosen to be,

$$w = 2.28 \left( U_p + 3.4 \cdot 10^{-3} C_2 \frac{V_{disp} (p_f - p_m)}{V_{ivc} p_{ivc}} T_{ivc} \right) \quad (5)$$

The variables are:

B	cylinder bore	$U_p$	mean piston speed
p	cylinder pressure	T	charge temperature
$p_m$	motored pressure	$V_{disp}$	displaced volume
$p_f$	firing pressure	$C_1, C_2$	tuning constants

This model gives the rate of the heat transfer  $\dot{Q}_{ht}$ . To simulate it in the crank angle domain it has to be scaled with the engine speed,  $n$ , which results in,

$$\frac{\delta Q_{ht}}{\delta \theta} = \frac{\delta Q_{ht}}{\delta t} \frac{\delta t}{\delta \theta} = \dot{Q}_{ht} \frac{n \pi}{30}$$

## 2.6 Cylinder volume

The cylinder volume is included in the heat release model and it depends on the crank angle  $\theta$ , crank radius  $a$ , connecting rod length  $l$ , piston area  $A$ , and clearance volume  $V_c$ .

$$V(\theta) = V_c + \frac{\pi B^2}{4} (l + a - a \cos \theta - \sqrt{l^2 - a^2 \sin^2 \theta})$$

The clearance volume  $V_c$  influences the maximum cycle temperature and pressure through its influence on compression ratio, and for heat release calculations the clearance volume is of great importance. The actual clearance volume,  $V_c$ , differs from engine to engine and it also differs between the cylinders in the same engine [4]. Therefore, it is not sufficient to calculate the clearance volume given the compression ratio data from the manufacturer.

## 2.7 A commonly used family of simulation models

The equations described in this chapter (Equations 2 to 5) constitute a family of models that are frequently used in the literature on one form or the other. There are basically two ways to change the model structure, one is to change the parameters and effects included and the second is to rearrange the equations. These are illustrated below.

By setting some parameters to determined values models of lower complexity are received: (1) With the crevice volume  $V_{cr}$  set equal to zero a model with net heat release and heat transfer is received. (2) With the heat transfer coefficient  $C_1$  set equal to zero we get a model that includes crevice effects and net-heat release. (3) With both  $V_{cr}$  and  $C_1$  equal to zero we get a net-heat release model. Note that in such a case it is more reasonable to exchange  $\gamma$  to a polytropic exponent that is constant independent of temperature which is consistent with the omission of loss mechanisms.

By rearranging (Equations 2 to 5), and interchanging inputs and outputs, two different models are received: One in which a measured cylinder-pressure trace is used as input and the gross heat-release trace calculated; In the other the heat-release trace is specified and the cylinder pressure is calculated. These two formulations can be used for estimating the model parameters and one issue here is to study how the different formulations influence the parameter estimation.

### Heat release simulation

The heat release model is stated such that the pressure and volume traces are given as input and the model then outputs the time or crank angle derivative of the net heat-release, i.e.

$$\frac{\delta Q_{ch}}{\delta \theta} = f\left(p, \frac{dp}{d\theta}, V, \frac{dV}{d\theta}\right) \quad (6)$$

where  $p$  and  $\frac{dp}{d\theta}$  are the pressure and differentiated pressure traces. Solving Equation (6) together with an initial condition produces the time history for the heat release  $Q_{ch}(\theta)$ .

To solve Equation (6) it is necessary to specify an initial value of  $Q_{ch}$ , in conjunction with the starting point of the simulation. This poses a problem for the determination of the best parameters. To illustrate this issue two simulations, with identical values of the model parameters but with changed starting points for the simulation, are shown in Figure 2. As it can be seen the starting point has

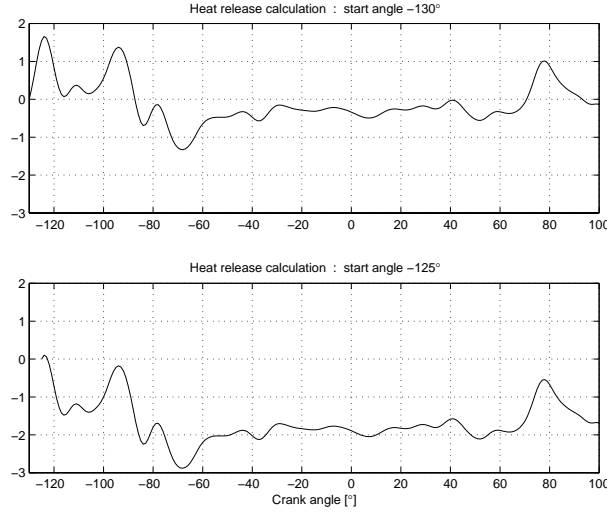


**Figure 2** Two traces with exactly the same parameters, but with changed starting points. The figure shows that the level of  $Q_{ch}$  has changed significantly.

a very large effect on the amount of heat released,  $Q_{ch}$ , which implies that the initial value will also have a large effect on the estimated parameters. There are two ways to overcome this problem: The first is to add a parameter for the initial value and include it in the parameter estimation; The second is to set the initial value to zero and calculate a mean value over e.g. the first  $80^\circ$  and then subtract it from the calculated heat release trace. The second procedure was chosen for its simplicity, and tests with the optimization procedure showed that the length of  $80^\circ$  was sufficiently long to give consistent parameter estimates.

### Pressure simulation

Solving Equation 2 for the pressure differential  $dp$  gives the following ordinary differential equation (ODE) which can be used to simulate the pressure.

$$\frac{dp}{d\theta} = \frac{\frac{dQ_{ch}}{d\theta} - \frac{\gamma}{\gamma-1} p \frac{dV}{d\theta} - \frac{dQ_{ht}}{d\theta}}{\frac{1}{\gamma-1} V + \frac{V_{cr}}{T_w} \left( \frac{T}{\gamma-1} - \frac{1}{b} \ln \left( \frac{\gamma-1}{\gamma'-1} \right) + T' \right)} \quad (7)$$

For this ordinary differential equation to be complete an initial value of the pressure must be specified. The starting point for the simulations is IVC, and therefore  $p_{ivc}$  is used as initial value. The pressure at IVC is not fully known, see the discussion in Section 2.3, so it is left for identification. Solving (7) produces the pressure

development,  $p$  provided the heat release trace  $Q_{ch}$ , and for parameter tuning the motored cycle is used, for which the heat release is equal to zero,  $dQ_{ch} = 0$ .

### Simulation environment

To obtain the heat release and pressure traces a Runge-Kutta ODE-solver in the Simulink [16] toolbox of Matlab was used. The solver was of order 4 with adaptive step length. The step-lengths, tolerances, and also the solver method, were changed in a systematic manner in-order to ensure that the simulation results did not depend on the numerical integration of the ODE:s.

## 3 Pressure Sensing and Sensor Modeling

The quality of the pressure data is crucial for the heat-release analysis and several papers are devoted to these issues, see for example [6, 4, 5]. In this section the attention is turned to the following three issues: Frequency contents of the pressure signal; Phasing of the pressure signal relatively the crank angle and cylinder volume; Characteristics of the pressure transducer and measurement system. Before entering these issues a short description is given of a normal pressure measurement setup.

Nowadays the in-cylinder pressure is measured using digital sampling systems where the sampling events are externally triggered using incremental encoders, see Figure 3. The pressure-measurement chain consists of pressure transducer, charge amplifier, and A/D converter. The pressure measurement will be discussed in Section 3.4. The optical encoder determines the sampling instants (for example it can give 360 pulses per revolution) and holds phase information of the pressure trace in relation to the crank angle. A signal that produces 1 pulse per revolution (or cycle) is often used to determine the location of the samples in relation to TDC.

### 3.1 Pressure frequency contents

Ten motored cycles have been measured at the engine speeds 800 rpm and 1600 rpm and Figure 4 shows their frequency contents. The pressure is a cyclic signal and the first peak in the spectrum appears at the engine-cycle frequency, i.e. for 800 rpm at  $\frac{800}{2.60} \approx 6.7$  Hz. Note that the spectra for the two signals have been plotted with different frequency scales, showing that the frequency contents clearly depends on the engine speed. Around the 40th harmonic it gets harder to distinguish the harmonics from the noise, i.e. for 800 rpm around 270 Hz.

Analysis of several data sets of motored pressure have shown that that there is usually information up to the 50th harmonic. Data from firing cycles have also been analyzed and peaks in the spectrum that are higher than the noise has occurred at much higher frequencies. Information up to the 140th harmonic has been observed under favorable conditions for the firing data. Thus, the sampling rate and the

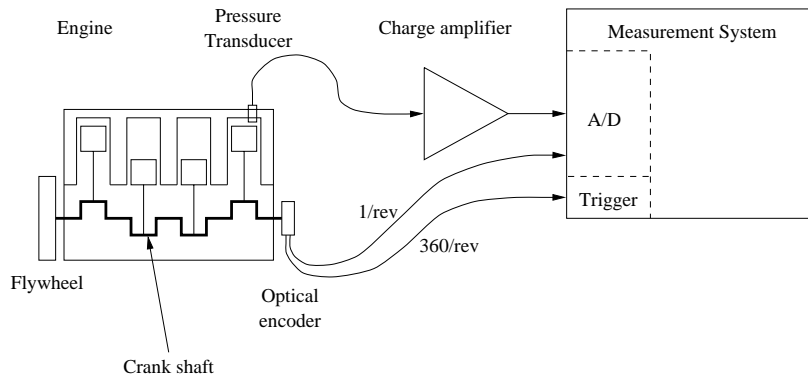


**Figure 3** Example of a pressure measurement setup, that samples the cylinder pressure based on the crank angle. The sample rate, in this configuration, is equal to one sample per crank angle degree.

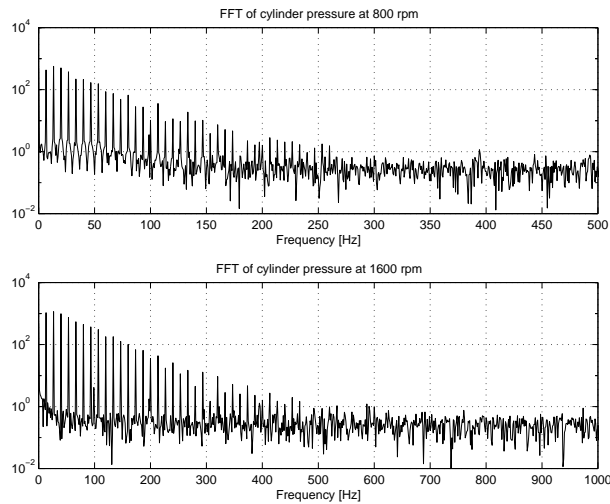


**Figure 4** Spectra for two (motored) cylinder pressure traces measured at engine speeds of 800 rpm and 1600 rpm. Note that the frequency scales are different for the two spectra. The first harmonic in the signal occurs at the frequency of the engine cycle i.e. for 800 rpm at 6.7 Hz. For both engine speeds the frequency contents become difficult to distinguish from noise around the 40th harmonic.

pre-filtering should be selected sufficiently above these frequencies to retain the information.

The signal to noise ratio (SNR) effects the number of harmonics that can be detected and for a different SNR more frequency components is visual in the spectrum. Furthermore, increasing the number of cycles included in the FFT calculation also increases the amplitude for the harmonic in the signal. Calculations and comparisons has shown that doubling the length of the data set only increases the number of harmonics that can be seen with only 1 or 2.

Normally the resolution of the incremental encoder, connected to the crank shaft, is set to a crank angle resolution of  $1^\circ$  per sample during the data acquisition. This gives a sufficiently high sampling frequency according to the discussion above. The resolution is further motivated by [11], that states that a sample rate of 1 sample per crank-angle degree is considered adequate for burn-angle analysis from heat-release calculations.

### 3.2 Phasing of the pressure signal

When collecting the pressure traces it is important that the phasing is preserved in the signal since the heat release calculation needs both the volume trace and the pressure trace. In the heat release analysis the cylinder volume is calculated using the crank angle obtained from the sampling.

There is an uncertainty in the exact crank angle positions for the sampling pulses which is due to that the mounting of the incremental encoder can not be performed with infinite precision. If we disregard that the crank shaft is flexible then the crank angle,  $\theta_i$ , at sample,  $i$ , can be modeled as having an unknown offset  $\theta_0$  from the true crank angle  $\theta_{\text{true},i}$

$$\theta_i + \theta_0 = \theta_{\text{true},i}$$

The determination of  $\theta_0$  is often called TDC determination, and it is generally considered that state of the art systems can determine the offset to an accuracy of  $\sim 0.1 - 0.2^\circ$  [4, 14]. Furthermore, in a multi-cylinder engine the crank-shaft torsion can also influence the accuracy. One interesting issue is to see if the offset  $\theta_0$  can be identified from the measured pressure.

### 3.3 Filtering and data collection

Despite that the crank angle offset has been accurately determined problems can still arise if proper care is not taken when the data is collected and processed. The following example illustrates the problem:

Cylinder-pressure data from a motored cycle has been collected at 800 rpm with a crank angle resolution of  $1^\circ$ . The noise in the signal is to be reduced by filtering the data with a cut-off frequency corresponding to 360 Hz. Figure 5 shows the result when two filters with the same cut-off frequency and filter order are used,

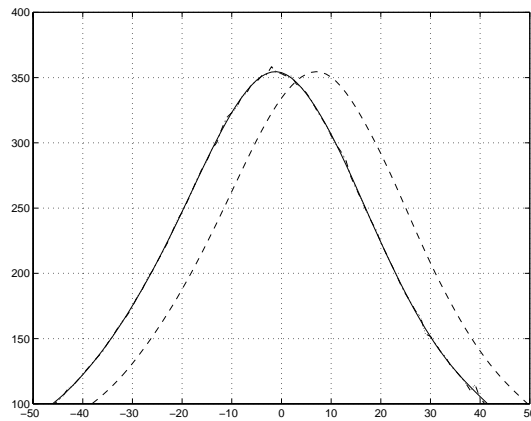


**Figure 5** Three pressure signals: Dash dotted – measured pressure, Solid – zero-phase filtered, Dashed – causally filtered. The two filters had the same order and the same cut-off frequency, but the causal filter causes a shift in peak pressure position of  $10^\circ$ .

one causal and one non-causal with zero-phase shift. The measured signal (dash-dotted) and the signal filtered with a non-causal filter (solid) is identical in phase, but the signal filtered with causal filter is shifted with as much as  $10^\circ$ .

When acquiring pressure data a pre-sampling filter should always be used to avoid aliasing. Such a filter is causal and inherently affects the phase of the sampled signals. Therefore, it is essential for the phasing of the pressure signal that the sampling rate and also the cut-off frequency of the anti-alias filter is sufficiently high. More sophisticated filtering techniques that preserve the phasing of the signals, can be applied when the data is sampled, such as non-causal filters with zero phase-shift. An example is the `filtfilt` function in the “Signal Processing Toolbox” of Matlab [17].

### Influence of anti-alias filter

The following example quantifies the phase-shift effect of a first order anti-alias filter. The transfer function for a first order filter with cut-off frequency  $\omega_c$  and unity gain is

$$H(j\omega) = \frac{1}{1 + \frac{j\omega}{\omega_c}}, \text{ with phase: } \arg[H(j\omega)] = -\arctan\left(\frac{\omega}{\omega_c}\right)$$

which results in the following response for a sinusoidal input,

$$\mathbf{y} = |H(j\omega)| \sin\left(\omega t - \arctan\left(\frac{\omega}{\omega_c}\right)\right) = |H(j\omega)| \sin\left(\omega\left(t - \frac{\arctan(\omega/\omega_c)}{\omega}\right)\right)$$

Thus, the time delay that the first order filter introduces is  $\tau_d(\omega) = \frac{\arctan(\omega/\omega_c)}{\omega}$ . This function has the following three important properties:

- 1)  $\tau_d(\omega)$  decreases monotonously with  $\omega$ .
- 2)  $\lim_{\omega \rightarrow 0^+} \tau_d(\omega) = \frac{1}{\omega_c}$ .
- 3)  $\tau_d(\omega_c) = \frac{\pi}{4\omega_c}$ .

We now see that if we sample the data with sampling time  $T_s = \frac{1}{f_s}$  and use a first order anti-alias filter with cut-off frequency  $f_c = f_s/2$  then the time delay, introduced by the filter, lies in the following interval

$$\frac{T_s}{4} = \frac{1}{4f_s} \leq \tau_d < \frac{1}{\pi f_s} = \frac{T_s}{\pi}$$

for frequencies in the range  $0 \leq f \leq f_s/2$ .

By sampling the cylinder pressure with a resolution of  $1^\circ$  then the anti-alias filter introduces a delay of  $\sim \frac{1}{\pi}^\circ$  at the lowest frequencies. Thus, the anti-alias filter will produce a delay in the order of  $0.3^\circ$  irrespectively of how accurate the phasing for the crank angle based sampling has been determined. If the filter order is increased or the cut-off frequency is decreased then the time delay will be even larger.

### Pressure differentiation

For the heat-release model the crank angle derivative of the pressure signal is required as input, see Equation 6. Also the numeric differentiation method can affect signal phasing of the pressure signal. A simple method that keeps the phase information is,

$$\frac{\partial p_m(\theta_i)}{\partial \theta} = \frac{p_m(\theta_{i+1}) - p_m(\theta_{i-1})}{\theta_{i+1} - \theta_{i-1}}$$

which is the standard differentiation procedure given in any numerical analysis textbook.

The main message in this section about pressure phasing and filtering has been to illustrate the following basic principle for collecting cylinder-pressure data:

Sample the data with a frequency that is sufficiently high so that the pre-sampling filter does not produce a significant phase shift, then perform data reduction, signal processing, and filtering off-line using non-causal filters with zero phase-shift.

### 3.4 Sensor modeling

Two models of different complexity for the pressure measurement chain will be derived and examined. The simplest model is that the actual and measured pressure are connected by a static relation that is considered constant during one engine cycle. The more complex model describes the drift of the charge amplifier which

gives a dynamic relation between the actual and measured cylinder pressure. Two phenomena influences the accuracy of the measured cylinder and amounts to an unknown offset in the measured pressure signal. The first is connected to the measurement chain and the second is connected to transducer's sensitivity to thermal shock.

The pressure transducer reacts to the pressure by producing a charge proportional to the pressure change this charge is then integrated by the charge amplifier. Therefore, the resulting voltage from the amplifier does not contain information about the absolute pressure level. Furthermore, leakage currents in the charge amplifier produces a signal that drifts towards an output equal to zero. Temperature variations in the sensor and sensor mounting change the transducer sensitivity and output. The variations in temperature during the engine cycle also amounts to a drift in the output, and thus an unknown absolute level.

### 3.5 Static sensor model

The measurement chain consisting of pressure transducer, charge amplifier, and data acquisition equipment has a static gain,  $C$ , from the sensor to the pressure measured value. With the pressure trace sampled at certain crank angle positions,  $\theta_i$ , a simple static model for the pressure sensor is,

$$p_m(\theta_i) = C p(\theta_i) + p_0 \quad (8)$$

where,  $p$ , is the true cylinder pressure and  $p_m$  the measured pressure. The gain,  $C$ , for the measurement chain is considered constant for all cycles but the offset,  $p_0$ , changes between cycles due to leakage in the charge amplifier and thermo-shock in the pressure transducer. The determination of the offset,  $p_0$ , is referred to as pegging the pressure signal, or cylinder pressure referencing, and it is generally recommended that the pegging is performed once for each pressure cycle [7, 6].

The total gain can be determined in at least three different ways, which are summarized in [18]: The first is to determine the gain for each component and multiplying them with each other; The second is to calibrate the total chain by applying a well determined pressure step and measure the result; The third is to calibrate the total chain in conjunction with a thermodynamic model. The third approach was used in [18] to get a good determination total gain for the pressure measurement chain, and it will also be tested here.

#### Dynamic sensor model

In the model above the offset is assumed to be constant during the cycle, which is only an approximation since the charge leakage and thermal drift influences the output during the cycle. Thermal shock has been investigated by many authors [4, 6, 19] and here the influence of the charge amplifier drift will be investigated.

A more detailed model of the pressure sensor is received when including the drift of the charge amplifier, which can be modeled as a leakage towards the mean

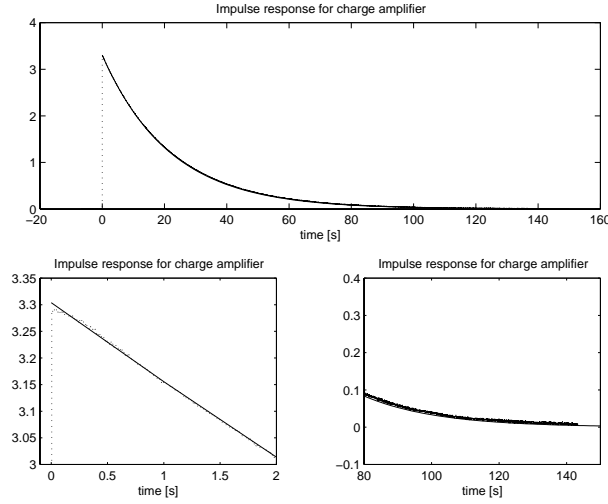


**Figure 6** Impulse response for the charge amplifier. At  $t=0s$  a charge of  $2.91\text{ nC}$  is given as input to the charge amplifier. Solid line – model output with  $\tau_c = 22\text{ s}$ . Dotted line – measured output from the charge amplifier.

value, or DC-component, of the measured pressure signal. The measurement chain containing charge leakage can be modeled as follows

$$p_m(s) = C \cdot G(s) \cdot p(s), \text{ where } G(s) = \frac{s}{s+1/\tau_c} \quad (9)$$

where  $s$  is the Laplace operator,  $C$  is the gain (same as for the static model), and  $\tau_c$  is the time constant for the leakage. Since this is a second order system it must be completed with an initial value,  $p_{in}$ . The output from this dynamic model is the measured pressure,  $p_m$ , but it can be also inverted to generate the cylinder pressure,  $p$ , as output.

This model is validated in Figure 6 which shows a calibration experiment that gives the time constant and the gain for the charge amplifier. The received time constant of  $\tau_c = 21.76$  seconds agrees well with the tabulated values in the reference manual for this amplifier setting. The amplifier setting normally used for has a tabulated sensitivity of  $\tau_c = 2.2$  seconds.

The effect that charge-amplifier leakage has on the measured cylinder pressure has been evaluated by simulating Equation (9) and compared with a model of an idealized charge amplifier (with an infinite time constant  $\tau_c = \infty$ ). An engine speed of 1000 rpm was chosen since the leakage effect is more pronounced at lower engine speeds, and the time constant for the charge amplifier model was changed in the range from  $\tau_c = 0.22$  to  $\tau_c = 22.00$  seconds. The results are shown in Table 1. The simulation result for  $\tau_d = 2.2\text{ s}$  is also shown in Figure 7 which displays a peak-to-peak drift of 0.36 % compared to the maximum of the pressure signal. As

$\tau_c$ [s]	$\max(\Delta p) - \min(\Delta p)$ [bar]	$\frac{\max(\Delta p) - \min(\Delta p)}{\max(p)}$
0.22	0.709	0.0361
0.70	0.225	0.0114
2.20	0.0710	0.00362
6.96	0.0224	0.00114
22.0	0.00710	0.000362

**Table 1** Influence of charge amplifier time constant  $\tau_c$  on the intra cycle measurement offset.  $\Delta p$  is the difference between ideal sensor and actual sensor.  $\max p$  is the maximum pressure during the cycle.

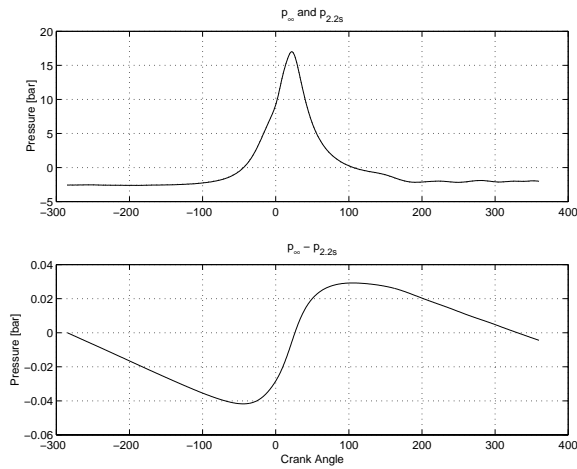


**Figure 7** Pressure signals for two different charge amplifiers, one with an infinite time constant,  $p_\infty$ , and one with a time constant of 2.2 s,  $p_{2.2s}$ .

it can be seen in the table the time constant of the charge amplifier has a small effect on the measured pressure trace during one engine cycle if the time constant is large, but reducing the time constant rapidly increases the effect. The simulations are performed for an engine speed of 1000 rpm and an increased engine speed will reduce the effect.

To compare the charge amplifier influence with the transducer thermo shock the data sheet for the transducer is utilized. The influence of thermal shock on the QC32C sensor used in the laboratory is tabulated for a cycle at 1300 rpm with a pressure peak of 75 bar [20], which amounts to a measurement drift less than 0.2 bar, i.e. about 0.3 %. The thermal drift is thus of the same order as the leakage for this setup.

The simulations above have quantified the effect of the charge amplifier time constant on the pressure output. It has been shown that the charge amplifier can have a significant effect on the pressure measurement if the time constant is small. For the sensor and charge amplifier in the laboratory, with  $\tau_c = 2.2$ , the charge amplifier has an affect of equal magnitude to the thermal shock.

## 4 Parameter Estimation Method

Previous sections have described the model a number of parameters that requires determination. In this and the following sections the unknown parameters are collected in a parameter vector denoted  $\Theta$ .

To determine the parameter values, that fit the model best to the measured data, a least squares criterion is used, and the parameter values that minimizes this criterion is chosen. The minimum is searched for using an optimization method which takes a set of parameter values  $\Theta$ , simulates the model, and predicts an output. Then it calculates the difference (residual) between model and measured outputs, a gradient direction, and an approximation to the Hessian. Finally it calculates an updated set of parameters. The three steps described above are repeated until there is no further improvement in the least squares criterion.

One possible way to tune the parameters would be to take a pressure and heat release signature for a firing cycle and use e.g. the pressure trace and the model to predict the heat release. The problem with this approach is that both the pressure trace and the true heat release trace must be known. Tuning the parameters to a motored cycle offers the benefit that the heat release trace is known, i.e. it is zero  $Q_{hr} = 0$ . The tuning should also be performed on a motored cycle obtained by skipped firing, which means that the engine is run under test conditions and then the ignition is skipped for one cycle. Under steady state conditions the initial condition for the motored cycle should be the same as for the preceeding cycles.

### 4.1 Formulation of residuals

The two different simulation models, Equation 6 and 7, are used to formulate two different residuals which are used to determine the parameters.

#### Heat-release residual

The heat release simulation equation requires the pressure as input, and using the static model Equation 8 the actual pressure,  $p$ , and its crank angle derivative can be calculated from the measured pressure trace  $p_m$  and its derivative as follows,

$$p = \frac{1}{C}(p_m - p_0) \quad \text{and} \quad \frac{dp}{d\theta} = \frac{1}{C} \frac{dp_m}{d\theta} \quad (10)$$

A heat release trace  $Q_i(\Theta)$  can be simulated using the model parameters  $\Theta$  and Equations 10 and 6. The subscript  $i$  in  $Q_i(\Theta)$  denotes the sampling index.

The actual heat released for the motored cycle is zero which gives the following residual to minimize

$$r_i(\Theta) = Q_i(\Theta) - 0 \quad (11)$$

### Pressure residual

The residual to minimize when using the pressure simulation model Equation 7 as criterion is stated as the difference between the pressure predicted by the model  $p_i$  and the measured pressure  $p_{m i}$ , which becomes (after including the sensor model, Equation (8))

$$r_i(\Theta) = C \cdot p_i(\Theta) + p_0 - p_{m i} \quad (12)$$

(Note, the parameters  $C$  and  $p_0$  are components in  $\Theta$ .)

## 4.2 Minimization procedure

The least squares criterion is used to select the best parameter values

$$V_N(\Theta) = \frac{1}{2} \sum_{i=1}^N (r_i(\Theta))^2 = \frac{1}{2} \mathbf{r}(\Theta) \mathbf{r}^T(\Theta)$$

here the residuals are collected in the vector  $\mathbf{r}(\Theta)$

$$\mathbf{r}(\Theta) = (r_1(\Theta), \dots, r_N(\Theta))$$

The minimization of  $V_N(\Theta)$  is a standard non-linear least-squares problem that can be solved by several methods described in e.g. [21, 22]. Here an algorithm of Levenberg-Marquardt type with a numerically computed gradient and an approximated Hessian has been used.

The algorithm needs the gradient which can be computed as,

$$\nabla V_N(\Theta) = J(\Theta) \mathbf{r}^T(\Theta)$$

where the Jacobian,  $J$ , is defined as  $J(\Theta) = [\nabla r_1(\Theta), \dots, \nabla r_N(\Theta)]$ . The residual gradients,  $\nabla r_i(\Theta)$  are computed numerically with a difference approximation,

$$\frac{\partial r_i(\Theta)}{\partial \Theta_j} = \frac{r_i(\Theta_j + \Delta\Theta_j) - r_i(\Theta_j)}{\Delta\Theta_j}$$

$r_i(\Theta_j + \Delta\Theta_j)$  is easily calculated with one simulation. For least squares problems there exists an approximation to the Hessian, which only uses the information from the Jacobian  $J$ . The Hessian is,

$$\nabla^2 V_N(\Theta) = J(\Theta) J^T(\Theta) + \sum_{i=1}^N r_i(\Theta) \nabla^2 r_i(\Theta)$$

and for  $\Theta$  close to optimum  $r_i(\Theta)$  is small, which gives the following approximation of the Hessian,

$$\nabla^2 V_N(\Theta) \approx H(\Theta) = J(\Theta) J^T(\Theta)$$

### Optimization procedure

With the parameters values given at optimization step,  $k$ , the next set of parameter values,  $\Theta$ , is updated by the following law

$$\Theta^{k+1} = \Theta^k + \mathbf{d}^k$$

in the Levenberg-Marquardt type methods the direction,  $\mathbf{d}^k$ , is chosen as the solution to the following equation

$$(\mathbf{H}(\Theta^k) + \nu \mathbf{I})\mathbf{d}^k = \mathbf{J}(\Theta^k)\mathbf{r}(\Theta^k)$$

With  $\nu = 0$  this is the Gauss-Newton method, and if  $\nu \rightarrow \infty$  the direction  $\mathbf{d}^k$  approaches the steepest descent direction. Generally it is not guaranteed that  $\mathbf{d}^k$  is a descent direction, for example if the problem is very non-linear or if the residuals,  $r_i$ , are large. Therefore, the parameter  $\nu$  is varied during the optimization to ensure that a descent direction is received. If  $V_N(\Theta^{k+1}) \geq V_N(\Theta^k)$  then  $\nu$  is increased and new values of  $\mathbf{d}^k$  and  $\Theta^{k+1}$  are computed. This step is repeated until a descent direction is received. To extend this simple method further with a line search has not been necessary since the procedure has always resulted in descent direction.

The stopping criterion for the search algorithm has been chosen as

$$\text{If } V_N(\Theta^k) - V_N(\Theta^{k+1}) < \epsilon V_N(\Theta^k) \text{ then stop}$$

where  $\epsilon$  is a chosen to be a small number. This means that the last iteration did not improve the objective function more than a certain degree.

The model parameters, see Table 2, have values that range over 7 decades and therefore the optimization is performed using a set of scaled variables. A linear transformation  $\mathbf{x} = \mathbf{D}\Theta$  with a diagonal matrix, where the diagonal elements are  $D_{i,i} = 1/\Theta_i$ , is applied to the initial guess so that the optimization procedure starts with a set of variables  $\mathbf{x}$  that are all equal to 1.

The optimization method, described above, converged after 3 to 12 iterations, depending on how many and which parameters were included in the optimization. For example, if the model is over-parameterized then the Hessian approximation is close to singular which makes it numerically difficult to invert, and the objective function does not decrease as fast as for a well posed optimization problem.

### 4.3 Parameter Evaluation

Two things are studied and used to evaluate the parameter values, after the optimization procedure has stopped at a point  $\Theta^*$ : the quadratic loss,  $V_N(\Theta^*)$ , and the Hessian approximation,  $\mathbf{H}(\Theta^*)$ . The quadratic loss is only used to supervise how good the resulting fit is.

Locally  $\mathbf{H}(\Theta^*)$  gives insight into how sensitive  $V_N(\Theta^*)$  is to a certain parameter or a direction. Especially interesting is the eigenvector that corresponds to the smallest eigenvalue of  $\mathbf{H}(\Theta^*)$ , since it points in the direction where  $V_N(\Theta^*)$  changes

least. This fact is used in to evaluate how important different parameters are for a good fit between the model and the measured data. To be able to compare the importance of the different parameters the Hessian is calculated and compared using the scaled parameters  $\chi$ . The reciprocal condition number,  $\kappa^{-1}$  is used to check how the Hessian is scaled.

In the following Sections an analysis is performed of how important different parameters are for the fit. The following procedure is used to study how the parameters are estimated

1. As a first step all parameters are included in the optimization.
2. Find the best parameters  $\Theta^*$  with the optimization procedure.
3. Study the reciprocal condition number and eigenvectors for  $H(\Theta^*)$ .
4. Remove the parameter with least influence on  $V_N$  from the optimization procedure and set it to a fixed value.
5. If there still remain free parameters goto step 2.

#### 4.4 Unknown parameters

The unknown parameters have been discussed previously in the text but they are summarized in Table Table 2, for convenience of referencing, before the parameter estimation results are discussed.

Param.	Description	Size
$\gamma_{300}$	ratio of specific heats	1.35 –
$C_1$	heat transfer parameter	1 –
$\theta_0$	crank angle phasing	1°
$V_c$	clearance volume	$6.3 \cdot 10^{-5} \text{ m}^3$
$V_{cr}$	single aggregate crevice volume	0.5 % of $V_{cr}$
$p_0$	bias in pressure measurements	0.1 bar
$C$	pressure measurement gain	1 –
$T_w$	mean wall temperature	450 K
$T_{ivc}$	mean charge temperature at IVC	300 K
$p_{ivc}$	cylinder pressure at IVC	0.5 bar

**Table 2** Tuning parameters in the heat release model. The values shown in the rightmost column give the approximate size.

## 5 Parameter Estimation Results

For evaluation ten cycles of pressure data have been collected in seven different motoring operating points: 800 rpm with throttle angles 0 %, 5 %, 10 %, and

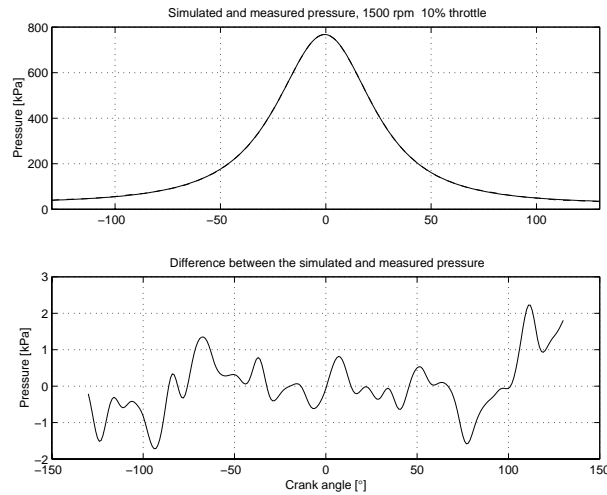


**Figure 8** The upper plot shows the measured pressure (solid line), and the output from the model (dashed line) the pressure that the model predicts, the signals are extremely close. The lower plot shows the difference between the measured and the model, and the conclusion is that the difference is very small.

15 %, and 1600 rpm with throttle angles 0 %, 10 %, and 15 %. Furthermore, data has been collected for four operating conditions with running engine. During the tests three different pressures were measured: in-cylinder pressure; intake manifold pressure, measured at the plenum; and exhaust pressure, measured at a distance of 70 cm from the exhaust valve. The intake and exhaust pressures were measured and used only for validation of the parameter estimation. The engine was a SAAB 2.3 l, 16 valve, normally aspirated engine, it's data is further tabulated in the appendix.

### Closeness of fit

To validate how close the measured cylinder pressure can be predicted the output from the optimization procedure is plotted in Figure 8. The model that is used includes heat transfer but not crevice flow. The simulated pressure signal,  $p$ , is generated with the parameters from the optimization procedure and compared with the measured pressure signal that is corrected with the parameters for the sensor model, i.e.  $\frac{p_m(\theta_i - \theta_0) - p_0}{C}$ . From the figure it can be seen that the difference between the measured signal and the model output is very small. Thus, it can be concluded that the optimization procedure does find model parameters that describes the measured data well.

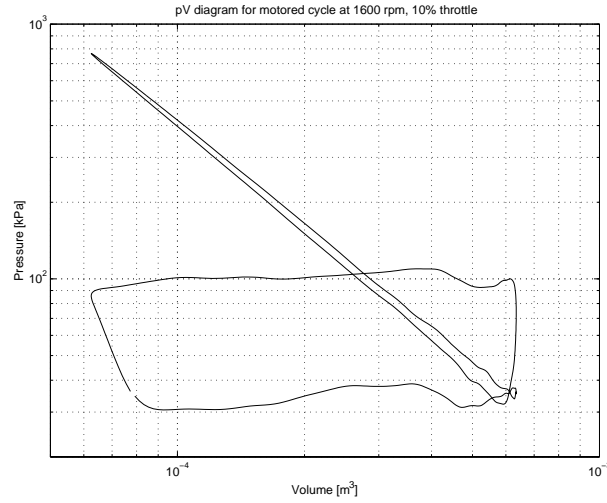


**Figure 9** Log-log  $pV$  diagram for pressure that has been optimized and the crank angle offset, sensor gain, and pressure offset has been included.

To verify, that the optimization procedure gives a pressure signal which has the correct properties, a  $pV$ -diagram is plotted in log-log scale in Figure 9. One verification of correctness seen in the plot is that during compression and expansion the diagram shows approximately straight lines. Another verification is that the edge is sharp at TDC and that lines do not cross each other at TDC, which would indicate wrong TDC phasing [4].

### 5.1 Pressure Residual

The results that are obtained from the minimization problem that is based on the pressure residual, Equation 12, is summarized below. As a first step all parameters are included in the optimization procedure.

#### Sensor gain, $C$ , and initial pressure, $p_{ivc}$

With all parameters free the Hessian has a reciprocal condition number of  $\kappa^{-1} \approx 10^{-17}$  and the are two components in the eigenvector that corresponds to the smallest eigenvalue are pressure gain,  $C$ , and the initial pressure,  $p_{ivc}$ . This indicates that the gain,  $C$ , is hard to determine if also the initial pressure,  $p_{ivc}$ , is free and the model can be viewed as over-parameterized. This can be motivated by studying the pressure development which approximately undergoes a polytropic compression and expansion, i.e.  $p = c \cdot V^{-k}$  where  $k$  is the polytropic expansion constant. The constant  $c$  can be found at IVC as  $c = \frac{p_{ivc}}{V_{ivc}^{-k}}$ . By scaling  $p_{ivc}$ ,

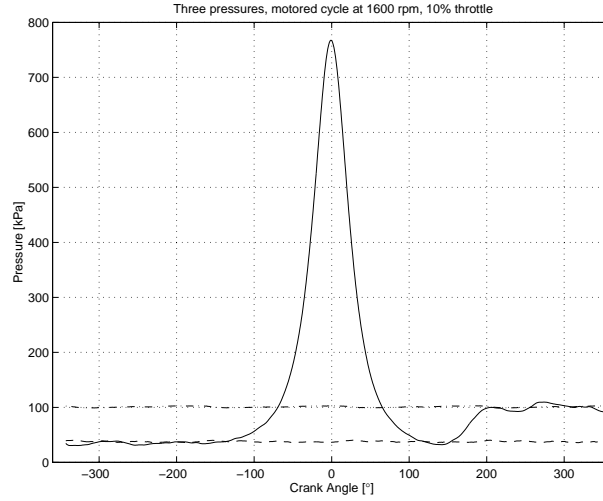


**Figure 10** Cylinder pressure, intake manifold pressure, and exhaust pressure for one motored cycle. A validation that with a known sensor gain,  $C$ , the initial pressure,  $p_{ivc}$ , can be estimated and the cylinder pressure is close to the intake and exhaust pressures during the intake and exhaust strokes.

the pressure trace,  $p = \frac{p_{ivc}}{V_{ivc}^{-k}} \cdot V^{-k}$ , also becomes scaled with the same constant which gives the same effect as a change in sensor gain.

There is still a possibility to estimate  $p_{ivc}$  given  $C$  and vice versa. This possibility can be used for cross validation of the initial pressure and sensor gain, at low speeds where a tuned intake system does not have a large effect. If the sensor gain is known then the initial pressure would approximately correspond to the intake manifold pressure during the intake stroke and to the exhaust pressure during the exhaust stroke. Figure 10 shows such an validation.

The initial pressure is difficult to determine without a sensor for absolute pressure mounted directly in the cylinder. To use the intake manifold pressure is another possibility but due to tuning and ram effects the pressure in the intake differs from the pressure in the cylinder. The gain,  $C$ , can be determined through calibration experiments and is therefore removed from the optimization and fixed to the value obtained from calibration.

### Heat transfer parameters $T_{ivc}$ , $C_1$ , and $T_w$

With all parameters except,  $C$ , free the reciprocal condition number was  $\kappa^{-1} \approx 3 \cdot 10^{-10}$ . The largest components in the eigenvector for the smallest eigenvalue corresponded to  $T_{ivc}$ ,  $C_1$ , and  $T_w$ . The structure of the heat-transfer correlation gives a hint to this dependence. The temperature is modeled as  $T = T_{ivc} \frac{pV}{p_{ivc}V_{ivc}}$

Throttle angle	Standard deviation for $V_{cr}$
0 %	9.6 % of $V_c$
5 %	2.2 % of $V_c$
10 %	0.7 % of $V_c$
15 %	0.5 % of $V_c$

**Table 3** Standard deviation for the estimated crevice volume, for an engine speed of 800 rpm. The standard deviation increases pronouncedly when the throttle angle decreases, which reduces the temperature difference between crevices and average charge temperature.

from this it can be seen that scaling the initial temperature  $T_{ivc}$  with  $\alpha$  also scales the average cylinder charge temperature,  $T$ , with  $\alpha$ . The variables  $T_{ivc}$ ,  $C_1$ , and  $T_w$  effects the heat transfer equation in approximately the following way

$$dQ_{ht} = C_1 (T - T_w) K$$

If the initial temperature  $T_{ivc}$  is scaled with  $\alpha$ , an identical model can be received received by scaling  $T_w$  with  $\alpha$  and  $C_1$  with  $\frac{1}{\alpha}$ .

$$dQ_{ht} = \frac{1}{\alpha} C_1 (\alpha T - \alpha T_w) K = C_1 (T - T_w) K$$

The above discussion illustrate that it is difficult to estimate all three parameters and therefore  $T_{ivc}$  is fixed to a value slightly above the ambient temperature since the parameters  $T_w$ ,  $C_1$ , can not easily be measured.

### Crevice volume, $V_{cr}$

With  $C$ , and  $T_{ivc}$  fixed  $\kappa^{-1}$  is further improved to  $\kappa^{-1} \approx 5 \cdot 10^{-9}$ . And the crevice volume corresponded to the smallest eigenvalue of  $H$ .

Especially for small throttle angles the crevice volume is difficult to identify from the pressure data, this is shows in the standard deviation for the estimated  $V_{cr}$  parameter, Table 3. One plausible explanation is that low cylinder pressures give low temperature differences between the wall and the mean gas temperature, which makes it hard to detect that the crevice effect. For several cycles even negative values of the crevice volume are received from the measured pressure data. This might indicate that the model does not correctly describe the actual loss mechanisms present in the combustion chamber during the motored tests. Both crevice effects and heat-transfer are loss mechanisms that have similar influence on the pressure and are hard to separate from each other. Combining the equations for the two mechanisms, with a negative  $V_{cr}$  and a large  $C_1$ , the actual pressure trace is sometimes better described than with parameter values that have physical meaning.

### Heat transfer coefficient $C_1$

With the crevice effect removed  $\kappa^{-1}$  was further improved further to  $\kappa^{-1} \approx 1 \cdot 10^{-6}$ , but the objective function did not change much. With  $C$ ,  $T_{ivc}$ , and  $V_{cr}$  removed the largest component in the eigenvector corresponded to the heat transfer coefficient  $C_1$ . When  $C_1$  is removed the objective function  $V_N(\Theta)$  increases, which indicates that the heat transfer  $C_1$  is important for describing the pressure development.

### The rest of the parameters

The value of  $\kappa^{-1}$  steadily increases if more parameters are removed from the optimization. The objective function also starts to increase when more parameters are removed from the optimization procedure, which indicate that they are necessary for a good fit. For the sake of completeness the order that the parameters were removed in the tests is given here:  $p_0$ ,  $T_w$ ,  $\theta_0$ ,  $V_c$ , and  $p_{ivc}$ , which leaves  $\gamma_{300}$ .

## 5.2 Heat-Release Residual

The criterion based on the heat release residual, Equation 6, has been analyzed in the same way as the pressure residual and the parameters that can be removed and the order in which they were removed agrees with the procedure described above for the pressure residual. However, there is one major difference between the heat release and the pressure residuals and that is in how the pressure sensor model is included. In the heat release residual the pressure sensor model must be inverted. This is analyzed below. Another minor difference is that  $p_{ivc}$  is not necessary in the heat release residual.

### Sensor gain, $C$ , and heat transfer coefficient, $C_1$

With all parameters free the reciprocal condition number was  $\kappa^{-1} \approx 5 \cdot 10^{-11}$ , which is not at all close to the machine precision. But if the parameters are studied during the optimization it can be seen that the parameter values for the heat transfer coefficient  $C_1$  tends to  $C_1 = 0$  and sensor gain  $C$  increases. The cause for this behavior can be seen by studying the least squares criterion with the residual described by Equation (11), which has a global minimum for  $C = \infty$  and  $C_1 = 0$ . Set for example  $C = \infty$  and  $C_1 = 0$  and insert into Equations 10, 4, and 1. Even if  $C_1$  is set to a fixed value during the optimization the gain  $C$  still increases, since by reducing  $p$  and  $dp$  in Equation (1) it also reduces the residual, but it eventually stops at a finite value.

## 5.3 TDC determination, $\theta_0$

There are several methods that can be used for determining the exact location of the top dead center (TDC), of which there are basically two different approaches. One approach is to directly measure the piston position in some way, e.g. by a dial indicator or by using microwaves. Measurements of the piston position should be

performed on both sides of TDC to reduce systematic errors in the determination [4, 5]. Another approach is to determine the position using motored cylinder pressure data and some knowledge about the process, e.g. a thermodynamic model [2, 3]. Also for such methods it is essential that data from both sides of TDC is used.

If TDC is determined by using a thermodynamic model and pressure data, the values that such a method gives depend on the model and its assumptions. The loss mechanisms, such as heat transfer, has an influence on how much before TDC the pressure peak appears. In one test heat release coefficient  $C_1$  was forced to change 40 %, which changed the estimated TDC phasing changed with  $\sim 0.1^\circ$ . This change is not large but it shows the dependence on the assumed heat release model. Since the minimization is performed over a large crank angle interval the influence of measurement noise is reduced.

The dependence on the thermodynamic model is further illustrated in Figure 11, where pressure data for three different operating conditions has been used to find crank angle phasing. The same model structure has been used in all three cases, which if the model fully captured all phenomena present would give the same values. For the same operating condition the crank offset is estimated to within  $0.1^\circ$ , which is very good and close the limit of how accurate the TDC can be determined. But for different operating conditions the offset is estimated only within  $0.5^\circ$ . This indicates that the model does not fully capture the appearance of the pressure signal with respect to changing operating conditions. Though, there are no numerical difficulties in identifying the crank angle offset  $\theta_0$ .

## 5.4 Cylinder pressure referencing

To determine the absolute cylinder pressure level is called absolute pressure referencing (or pressure pegging). The determined absolute value of the cylinder pressure has an influence on many parameters that are calculated from cylinder pressure, such as: polytropic indexes for compression and expansion, heat release energy and rate, estimated charge temperature as well as other [4]. Randolph [6] described nine, and evaluated four different methods, for cylinder pressure referencing, where two of the methods were: (1) Forcing a polytropic compression with a fixed polytropic coefficient  $k$ . (2) Forcing a polytropic compression with a variable  $k$ . Both methods are sensitive to noise in the measured pressure signal, especially number 2 in it's calculation of the polytropic exponent. Both also have the drawback of assuming a polytropic compression, which means that they are sensitive to the TDC phasing since the volume depends on  $\theta_0$ .

The method investigated here addresses the problems described above. This is done by performing a total minimization including the pressure referencing, the influence of crank angle phasing, and a model for the thermodynamic processes in the cylinder (which is more than just assuming polytropic compression). Furthermore, the optimization is performed over all samples from IVC to EVO which reduces the influence of measurement noise.

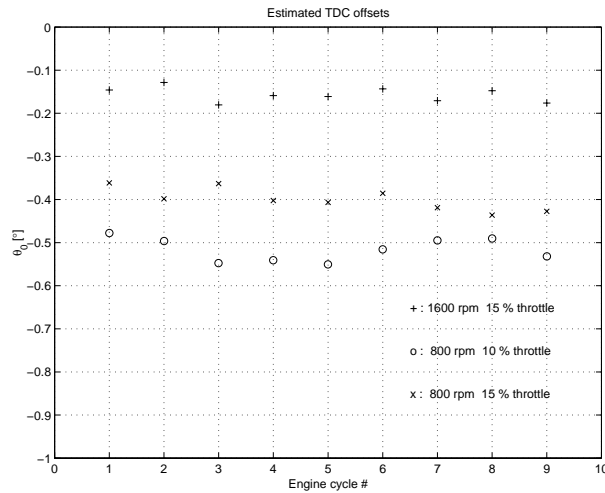


**Figure 11** Estimated TDC offset for crank angle measurements. The values that are estimated for one operating condition is very close to each other (within  $\sim 0.1^\circ$ ), but between the operating conditions the offset varies ( $\sim 0.5^\circ$ ).

### Pressure measurement corrections

Both TDC determination and absolute pressure referencing by using thermodynamic models have been given much attention in the literature, and they have often been considered as separate problems. It has in both cases been noted that the procedures slightly depends on each other, especially the absolute pressure referencing techniques depends on the phasing of the pressure trace. The method discussed here addresses both issues at the same time.

### 5.5 Parameter variations

Comparing the parameters that are estimated, for different cycles at the same operating condition, shows that there are cycle-by-cycle variations present. The presence of variations indicates that it is not sufficient just to tune the parameters on one motored cycle, instead several cycles should be used and an average of the estimated parameters should be used in the subsequent heat-release calculation.

### 5.6 Which criterion to minimize?

The criterion that is based on minimizing the pressure residual, Equation (12), has for the same number of parameters had better numerical properties concerning the Hessian. Also when there is much noise in the pressure signal the pressure

residual is better, this is due to the calculation of the differentiated pressure trace. In most cases the pressure residual converges 1 or 2 steps faster than the heat release residual. But no significant differences in estimated parameters could be discerned for the two methods. One benefit with the heat release residual is that, when used in conjunction with a heat release analysis program, the same model and implementation can be used for both heat release analysis and parameter estimation.

## 6 Conclusions

A systematic method for identifying unknown or non-measured parameters in heat release models has been presented. The question that has been addressed is what model parameters can be identified by measuring the in-cylinder pressure. To have a well determined reference for the heat release, the identification is performed for a motored cycle that is obtained by skipped firing.

The parameters  $\gamma$ , crank angle offset, pressure sensor offset, and IVC cylinder pressure are identifiable without numerical difficulties. At least one of the parameters initial temperature, wall temperature, and heat transfer coefficient, included in the heat transfer equations, must be fixed to a constant value or else the model is over parameterized. It is recommended that the initial temperature is taken from other measurements. The combination of the loss mechanisms, crevice effect and heat transfer, also makes it hard to identify the separate effects. The pressure sensor gain can not be identified unless some assumptions are made about either the initial pressure or the heat transfer.

The systematic method reveals if there are ambiguities in the model and between the model and measured signal, for example parameters that are impossible to identify or that phenomena are modeled in a way that does not explain the measurements. In conclusion, this is a first step towards a systematic method for estimating heat release model parameters that does not include arbitrary choices of parameter values in the modeling.

## References

- [1] Kwang Min Chun and John B. Heywood. Estimating heat-release and mass-of-mixture burned from spark-ignition engine pressure data. *Combustion Sci. and Tech.*, Vol. 54:133–143, 1987.
- [2] Marek J. Staś. Thermodynamic determination of T.D.C. in piston combustion engines. *SAE Technical Paper 960610*, 1996.
- [3] Mitsue Morishita and Tadashi Kushiyama. An improved method for determining the TDC position in a pv-diagram (first report). *SAE Technical Paper 970062*, 1997.

- [4] Charles A. Amann. Cylinder-pressure measurement and its use in engine research. *SAE Technical Paper 852067*, 1985.
- [5] David R. Lancaster, Roger B. Krieger, and John H. Lienesch. Measurement and analysis of pressure data. *SAE Technical Paper 750026*, 1975.
- [6] Andrew L. Randolph. Methods of processing cylinder-pressure transducer signals to maximize data accuracy. *SAE Technical Paper 900170*, 1990.
- [7] Michael F. J. Brunt and Christopher R. Pond. Evaluation of techniques for absolute cylinder pressure correction. *SAE Technical Paper 970036*, 1997.
- [8] W. J. D. Annand. Heat transfer in the cylinders of reciprocating internal combustion engines. *Proc. Instn. Mechanical Engineers*, Vol. 177(36), 1963.
- [9] G. Woschni. A universally applicable equation for the instantaneous heat transfer coefficient in the internal combustion engine. *SAE Technical Paper 670931*, 1967.
- [10] Andrzej Wolff, Konstantinos Boulouchos, and Rene Mueller. A computational investigation of unsteady heat flux through an I.C. engine wall including soot layer dynamics. *SAE Technical Paper 970063*, 1997.
- [11] Michael F. J. Brunt and Andrew L. Emtage. Evaluation of burn rate routines and analysis errors. *SAE Technical Paper 970037*, 1997.
- [12] J. A. Gatowski, E. N. Balles, K. M. Chun, F. E. Nelson, J. A. Ekchian, and J. B. Heywood. Heat release analysis of engine pressure data. *SAE Technical Paper 841359*, 1984.
- [13] Lennart Ljung. *System Identification Theory for the User*. Prentice Hall, 1987.
- [14] J. B. Heywood. *Internal Combustion Engine Fundamentals*. McGraw-Hill series in mechanical engineering. McGraw-Hill, 1988.
- [15] Frank W. Schmidt, Robert E. Henderson, and Carl H. Wolgemuth. *Introduction to Thermal Sciences*. John Wiley & Sons, 2 edition, 1993.
- [16] The Math Works Inc., 24 Prime Park Way, Natick, MA 01760-1500. *Simulink – Dynamic System Simulation for MATLAB*.
- [17] The Math Works Inc., 24 Prime Park Way, Natick, MA 01760-1500. *Signal Processing Toolbox – User’s Guide*.
- [18] Bengt Johansson. *On Cycle to Cycle Variations in Spark Ignition Engines*. PhD thesis, Lund Institute of Technology, 1995.
- [19] E. Rosseel, R. Sierens, and R.S.G Baert. Evaluating piezo-electric transducer response to thermal shock from in-cylinder pressure data. *SAE Technical Paper 1999-01-0935*, 1999.

- [20] AVL LIST GmbH. *AVL Pressure Transducers for Engine Test Instrumentation*.
- [21] Åke Björk. *Numerical Methods for Least Squares Problems*. SIAM, 1996.
- [22] David G. Luenberger. *Linear and Nonlinear Programming*. Addison Wesley, 1984.

## Appendix

Data collection has been performed on a SAAB 2.3 l, four cylinder, four stroke, 16 valve, fuel injected, normally aspirated, production engine equipped with an ECU. The engine is connected to a Schenck “DYNAS NT 85” AC dynamometer, with an electronic control system. Table 4 shows the data for the engine.

Bore (B)	90	mm
Stroke (L)	90	mm
Swept volume (V-V <sub>c</sub> )	2290	cm <sup>3</sup>
Connecting rod (l)	147	mm
Crank radius (a)	45	mm
Weight	160	kg
Compression ratio (rc)	10.1	
Intake valve closing	53°	ABDC
Intake valve opening	50°	BBDC

**Table 4** Data for the engine that is used in the experiments.

# A Parametric Study of Optimal Spark Advance and the Influence of Cycle-to-Cycle Variations<sup>1</sup>

Lars Eriksson

*Vehicle Systems, ISY  
Linköping University, SE-581 83 Linköping  
SWEDEN*

## Abstract

Most of today's spark-advance controllers operate in open loop but there are several benefits of using feed-back or adaptive schemes based on combustion descriptors deduced from the cylinder pressure. A systematic study of how different engine conditions change the combustion descriptors, at optimal ignition timing, is performed. The analysis is performed using a one-zone heat-release model and varying the model parameters. The combustion descriptors that are studied are: position of the pressure peak, mass fraction burned levels of 30%, 45%, 50%, and 90%, and the pressure ratio.

The peak pressure position and the positions for 45% – 50% mass fraction burned does not change much when the flame development angle and rapid burn angle change in wide ranges. Considering only the mass fraction burned trace it is shown that levels between 45% and 50% changes least. The pressure ratio produces values similar to the mass fraction burned and requires no separate treatment. The loss in net indicated torque is less than 0.4% if the spark advance is controlled using the peak pressure position or the position for 45% mass fraction burned even for large variations in the burn angles. Cycle-to-cycle variations do not have a significant effect on the optimal ignition timing and it suffices to evaluate the mean values for the burn rate parameters.

---

<sup>1</sup>This is an extended version of the conference paper "Spark Advance for Optimal Efficiency" by Lars Eriksson, *SAE Technical Paper 1999-01-0548*, Detroit, MI, March, 1999.

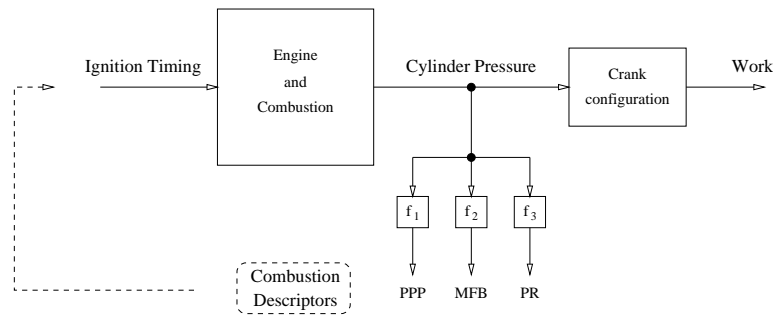


**Figure 1** Closed loop schemes for spark advance control have been presented that utilize the three combustion descriptors, shown in the figure, as a sensor for optimal spark advance. The three combustion descriptors are: peak pressure position (PPP), mass fraction burned (MFB), and the pressure ratio (PR).

## 1 Introduction

Development in the area of computerized engine controls has approached the point where they are feasible to utilize for direct combustion measurements and for on-line engine optimization. The development strives to meet the challenges of stricter emission regulations and the customers demand for better fuel economy. The spark advance by itself affects nearly all engine outputs, and is thereby an important parameter that requires precise control in todays and future engines. Most of todays production systems for spark advance control are open loop schemes that rely on look-up tables obtained by extensive calibration. Closed-loop schemes have the potential to improve performance and reduce the calibration effort but they require some kind of sensor.

Different sensing strategies have been presented that relate variables deduced from the in-cylinder pressure, such as peak pressure position (PPP), mass fraction burned (MFB), or pressure ratio (PR), to when the spark advance gives maximum brake torque (MBT). The variables will be referred to as *combustion descriptors* since they include a compact description of the combustion phasing. Feedback and calibration schemes that utilize these descriptors have reported good results [1, 2, 3, 4]. Figure 1 shows a schematic picture of the situation. The robustness of such a system will depend on how sensitive the combustion descriptors are with respect to changes in non-measured engine or environmental conditions, since they don't measure the efficiency or torque directly. This poses the question that outlines this work: –At MBT timing, how do the combustion descriptors vary when the engine and environmental conditions change?

To perform experiments on a real engine that cover all possible cases of engine and environmental conditions would be very expensive and time consuming. How-

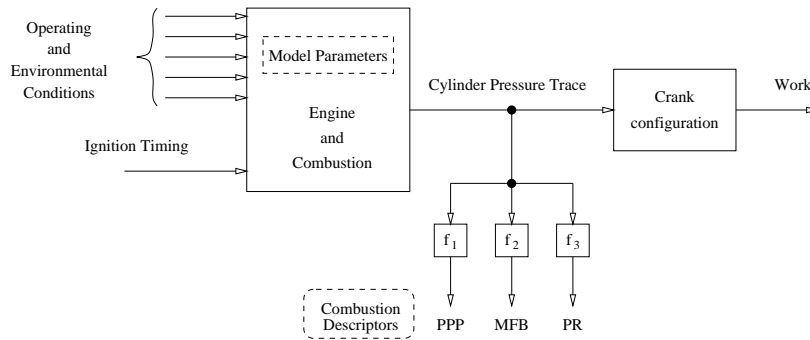


**Figure 2** Environmental and engine conditions affect how the cylinder pressure develops and thus the optimal spark advance. Changes in conditions can also be represented by changes in model parameters, and in the simulation evaluation the model parameters are varied and their influence on the combustion descriptors are mapped.

ever, an alternative way that is very informative is to use a model that describe the system sufficiently well and vary the conditions in the model. The latter approach is used here where modeling and simulation of the cylinder pressure is used in a systematic way to gain insight into how the spark advance positions the pressure trace and mass fraction burned profile for maximum work. The influence that varying conditions have on the *combustion descriptors* at optimal ignition timing is investigated by varying parameters in the model.

## 1.1 Outline of Investigation

Background material on spark-advance control, the combustion descriptors, and the one-zone heat-release model is given in Sections 2 to 4. The heat-release model used here was presented by Gatowski et. al [5], and is well known and much used. The model includes the loss mechanisms of heat transfer and crevice flow and can accurately describe the pressure development. In Section 5 a data set, covering the engine operating range, is used to build a parameter data-base over the rate of heat-release and the cycle-to-cycle variations. The experimental data is further examined with respect to flame development and rapid burning and how they depend on operating condition and ignition angle.

Engine conditions, see Figure 2, such as fuel, air humidity, EGR dilution, aging, wear, as well as several other influence the model parameters. One example is the air humidity which changes how fast the flame develops,  $\Delta\theta_a$ , and burns,  $\Delta\theta_b$ , and it also changes the energy contents  $Q_{in}$  and thermodynamic properties. Instead of varying the engine conditions directly the model parameters are studied in the simulation, see Figure 2.

In Section 6 the parametric study is described. The model parameters related to burn rates, loss mechanisms, energy content, and thermodynamic properties are varied and for each parameter value the ignition timing that maximizes the produced work is searched for. When the optimal ignition timing is found, the pressure and mass fraction burned traces are calculated and compared. The results are trends that illustrate how different model parameters influence the deduced variables. A quantification of the how much is lost when a deduced variable is used for control and the conditions is also performed.

The simulation study is first performed without considering cycle-to-cycle variations, and then it is shown in Section 8 that the cycle-to-cycle variations do not significantly change the results. Finally two issues that are relevant for a spark advance control system are studied in Section 9. The ambiguity in the determination of how a certain peak pressure position relates to early or late combustion is pointed out, and it is shown that the ambiguity becomes pronounced for conditions with rapid burning angle larger than  $37^\circ$  which only occurs at idle conditions. The other issue discussed is the gain from spark advance to the combustion descriptors.

## 2 Spark advance control

Spark-advance control deals with determination of the engine position where the spark plug shall ignite the air-fuel mixture and start the combustion. Engine efficiency and emissions are directly affected by the spark advance, due to its influence on the in-cylinder pressure. The purpose of the engine (and combustion) is to produce work and the optimal spark advance is here defined as the spark advance that gives maximum work if all other parameters are held constant. Emission regulations and engine knock sometimes restrict the spark advance setting from being at optimum, but this is not a topic here.

### Open-loop control

Today, most spark-advance controllers are open-loop systems, that measure a number of parameters known to affect the spark advance and compensate for their effects. Extensive testing and calibration, during the design phase of the engine, results in a nominal spark-advance schedule. Such a calibrated schedule is conservative since it has to guarantee good performance over the entire range of the non-measured parameters, and also be robust to aging. If all parameters that affect the spark advance were measured, and their effects and interactions were properly accounted for, it would be possible to determine the best spark advance. However, such a system would be too expensive due to the measurements and testing required to incorporate it in a production car.

### Feed-back or adaptive control

A different approach is to measure the result of the spark setting rather than measuring all the parameters known to affect the spark advance. Such a scheme

can still maintain the optimal spark advance even for large changes in non-measured parameters. This requires a measurement of parameters directly resulting from the actual combustion and that are related to the produced work. One of the first attempts to use feedback control to maintain optimal performance was made by Draper and Li [6]. They used a dither technique and applied it to a single cylinder engine. Schweitzer et. al. [7] extended the work to a multi-cylinder engine. These systems rely on the dithering signal that constantly changes the ignition and excites the system in order to determine if the ignition is at optimum or not.

Another technique is to utilize some kind of sensor that directly measures the result from the combustion and then relate the measurement to the maximum work. One example is the cylinder pressure which is important since it together with the volume gives the work that is produced  $W_c$ , i.e.  $W_c = \oint p \, dV$ .

## 2.1 Spark Advance and Cylinder Pressure

The spark advance positions the combustion and cylinder pressure development in relation to the crank shaft rotation, see Figure 3. Under normal driving conditions the mixture is ignited around  $15 - 30^\circ$  before the piston has reached top dead center (TDC), and the pressure reaches its maximum around  $15 - 20^\circ$  after TDC. The figure shows three different pressure traces resulting from three different spark timings. An earlier spark advance normally gives a higher maximum pressure and temperature, which occur at earlier crank angles. The spark advance for maximum brake torque (MBT) is close to SA2, for the conditions shown in the figure, and the resulting pressure peak lies around  $17^\circ$  after TDC.

With too early ignition timing the pressure rise starts too early and counteracts the piston movement. This can be seen in the figure for SA1 where the pressure rise starts  $20^\circ$  before TDC. With an early ignition there are also increased losses due to heat transfer to the walls and flows into and out of crevices. With an early ignition timing the temperature will rise earlier and more energy will be dissipated during the cycle. Similarly, will the earlier combustion, which results in a maximum pressure, force more of the gases into the crevices with an early ignition timing.

Too late ignition produces a pressure increase that comes too late so that work is lost during the expansion phase. In Figure 3, the pressure increase for spark advance SA3 starts as late as at TDC. But work is also gained, partly due to the later start of the effects mentioned above, which can be seen in the figure. The pressure trace from the spark advance, SA3, is higher than the others at crank angles over  $35^\circ$ . However, this gain in produced work can not fully compensate for the loss early in the expansion phase, and work is lost compared to the optimal spark advance.

## 3 Empirical Rules for Optimal Spark Advance

There exists several empirical rules that relates variables deduced from the pressure trace to the optimal spark advance. The variables “describe” how the pressure

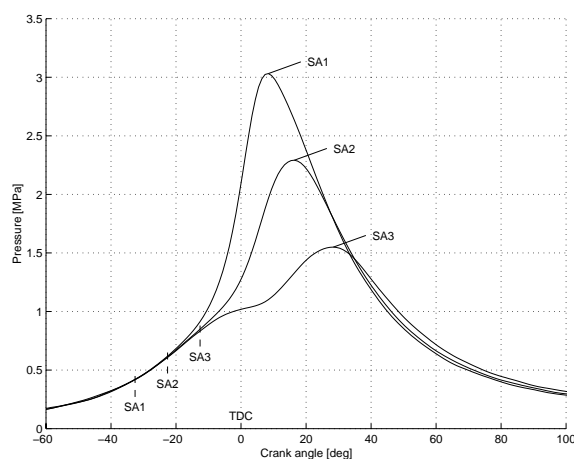


**Figure 3** Three pressure traces resulting from three different spark advances. The different spark advances are; SA1: spark advance  $32.5^\circ$  before top dead center (TDC), SA2:  $22.5^\circ$  before TDC, SA3:  $12.5^\circ$  before TDC. The optimal spark advance is close to SA2.

development is phased in relation to the crank angle revolution. Three well known *combustion descriptors* are summarized below.

### Peak Pressure Concept [1]

The optimal spark advance positions the pressure trace in a way that compromise between the effects mentioned above. To define the position of the in-cylinder pressure relative to TDC, the peak pressure position (PPP) can be used, Figure 4. The PPP is the position in crank angle where the in-cylinder pressure takes its maximal value.

It was shown by Hubbard et. al. that for MBT timing the position for the pressure peak is fairly constant, around  $16^\circ$  ATDC, regardless of operating condition [1]. A spark-advance control algorithm that maintains a constant peak pressure position (PPP) is therefore close to optimum. This scheme has been validated and used by several authors [8, 3, 9].

### Mass fraction burned (MFB)

Another possibility for describing the position of the combustion is to use the mass fraction burned profile  $x_b(\theta)$ . Heywood [10] states that with optimal spark timing half of the charge is burned (50% mass fraction burned) about  $10^\circ$  after TDC. This has been further investigated and supported by Bargende [4]. Other possible measures of good combustion could be the positions for 30% or 90% mass fraction

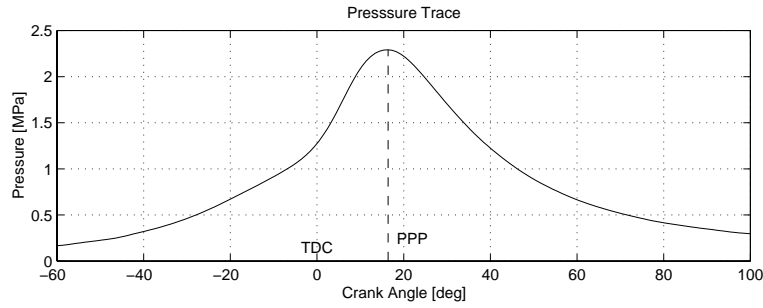


**Figure 4** The PPP (Peak Pressure Position) is the position in crank angles for the pressure peak. It is one way of describing the position of the pressure trace relative to crank angle.

burned. A mass fraction burned profile is shown in Figure 5 which indicates the positions for 30%, 50%, and 90% mass fraction burned.

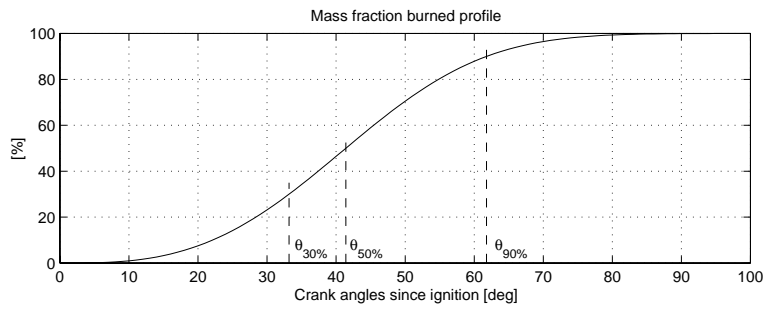


**Figure 5** The mass fraction burned profile  $x_b(\theta)$  with the three positions for 30%, 50%, and 90% mass fraction burned marked.

### Pressure ratio management (PR) [2]

A third way to define the combustion position and spark advance efficiency is to use the pressure ratio. The pressure ratio is defined using the ratio between a pressure from a firing cycle,  $p_f(\theta)$ , and the pressure from a motored cycle,  $p_m(\theta)$ ,

$$PR(\theta) = \frac{p_f(\theta)}{p_m(\theta)} - 1$$

The pressure ratio can be normalized with its maximum,

$$PR_N(\theta) = \frac{PR(\theta)}{\max PR(\theta)}$$

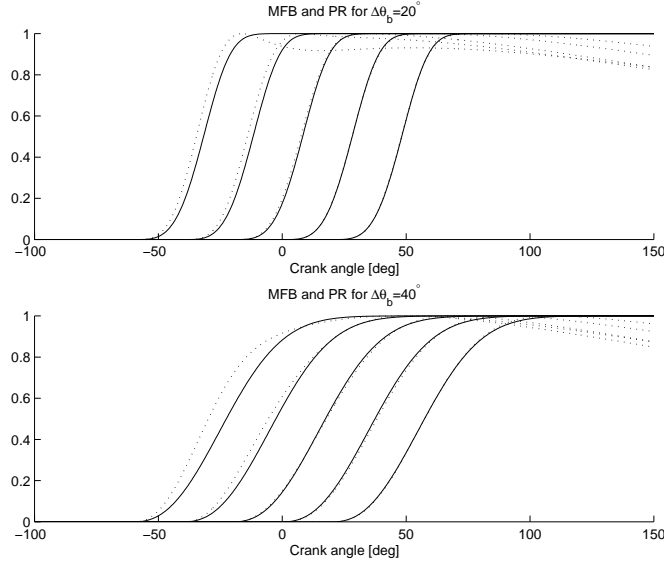


**Figure 6** Comparison of pressure ratio (dotted) and mass fraction burned (solid) traces, for five ignition timings,  $\theta_{ig} \in \{-60^\circ, -40^\circ, -20^\circ, 0^\circ, 20^\circ\}$ , and two rapid-burning angles,  $\Delta\theta_b \in \{20^\circ, 40^\circ\}$ . The difference is small when the burning occurs around and after TDC.

which results in a trace that is very similar to the mass fraction burned. An alternative way to normalize  $PR(\theta)$  is to use the pressure ratio at a certain crank angle, when the combustion is assumed to be complete, e.g.  $PR_N(\theta) = \frac{PR(\theta)}{PR(100^\circ)}$ . In the same way as for the mass fraction burned the position where the normalized pressure ratio equals  $PR_N(\theta) = 0.5$  has been proposed as a descriptor of the optimal combustion position.

### 3.1 Comparison of PR and MFB

The normalized pressure ratio  $PR_N(\theta)$  is very similar to the mass-fraction burned trace  $x_b(\theta)$ , and the difference between them is investigated in this section. For ignition control the interesting part to examine is the difference between the positions where  $PR_N(\theta) = 0.5$  and  $x_b(\theta) = 0.5$ . Simulations, using the model that will be described in Section 4, are used to quantify the difference. The ignition angle and the rapid burning angle  $\Delta\theta_b$  has most influence on the difference.

Figure 6 shows how the mass fraction burned and pressure traces differ for changing ignition timings  $\theta_{ig}$  and rapid burning angles  $\Delta\theta_b$ . The trend is that there is a minimum in the difference when the combustion is positioned around TDC and increases as the spark advance is advanced or retarded far from the

$\theta_{ig}$	$\Delta\theta_b = 20^\circ$		$\Delta\theta_b = 40^\circ$	
	$\Delta\theta_{50\%}$	$\Delta\theta_{45\%}$	$\Delta\theta_{50\%}$	$\Delta\theta_{45\%}$
$-60^\circ$	$2.97^\circ$	$2.93^\circ$	$5.25^\circ$	$5.29^\circ$
$-50^\circ$	$2.57^\circ$	$2.56^\circ$	$3.02^\circ$	$3.27^\circ$
$-40^\circ$	$1.76^\circ$	$1.79^\circ$	$0.74^\circ$	$1.03^\circ$
$-30^\circ$	$0.87^\circ$	$0.93^\circ$	$-0.70^\circ$	$-0.51^\circ$
$-20^\circ$	$0.26^\circ$	$0.31^\circ$	$-1.30^\circ$	$-1.20^\circ$
$0^\circ$	$-0.04^\circ$	$-0.00^\circ$	$-1.03^\circ$	$-1.03^\circ$
$20^\circ$	$0.21^\circ$	$0.23^\circ$	$-0.12^\circ$	$-0.14^\circ$

**Table 1** The difference in crank angle between 50% mass fraction burned and pressure ratio (PR)=0.5 for different rapid burn angles and ignition angles. The optimal ignition timing for these conditions are  $\theta_{ig} \in [-30^\circ, -15^\circ]$  and for these ignition angles the difference is only in the order of one degree.

optimal spark advance. Table 1 summarizes the difference between the pressure ratio and the mass fraction burned trace for different ignition angles and rapid burn angles. Optimal ignition timing is around  $-30^\circ$  to  $-15^\circ$  and at such conditions the difference is in the order of  $1^\circ$  which is very small. Therefore, only the mass fraction burned trace will be considered in the parametric study, in Section 6, since the pressure ratio will produce results that are very close to the mass fraction burned.

## 4 Heat-release model

This section describes the one-zone heat-release model based on the first thermodynamic law that is used both for evaluation of engine data and in the simulation evaluation.

The article by Gatowski et.al. [5] develops, tests and applies the heat release analysis procedure used here. It maintains simplicity while still including the effects of heat transfer and crevice flows. The model has been widely used and the phenomena that it takes into account are well known [10]. Therefore, only a short summary of the model is given here and a more detailed description is provided, of the model and the assumptions made during the modeling, in Appendix A.

The expression derived for the chemical heat release  $\delta Q_{ch}$  is

$$\delta Q_{ch} = \frac{\gamma}{\gamma-1} p dV + \frac{1}{\gamma-1} V dp + \delta Q_{ht} + \frac{dp V_{cr}}{T_w} \left( \frac{T}{\gamma-1} - \frac{1}{b} \ln \left( \frac{\gamma-1}{\gamma'-1} \right) + T' \right) \quad (1)$$

Equation 1 represents the chemical or gross heat release, and to completely solve it an expression for the heat transfer,  $\delta Q_{ht}$ , is needed. Woschni's correlation [11] is used here.

## 4.1 Heat-Release Calculation

The heat release analysis takes as input the pressure and volume traces and their derivatives and gives as output time or crank angle derivative of the net heat-release. Provided a measured pressure Equation 1 can easily be numerically integrated which gives the heat release trace  $Q_{ch}(\theta)$ . Assuming that the mass of mixture that burns is proportional to the released heat, then the mass fraction burned trace can be calculated by normalizing the heat-release trace

$$x_b(\theta) = \frac{Q_{ch}(\theta)}{\max Q_{ch}(\theta)}$$

The heat-release analysis is used to analyze pressure data, measured on the engine, and determine the best model parameters. Among others the crank angles for 10% and 85% mass fraction burned are determined.

## 4.2 In-Cylinder Pressure Simulation

A model for simulating the in-cylinder pressure trace can easily be derived by solving Equation 1 for the pressure differential,  $dp$

$$dp = \frac{\delta Q_{ch} - \frac{\gamma}{\gamma-1} p dV - \delta Q_{ht}}{\frac{1}{\gamma-1} V + \frac{V_{cr}}{T_w} \left( \frac{T}{\gamma-1} - \frac{1}{b} \ln \left( \frac{\gamma-1}{\gamma'-1} \right) + T' \right)} \quad (2)$$

This is an ordinary differential equation that easily can be solved numerically if it is provided with a heat-release trace,  $\delta Q_{ch}$ . For this purpose the well-known Wiebe function is used in its differentiated form.

The Wiebe function has the following appearance

$$x_b(\theta) = 1 - e^{-\alpha \left( \frac{\theta - \theta_0}{\Delta\theta} \right)^{m+1}} \quad (3)$$

and its differentiated form is

$$\frac{d}{d\theta} x_b(\theta) = \frac{\alpha (m+1)}{\Delta\theta} \left( \frac{\theta - \theta_0}{\Delta\theta} \right)^m e^{-\alpha \left( \frac{\theta - \theta_0}{\Delta\theta} \right)^{m+1}}$$

where  $\theta_0$  is the start of the combustion,  $\Delta\theta$  is the total combustion duration, and  $\alpha$  and  $m$  are adjustable parameters. Note that the Wiebe function is over parameterized in  $\alpha$ ,  $m$ , and  $\Delta\theta$ , since for example the sets [ $\alpha = 1$ ,  $\Delta\theta = 1$ ,  $m = 1$ ] and [ $\alpha = 4$ ,  $\Delta\theta = 2$ ,  $m = 1$ ] give identical functions.

Two parameters that are commonly used to characterize the mass fraction burned profiles are the *flame development angle*,  $\Delta\theta_d$ , and *rapid burning angle*,  $\Delta\theta_b$  (see Figure 7). Here the flame development angle,  $\Delta\theta_d$ , is the crank angle from ignition to 10% mass fraction burned, and the rapid burning angle,  $\Delta\theta_b$ , is the crank angle from 10% to 85% mass fraction burned. The burn angle parameters can be used to calculate the parameters in the Wiebe function. Due to the

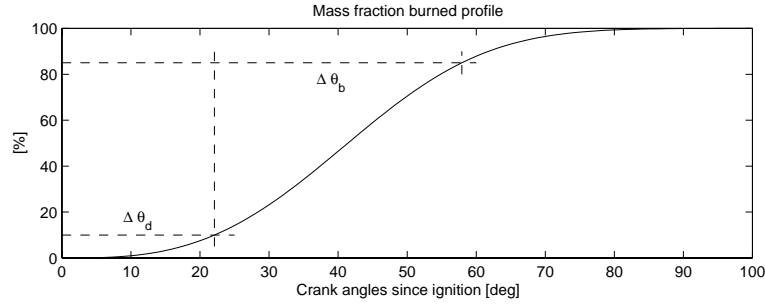


**Figure 7** The mass fraction burned profile with the flame development angle,  $\Delta\theta_d$ , and rapid burning angle,  $\Delta\theta_b$  marked.

over parameterization either  $\Delta\theta$  or  $\alpha$  must be specified for a unique solution, and by specifying  $\Delta\theta$  beforehand the Wiebe parameters can be calculated using the following scheme:

$$\begin{aligned} m &= \frac{\ln\left(\frac{\ln(1-0.1)}{\ln(1-0.85)}\right)}{(\ln(\Delta\theta_d) - \ln(\Delta\theta_d + \Delta\theta_b))} - 1 \\ \alpha &= -\ln(1-0.1) \left(\frac{\Delta\theta}{\Delta\theta_d}\right)^{m+1} \end{aligned}$$

The differentiated Wiebe function produces the profile for the mass fraction burned,  $\frac{dx_b}{d\theta}$ . The fuel mass,  $m_f$  together with its specific heating value,  $Q_{HV}$  gives the following equation for the heat release rate,

$$\frac{dQ_{ch}}{d\theta} = m_f Q_{HV} \eta_f \frac{dx_b}{d\theta} = Q_{in} \frac{dx_b}{d\theta}$$

where  $\eta_f$  represents the combustion efficiency. The parameters  $m_f Q_{HV} \eta_f$  are lumped together in  $Q_{in}$  for convenience. The parameters  $Q_{in}$ ,  $\Delta\theta_d$ , and  $\Delta\theta_b$  are all determined using the previously described heat release model and the engine data that will be described in the next section.

## 5 Engine Data and Model Parameters

In this section experimental data are analyzed using the heat-release model. Variations in flame development angle  $\Delta\theta_d$  and rapid burn angle  $\Delta\theta_b$  are studied with respect to their variations with operating condition and ignition angle. Furthermore, a simple model is developed that describes how  $\Delta\theta_d$  depends on the ignition angle. The experimental data are also used to determine a nominal set of model parameters that will be used in the simulation evaluation.

Cylinder pressures are collected on a SAAB 2.3 liter, normally aspirated, production engine, covering the engine operating range of engine speeds 1000, 1500,

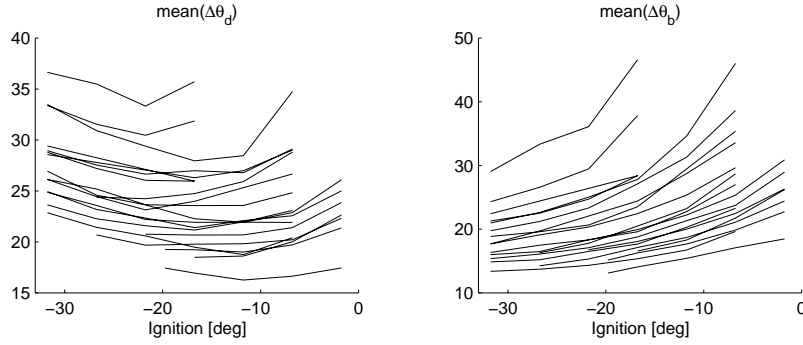


**Figure 8** Variations in  $\Delta\theta_d$  and  $\Delta\theta_b$  as a function of ignition angle. The different lines represent one operating condition with respect to engine speed and load.

2300, 3500 rpm and engine loads 0, 20, 50, 90, and 130 Nm. The operating conditions were selected to cover most of the normal driving conditions. In each operating condition the spark advance has been changed in the range  $35^\circ$  BTDC to TDC (except when the knock limit was reached). For each operating condition and spark advance, which sums up to 107 data sets, 300 engine cycles have been collected and analyzed.

### 5.1 Study of burn-angle variations

The flame development angle,  $\Delta\theta_d$ , and rapid burning angle,  $\Delta\theta_b$ , are central in the description of how the combustion propagates and the cylinder pressure develops and as a first step these parameters are studied. Heat-release traces have been calculated for 150 cycles in each dataset, using the heat-release model, described in Section 4, and the burn angles have been determined from the heat-release traces. Brunt and Emtage [12] performed an investigation of burn rate analysis errors and concluded that 150 cycles should be adequate for burn angle statistics.

### 5.2 Burn angles and spark advance

Figure 8 displays how the burn angles change with the ignition angle. The trend in the data is that  $\Delta\theta_d$  first decreases and then increases as the ignition angle is changed from very early to very late ignition. The minimum for the flame development angle  $\Delta\theta_d$  is attained in a position described approximately by the following relation

$$\min \Delta\theta_d \approx -2\theta_{ig}^* = -2 \arg \min_{\theta_{ig}} \Delta\theta_d(\theta_{ig})$$

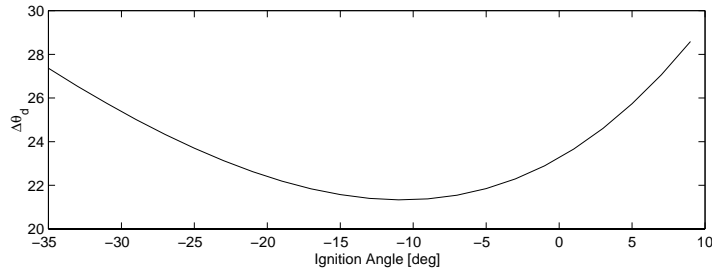


**Figure 9** Simulation of how the ignition angle influences the flame development angle,  $\Delta\theta_d$ , through the laminar burning velocity, the result agrees well with the experimental data in Figure 8. The minimum for  $\Delta\theta_d$  is  $22^\circ$  which occurs around  $\theta_{ig} \approx 11^\circ$ .

The decreasing and then increasing trend in the data is due to that the flame development and the pressure development are connected through the laminar burning velocity,  $S_L$ . Increasing the laminar burning velocity increases the rate of combustion and thus decreases the flame development angle. The laminar burning velocity is influenced by the pressure and the following power relation, which is derived from Heywood [10] in Appendix B, models the dependence

$$S_L = k_1 p^{k_2}$$

here  $k_1$  and  $k_2$  are positive constants that depend on initial temperature and pressure for the cycle, fuel used, equivalence ratio, and burned gas diluent fraction. Thus, increasing the pressure will decrease the flame development angle.

The influence that the ignition instant has on the of flame development is illustrated in the following examples: 1) For a very early ignition the pressure is low during the flame development phase which gives large  $\Delta\theta_d$ . 2) When the ignition angle is very late, the flame development phase is still in progress after TDC, and for very late conditions the pressure starts to decrease due to the expanding volume during the flame development phase which also increases  $\Delta\theta_d$ . In between these two cases the flame development is centered around TDC, with a high pressure, which produces the minimum flame development angle.

### Burn rate model

A simple model, for the early flame propagation and combustion, is developed in Appendix C that supports the explanation above. The flame-development angles that are received from the model for different ignition angles are shown in Figure 9 and the simulation results agree well with the experimental data shown in Figure 8. The model is based on the relations provided in Heywood [10] and an assumption

of spherical flame propagation which specifies the burn-rate through

$$\frac{dm_b}{dt} = S_L A_f \rho_u \quad (4)$$

where  $\rho_u$  is the unburned fluid density. The burn-rate specifies the mass-fraction burned which in its turn is used to calculate the volume-fraction burned. Finally, the flame-front area,  $A_f$ , is determined using the assumption of spherical flame-propagation. Note, this is an alternative to using the Wiebe-function for specifying how the fuel-mass burns. For more complex models see e.g. [10, 13, 14].

### Rapid burning angle

Figure 8 also shows that the rapid burning angle,  $\Delta\theta_b$ , increases with increasing ignition angle. The rapid burning angle also depends on pressure development and laminar burning velocity, in a similar way as the  $\Delta\theta_d$ , but during this phase the flame area is much bigger and it is therefore also influenced by turbulence. When the ignition is much earlier than shown in the figure,  $\Delta\theta_b$  is expected to increase for the same reasons as  $\Delta\theta_d$ . But this is not further investigated since the ignition for engines is normally retarded towards TDC from MBT, rather than advanced to positions earlier than MBT.

One measure of the cycle-to-cycle variations is the standard deviation which is shown in Figure 10. The figure shows that the cycle-to-cycle variations increase with increasing ignition angle. The correlation coefficient between  $\Delta\theta_d$  and  $\Delta\theta_b$  is shown in Figure 11, which clearly indicates that there is a dependence between the two burn angles. It is also apparent that the correlation coefficient shows a trend to increase with increased ignition angles.

### 5.3 Burn angles and engine speed

The influence of engine speed on  $\Delta\theta_d$  and  $\Delta\theta_b$  is shown in the two top plots in Figure 12. For low speeds the burn angles increase with increasing engine speeds, and for high speeds the burn angles decrease with increasing engine speed. A dependence on engine speed is natural since the laminar flame speed gives the burning as a function of time, see Equation 4, while the burn angles are functions of crank angle and they are related through  $d\theta = \frac{2\pi N}{60} dt$ , where  $N$  is the engine speed in rpm. But the phenomena are complex and the laminar burn velocity alone does not provide a sufficient explanation since burning also depends on turbulence. One interesting question is why the burn angles decrease for high engine speeds. A plausible explanation is that an increased engine speed increases the turbulence which increases the effective laminar burning area and thus decreases the flame development angle. Another contributor can be that an increased engine speed increases the engine temperature which in turn increases the laminar burn velocity.

The two top plots of Figure 13 show how the standard deviations change with the engine speed. There is a trend that an increased engine speed increases the cycle-to-cycle variations for all conditions except for the lowest load which shows a decreasing trend.

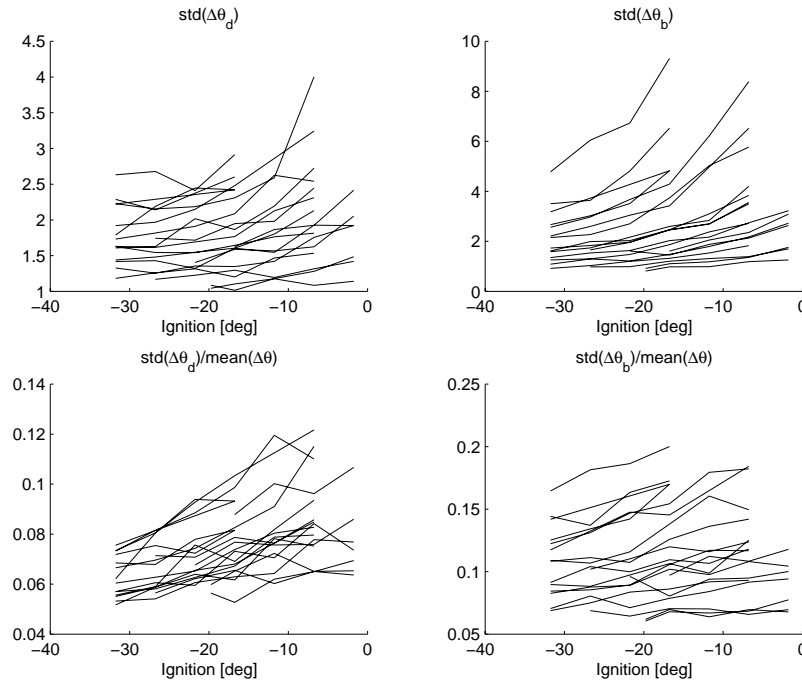


**Figure 10** Standard deviations for  $\Delta\theta_d$  and  $\Delta\theta_b$  for different ignition angles. The standard deviations increase as the ignition angle is increased.

The left plot in Figure 14 shows how the correlation coefficient varies with the engine speed. No obvious trend is visible, except than the dispersion in the correlation coefficient increases for decreasing engine speed.

#### 5.4 Burn angles and engine load

The two bottom plots in Figure 12 show that both burn angles decrease with engine load. This is due to that for higher loads the pressure, and density during the combustion are higher which increases the burn rate and thus decreases the burn angles, other effects such as in cylinder velocities and turbulence does also play a role. Also the standard deviations and correlation coefficient decrease when the load increases, Figures 13 and 14.

#### 5.5 Summary of burn-angle variations

Table 2 summarizes the trends in the different parameters derived from the burn angles that are due to changing engine conditions. *Ignition timing*: The cyclic variability increases as the ignition timing is delayed, and so does the correlation

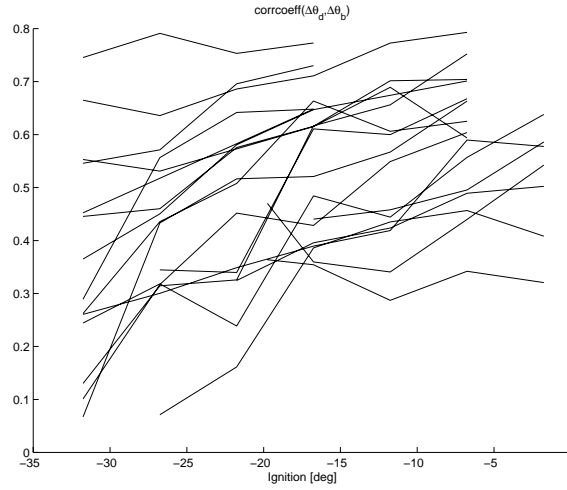


**Figure 11** Correlation coefficient between  $\Delta\theta_d$  and  $\Delta\theta_b$  for different ignition angles. There is a clear correlation between  $\Delta\theta_d$  and  $\Delta\theta_b$  for several operating conditions and the trend is that the correlation increases as the ignition angle is increased.

between  $\Delta\theta_d$  and  $\Delta\theta_b$ . *Engine load:* All parameters calculated from the burn angle decrease with increasing engine load. *Engine speed:* For the engine speed there is an increase in cyclic variability with increasing engine speed. The dependence and correlation between the burn angle parameters have been investigated by several others and many results are summarized in Section 9.4.2 in Heywood [10].

## 5.6 Burn-angle parameters for 1500 rpm 50 Nm

For this operating condition the parameters were varied within the following ranges when the ignition  $\theta_{ig}$  is varied from  $-30^\circ$  to  $-5^\circ$ .

$$\begin{aligned} \Delta\theta_d &\in (21, 26) && \text{min for } \theta_{ig} \approx -17 \\ \Delta\theta_b &\in (15, 30) && \nearrow \theta_{ig} \Rightarrow \nearrow \theta_b \end{aligned}$$

A simple model that well describes the mean values for these parameters is:

$$\begin{aligned} \Delta\theta_d &= 0.0149 \theta_{ig}^2 + 0.492 \theta_{ig} + 26.7 \\ \Delta\theta_b &= 0.0156 \theta_{ig}^2 + 0.978 \theta_{ig} + 31.0 \end{aligned} \quad (5)$$

Using this model the optimal ignition timing has been determined in simulation to  $\theta_{ig} = -21^\circ$  which agrees well with the measured MBT timing of  $\sim 20^\circ$ . Good approximations for the burn rate parameters at ignition timings close to optimum

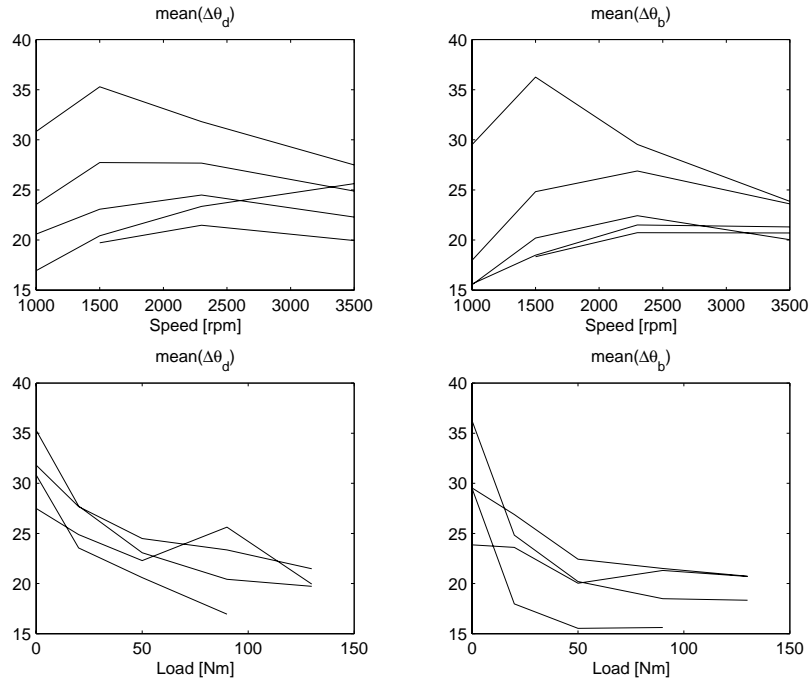


**Figure 12** Variations in  $\Delta\theta_d$  and  $\Delta\theta_b$  as a function of engine speed and engine load.

are  $\Delta\theta_d = 23$  and  $\Delta\theta_b = 17$ . This simple model is used to determine the gain from ignition to peak pressure position or from ignition to a certain mass-fraction burned level in Section 9.3.

## 5.7 Nominal Model Parameters

The heat-release model consists of several parameters that have been determined using the cylinder pressure data described in the beginning of this section. The parameters have been identified using a method that minimizes the prediction error. The method is further described in [15].

The parameter identification and analysis of the data set produced a set of nominal parameters that is used through out the simulation evaluation. For the simulation study the operating condition 2300 rpm and 50 Nm was chosen since it represents a normal driving condition. The parameters that are varied in the simulation evaluation and their values are given in Table 3. A more detailed description of the parameters and the effects that they model is given in Appendix A.

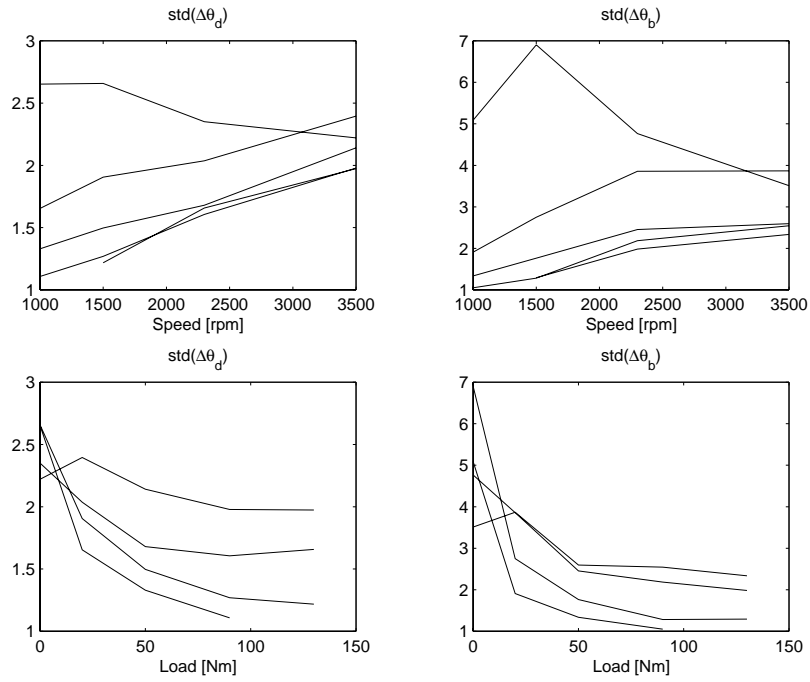


**Figure 13** The standard deviations for  $\Delta\theta_d$  and  $\Delta\theta_b$  as a function of engine speed and engine load.

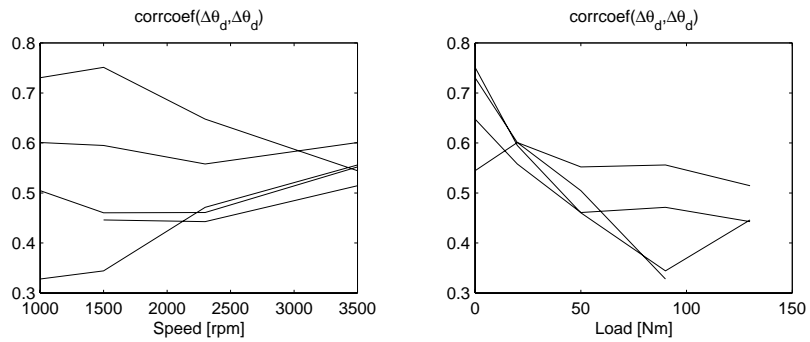


**Figure 14** Coefficient of correlation between  $\Delta\theta_d$  and  $\Delta\theta_b$  as a function of engine speed and engine load.

	$\theta_{ig}$	N	$T_L$
mean( $\Delta\theta_d$ )	$\searrow \nearrow$	$\nearrow \searrow$	$\searrow$
mean( $\Delta\theta_b$ )	$\nearrow$	$\nearrow \searrow$	$\searrow$
std( $\Delta\theta_d$ )	$\nearrow$	$\nearrow (?)$	$\searrow$
std( $\Delta\theta_b$ )	$\nearrow$	$\nearrow (?)$	$\searrow$
corcoef( $\Delta\theta_d, \Delta\theta_b$ )	$\nearrow$	$\rightsquigarrow$	$\searrow$

**Table 2** A qualitative representation of how the burn-angle parameters vary with increasing ignition angle  $\theta_{ig}$ , engine speed N, and engine load  $T_L$ . The symbols have the following meaning:  $\searrow$  – decreasing trend,  $\nearrow$  – increasing trend,  $\rightsquigarrow$  – no apparent trend,  $\searrow \nearrow$  – first decreases then increases,  $\nearrow \searrow$  – first increases then decreases, (?) – there are data that contradicts the trend.

Param.	Value	Param.	Value
$\Delta\theta_d$	23°	$V_{cr}$	0.5%
$\Delta\theta_b$	17°	$Q_{in}$	600 J
$C_1$	1	$\gamma_{300}$	1.34
$C_2$	0.5		

**Table 3** Nominal model parameter values that has been used during the evaluation. The parameters are:  $\Delta\theta_d$  and  $\Delta\theta_b$  – burn rate parameters,  $C_1$  and  $C_2$  – heat transfer parameters,  $V_{cr}$  – crevice volume given in % of clearance volume,  $Q_{in}$  – input energy,  $\gamma_{300}$  – ratio of specific heats for the temperature  $T = 300K$ .

### 5.8 Mean values for the burn rates

Figure 15 shows averaged values for the burn-rate parameters at different operating conditions, each mark in the plot represents one speed, load, and spark advance. As it can be seen in the figure the burn-rate parameters lie in the following ranges

$$\begin{aligned} \Delta\theta_d &\in [16, 37] \\ \Delta\theta_b &\in [13, 38] \end{aligned} \quad (6)$$

These values will be used as a basis in the simulation study especially in the study of how the burn rate effects the deduced variables.

## 6 Simulation evaluation of engine efficiency

The results from the last two sections are a model and set of nominal model parameters that can be used to simulate the cylinder pressure. Now the attention is

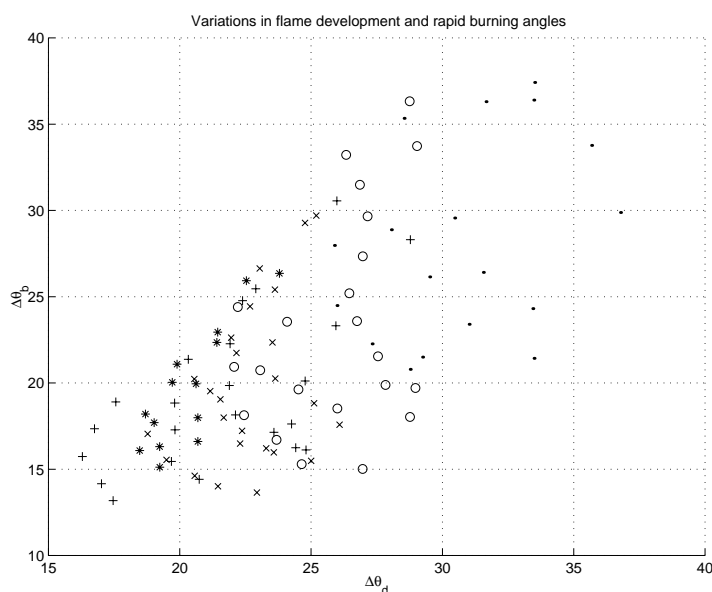


**Figure 15** Variations in the flame development angle,  $\Delta\theta_d$ , and rapid burning angle,  $\Delta\theta_b$ , for the data set. Each mark in the plot represents the mean value for the parameter, calculated from 150 cycles at each operating condition i.e. for one speed, load, and ignition timing. The different shapes represent different loads:  $\circ$ -0 Nm,  $\times$ -20 Nm,  $+$ -50 Nm,  $*$ -90 Nm, and  $\cdot$ -130 Nm

turned to the question that was posed in the introduction and refined in Section 1.1 with help from Figure 2: –How do the *combustion descriptors* vary when the model parameters change?

The method that is used to solve this question is outlined in Figure 16. The model parameters, described in Table 3, are varied and for each set of parameter values the optimal ignition timing is determined using an optimization procedure and finally the values of the combustion descriptors at the optimum is stored. With optimal ignition timing it is meant the spark advance that maximizes the produced work.

The spark advance has only a minor influence on the pumping process of the engine, see Figure 17. By delaying the ignition instant the pressure and temperature will become slightly higher when the exhaust valve opens but this increase does not significantly contribute to the exhaust and intake processes. During the simulation and search for optimal spark advance, it is therefore assumed that the ignition timing that maximizes the indicated work from IVC to EVO also maximizes the brake work.

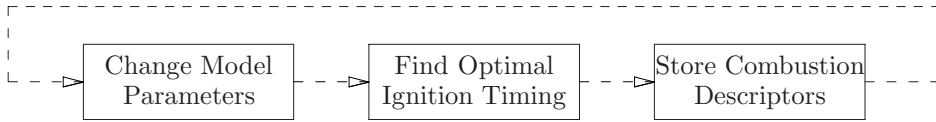


**Figure 16** The method for studying the how different model parameters influence the combustion descriptors at optimal ignition timing and.

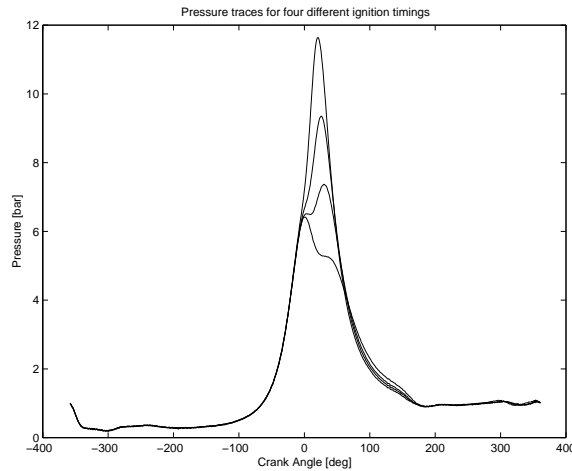


**Figure 17** Validation that the ignition does not significantly change the intake and exhaust processes. In the engine data plotted the four ignition angles ranged from  $-23^\circ$  to  $-8^\circ$  BTDC. Even though, the ignition angle changed the pressure during the exhaust and intake strokes does not change, and thus the pumping work is not significantly influenced by the ignition timing.

### Optimization procedure

The optimization problem, for finding the optimal spark advance, that is solved during the evaluation is stated as: Find the ignition angle,  $\theta_{ig}^*$ , that maximizes the work,  $W$ , from IVC to EVO, i.e.

$$\theta_{ig}^* = \arg \max_{\theta_{ig}} W(\theta_{ig})$$

The search is performed using a univariate maximization technique, similar to golden section search, which gradually reduces the interval for the optimum, see e.g. [16]. During the search the pressure trace  $p(\theta, \theta_{ig})$  and crank shaft torque

$M(\theta, \theta_{ig})$  are simulated for a given ignition angle  $\theta_{ig}$ , and the work is integrated from the torque

$$W(\theta_{ig}) = \int_{-130^\circ}^{130^\circ} M(\theta, \theta_{ig}) d\theta$$

Then the work  $W(\theta_{ig})$  is compared with previous results and a new  $\theta_{ig}$  is calculated. The interval for the optimum  $\theta_{ig}$  is gradually reduced by the search method and when the interval is smaller than  $0.01^\circ$  the optimization exits.

### Outline of Parameter Variations

The following sections show the results from the evaluation of how the model parameters in Table 3 affect the combustion descriptors deduced from the cylinder pressure. First the influence of the flame development and rapid burn parameters are investigated by varying  $\Delta\theta_d$  and  $\Delta\theta_b$  and having all other parameters fixed to their nominal values given in Table 3. For each pair of values for  $\Delta\theta_d$  and  $\Delta\theta_b$  the optimal spark advance is determined, and the pressure and heat release trace are calculated. The combustion descriptors are then determined and their variations and trends are plotted.

In Section 6.2 the influence of heat transfer and a correlation between the burn angles are investigated. In Section 6.3 the crevice volume and heat transfer from the combustion is investigated. Finally in Section 6.4 the influence of energy contents and thermodynamic property is investigated.

## 6.1 Flame Development and Rapid Burn

The first analysis is performed by varying the flame development angle,  $\Delta\theta_d$ , and rapid burning angle,  $\Delta\theta_b$ , see Figure 7 for their definitions. These combustion related angles depend on various measured parameters such as engine speed, engine load, and engine temperature, they also depend on several non-measured parameters such as air humidity, dilution by excess air and EGR. The desired property of the combustion descriptor is that it should not depend on changes in these parameters (nor in any other non-measured parameter).

The data set from the engine test cell provides information on how  $\Delta\theta_d$  and  $\Delta\theta_b$  vary with engine speed, engine load and ignition angle. Each mark, in Figure 15, is averaged over 150 consecutive cycles at constant engine speed, engine load, and spark advance. As it can be seen in the figure the parameters lie in the ranges  $\Delta\theta_d \in [16, 37]$ , and  $\Delta\theta_b \in [13, 38]$ . For the simulation evaluation the following larger set of parameter values is used,

$$\begin{aligned} \Delta\theta_d &\in [15, 45] \\ \Delta\theta_b &\in [5, 45] \end{aligned} \quad (7)$$

These ranges over-estimate the variations in the parameters at the optimal spark advance since the figure includes all operating conditions and all spark advances in the measured data.

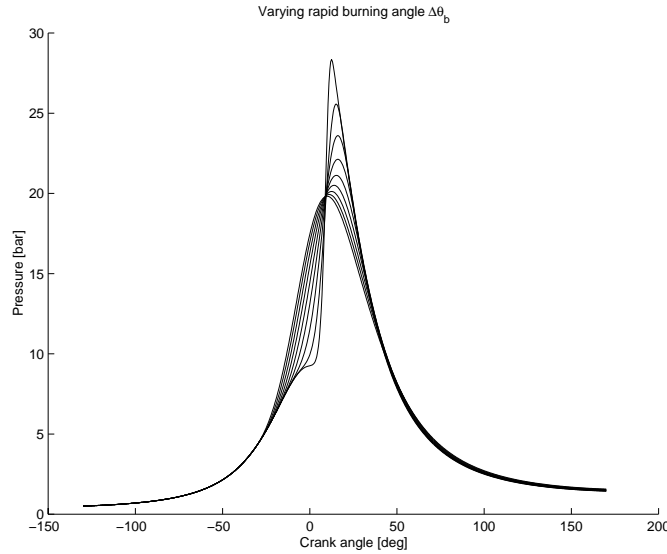


**Figure 18** Pressure traces for optimal spark advance for changes in rapid burning angle  $\Delta\theta_b$ . The flame development angle is  $\Delta\theta_d = 20^\circ$  for the plot in this figure.

### Pressure traces and heat release rates

Figures 18 and 19 show how the rapid burn rate  $\Delta\theta_b$  effects the position of the pressure trace and the heat release trace at optimal spark advance. Figure 19 shows how the combustion is positioned for varying rapid burn angles at optimal ignition timing. For increasing rapid burn angles the optimal ignition occurs earlier and the burning of the fuel is centered around a position slightly after TDC. Studying Figure 19 it is clear that the crank angle positions for 50% mfb are very close for all traces. This is the basic idea behind the empirical rule for positioning the 50% mass fraction burned at a pre-determined crank angle (for example  $9^\circ$  ATDC).

The evaluation below shows how the burn-rate parameters,  $\Delta\theta_d$  and  $\Delta\theta_b$  influence the optimal ignition timing, as well as how the peak pressure position and the mass fraction burned traces are positioned at optimal ignition timing for varying burn rate parameters.

### Ignition timing

The optimal ignition timing is directly influenced by the changes in burn rate and varies in wide range, which can be seen in Figure 20. Each circle in the plot represents one set of values for  $\Delta\theta_d$  and  $\Delta\theta_b$ . The optimal spark advance increases when flame development angle,  $\Delta\theta_d$ , and rapid burning angle,  $\Delta\theta_b$ , increase.

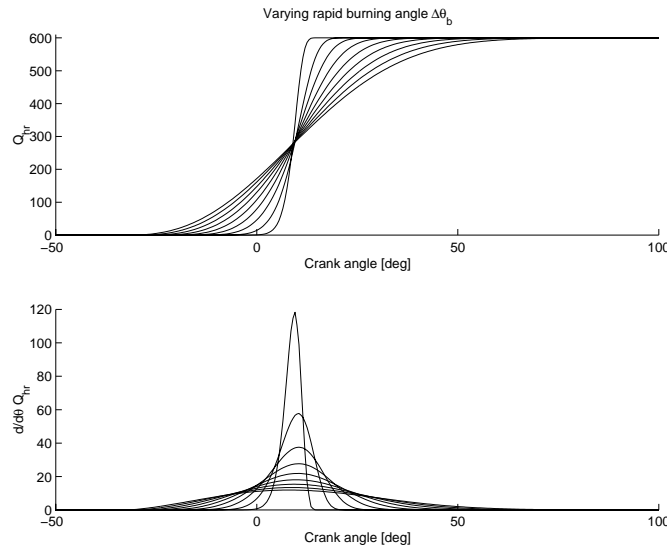


**Figure 19** Heat release traces for optimal spark advance for changes in rapid burning angle  $\Delta\theta_b$ . The flame development angle is  $\Delta\theta_d = 20^\circ$  for the plot in this figure.

### Peak pressure position

The peak pressure position (PPP or  $\theta_{pp}$ ) at MBT timing for changing burn rate parameters is displayed in Figure 21. The figure shows that the optimal ignition timing results in a pressure peak that is positioned in the range  $10^\circ$  to  $17^\circ$  ATDC for large changes in the flame development angle,  $\Delta\theta_d$ , and rapid burning angle,  $\Delta\theta_b$ . This corresponds well with earlier measurements for the engine which has shown that the optimal spark advance results in a peak pressure position around  $14^\circ$  to  $16^\circ$  ATDC [9]. Two things are worth to mention: First and most important, the optimal PPP only changes  $7^\circ$  while the optimal spark advance changes  $50^\circ$  (this has been reported earlier [1]). Second, the rapid burn angle has more influence on the optimal PPP than the flame development angle.

### Mass fraction burned

Figure 22 shows an enlargement around levels of 40 – 55% mass fraction burned which gives another view of the results in Figures 23 and 24. As it can be seen in the figure the traces are very close together for mass fraction burned levels in the range 45 – 50%. From the figure it is evident that positions for higher or lower levels than 45 – 50% will result in larger changes when the burn angles vary. For variations in flame development angle and rapid burn angle only, the 45% and 50% mass fraction burned position are good measures of the combustion efficiency since

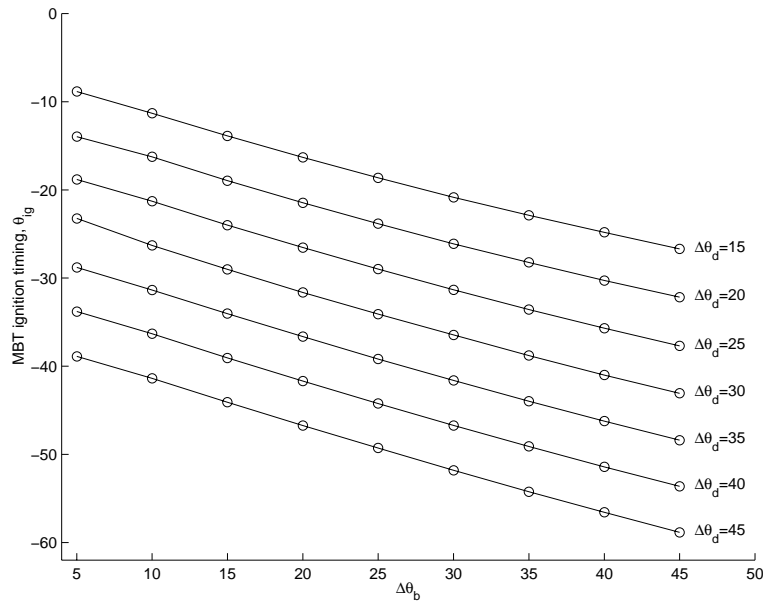


**Figure 20** Changes in the optimal ignition angle as a function of flame development angle,  $\Delta\theta_d$ , and rapid burning angle,  $\Delta\theta_b$ . The x-axis gives values for  $\Delta\theta_b$ , the lines represent constant  $\Delta\theta_d$ , and the y-axis gives the optimal ignition timing MBT timing.

it changes less than  $2^\circ$  at MBT timing, even for large changes in the burn angles.

The positions for 45% and 50% mass fraction burned ( $\theta_{45\%}$  and  $\theta_{50\%}$ ) are displayed in Figures 23 and 23 for varying  $\Delta\theta_d$  and  $\Delta\theta_d$ . The variations are at a minimum for ratios between 45% and 50%, but if there is a correlation between  $\Delta\theta_d$  and  $\Delta\theta_b$  then  $\theta_{45\%}$  is slightly better, this is further illustrated in the next section where a correlation between the burn angles is simulated together with the heat transfer is evaluated.

## 6.2 Heat Transfer and Burn Rate

The heat transfer is influenced by many operating parameters among others swirl, tumble, and turbulence which depends on engine design, as well as engine speed and engine temperature. In the Woschni heat-transfer correlation the heat transfer coefficient  $C_1$  is normalized such that it normally for SI engines lies around  $C_1 \approx 1$ . For the engine data used here  $C_1 = 1$  also gave a good fit. In the simulations the heat transfer coefficient is changed in the interval

$$C_1 \in [0.0, 3.2]$$

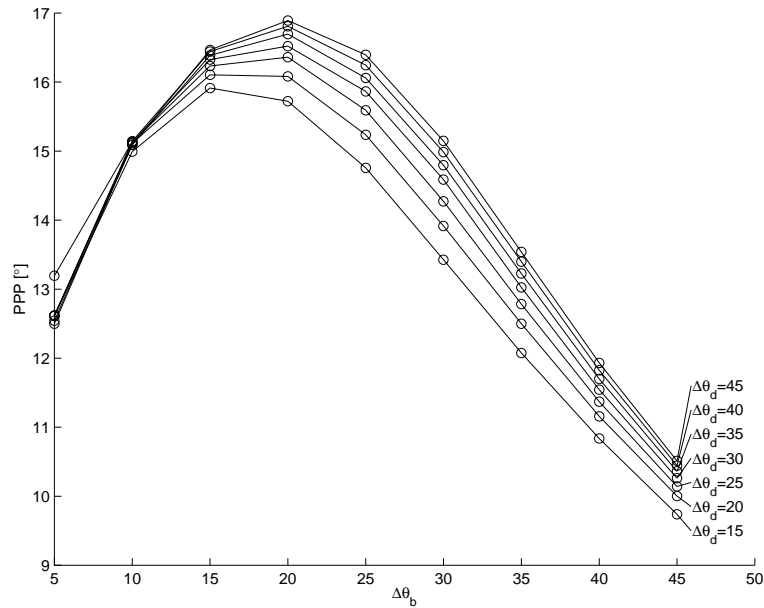


**Figure 21** The peak pressure position (PPP) for optimum spark advance (MBT timing) as a function of flame development angle,  $\Delta\theta_d$ , and rapid burning angle,  $\Delta\theta_b$ .

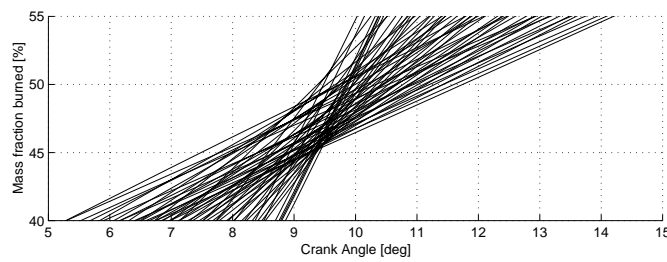


**Figure 22** Enlargement of the mass fraction burned traces shown in Figure 19 and with all other traces added. The plot shows that mass fraction burned levels between 45% and 50% are contained in a narrow region for a variety of flame development and rapid burn angles.

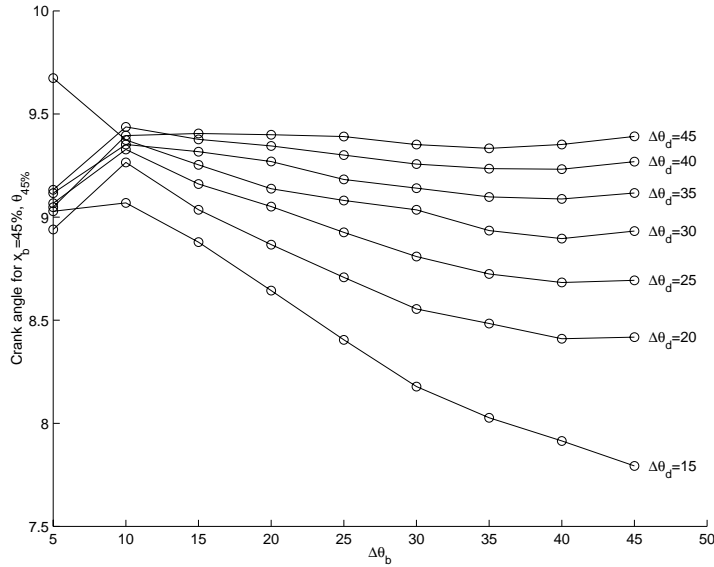


**Figure 23** Changes in the 45% mass fraction burned for optimum ignition as a function of flame development angle,  $\Delta\theta_d$ , and rapid burning angle,  $\Delta\theta_b$ .

The influence of the burn rate is further evaluated by changing  $\Delta\theta_d$  and  $\Delta\theta_b$  according to the following linear relation

$$\Delta\theta_b = 12 + (\Delta\theta_d - 15) \frac{38 - 12}{35 - 15} \quad (8)$$

where  $\Delta\theta_d$  is varied in the interval

$$\Delta\theta_d \in [10, 40]$$

The linear relation 8 represents variations in the burn rates that lies on a line in Figure 15, going through the points  $\Delta\theta_d = 15$ ,  $\Delta\theta_b = 12$  and  $\Delta\theta_d = 35$ ,  $\Delta\theta_b = 38$ .

### Optimal spark advance MBT

The optimal spark advance (MBT timing) is shown in Figure 25 for changes in heat transfer and heat release rate. The optimal spark advance decreases with increasing heat transfer and increases with longer  $\Delta\theta_d$  and  $\Delta\theta_b$ .

### Peak pressure position

The optimal peak pressure position (PPP) for changing heat transfer coefficients and burn rates are shown in Figure 26. The optimal position varies between 5 and

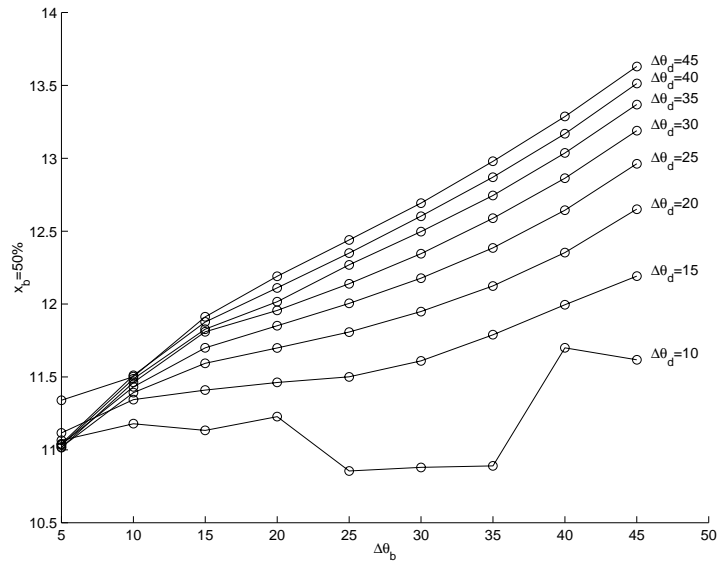


**Figure 24** Changes in the 50% mass fraction burned for optimum ignition as a function of flame development angle,  $\Delta\theta_d$ , and rapid burning angle,  $\Delta\theta_b$ .

25° ATDC. Increasing the heat transfer increases the optimal PPP,  $\theta_{pp}$ , while increasing the burn angles according to Equation 8 produce a more complex behavior in the optimal PPP. The variations follow the behavior of Figure 21: for small and large  $\Delta\theta_b$  the optimal  $\theta_{pp}$  occurs early, and for a position in between the optimal  $\theta_{pp}$  has a maximum.

### Mass fraction burned

Figure 27 displays the optimal position for 45% mass fraction burned,  $\theta_{45\%}$ , when the heat transfer and burn rate varies. Increasing the heat transfer increases  $\theta_{45\%}$ , while changes in the burn angles only produce a change of 1° in  $\theta_{45\%}$ . The position for 50% mass fraction burned has also been studied and the behavior for changing heat transfer was almost identical to the 45% mass fraction burned position, while for changes in the burn angles the optimal position changed 3° (which three times larger than for  $\theta_{45\%}$ ). The conclusion is: when there is correlation between the burn angles then a criteria based on 45% mass fraction burned is slightly better than a criteria based on 50% mass fraction burned.

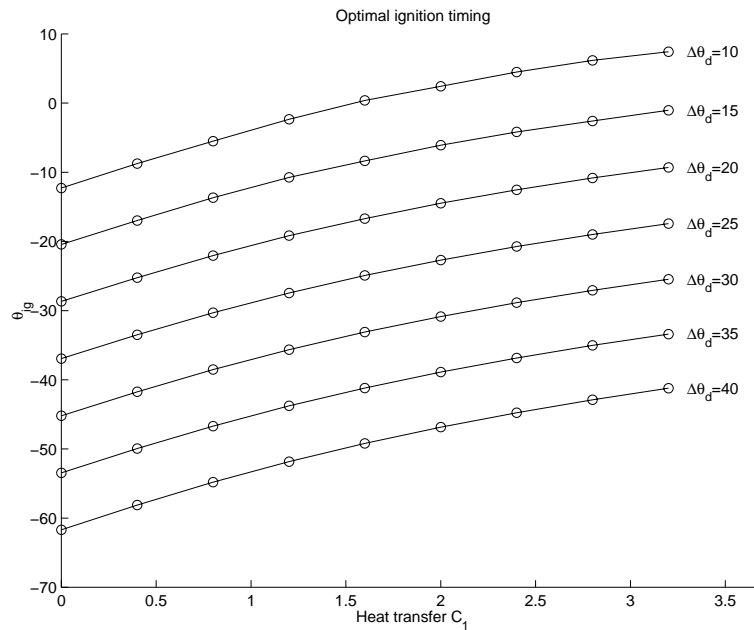


**Figure 25** Changes in the optimal ignition angle as a function of heat transfer coefficient  $C_1$  and changes in burn rate through  $\Delta\theta_b = 12 + (\Delta\theta_d - 15)/20 * 26$ .

### 6.3 Crevice Volume and Heat Transfer

The correlation parameter  $C_2$ , in the Woschni heat transfer correlation, reflects an increase in heat transfer due to the influence that the combustion has on charge movement. It usually lies around  $C_2 \approx 1$ , and  $C_2 = 0.5$  produced a good fit to the engine data. The crevice volume,  $V_{cr}$ , takes into account the losses for flows into and out of crevices. The crevice volume is given in percent of clearance volume, and reasonable values are 1–2% [5]. These parameters are changed in the following ranges  $C_2 \in [0, 1.5]$ ,  $V_{cr} \in [0, 1.5]$ .

#### Influence on PPP and MFB

The optimal PPP for changes in heat transfer coefficient,  $C_2$ , and crevice volume,  $V_{cr}$  is displayed in Figure 28. Increasing  $C_2$  delays the optimal position and increasing the crevice volume has only a slight affect. The influence of the crevice volume is more pronounced for cycles with high pressures, i.e. with early ignition timings where the pressure peaks early.

The influence of changing  $C_2$  and  $V_{cr}$  on the optimal 45% mass fraction burned position is the same as that of the optimal peak pressure position. While  $\theta_{pp}$  varies

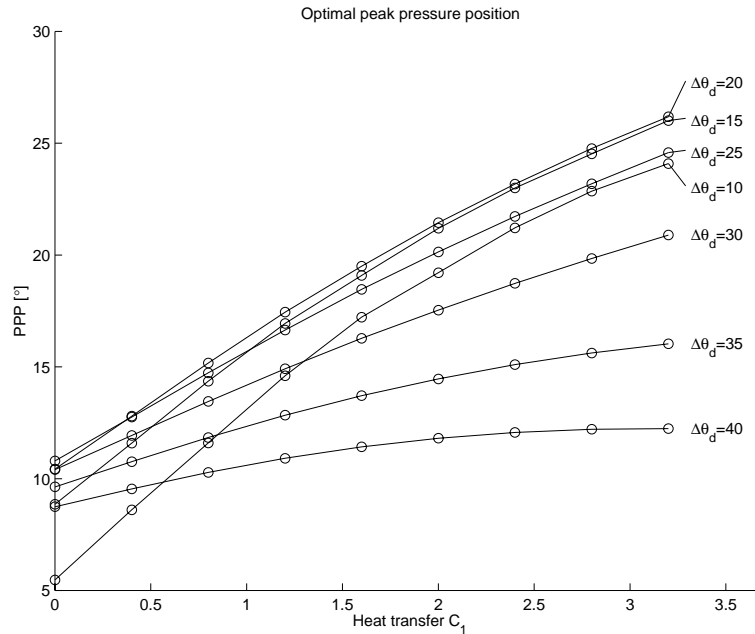


**Figure 26** Changes in the optimal peak pressure position (PPP) as a function of heat transfer coefficient  $C_1$  and changes in burn rate through  $\Delta\theta_b = 12 + (\Delta\theta_d - 15)/20 * 26$ .

from  $12^\circ$  to  $24^\circ$ , then  $\theta_{45\%}$  varies from  $3^\circ$  to  $17^\circ$ .

#### 6.4 $Q_{in}$ and $\gamma_{300}$

The input energy changes mainly with changing fuel and with mixture strength. The offset parameter  $\gamma_{300}$  which represents  $\gamma = \frac{c_v}{c_p}$  at  $T = 300^\circ\text{K}$  and also depends on the mixture. These parameters were changed in the ranges

$$\begin{aligned} Q_{in} &\in [500, 600] \\ \gamma_{300} &\in [1.3, 1.4] \end{aligned}$$

Changing  $Q_{in}$  results in very small changes in the optimal spark advance and the optimal values for the optimal PPP and MFB, all changes were less than:

$$\begin{aligned} 0.4^\circ &\text{ degrees for } \theta_{ig} \\ 0.4^\circ &\text{ degrees for } \theta_{50\%} \text{ and } \theta_{45\%} \\ 0.45^\circ &\text{ degrees for } \theta_{PP} \text{ or (PPP)}. \end{aligned}$$

Changing  $\gamma_{300}$  also results in small changes in optimal spark advance and the optimal values for the criteria, all changes were less than:

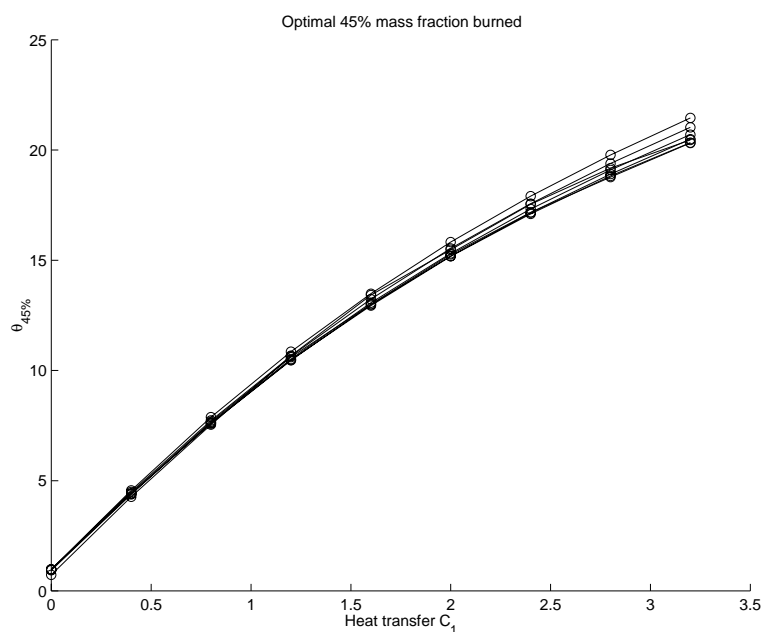


**Figure 27** Changes in the optimal position for 45% mass fraction burned position as a function of heat transfer coefficient  $C_1$  and changes in burn rate through  $\theta_b = 12 + (\theta_d - 15)/20 * 26$ .

2.2° degrees for  $\theta_{ig}$   
 2.2° degrees for  $\theta_{50\%}$  and  $\theta_{45\%}$   
 1.7° degrees for  $\theta_{PP}$  or (PPP).

## 6.5 Evaluation of loss

The interesting question that remains is: –How much work is lost if the ignition is not maintained at its optimum? The efficiency that is studied is the net indicated efficiency which represents a wide open throttle (WOT) condition, while a part load condition would increase the loss since the pumping work must be taken into consideration. As parameters for the simulation evaluation the nominal parameter values given in Table 3. Some rules of thumb can be picked out of the figure: 1) A one degree change off from optimal ignition timing will produce a loss of 0.03 percent. 2) Ten degrees off from optimum gives a loss of 3 percent. 3) A one percent loss occurs for an ignition  $5.8^\circ$  off from optimum. Note once again that these figures if valid for the net indicated efficiency.

Variations with operating condition in the burn angles will produce a changed optimal value for the ignition. Studying the simulation results in Figures 21, 23, and 24 we see that the combustion descriptor, peak pressure position and the

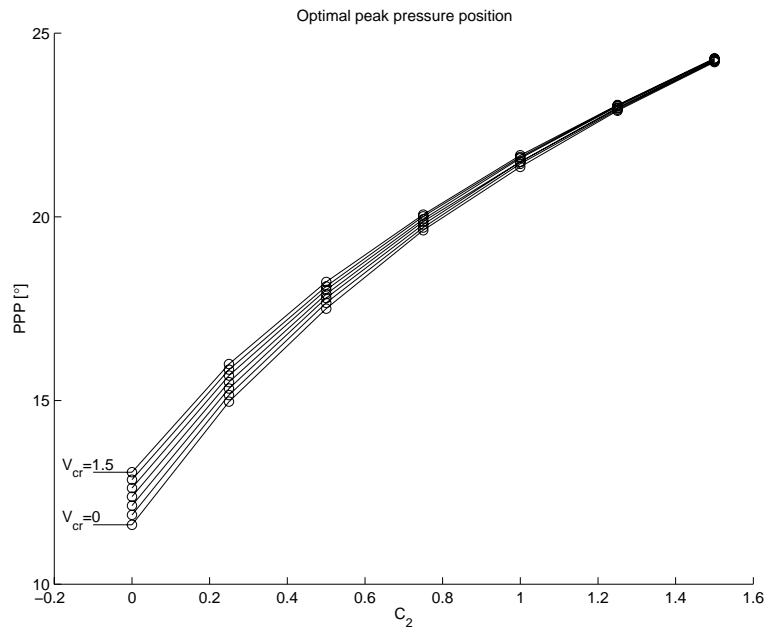


**Figure 28** Changes in the optimal peak pressure position as a function of heat transfer coefficient  $C_2$  and changes in crevice volume.

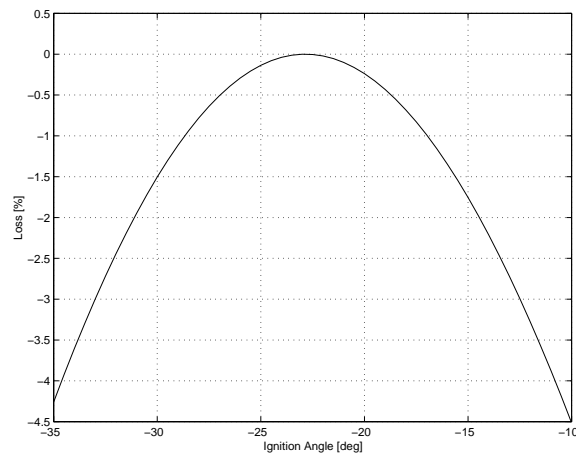


**Figure 29** Net indicated efficiency as a function of ignition angle, the optimal value for the ignition is  $\theta_{i0} = 22.9^\circ$ . The plot is generated with the model parameters at their nominal values.

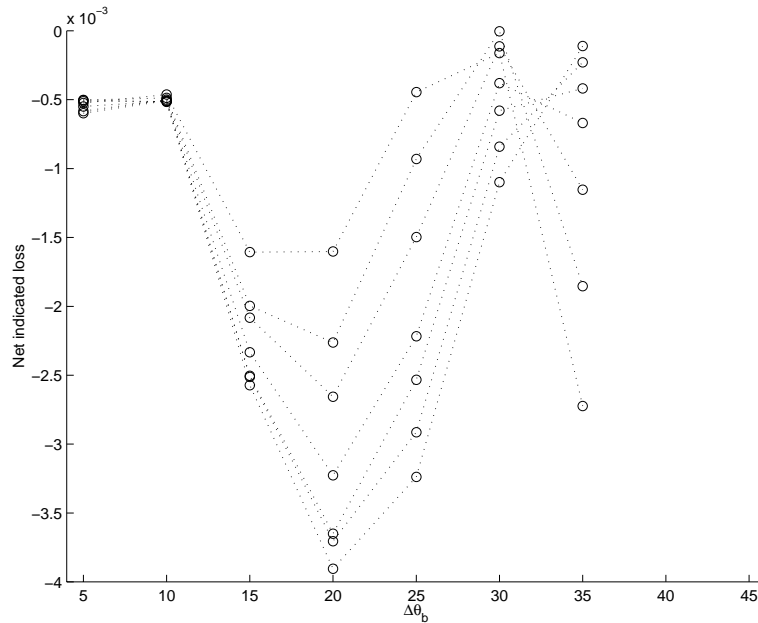


**Figure 30** The loss of not maintaining the peak pressure position at its optimum. In the plots the peak pressure has been kept at a position of  $14^\circ$  ATDC and the loss in efficiency compared to the optimal ignition. It can be seen that the loss is less than 0.4%.

positions for 45 and 50% mass fraction burned varies slightly with the burn angles. The main question is how much is lost when the combustion descriptor is controlled to a value off optimum. For the mfb-traces the question is elementary since the a change in desired position will change the ignition equally much. Figure 23 suggests that if the position for 45% mfb is controlled to  $9^\circ$  ATDC then the ignition timing will at most be 1.2 degrees off optimum thus the loss will be much less than 0.1%. However, the peak pressure position is not as easy as the mfb to analyze directly, therefore a simulation evaluation is necessary. By controlling the peak pressure position to a certain pre-determined value and comparing the produced work to the work for the optimal ignition timing the loss in not maintaining the ignition at an optimal ignition timing can be calculated. Studying Figure 21 and considering only variations for the rapid burn angle in the range  $\Delta\theta_b \in [10, 35]$  we see that a good trade off for the optimal PPP lies close to  $14^\circ$ . Figure 30 shows the loss when the peak pressure position has been controlled to  $14^\circ$  and the output work has been compared to the optimal work. Thus the loss is less than 0.4% for this choice of reference value and range of burn rate parameters.

## 7 Summary of simulation evaluation

Table 4 summarizes the simulation evaluation and shows the influence of different model parameters on the different combustion descriptors. As it can be seen in the table the position for 45% mass fraction burned has smallest variations for varying burn angles, especially when there is a correlation between flame development angle and rapid burn angle (row 4 in the table).

Param.	$\theta_{ig}$	$\theta_{pp}$	$\theta_{45\%}$	$\theta_{50\%}$
$\Delta\theta_d$	30°	2.0°	1.5°	1.5°
$\Delta\theta_b$	18°	7.5°	1.2°	1.3°
$C_1$	19°	18°	20°	21°
$\Delta\theta_d$ & $\Delta\theta_b$	50°	15°	1.0°	3.0°
$C_2$	15°	13°	15°	15°
$V_{cr}$	1.6°	1.5°	1.6°	1.6°
$Q_{in}$	0.4°	0.45°	0.4°	0.4°
$\gamma_{300}$	2.2°	1.7°	2.2°	2.2°

**Table 4** Summary of how much the different model parameters influence the different combustion descriptors in the simulations.

All variables are directly influenced by the amount of heat transfer, when the heat transfer increases the optimal position for the burning of fuel is later in the cycle. This agrees with what has been reported by Hubbard et. al. [1] for the peak pressure position. Furthermore, the simulation has also shown that the influence of heat transfer and crevice volume on the combustion descriptors is small.

### 7.1 Validation of relevance of study

One remaining question is whether or not the evaluation produces results for the deduced variables that agrees with engine measurements. The results from the evaluation of burn rate parameters and the optimal PPP, Figure 21, predicts that the optimal value for this engine lies in range 11° to 17°. Torque and pressure measurements for a wide range of operating conditions has shown that the peak pressure position for MBT timing most often occurs between 14° and 16° [17], which coincide with the results from the evaluation. Additionally, as it was mentioned earlier the influence of heat transfer also agrees with that reported by others.

## 8 Cycle-to-cycle variations

So far the simulations, described in the previous sections, has been performed for the mean values of the burn angles ( $\Delta\theta_d$  and  $\Delta\theta_b$ ). Cycle-to-cycle variations are always present in SI engines and it is therefore an important issue to investigate if

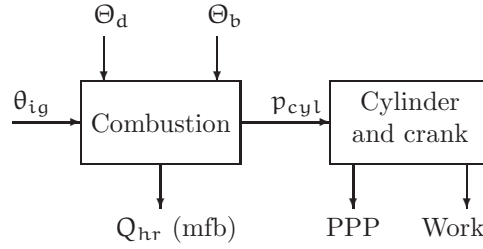


**Figure 31** Model of the combustion process where the parameters  $\theta_{ig}$ ,  $\Theta_d$ , and  $\Theta_b$  are inputs and the mass fraction burned, cylinder pressure, PPP, and work are outputs.  $\theta_{ig}$  is a deterministic variable while  $\Theta_d$ , and  $\Theta_b$  are stochastic variables.

the cycle-to-cycle variations in the burn rates change the criteria for optimal spark advance. To evaluate the influence of cycle-to-cycle variations on the criteria a stochastic model of the burn angle parameters has been used.

In Figure 31 the model of the combustion process is shown, where the burn angle parameters,  $\Delta\theta_d$  and  $\Delta\theta_b$ , are modeled as stochastic variables  $\Theta_d$  and  $\Theta_b$ . The work, mass fraction burned, and PPP are all modeled as a function of the two stochastic variables  $\Theta_d$ , and  $\Theta_b$  and the deterministic ignition timing  $\theta_{ig}$ . The work for one cycle can be expressed as

$$\text{Work}(\theta_{ig}) = w(\Theta_d, \Theta_b, \theta_{ig})$$

The optimal spark advance,  $\theta_{ig}^*$ , which maximizes the work output  $W(\theta_{ig})$  in the presence of variations, can mathematically defined as

$$\theta_{ig}^* = \arg \max_{\theta_{ig}} E[w(\Theta_d, \Theta_b, \theta_{ig})] \quad (9)$$

where  $E[\cdot]$  represents the expectation with respect to the stochastic variables. What has been investigated in the previous sections is the following

$$\theta_{ig}^\circ = \arg \max_{\theta_{ig}} w(E[\Theta_d], E[\Theta_b], \theta_{ig}) \quad (10)$$

and the question is thus how much the optimum differ, i.e.  $\Delta = \theta_{ig}^* - \theta_{ig}^\circ$ .

The expectation in Equation 9 is defined as

$$W(\theta_{ig}) = E[w(\Theta_d, \Theta_b, \theta_{ig})] = \iint_{\mathbb{R}^2} w(\theta_d, \theta_b, \theta_{ig}) f_{\Theta_d, \Theta_b}(\theta_d, \theta_b) d\theta_d d\theta_b \quad (11)$$

where  $f_{\Theta_d, \Theta_b}(\theta_d, \theta_b)$  is the two-dimensional probability density function (pdf) for the stochastic variables  $\Theta_d$ , and  $\Theta_b$ . The MBT timing,  $\theta_{ig}^*$ , is received when

maximizing the work in the equation above

$$\theta_{ig}^* = \arg \max_{\theta_{ig}} W(\theta_{ig})$$

The function  $w(\theta_d, \theta_b, \theta_{ig})$  is deterministic and can be simulated using the model described in Section 4. The only thing needed for the calculations is the pdf  $f_{\Theta_d, \Theta_b}(\theta_d, \theta_b)$ , and it is derived from measurement data using the procedure described below. Finally, the double integral in Equation 11 is discretized by dividing the area into a number of rectangles and assuming that  $f_{\Theta_d, \Theta_b}(\theta_d, \theta_b)$ , and  $w(\theta_d, \theta_b, \theta_{ig})$  are constant in each rectangle.

### 8.1 Derivation of the pdf

The probability density function (PDF) has been created following the eight steps described below. Figure 32 illustrates the results from four of the steps. To get an estimate of how much the optimum can change with cycle-to-cycle variations, the operating condition with the largest cycle-to-cycle variations in  $\Delta\theta_d$  and  $\Delta\theta_b$  is used for the simulations.

- 1) Select the data set with the largest variations.
- 2) Subtract the mean values for  $\Delta\theta_d$  and  $\Delta\theta_b$ .
- 3) Find the principal components  $x$ ,  $y$  and present the data in the principal components. (The result from steps 1 to 3 is illustrated in (a) and (b) in Figure 32).
- 4) Assuming independence for the principal components.
- 5) Estimate the pdf for each component direction,  $f_X(x)$  and  $f_Y(y)$ . Figure 33 shows a test of normality in the  $x$  and  $y$  directions and the result is that the  $y$  direction seems to be well described by a Normal distribution. As a result  $f_X(x)$  is modeled using a smoothed version of the data and  $f_Y(y)$  is assumed to be Normal distributed. (The pdf's are shown in (c) in Figure 32.)
- 6) The two-dimensional PDF is then calculated as follows, using the assumption of independence  $f_{XY}(x, y) = f_X(x) \cdot f_Y(y)$ .
- 7) Substitute variables back to  $\Delta\theta_d$ , and  $\Delta\theta_b$ . (This is shown in (d) in Figure 32.)
- 8) Translate the PDF back using the mean values subtracted in step 2 for  $\Delta\theta_d$  and  $\Delta\theta_b$ .

#### Validation of the stochastic model

To validate the pdf it has been compared with the raw data, by dividing the area into smaller regions  $\Omega_i$  and comparing the number of data in the region  $N_i$  with the probability received from the integral

$$N \cdot \iint_{\Omega_i} f_{XY}(x, y) dx dy$$

( $N$  is the total number of data). The agreement was good between raw data and the numbers that were predicted by the pdf-integral and therefore the derived pdf was accepted as a model for the burn rate variations.

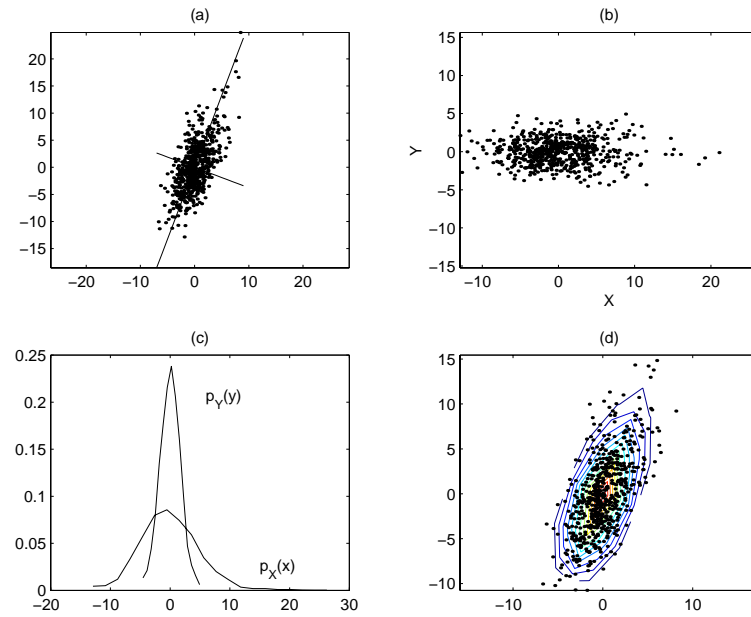


**Figure 32** Four of the steps in deriving the pdf for the burn-rate parameters are shown. a) Find principal components. b) “Rotation” to principal components  $(x, y)$ . c) pdf for principal components. d) Rotation back to burn rate parameters.

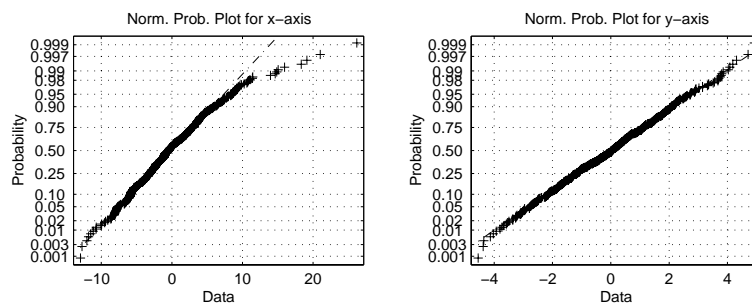


**Figure 33** Test of normality for data averaged over the principal components. The x-component does not fit a Normal distribution while the y-components does.

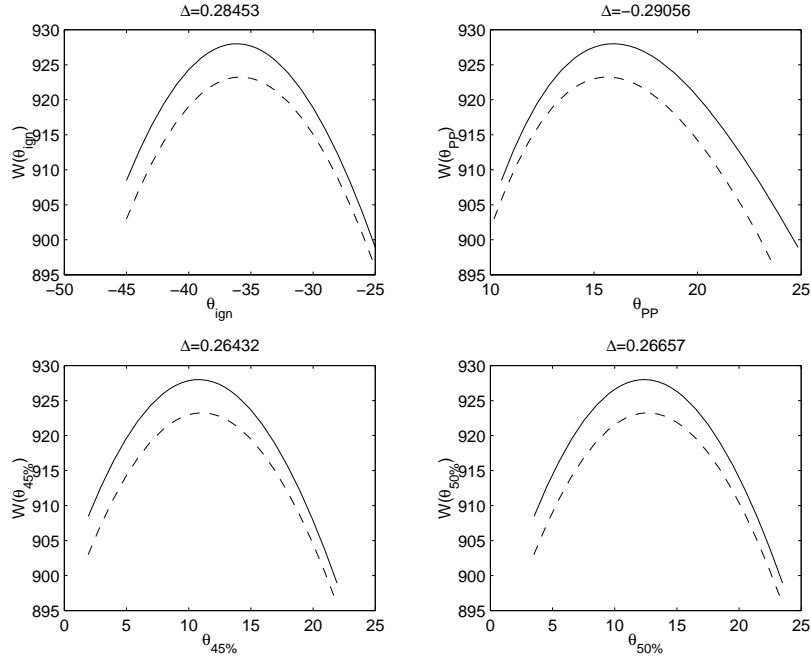


**Figure 34** The output torque, peak pressure position, 45% and 50% mass fraction burned as a function spark advance. Solid lines – no cycle-to-cycle variations. Dashed lines – parameters influenced by cycle-to-cycle variations.

## 8.2 Influence of cycle-to-cycle variations

Values for  $\theta_{pp}$ ,  $\theta_{45\%}$ , and  $\theta_{50\%}$  can be calculated in the same manner as the work in Equation 11, and the influence of cycle-to-cycle variations on these parameters can thus be determined. Straight-forward simulations is used to calculate the deterministic function  $w(\theta_d, \theta_b, \theta_{ig})$ , and the expected work  $E[W]$  can finally be calculated. Figure 34 shows the result from the analysis. The solid lines represent a simulation where no cycle-to-cycle variations (ccv) are present (Equation 10), and the dashed lines when cycle-to-cycle variations are present (Equation 10). To generate each line, a sweep with the ignition angle has been performed, and the maximum in each plot represents MBT timing. The delta,  $\Delta$ , is defined as the difference between the max positions for the simulation with ccv and the maximum position for the the simulation without ccv. The table below summarize the influence of cycle to cycle variations on the different criteria.

Parameter	Change in optimum, $\Delta$
$\theta_{ig}$	$0.28^\circ$
$\theta_{pp}$	$-0.29^\circ$
$\theta_{45\%}$	$0.26^\circ$
$\theta_{50\%}$	$0.27^\circ$

As it can be seen the influence on the criteria is very small and the error that has been made in the analysis earlier can thus be neglected. However, the reduction in output work due to cycle-to-cycle variations is still significant since it influences the engine performance.

## 9 Issues Relevant for Feedback Control

Beside the robustness there are also some other things that influence the performance of a feedback controller, and some issues are discussed here.

### 9.1 Ambiguity in PPP

For very late ignition timings the pressure rise from the combustion will come too late so that the pressure will attain its maximum close to TDC. This ambiguity will always occur. Increasing the rapid burn angle,  $\Delta\theta_b$ , decreases the ignition angle where the position for the pressure peak starts moving towards PPP, see Figure 35. The trend becomes more pronounced when the rapid burn angle,  $\Delta\theta_b$ , is increased above  $37^\circ$ . Note that the values for the rapid burning angle in the figure are very large compared to the ones obtained from the engine data, Figure 15. The ambiguity has also been pointed out by Matekunas [18]. The numerator in Equation 2 gives insight into what happens (the denominator is always positive). During the expansion the pressure rise  $dp$  due to combustion  $dQ_{ch}$  competes with the pressure decrease due to the expanding volume  $p dV$  and the peak pressure occurs at the position where these are equal (if there is no heat transfer). At TDC  $dV$  is zero, it then increases with the crank angle and the maximum is attained slightly before  $\theta = 90^\circ$ . Increasing  $\Delta\theta_b$  decreases the burn rate  $dQ_{ch}$ , see e.g. Figure 19. With these two trends competing the pressure will attain its maximum earlier for increasing values of  $\Delta\theta_b$ .

#### Implications for control

The determination of the peak pressure position is a simple task but under low load conditions, where the rapid burn angle becomes large and the cycle-to-cycle variations also are large, then it can be difficult to infer from only the peak pressure position whether the cycle is slow burning or fast burning. It can thus be difficult to perform the spark advance updating based on only the PPP information for conditions where the rapid burning angle is large. However, in the measured data only conditions close to idle pose problems since they are the only ones that have large values of  $\Delta\theta_b$ .

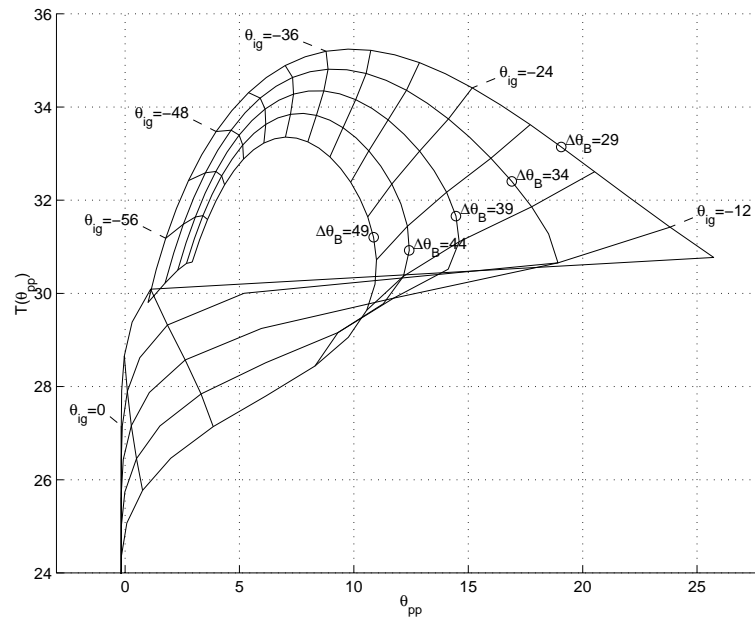


**Figure 35** A carpet plot showing the output torque  $T$  as a function of the three values: peak pressure position  $\theta_{pp}$ , rapid burning angle  $\Delta\theta_b$ , and ignition angle  $\theta_{ig}$ . The ignition timing was varied from  $60^\circ$  BTDC to  $10^\circ$  ATDC. For very late ignition timings TDC is detected as peak pressure position. The flame development angle was fixed to  $\Delta\theta_d = 25^\circ$  for all conditions simulated. Note that the rapid burn angles were chosen very large compared to the engine data shown in Figure 15.

## 9.2 Determination of the Combustion Descriptors

Another issue that has not yet been addressed is the retrieval of the combustion descriptors, and the accuracy of the pressure data. The algorithm for finding PPP is more simple than that of finding the mass fraction burned. To find the peak pressure position, it is necessary to have the correct crank angle phasing and a simple peak search can be utilized. Systems for determining the peak pressure have also been implemented in purely hardware. To determine the mass fraction burned profile it is necessary to have, correct phasing, a correct offset of the pressure signal, and a heat-release model. But with the pressure signal directly available and a fast enough micro processor the difference in complexity is of little importance.

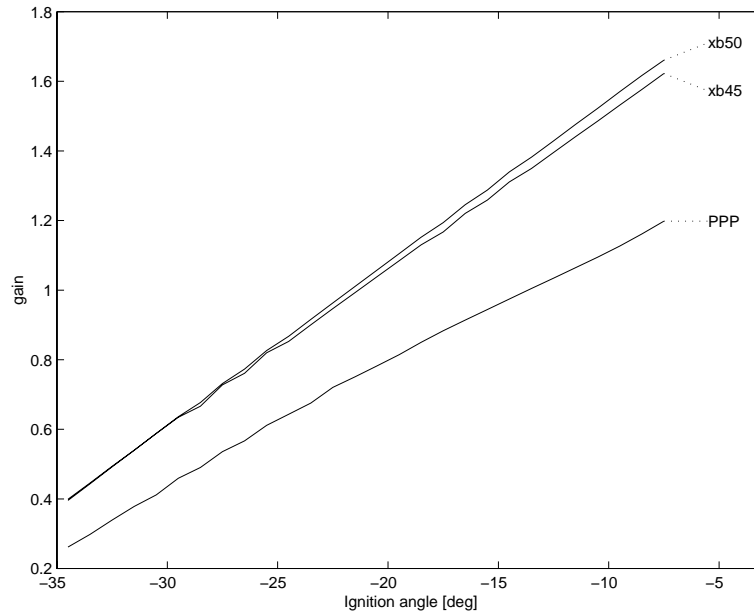


**Figure 36** Evaluation of the how the gain changes for different ignition angles in one operating condition. The lines represent: *xb50* – gain for  $\theta_{50\%}$ , *xb45* – gain for  $\theta_{45\%}$ , and *PPP* – gain for *PPP*.

### 9.3 Gain evaluation

The performance of a feedback controller can be enhanced if knowledge of the cycle-to-cycle variations (noise) and the gain for the system is known. Cycle-to-cycle variations have already been studied in Section 5 and the issue remaining here is to investigate how the gain, from ignition to combustion descriptor, changes when the ignition timing itself changes, for a typical operating condition. The model for how the burn angles vary with the ignition angle for 2300 rpm and 50 Nm, Equation 5, is used to determine the gain. The simulation results are shown in Figure 36, where the gain for the *PPP* is defined as

$$\text{gain} = \frac{\Delta \text{PPP}}{\Delta \theta_{ig}}$$

and the gains for 45 and 50% mass fraction burned positions are defined analogously.

There are significant variations in the gain as the ignition timing varies. At optimal ignition timing ( $\theta_{ig} = -21^\circ$ ) the gain is approximately unity for positions of 45 and 50% MFB and about 0.8 for the *PPP*. The linear dependence of the gain on the ignition comes from the quadratic model of the burn angles, Equation 5.

Another interesting thing shown in the figure is that the gain for the PPP is lower than for the MFB, this is due to the flattening influence that increasing crank angles (after TDC) have on the pressure development.

## 10 Summary and Conclusions

Three combustion descriptors deduced from the in-cylinder pressure have been studied. They are: peak pressure position, different levels of the mass fraction burned and, the pressure ratio. The combustion descriptors are related to the MBT timing, and have the potential of being used as sensed variables for feedback control of the spark advance. A desirable property is that the combustion descriptor is insensitive to non-measured changes in engine or environmental conditions. The three combustion descriptors were studied with respect to changes in burn angle parameters, heat transfer parameters, crevice volume, input energy, and ratio of specific heat. The main conclusions are:

- The peak pressure position and the positions for 45%–50% mass fraction burned does not change much when the flame development angle and rapid burn angle change in wide ranges.
- Considering only the mass fraction burned it is shown that the position for levels between 45% and 50% varies least when the burn angles change. When there is a correlation between the burn angles then the position for 45% is better than 50%.
- By controlling the combustion descriptors to constant positions ( $14^\circ$  for peak pressure position and  $9^\circ$  for the 45% mass fraction burned level) the loss in net indicated work is less than 0.4% even under large changes in the burn angles.
- The cycle-to-cycle variations have only a minor influence the optimal spark advance. The criteria based on the combustion descriptors can, without significant loss of information, be evaluated considering only the mean values for the burn angle parameters.
- The pressure ratio is very similar to the mass fraction burned, and no separate treatment is needed.
- The optimal value for combustion descriptors is influenced by the heat transfer. An increased heat transfer moves the optimum to a later position.
- The crevice flow, input energy, and ratio of specific heat at  $300^\circ$  do not have a large influence on the optimal value of the combustion descriptor.
- There is an ambiguity in the peak pressure position which is significant only for large values ( $> 37^\circ$ ) of the rapid burning angle. The ambiguity can occur at idle and also for very late ignition timings.

## References

- [1] M. Hubbard, P. D. Dobson, and J. D. Powell. Closed loop control of spark advance using a cylinder pressure sensor. *Journal of Dynamic Systems, Measurement and Control*, pages 414–420, December 1976.
- [2] Frederic A. Matekunas. Engine combustion control with ignition timing by pressure ratio management. US Pat., A, 4622939, Nov. 18 1986.
- [3] K. Sawamoto, Y. Kawamura, T. Kita, and K. Matsushita. Individual cylinder knock control by detecting cylinder pressure. *SAE paper No. 871911*, 1987.
- [4] Michael Bargende. Schwerpunkt-kriterium und automatische klingelerkennung. *Motor Technische Zeitschrift*, Vol. 56(10):632–638, 1995.
- [5] J. A. Gatowski, E. N. Balles, K. M. Chun, F. E. Nelson, J. A. Ekchian, and J. B. Heywood. Heat release analysis of engine pressure data. *SAE Technical Paper 841359*, 1984.
- [6] C.S. Draper and Y.T. Li. Principles of optimizing control systems and an application to the internal combustion engine. *ASME Publication*, September 1951.
- [7] P.H. Schweitzer, Carl Wolz, and Frank DeLuca. Control system to optimize engine power. *SAE Technical Paper 660022*, 1966.
- [8] I. Glaser and J. D. Powell. Optimal closed-loop spark control of an automotive engine. *SAE paper No. 810058*, pages 11–21, 1981.
- [9] Lars Nielsen and Lars Eriksson. An ion-sense engine-fine-tuner. *IEEE Control Systems (special issue on powertrain control)*, Vol. 18(5):43–52, October 1998.
- [10] J. B. Heywood. *Internal Combustion Engine Fundamentals*. McGraw-Hill series in mechanical engineering. McGraw-Hill, 1988.
- [11] G. Woschni. A universally applicable equation for the instantaneous heat transfer coefficient in the internal combustion engine. *SAE Technical Paper 670931*, 1967.
- [12] Michael F. J. Brunt and Andrew L. Emtage. Evaluation of burn rate routines and analysis errors. *SAE Technical Paper 970037*, 1997.
- [13] S.D. Hires, R.J. Tabaczunski, and J.M. Novak. The prediction fo ignition delay and combustion intervals for a homogeneous charge, spark ignition engine. *SAE Technical Paper 780232*, 1978.
- [14] Bengt Johansson. *On Cycle to Cycle Variations in Spark Ignition Engines*. PhD thesis, Lund Institute of Technology, 1995.

- [15] Lars Eriksson. Requirements for and a systematic method for identifying heat-release model parameters. *Modeling of SI and Diesel Engines*, SP-1330(SAE Technical Paper no.980626):19–30, 1998.
- [16] Philip E. Gill, Walter Murray, and Margaret H. Wright. *Practical Optimization*. Academic Press, 1981.
- [17] Lars Eriksson, Lars Nielsen, and Mikael Glavenius. Closed loop ignition control by ionization current interpretation. *SAE SP-1236*, (SAE paper No. 970854):159–166, 1997.
- [18] Frederic A. Matekunas. Spark ignition engines – combustion characteristics, thermodynamics, and the cylinder pressure card. Central States Section, The Combustion Institute, March 19-20 1984. Minneapolis, Mn.
- [19] Frank W. Schmidt, Robert E. Henderson, and Carl H. Wolgemuth. *Introduction to Thermal Sciences*. John Wiley & Sons, 2 edition, 1993.
- [20] W. J. D. Annand. Heat transfer in the cylinders of reciprocating internal combustion engines. *Proc. Instn. Mechanical Engineers*, Vol. 177(36), 1963.

## A Heat-Release Model

This appendix describes the one-zone heat-release model that has been used in this work. The model has been widely used and the phenomena that it takes into account have been described earlier in the literature [5, 10]. Basically the model is a one-zone model based on the first thermodynamic law, in which some parameters are not fully known. Some of the processes that influences the cylinder pressure are combustion, volume changes, heat transfer to the chamber walls, and mass leakage to the crevices. The article by Gatowski et.al. [5] develops, tests and applies the heat release analysis procedure used here. The model maintains simplicity while still including the effects of heat transfer and crevice flows.

### A.1 Energy conservation equation

The combustion process is considered as a separate heat addition process and the contents of the chamber is regarded as a single fluid. In the model the thermodynamic properties of the fluid are represented by a linear approximation for  $\gamma(T)$ . Straightforward heat transfer and crevice models are used to complete the energy balance in the first thermodynamic law

$$\delta Q_{ch} = dU_s + dW + \delta Q_{ht} + \sum_i h_i dm_i$$

Here the conventions, following [5, 10], are used:  $\delta Q_{ch}$  is the chemical energy that is added to the fluid through combustion;  $dU$  is the increase in internal energy which is considered as only a function of mean charge temperature,  $U_s = m_c u(T)$ ,

where both products and reactants are referred to the same datum;  $dW$  is the work produced by the fluid on the piston, i.e.  $p dV$ ;  $\delta Q_{ht}$  is the heat transfer from the fluid to the cylinder walls;  $h_i dm_i$  is the enthalpy for the mass flow out of the cylinder.

The single mass flux considered is the gas flow into and out of crevices,  $dm_i = dm_{cr} = -dm_c$ . In this model no blow-by is considered. The mean temperature for calculating the internal energy is computed using the ideal gas law  $T = \frac{pV}{m_c R}$ , which is close to the mass averaged cylinder temperature since the molecular weights of the reactants and the products are almost identical [5]. Using the statements above, the ideal gas law, and assuming that the change in the gas constant can be neglected, then the following expression can be derived

$$\delta Q_{ch} = \frac{c_v}{R} V dp + \frac{(c_v + R)}{R} p dV + (h' - u + c_v T) dm_{cr} + \delta Q_{ht} \quad (12)$$

$dm_{cr} > 0$  for flows out of the cylinder into the crevice, and  $h'$  is evaluated at cylinder conditions when  $dm_{cr} > 0$  respectively at crevice conditions otherwise.

## A.2 Thermodynamic properties

The most important thermodynamic property used for calculating the heat release rates for engines is the ratio of specific heats,  $\gamma$ . It is important since it affects how accurate changes in the internal energy of the working fluid can be represented. The ratio of specific heats,  $\gamma$ , decreases with the fuel/air mixture, and it also decreases with the temperature.

### Model of $\gamma$

A simple model of gamma is to describe it as a linear function of temperature which can be parameterized as,

$$\gamma(T) = \gamma_{300} + b(T - 300)$$

where  $\gamma_{300}$  and  $b$  are constants. The approximation in this model is consistent with the other components of the one-zone heat-release model, and it is sufficient for calculating burning rates and the overall energy balance [5].

Changing the air/fuel ratio mainly changes the parameter  $\gamma_{300}$ , while the change in  $b$  is relatively small. For evaluation of data from a motored cycle the parameter  $b$  is fixed to  $b = -2.487 \cdot 10^{-4}$  which represents the slope of  $\gamma(T)$  in the range  $T \in [300K, 1000K]$ . For firing cycles a value of  $b = -7.0 \cdot 10^{-5}$  is used which approximates the slope for both products and reactants when  $T \in [300K, 2500K]$ .

## A.3 Crevice model

The crevice walls cool the gas in the crevices to a temperature close to the wall temperature, therefore crevices may contain substantial amounts of gas when the

cylinder pressure is very high. The percentage of the original charge present in the crevices at the end of the combustion can approach 10% [5]. A simple model which does not account for blow-by is to consider a single aggregate crevice volume which has same gas temperature as the walls and the same pressure as the cylinder, i.e.  $m_{cr} = \frac{pV_{cr}}{RT_w}$ .

Using the model for  $\gamma$  the factor that multiplies  $dm_{cr}$  in Equation 12 can be rewritten, and with the crevice model the heat release model now becomes,

$$\delta Q_{ch} = \frac{\gamma}{\gamma-1} p dV + \frac{1}{\gamma-1} V dp + \delta Q_{ht} + \frac{dp V_{cr}}{T_w} \left( \frac{T}{\gamma-1} - \frac{1}{\gamma'} \ln \left( \frac{\gamma-1}{\gamma'-1} \right) + T' \right)$$

(For an explanation of the primed quantities,  $\gamma'$  and  $T'$ , see the text after Equation 12). This is an equation which represents the chemical or gross heat release, and to complete it models for heat transfer must be added.

#### A.4 Temperature model

The temperature is needed in the heat transfer model and for  $\gamma(T)$ , and the ideal gas law  $pV = mRT$  is used to calculate the temperature. By knowing the temperature at some known datum, e.g. IVC, the ideal gas law can be rewritten to

$$pV = \frac{p_{ivc} V_{ivc}}{T_{ivc}} T$$

which eliminates  $m$  and  $R$ . The model gives the mean charge temperature at a given pressure and volume during the combustion cycle from IVC to EVO.

#### A.5 Convective Heat Transfer

The magnitude of the rate of energy transfer by convection, which occurs in a direction perpendicular to the surface fluid interface,  $\dot{Q}_{ht}$ , is obtained by use of an expression referred to as Newton's law of cooling

$$\dot{Q}_{ht} = h A \Delta T = h A (T - T_w)$$

where  $A$  is the surface area of the body which is in contact with the fluid,  $\Delta T = T - T_w$  is the appropriate temperature difference, and  $h$  is the convection heat transfer coefficient. The most important task is to accurately predict the magnitude of the convection heat transfer coefficient. Since this quantity is a composite of both microscopic and macroscopic phenomena, many factors must be taken into consideration. For many flow geometries,  $h$ , is given by the relation [19, 20, 11]

$$Nu = C (Re)^m (Pr)^n$$

The correlation used to calculate the instantaneous spatially averaged heat transfer is based on the form proposed by Woschni [11], which essentially is a

Nusselt-Reynolds number of the form  $Nu = 0.035Re^m$ .

$$h = \frac{131B^{0.2}C_1p^{0.8}w^{0.8}}{T^{0.53}}$$

where,

$$w = 2.28 \left( U_p + 3.4 \cdot 10^{-3} C_2 \frac{V_{disp}}{V_{ivc}} \frac{(p_f - p_m)}{p_{ivc}} T_{ivc} \right)$$

The variables are:

B	cylinder bore	$U_p$	mean piston speed
p	cylinder pressure	T	charge temperature
$p_m$	motored pressure	$V_{disp}$	displaced volume
$p_f$	firing pressure	$C_1, C_2$	tuning constants

This model gives the rate of the heat transfer  $\dot{Q}_{ht}$ . To simulate it in the crank angle domain it has to be scaled with the engine speed,  $n$ , which results in,

$$\frac{\delta Q_{ht}}{\delta \theta} = \frac{\delta Q_{ht}}{\delta t} \frac{\delta t}{\delta \theta} = \dot{Q}_{ht} \frac{n \pi}{30}$$

## B Laminar burning velocity

This section aims at deriving an expression for the laminar burning velocity which for a given initial condition only depends on the pressure. Data for the laminar burning velocity at different pressures and temperatures have been fitted to the following power law Heywood (p.403) [10]

$$S_L = S_{L,0} \left( \frac{T_u}{T_0} \right)^\alpha \left( \frac{p}{p_0} \right)^\beta \quad (13)$$

where  $T_0 = 298$  K and  $p_0 = 1$  atm are reference states,  $S_{L,0}$ ,  $\alpha$ , and  $\beta$  are constants for a given fuel, equivalence ratio, and burned gas diluent fraction. An expression for the laminar burning velocity which only depends on the pressure can be derived using the isentropic relation for state changes in pressure and temperature

$$\frac{T_u}{T_i} = \left( \frac{p}{p_i} \right)^{1-1/\gamma} \quad (14)$$

where  $T_i$  and  $p_i$  represents the pressure and temperature at some state in the cycle, and  $\gamma$  is the ratio of specific heats. Inserting (14) into (13) and lumping all things except the pressure into constants we get

$$S_L = k_1 \cdot p^{\alpha+\beta-\alpha/\gamma} = k_1 \cdot p^{k_2}$$

where  $k_1$  and  $k_2$  are constants that depend on  $S_{L,0}$ ,  $\alpha$ ,  $\beta$ ,  $\gamma$ ,  $T_0$ ,  $p_0$ ,  $T_i$ , and  $p_i$ . Values for the constants  $\alpha$ ,  $\beta$ , and  $S_L$  are given as functions of the equivalence ratio (Heywood [10] p. 403)

$$\begin{aligned}\alpha &= 2.18 - 0.8(\phi - 1) \\ \beta &= -0.16 + 0.22(\phi - 1) \\ S_{L,0} &= B_m + B_\phi(\phi - \phi_m)^2\end{aligned}$$

where  $\phi$  is the fuel/air equivalence ratio and where  $B_L$  and  $B_\phi$  are constants depending on the fuel. The following expression can be derived for  $k_2$

$$k_2 = 2.02 - \frac{2.18}{\gamma} - \left(0.58 - \frac{0.8}{\gamma}\right)(\phi - 1)$$

which is positive for all normal values of  $\gamma$  and  $\phi$ . Using data available in Heywood [10] it can also be shown that  $k_1 > 0$  for  $\phi \in [0.7, 1.5]$  (which covers the fuel/air range of interest). Hence, it is shown that  $k_1$  and  $k_2$  are positive in the range of interest and that the laminar burning speed increases with increasing pressures during the cycle.

## C Early combustion development

The model developed here is used to explain the flame development angle,  $\Delta\theta_d$ , as a function of ignition angle,  $\theta_{ig}$ . The basis for the model is the expression for laminar burn velocity, Equation 13, and the assumption that the flame is spreading spherically in the cylinder. Neglecting the loss mechanisms and assuming an ideal gas with constant specific heats then the first law of thermodynamics can be rewritten to

$$\delta Q_{ch} = \frac{\gamma}{\gamma - 1} p dV + \frac{1}{\gamma - 1} V dp$$

which gives the following expression for the pressure differential

$$dp = \frac{\delta Q_{ch} - \frac{\gamma}{\gamma - 1} p dV}{\frac{1}{\gamma - 1} V} \quad (15)$$

The heat released is assumed to be proportional to the mass of mixture burned  $\delta Q_{ch} = q_{in} dm_b$ . The mass burn-rate is specified through

$$\frac{dm_b}{dt} = S_L A_f \rho_u \quad (16)$$

where  $\rho_u$  is the unburned gas density. Assuming that the unburned gas is an ideal gas which is isentropically compressed, then the density can be calculated provided initial conditions and the pressure. The assumption of spherical flame propagation provides the connection between the enflamed volume  $V_f$  and the flame-front area

A<sub>f</sub>. The volume fraction enflamed  $y_b$  can be expressed in terms of the mass fraction burned Heywood (p.392) [10]

$$y_b = \left\{ 1 + \frac{\rho_b}{\rho_u} \left( \frac{1}{x_b} - 1 \right) \right\}^{-1} \quad (17)$$

where the density ratio  $\frac{\rho_u}{\rho_b}$  depends on several parameters but is, for most SI-engine conditions, close to 4. This gives the volume burned  $V_b = y_b V(\theta)$

Equations 15 to 17 represent a closed system of equations that produce a second order ordinary differential equation which is easily solved numerically. The only remaining difficulty is the singularity at the ignition instant where the enflamed volume is zero and thus the enflamed area also is zero which would not produce any burn rate at all. To overcome this simulation difficulty the spark discharge is assumed to produce a volume equivalent to a cylinder with length 1 mm and diameter 0.01 mm, which represents a narrow shape that mimics the spark discharge.